“Success consists of going from failure to failure without loss of enthusiasm.”

Winston Churchill

Promotors: Prof. dr. ir. Geert Haesaert

Prof. dr. ir. Kris Audenaert

Department of Applied Biosciences, Faculty of Bioscience Engineering, Ghent University, Ghent, Belgium

Prof. dr. ir. Monica Höfte

Department of Crop Protection, Faculty of Bioscience Engineering, Ghent University, Ghent, Belgium

Prof. dr. apr. Sarah De Saeger

Department of Bioanalysis, Faculty of Pharmaceutical Sciences, Ghent University, Ghent, Belgium

Dean: Prof. dr. ir. Marc Van Meirvenne (acting)

Rector: Prof. dr. Anne De Paepe

UNIVERSITEIT GENT

FACULTY OF BIOSCIENCE ENGINEERING

A unique chemotype and genome dynamics: the key to success for *Fusarium poae*?

Adriaan Vanheule

Thesis submitted in fulfillment of the requirements for the degree of

Doctor (PhD) of Applied Biological Sciences: Agricultural Sciences

Nederlandse vertaling van de titel:

Een uniek chemotype en genoom dynamiek: de sleutel tot succes voor *Fusarium poae*?

Refer to this thesis as:

Vanheule, A. (2015) A unique chemotype and genome dynamics: the key to success for *Fusarium poae*? PhD Thesis, Ghent University, Ghent, Belgium.

Cover: microconidia of *Fusarium poae* at 20x magnification

ISBN number: 978-90-5989-865-3

Members of the jury

Prof. dr. ir. Nico Boon (chairman)

Laboratory of Microbial Ecology and Technology, Department of Biochemical and Microbial Technology, Faculty of Bioscience Engineering, Ghent University, Ghent, Belgium

Prof. dr. ir. Geert Haesaert (promotor)

Department of Applied Biosciences

Faculty of Bioscience Engineering, Ghent University, Ghent, Belgium

Prof. dr. ir. Kris Audenaert (promotor)

Department of Applied Biosciences

Faculty of Bioscience Engineering, Ghent University, Ghent, Belgium

Prof. dr. apr. Sarah De Saeger (promotor)

Laboratory of Food Analysis, Department of Bioanalysis

Faculty of Pharmaceutical Sciences, Ghent University, Ghent, Belgium

Prof. dr. ir. Monica Höfte (promotor)

Laboratory of Phytopathology, Department of Crop Protection

Faculty of Bioscience Engineering, Ghent University, Ghent, Belgium

Dr. Robert Proctor

National Center for Agricultural Utilization Research, Agriculture Research Service

US Department of Agriculture, Peoria, United States

Dr. Susanne Vogelgsang

Institute for Sustainability Sciences

Agroscope, Zürich, Switzerland

Prof. dr. ir. Tina Kyndt

Department of Molecular Biotechnology

Faculty of Bioscience Engineering, Ghent University, Ghent, Belgium

Dr. Cees Waalwijk

Bio-interactions and Plant Health

Wageningen UR, Wageningen, the Netherlands

Prof. dr. ir. Yves Briers

Department of Applied Biosciences

Faculty of Bioscience Engineering, Ghent University, Ghent, Belgium

Table of contents

Abbreviations

AA	Amino acid
ABC	ATP binding cassette
ADON	Acetyldeoxynivalenol
AFLP	Amplified fragment length polymorphism
ANEO	Acetylneosolaniol
A-T2	Acetyl-T2 toxin
bp	basepairs
BEAU	Beauvericin
BUSCO	Benchmarking universal single-copy orthologs
CAL	Calonectrin
CBS	Centraalbureau voor schimmelcultures
CCα	Decision limit
CCβ	Detection capability
CO	Cut-off level
CWDE	Cell wall degrading enzymes
DAS	Diacetoxyscirpenol
DNA	Deoxyribonucleic acid
DOM	Deepoxy-deoxynivalenol
DON	Deoxynivalenol
DON-3G	Deoxynivalenol-3-glucoside
EF-1α	Elongation factor 1α
EFSA	European Food Safety Authority
ENN	Enniatin
FAO	Food and Agriculture Organization of the United Nations
FGSC	*Fusarium graminearum* species complex
FHB	*Fusarium* Head blight
FUM	Fumonisin
FUS-X	Fusarenon-x
GS	Gene swap
hai	Hours after inoculation
hyg	Hygromycin

INS	Insertion
ISSR	Inter simple sequence repeat
JA	Jasmonic acid
KO	Knockout
LC	Liquid chromatography
LOAEL	Lowest observed adverse effect level
LOD	Limit of detection
LOQ	Limit of quantification
LTR	Long terminal repeat
MAS	Monoacetoxyscirpenol
MFS	Major facilitator superfamily
MITE	Miniature inverted-repeat transposable element
MON	Moniliformin
MS	Mass spectrometry
MUCL	Mycothèque de l'Université catholique de Louvain
Mya	Million years ago
NEO	Neosolaniol
NGS	Next generation sequencing
NIV	Nivalenol
NOAEL	No observed adverse effect level
NOR	Nucleolus organizer region
ORF	Open reading frame
PAO	Polyamine oxidase
PCR	Polymerase chain reaction
PDA	Potato dextrose agar
PDB	Protein Data Bank
PKS	Polyketide synthase
PHS	Pentahydroxyscirpene
qPCR	quantitative PCR
QTL	Quantitative trait locus
RAPD	Random amplified polymorphic DNA
rDNA	Ribosomal DNA
RFLP	Restriction fragment length polymorphism

RIP	Repeat induced point mutation
RNA	Ribonucleic acid
RNAseq	RNA sequencing
RPB	DNA-directed RNA polymerase II
SA	Salicylic acid
SCR	Scirpentriol
SMC	Secondary metabolite biosynthesis cluster
SMRT	Single molecule real time
SNP	Single nucleotide polymorphism
TAS	Triacetoxyscirpenol
TE	Transposable element
TF	Transcription factor
TIR	Terminal inverted repeat
UTR	Untranslated region
VC	Variation coefficient
VCG	Vegetative compatibility group
WGS	Whole genome sequencing
WT	Wild type
ZAN	Zearalanone
ZEL	Zearalenole
ZEN	Zearalenone

Chapter 1: Problem statement, objectives and outline

The emergence, evolution and spread of new fungal diseases and new variants of existing diseases on agriculturally important crops is considered to be one of the main threats to worldwide food availability and safety (Fisher et al., 2012). Feeding an estimated 9.5 billion people in 2050 will require the international community to increase productivity of the existing range of crops, as well as to improve the inherent resistance of the highest yielding cultivars. Fisher et al. (2012) have shown that even relatively low levels of disease on the most important agricultural crops in 2011 resulted in yield losses that would have been enough to feed 8.5% of the world's population.

One of the most important agricultural crops is wheat, the number three grain crop in the world after maize and rice (Shewry, 2009). Domestication of wheat started in the Fertile Crescent circa 10 000 years ago and encompassed the transformation of a natural ecosystem into an agro-ecosystem. The gradual selection of performant cultivars and desirable phenotypes led to a depletion of genetic diversity, more dense cultivation and monoculture growth schemes. Stukenbrock and McDonald (2008) concluded that this had, and has, an important conducive effect on fungal populations, and led to the co-domestication of plant pathogens. On the other hand, various processes lead to the emergence of new (variants of) fungal pathogens, and human intervention with new resistant crops and antifungals accelerates fungal evolution. What results is a continued "arms race" between fungal pathogens and their hosts. The genomics era has made it feasible to study this interaction and the evolution of plant pathogens at a previously impossible depth.

Fusarium Head Blight (FHB) is an important disease on small grain cereals such as wheat, barley and oats (Parry et al., 1995). While this disease is caused by a whole range of *Fusarium* species (hereafter named the FHB complex), *F. graminearum* is widely considered as the most important (Goswami and Kistler, 2004). This complex is not fixed, and it varies depending on climatic conditions, geography, host cultivar, fungicide application and other agricultural practices. Species such as *F. langsethiae* and *F. poae* have gained importance in recent years as they have become prominent members of the FHB complex. The risk associated with infection by these species originates primarily from the toxic secondary metabolites called mycotoxins that they deposit in the host matrix. Through processing of the cereals, these end up in the food and feed chain where they pose a significant risk to human and animal health.

The aim of this PhD thesis was to gain an improved understanding of *F. poae*, which has been described as a prominent member of the FHB complex in Belgium and other European countries (Xu et al., 2005; Audenaert et al., 2009). Broadly, this thesis is divided into two major parts. In a first part (comprising Chapters 2 and 3), it is investigated whether, in fact, *F. poae* may be designated as "successful". Within the context of this thesis, a successful pathogen is considered a pathogen that manages to establish colonization of its host, regardless of whether that leads to detectable symptoms or not. Questions that are considered in the first part of this thesis are what is the incidence and abundance of *F. poae* in Belgium? Is it an emerging pathogen, or has it been prominent for a long time? What is its epidemiology like, and are there similarities or differences with other FHB pathogens? Is it efficiently controlled by fungicide application?

The second part, comprising Chapters 4, 5, and 6, attempts to uncover potential "keys to success" for *F. poae*. What mycotoxins does it produce, and how does it do this? Is there large genetic variability present in the population, and how does this correlate with mycotoxin production? Does it reproduce sexually? Can any genomic determinants explain for its persistence? Finally, in Chapter 7, we try to determine whether the new information on this organism may indeed be linked to its "success".

Chapter 2 reviews the current state-of-the-art on *F. poae* and other FHB causing species, particularly *F. langsethiae*, and highlights if and how they may have emerged in recent decades. Additionally, the epidemiology and taxonomy of *F. poae* and *F. langsethiae* are reviewed and compared to other *Fusarium* species.

Chapter 3 details a survey that was carried out in Belgian fields and markets to assess the prevalence of different *Fusarium* species and their mycotoxins. *F. poae* is confirmed as an important species on wheat, and *F. langsethiae* is shown to be associated with a complex of trichothecene mycotoxins.

In **Chapter 4**, the genomes of four *F. poae* isolates are sequenced, and for one isolate novel long read sequencing was performed, making it possible to assemble the genome to a highly contiguous level. This allows for an in depth look at the genome dynamics within *F. poae*, and shed light on an active exchange between two distinct classes of co-occuring chromosomes. Finally, significant indications of a combination of sexual and asexual reproduction are found for *F. poae*.

Chapter 5 widens the scope to a broad collection of *F. poae* isolates and uses the amplified fragment length polymorphism technique (AFLP) to investigate population genetics. The toxigenic potential of the isolates is assessed at the chemotype and genotype level, and it was observed that almost all isolates produce an unusual combination of trichothecene mycotoxins.

This chemotype detected in Chapter 5, is investigated in depth in **Chapter 6**. The organization of the trichothecene biosynthesis genes is taken from the sequenced genomes, and fungal transformation and *in silico* simulations are undertaken to identify the physiological mechanism behind this unusual chemotype.

Finally, in **Chapter 7** the gathered results are combined in an overall discussion and identification of future perspectives. The unique chemotype and genome dynamics of *F. poae* appear unlinked, but they may each have contributed in their own right to the success of *F. poae* as a pathogen, by providing the tools for more rapid adaptation and evolution, and a more toxic arsenal of secondary metabolites than closely related species in the FHB complex.

Chapter 2: General introduction

Parts of this chapter were redrafted from:

Audenaert, K, Vanheule, A, Höfte, M, Haesaert, G. (2013) Deoxynivalenol: a major player in the multifaceted response of *Fusarium* to its environment. Toxins, 6, 1-19.

Audenaert, K, Landschoot, S, Vanheule, A, Waegeman, W, De Baets, B, Haesaert, G. (2011) Impact of fungicide timing on the composition of the *Fusarium* head blight disease complex and the presence of deoxynivalenol (DON) in wheat, in: Fungicides - Beneficial and Harmful Aspects, edited by Nooruddin Thajuddin, INTECH Open Access Publisher.

2.1 Taxonomy and phylogeny of *Fusarium* species

The genus *Fusarium* belongs to the Ascomycota phylum of fungi. Members of the genus are ubiquitous and are known to infect plants and immuno-compromised humans (Booth, 1971; Nucci and Anaissie, 2007). Their epidemiologies are diverse and include saprophytes, endophytes and prominent plant pathogens, responsible for some of the most economically devastating diseases of important agricultural crops, vegetables and ornamentals. Some of these pathogens are toxigenic and produce an arsenal of mycotoxins that in turn are responsible for serious threats to human and animal health (D'mello et al., 1999).

The taxonomy and circumscription of *Fusarium* is complex. In the past, classification of *Fusarium* species depended on their morphology, which was used to group species into "sections". Up to 17 sections have been described (Gerlach and Nirenberg, 1982).

Leslie (1991) noted that based solely on morphology, it was not always possible to distinguish the organisms within a "section" to the species level. Classification of *Fusarium* species therefore evolved to include the ability of individuals to mate with one another, leading to viable offspring: if so, they are part of the same "mating population" – and presumably the same species (Leslie, 1991). Reports exist however of individuals from different species that lead to viable offspring after mating (Nor, 2014).

Today, molecular techniques using conserved "barcoding genes" have become the standard for the classification of *Fusarium*, and inferring the relation between different species (Geiser et al., 2004). The evolutionary phylogeny of all medically and agriculturally important *Fusarium* species was investigated by O'Donnell et al. (2013). Using combined *RPB1+RPB2* (DNA-directed RNA polymerase II, largest and second largest subunit) sequences, these authors inferred the evolutionary phylogeny of 93 *Fusarium* species, the result of which can be found in **Figure 2.1**. Where appropriate, these species have been grouped into species complexes, shaded grey in the figure. Four of these complexes are discussed in the following graph, and they are marked in **Figure 2.1** with red asterisks.

The *F. solani* and the *F. oxysporum* complexes are divided into *formae speciales*, capable of infecting different hosts depending on whichever virulence factors are encoded within their genome. Within the *F. solani* complex, *F. solani* f. sp. *pisi* (Coleman et al., 2009) infects pea, and other species within the complex are responsible for Sudden Death Syndrome of soybean. Members of the *F. oxysporum* complex are responsible for vascular wilt of a plethora of hosts (Michielse and Rep, 2009). Well-known examples include *F. oxysporum* f. sp. *lycopersici* (Ma

et al., 2010) infecting tomato and *F. oxysporum* f. sp. *cubense* infecting banana. The latter is considered an acute threat to worldwide banana production (Kema and Weise, 2013). The *F. fujikuroi* species complex, with its different geographic lineages, comprises dozens of species colonizing a wide range of plants (Kvas et al., 2009). Important examples are *F. fujikuroi* which infects rice leading to *bakanae* disease (Wiemann et al., 2013), and *F. verticillioides* which infects maize leading to ear rot (Logrieco et al., 2002).

The focus of this PhD is on the *sambucinum* species complex which includes *F. graminearum*, *F. langsethiae* and *F. poae* among others. These species infect primarily small grain cereals such as barley, wheat and oats, leading to FHB or "scab". This leads to shriveling of the grain with lower thousand kernel weight as a consequence (Parry et al., 1995). However, importantly, the contamination of the host with mycotoxins adds another layer of damage with significant economic consequence. Nganje et al. (2004) estimate that from 1998 to 2000 the direct economic loss due to FHB in the United States was 870 million US dollars in wheat and barley. A FHB epidemic in the US during the 1990s caused up to 3 billion US dollars in losses according to Windels (2000). Various classes of mycotoxins are produced by *Fusarium* species, and O'Donnell et al. (2013) pinpointed when the biosynthesis of four of the most important chemical classes of mycotoxins and other secondary metabolites was gained in the evolutionary history of the genus *Fusarium* ("birth" of the secondary metabolite biosynthesis). These four classes of metabolites (fusarins, fumonisins, gibberellins and trichothecenes) are superposed on **Figure 2.1**.

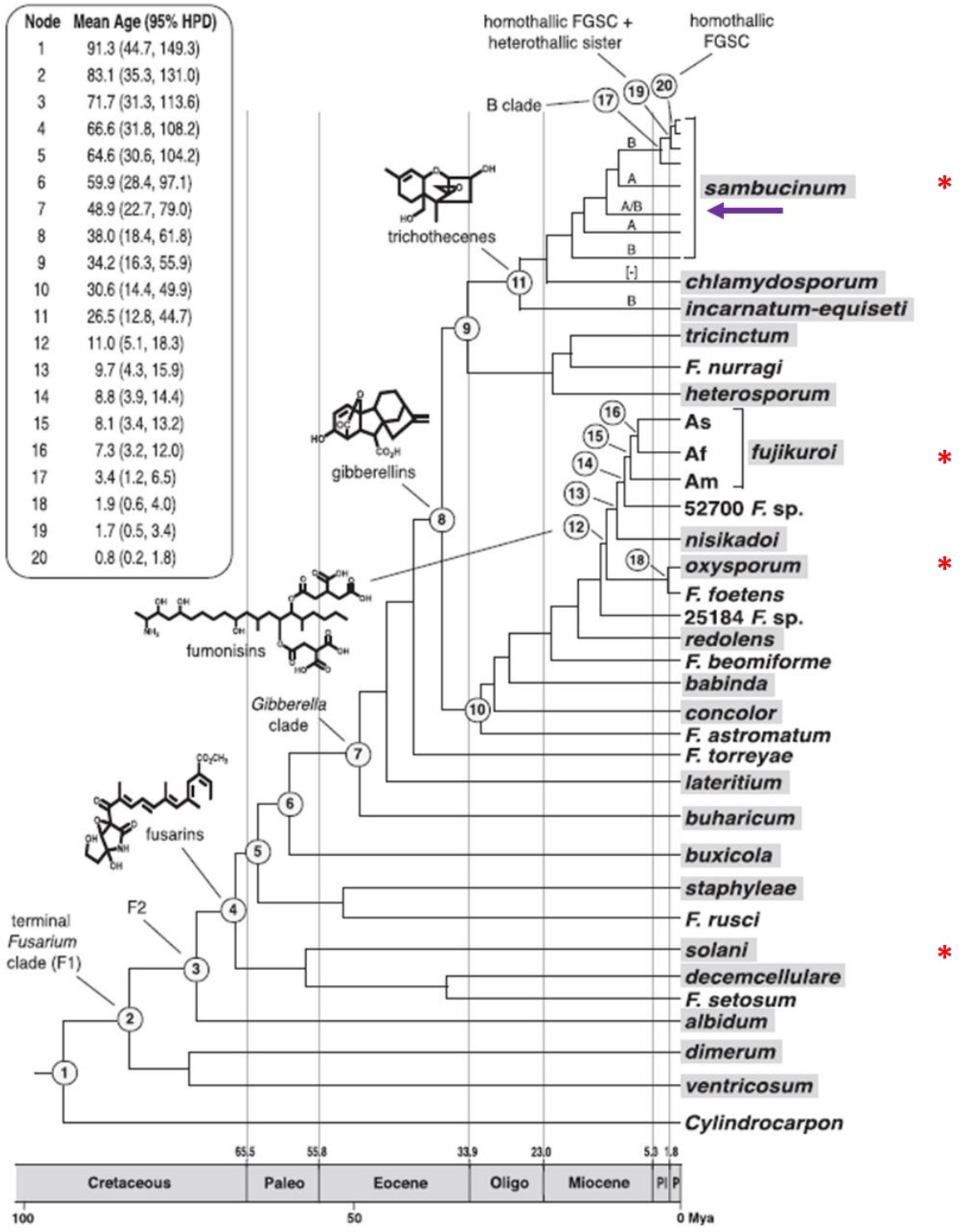

Figure 2.1 – Evolutionary phylogeny of *Fusarium* species as reported by O'Donnell et al. (2013). These authors built the tree based on combined *RPB1*+*RPB2* sequence. For 20 nodes (numbered), estimated divergence times have been calculated by these authors. Labelled nodes include the origin of certain lineages (such as the FGSC (*Fusarium graminearum* species complex) and the type B trichothecene producing lineage), and the estimated point where the capability to produce important secondary metabolites was gained (fusarins, fumonisins, gibberellins and trichothecenes). All species complexes are shaded in grey. Four of the most important species complexes are elaborated upon in the text and are designated with red asterisks. This thesis deals especially with the *sambucinum*

complex (upper side of the tree). *F. poae* is part of the *sambucinum* species complex (A/B lineage; purple arrow).

Evolutionary phylogeny as depicted by the *RPB1+RPB2* tree does not necessarily line up with morphological similarity as defined by the previously described "sections" (**Figure 2.2**). *F. sporotrichioides*, *F. langsethiae* and *F. poae* belong to the section *Sporotrichiella*, based on the morphology that they share: particularly the pyriform shaped microconidia which are abundantly produced by these species. The genetic relationship between the three species was the subject of an early 2000s EU COST action which culminated in a 2004 special issue of the International Journal of Food Microbiology (Torp and Adler, 2004). The papers in this special issue lay the framework for *F. langsethiae* as a novel species, that had previously been described only as "powdery *F. poae*" because of their morphological similarities (Torp and Nirenberg, 2004). The conclusion of this project, summarized in a polyphasic paper (Schmidt et al., 2004a), was that the three taxa are well separated and *F. sporotrichioides* and *F. langsethiae* are closely related sister species, in turn closely related to *F. poae*. As **Figure 2.2** shows, *F. poae* is not a direct sister species of *F. sporotrichioides* and *F. langsethiae*, while these three species are grouped within the same section based on morphology (*Sporotrichiella*).

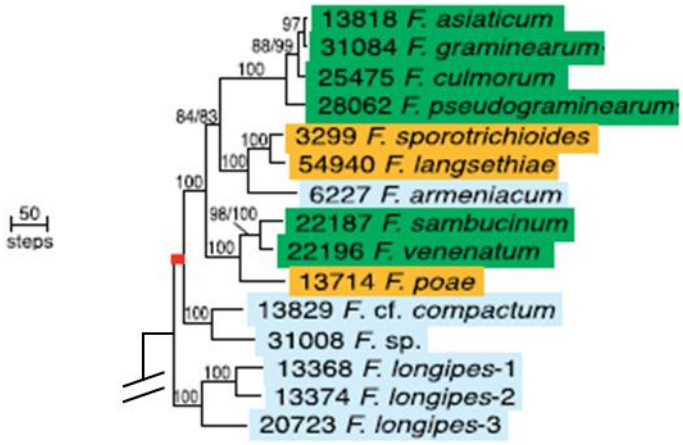

Figure 2.2 – Extract from a phylogenetic tree from O'Donnell et al. (2013) representing the *sambucinum* species complex based on *RPB1+RPB2* sequences. Species names are colored according to "sections", classifications of *Fusarium* based on morphology (Gerlach and Nirenberg, 1982). The orange section is *Sporotrichiella*, the green section is *Discolor* and the lightblue section is *Gibbosum*. It can be seen that the phylogeny of the species does not fully line up with their morphological similarity as defined by the sections.

Another major development of the last decade is the elucidation of the *F. graminearum* – clade of species. In the past, "*F. graminearum sensu lato*" was used to designate a species complex of *F. graminearum sensu stricto* and several sister lineages (*Fusarium graminearum* species

complex; FGSC). O'Donnell et al. (2004) identified nine distinct lineages within the *F. graminearum* clade and elevated them to species level. These include *F. graminearum sensu stricto*, *F. meridionale*, *F. asiaticum* and *F. boothii* as prominent disease causing species. Since 2004, more species have been discovered that are part of the *F. graminearum* species complex, including *F. gerlachii* and *F. vorosii* in 2007 (Starkey et al., 2007), *F. aethiopicum* in 2008 (O'Donnell et al., 2008), *F. ussurianum* in 2009 (Yli-Mattila et al., 2009) and *F. nepalense* and *F. louisianense* in 2011 (Sarver et al., 2011). Finally, Aoki et al. (2012) described a sixteenth species within the FGSC in 2012 which has not been formally described yet.

In addition to novel species being identified and species complexes being unraveled, the guidelines for correct nomenclature of fungal species have been a contentious issue. For sexual species, it was common to identify the species by the name of its teleomorph (given to its sexual stage), such as *Gibberella zeae* for *F. graminearum* and *Nectria haematococca* for *F. solani*. This led to dual nomenclature for many species. For this reason, a "one fungus, one name" policy has recently been adopted (Geiser et al., 2013).

2.2 Modes of reproduction in *Fusarium* species

Throughout the genus *Fusarium*, species show diverse modes of reproduction: putatively asexual, sexual in a heterothallic fashion and sexual in a homothallic fashion (see **Box 2.1**). Asexual species reproduce by the formation of conidia, propagules that are the result of mitotic divisions containing the exact same genetic material as the parent and that are therefore clonal. The benefits of clonal propagation include a rapid spread of successful genotypes, and the conservation of successful combinations of alleles which may otherwise be distorted by meiotic crossover. On the other hand, species that rely solely on clonal reproduction may loose genetic diversity and the power to adjust to adverse conditions, or gradually accumulate deleterious mutations (Lynch et al., 1993). Sexual species have the advantage of novel genotypes being generated through recombination, and the sexual propagules are often reinforced structures capable of enduring stress-related conditions (Neiman, 2005). Moreover, a fungal-specific defense mechanism against potentially disruptive transposable elements is only functional during meiosis (see Chapter 4).

For several *Fusarium* species, sexual reproduction has not been witnessed in the field, but it is suspected that they do contain a "cryptic" sexual cycle (Turgeon, 1998). *F. poae* is considered to be such a species, as isolates of both required mating types have been identified but a sexual

cycle has never been observed (Kerenyi et al., 2004). *F. oxysporum* is an example of a species reproducing strictly asexually.

Box 2.1: Modes of reproduction in fungi

Fungi reproduce either asexually or sexually. Asexual reproduction has the benefit of rapid dispersal of successful genotypes by the production of large numbers of conidia which contain the exact same genetic material as the parent. Sexual reproduction on the other hand results in new, potentially advantageous combinations of genes in offspring by recombination during meiosis. Moreover, sexual propagules are often capable of enduring adverse conditions, and a fungal-specific defense mechanism against potentially disruptive transposable elements is only active during meisosis (see Chapter 4). The sexual cycle in fungi is partly regulated by the genes that occupy the mating locus, and the two versions of this locus are called "idiomorphs" as they share no similarity to one another (opposed to alleles of the same gene). Heterothallic species contain the genes from either the MAT1-1 or MAT1-2 idiomorph in their genome. These require a partner of the opposing mating type to enter meiosis and are self-sterile. The Figure in this Box shows this for *F. pseudograminearum* (annotations extracted from NCBI accessions HG323867 and HG323861 respectively). Homothallic species such as *F. graminearum* contain the genes from both idiomorphs tightly linked, and these organisms are self-fertile and do not need a partner of the opposing mating type to cross (annotation extracted from NCBI accession HG970333). Black lines indicate homologous sequences, crossed lines indicate that the sequence is inverted. The flanks of the idiomorphs are circled with black lines, and this is sequence which is universally shared between the different species/isolates. Only the composition of the idiomorphs differs between them. Within the genus *Fusarium* is it speculated that heterothallism is the ancestral mode of reproduction and the homothallic configuration resulted from a complex fusion event (O'Donnell et al., 2004).

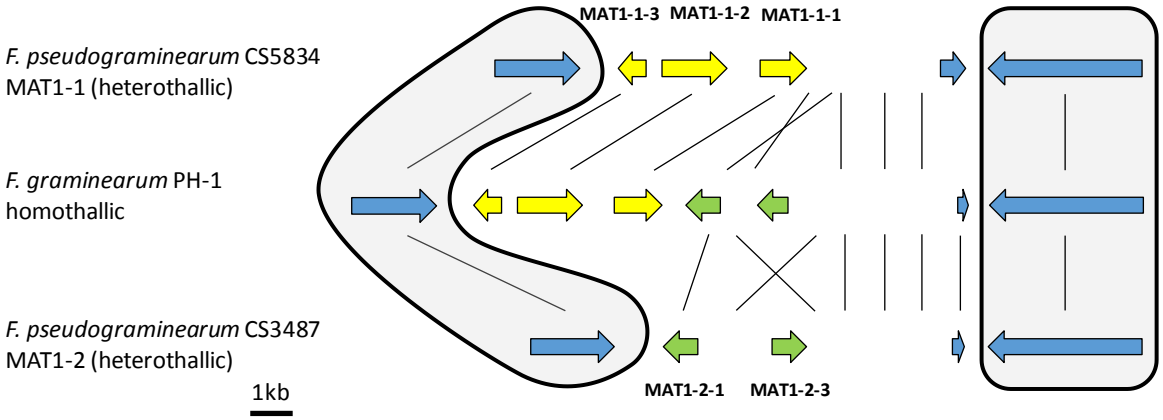

For other *Fusarium* species, it is certain that a sexual stage exists because the sexual structure has been witnessed and a teleomorph is described. Examples include *F. graminearum*, *F. avenaceum* and *F. solani*. As is stated in **Figure 2.1**, within the *sambucinum* species complex, both homothallic and heterothallic species exist (see nodes 19 and 20 in **Figure 2.1**). Notably, species within the FGSC are homothallic (indicated at node 20 in **Figure 2.1**), indicating that

they do not need a mating partner to engage in a sexual cycle, and they are self-fertile (O'Donnell et al., 2004). This is different from closely related species such as *F. pseudograminearum* and *F. culmorum,* which are heterothallic and need a partner of the opposite mating type to enter meiosis.

F. graminearum reproduces mainly sexually (Manstretta et al., 2015). As a homothallic species, it is able to self, leading to "clonal ascospores", but it also engages in outcrossing with other homothallic *F. graminearum* isolates (Bowden and Leslie, 1999) giving rise to "recombinant ascospores" (Ma et al., 2013). The nature of the agro-ecosystem may influence the mode of reproduction of a pathogen (Stukenbrock and McDonald, 2008). This was recently demonstrated in Canada where regional factors influenced *F. graminearum* population dynamics (Kelly et al., 2015). In accordance with this finding, Liang et al. (2015) have suggested that *F. graminearum* populations on wheat are sexually more active than populations on barley in the upper Midwestern United States.

The different modes of dispersal in sexual and asexual species, and the different ways that they may cope with newly released antifungals or crop varieties have a profound effect on their epidemiology and the measures that should be taken for durable disease management (McDonald and Linde, 2002). Pathogens with a mixed reproduction system have the greatest potential for evolution, as sexual recombination may be able to overcome resistance gene pyramids in the plant and virulent lineages may easily spread clonally. *Puccinia graminis* f. sp. *tritici*, the causal agent of wheat stem rust is currently one of the greatest threats to worldwide wheat production due to the emergence in 1999 of a virulent pathotype Ug99 (Singh et al., 2011). *Phytophthora infestans* which causes late blight in potato and was responsible for the Irish potato famine in the 1840s has traditionally been an asexual species in Europe with only a single mating type occurring, until the introduction of the opposing mating type during the 1970s. Since then it has begun to reproduce sexually leading to offspring which is able to overcome popular resistance genes in the plant, however these genotypes have only seen limited clonal spread up to now (Li et al., 2012).

2.3 *Fusarium* head blight on small grain cereals

The latest complete figures of the Food and Agriculture organization of the United Nations (FAO) highlight the importance of wheat, barley and oats in worldwide agriculture. In 2012, wheat constituted 27% of the Belgian total arable soil (217 060 ha of 801 800 ha total). Worldwide this was 15.5%. In Belgium, barley is grown on 5.7% of available arable land,

worldwide this percentage is 3.5%. Wheat is particularly important for food and feed production and is in many countries a staple food. Currently up to 50% of wheat harvest may be lost globally as a result of various pests and diseases (Oerke, 2006). Barley is primarily a feed component and is the main input stream of the malting and beer industry.

The term FHB is used to identify a set of symptoms on small grain cereals caused by a number of species which regularly co-occur on their host. These symptoms include bleaching of the wheat ear and shriveling of the grains. In the United States FHB may lead to economic losses in excess of one billion USD per year (McMullen et al., 2012). Depending on the small grain cereal crop, yield losses may range up to 50% in severe FHB epidemics (Parry et al., 1995).

F. graminearum is the most important member of the FHB complexs. It is a fairly aggressive pathogen and a primary invader of healthy tissue (Walter et al., 2010). *F. culmorum* is a closely related species, and has in the past been implicated in FHB epidemics (Scherm et al., 2013). Within the European *Fusarium* population on wheat and barley, these two species are the most aggressive and likely account for most of the easily discerned damages such as the typical bleaching. However, there are several other species which may occur on the ears of the plant. Examples are *F. poae*, *F. langsethiae* and *F. avenaceum*. *F. poae* has been increasingly detected by several researchers over the past decade (Xu et al., 2005; Audenaert et al., 2009). *F. langsethiae* is of major importance in oat cultivation (Imathiu et al., 2013). *F. avenaceum* is a typically generalist fungus which may occupy the wheat ear (Lysoe et al., 2014).

The damage these pathogens cause to the cereal ear is not limited to the introduction of morphological symptoms. Less visible, but likely accounting for more economical damages and food safety concerns, is the deposition of mycotoxins in the cereal matrix. While the visible damage of species such as *F. poae*, *F. langsethiae* and *F. avenaceum* may be disputable, their production of toxic compounds in the host is not (Thrane et al., 2004; Vogelgsang et al., 2008b).

Mycotoxins are toxic secondary metabolites produced by fungi. They are toxic in the sense that they are damaging to often both plant and animal cells, and can lead to health issues as a result of chronic exposure, or in some cases to acute toxicity (Placinta et al., 1999). They are secondary metabolites, which implies that they are dispensable for standard vegetative growth, but in many cases they may be involved in host infection or stress coping mechanisms (Reverberi et al., 2010). Their production depends on a range of environmental and genetic factors. The specific roles these compounds play in the life cycle of the organism is the subject of research. Deoxynivalenol (DON) and its acetylated derivatives (ADON) are the most

important trichothecene mycotoxins produced by *Fusarium* species, particularly *F. graminearum*.

2.4 FHB severity and composition are dynamic

The complex of species co-occurring on the cereal ear is not static. The population may evolve during the growing season, may differ between growing seasons and may be implicated in large population shifts when studied over multiple years. For example, during the growing season, Xu et al. (2008) found that from the milky ripe stage (Z77) to harvest time, *F. avenaceum* and *Microdochium majus* (another member of the FHB complex) showed a dramatic increase in fungal biomass in spikelets at the expense of *F. culmorum* in particular.

Multi-year studies allow for the evolution of the FHB complex to be monitored. Research carried out at Ghent University (**Figure 2.3**) shows that the composition of the complex, represented by the five most dominant species, is highly variable over the sampled years. In some years (2007, 2008), *F. poae* occurred in almost half of the sampled ears.

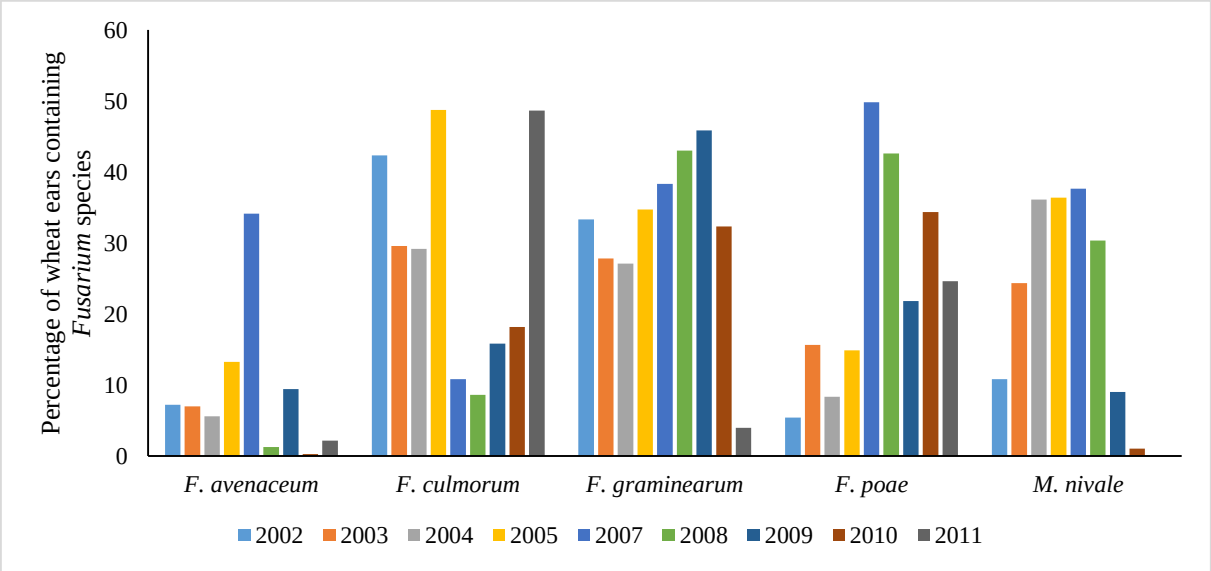

Figure 2.3 – Multi-year survey carried out in Flanders, Belgium to monitor the composition of the FHB population on wheat. Percentage of wheat ears (average 228 ears of multiple cultivars on ~9 locations tested every year) that contain *Fusarium* species are given. Presence of *Fusarium* species is determined by diagnostic PCR, methods are described in Audenaert et al. (2009). *Microdochium (M.) nivale* is a species that is frequently implicated in the FHB complex. No species sampling was performed in 2006. This graph is based upon data gathered in a PhD project at Ghent University (Landschoot, 2012).

Multiple FHB species may co-occur on the same ear and their presence may even be significantly correlated (Xu et al., 2008; Audenaert et al., 2009). Analyses carried out at Ghent University indicate that the FHB composition becomes more complex as the general disease

severity becomes higher (**Figure 2.4**; dataset and materials and methods described in Landschoot (2012)). *In vivo* artificial inoculation studies have shown that usually only one species is dominant in the wheat ear (Siou et al., 2015), which may be different under natural circumstances (Waalwijk et al., 2003).

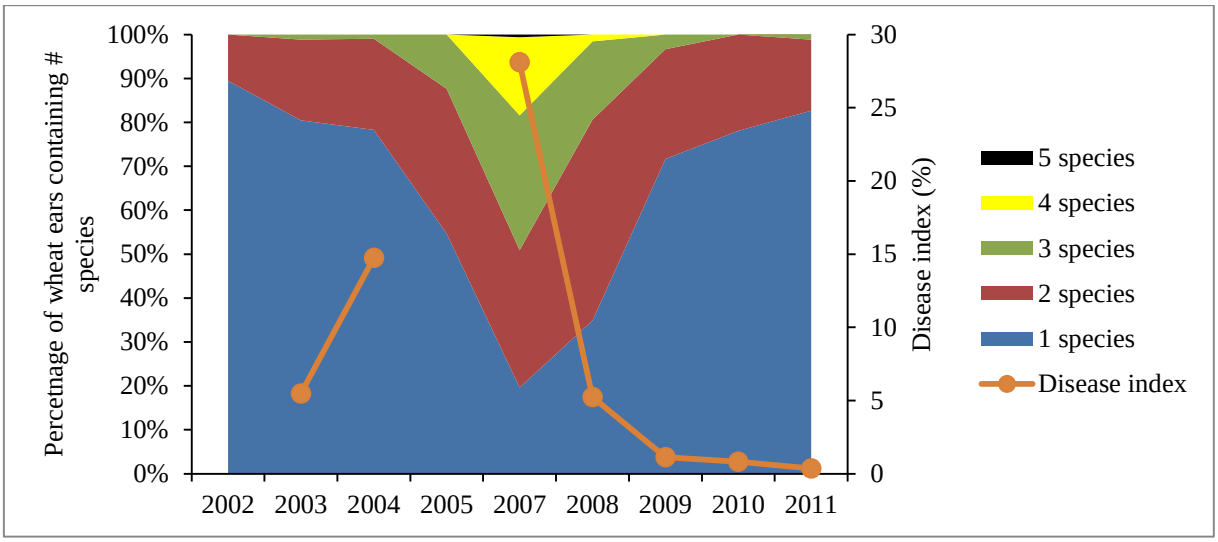

Figure 2.4 – Relation between disease index and complexity of the FHB population occupying wheat ears. Data is shown for on average 228 ears per year. In 2005, species were sampled but disease index was not determined. No species were sampled in the 2006 growing season and this year is skipped in the graph. Disease index is a composite measure for the severity of FHB. This graph is based upon data gathered in a PhD project at Ghent University (Landschoot, 2012).

Various environmental and agronomic variables influence the severity and the composition of the FHB (Landschoot et al., 2012). The influence of previous crops and other agronomic practices such as tillage versus no-tillage has been extensively investigated for several *Fusarium* species. Wheat after maize, and no-tillage, consistently give a higher risk for FHB infection and DON contamination (Dill-Macky and Jones, 2000). This is related to the enhanced opportunities for inoculum build-up outside of the growing season, as crop debris with *Fusarium* biomass remains at the surface of the field. Notably, for *F. poae*, no relationship to previous cropping factors has been uncovered (Thorp and Jennings, 2015). Uncertainty remains however, as Yli-Mattila (2010) indicates that tillage increases the *F. poae* contamination, opposite to the situation for *F. graminearum*. Importantly, weather conditions may impact the composition and severity of FHB (Doohan et al., 2003; Landschoot et al., 2012). The importance of relative humidity during flowering for the development of FHB has been extensively illustrated (Xu, 2003). **Figure 2.5** shows the influence of relative humidity in June and mean temperature during winter on overall *Fusarium* disease severity (research carried out at Ghent University). The list of variables impacting the composition and severity of FHB

presented here is not exhaustive, and other environmental and agronomic factors play a role such as fertilization (Lemmens et al., 2004), fungicide use (Audenaert et al., 2011), crop species and varieties (Mesterhazy, 1995), various meteorological parameters at the time of flowering (Landschoot et al., 2012), etcetera. Multiple reviews and studies have been published that go deeper into the wide range of environmental variables impacting FHB (Parry et al., 1995; Xu, 2003; Landschoot et al., 2012). A recently developed predictive model for FHB in Belgium uses up to 70 meteorological and other variables (Landschoot et al., 2013).

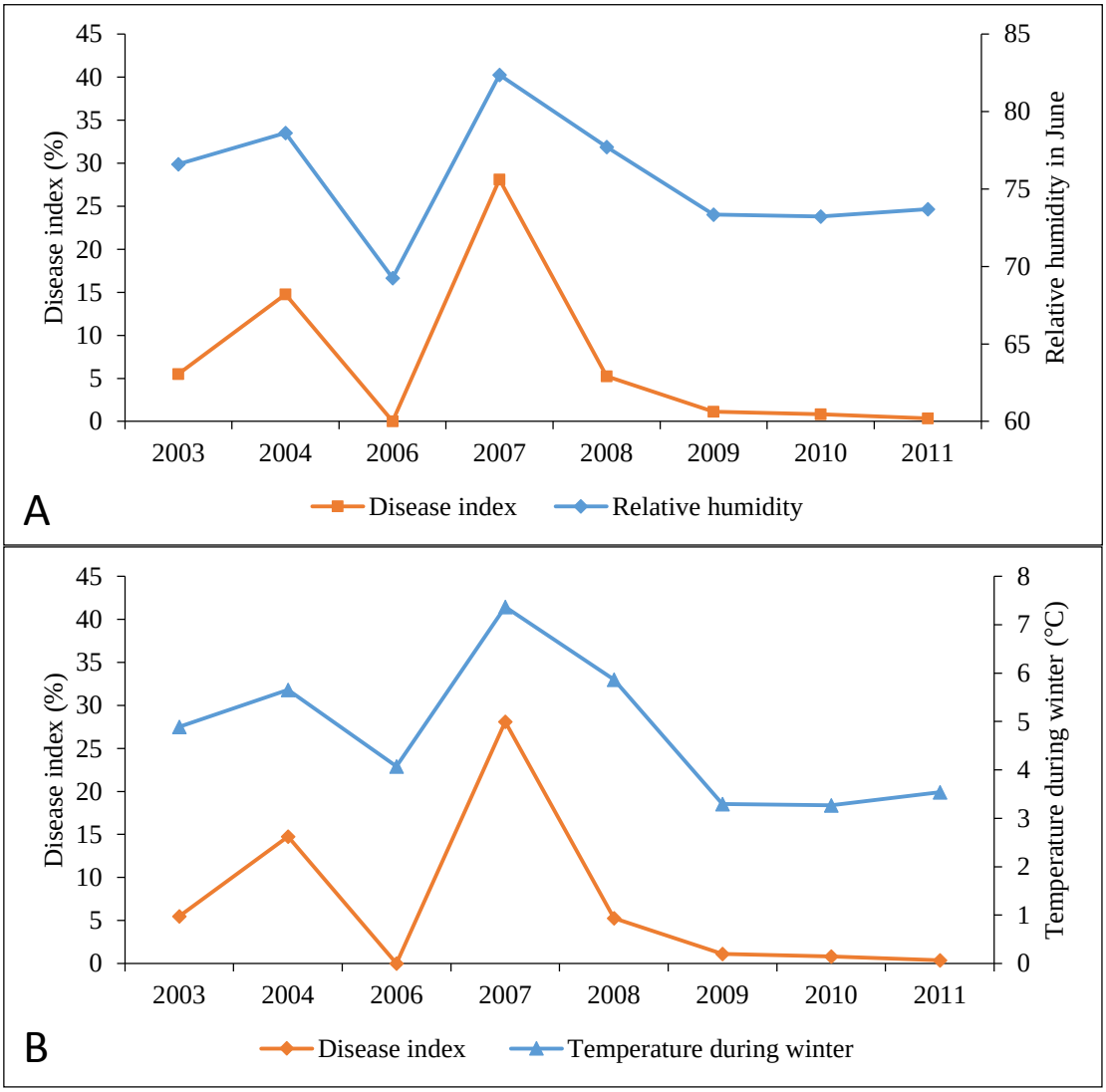

Figure 2.5 – Pattern of selected weather variables compared with overall Fusarium disease severity for the 2003-2011 growing seasons. Disease index is a composite measure for the severity of FHB. This graph is based upon data gathered in a PhD project at Ghent University (Landschoot, 2012). In 2005, no disease index was determined and this year is skipped in the graph. A: relative humidity (averaged over all days in June) and disease index are correlated. B: mean temperature during winter (averaged over four months: November, December, January and February) and disease index are correlated.

When the evolution of the FHB complex is monitored over greater time periods, major populations shifts or geographic migration patterns may be detected (van der Lee et al., 2015). In the Netherlands, a major shift from *F. culmorum* dominated populations to *F. graminearum* dominated ones has occurred at the end of the last century. The authors who have observed this shift have speculated that increased maize acreage, the ability of *F. graminearum* to readily form ascospores and worldwide climate changes could account for this major shift (Waalwijk et al., 2003). Also in the United States, the increased dominance of *F. graminearum* has led to a global re-emergence of FHB as a disease (Goswami and Kistler, 2004).

While the shift from *F. culmorum* to *F. graminearum* was noted by several researchers (Kosiak et al., 2003; Waalwijk et al., 2003) and has been generally accepted, other evolution in the FHB complex are less straightforward. Two morphologically closely related species (Schmidt et al., 2004a) which may be subject to drastic population trends are *Fusarium poae* and *Fusarium langsethiae*. Both species are among the most frequently detected FHB pathogens on small-grain cereals, where *F. poae* appears to be frequently recovered from barley and wheat, and *F. langsethiae* infestation is especially problematic in oats.

F. poae has been included in field surveys since the late-eighties of last century. Even at that time, it was often among the most common detected FHB pathogens in geographically distant places, such as Norway (Haave, 1985), Canada (Clear and Patrick, 1993) and the United Kingdom (Polley and Turner, 1995). Today it is still one of the most frequently detected species in wheat, barley and oats. Recent studies that show *F. poae* is among the dominant species in wheat include Wagacha et al. (2010), Lindblad et al. (2013) and Lazzaro et al. (2015), who analyzed samples from Kenya, Sweden and Italy respectively. Fredlund et al. (2013) noted a similar finding in oats. In barley, Nielsen et al. (2014) showed that *F. poae* is the dominant species in the United Kingdom. This finding holds true over a wide array of detection methods. In our analyses at Ghent University, we used in different studies diagnostic PCR (Audenaert et al., 2009) as well as qPCR (Chapter 3 of this thesis), both designating *F. poae* as one of the dominant species in Flanders. However, it must also be noted that *F. poae* is not always among the most frequently detected species when FHB is investigated, different from *F. graminearum* which is consistently detected as the most important cause of FHB.

The first reports dealing with *F. langsethiae* originate from the mid-nineties, at which time it was termed "powdery *F. poae*" (Torp and Langseth, 1999; Kosiak et al., 2004), and isolates of the species were in the past indeed sometimes identified as *F. poae* (Knutsen et al., 2004). It is unclear how frequently this may have occurred and when *F. langsethiae* was therefore first

detected. It has been detected in British wheat samples that were isolated in the early 1900s (dr. Cees Waalwijk, personal communication).

2.5 *F. graminearum* pathogenesis

F. graminearum is currently the most important pathogen within the FHB complex, and its distribution is near cosmopolitan. For this reason, *F. graminearum* infection has been studied more in depth than any other *Fusarium* – host interaction, but nevertheless the categorization of its mode of pathogenicity has been troublesome. Jansen et al. (2005) set out to identify whether the typical *F. graminearum* mediated necrosis is preceded by a biotrophic phase. They found that as soon as the fungal hyphae enter the cytosol of the wheat or barley epicarp cells, cell death was induced. Therefore, a strict biotrophic phase whereby nutrients are exchanged between the pathogen and the host in specialized structures does not occur. However, a multitude of reports indicate that *F. graminearum* infection is organized into distinct phases, and that it may be classified as a hemibiotroph or hemibiotroph-like pathogen (Kazan et al., 2012).

The precise series of events from spore landing to successful pathogenesis in *F. graminearum* has recently been reviewed (Walter et al., 2010; Audenaert et al., 2014). In wheat, penetration of the anthers during flowering is the preferred infection route. Up to two days after this initial infection, hyphae may grow subcuticularly and intercellularly in the glume, palea and lemma of the spikelet. Spreading to other spikelets besides the primary infection spikelet depends in wheat on DON production that hampers the host's reinforcement of the rachis (Jansen et al., 2005). In barley, DON is less of a virulence factor, as both wildtype and *Tri5* knockout isolates are inhibited at the rachis. The same conclusion was reached by Maier et al. (2006) who found that infection of barley was not linked to trichothecene biosynthesis. Indeed, barley has been identified as containing natural resistance against FHB which prohibits the pathogen from spreading within the ear. In wheat, *F. graminearum* spreads throughout the ear beyond the initial spikelet and produces DON in large amounts, and complete necrosis is accomplished and the typical bleaching of the ears are apparent symptoms.

The division into a non-necrotic and necrotic phase of *F. graminearum* infection is substantiated by transcriptomics analysis performed in wheat by Ding et al. (2011). These authors determined that in a first stage, signaling pathways mediated by salicylic acid (SA) are upregulated followed at later time points by pathways mediated by jasmonic acid (JA). SA and JA are implicated in defense against biotrophs respectively necrotrophs. The sequential and

meticulously timed defense strategy of wheat against hemibiotrophic *F. graminearum* (Pritsch et al., 2000) was confirmed by Ameye et al. (2015). In barley different stages of infection were elucidated by Boddu et al. (2006), who coupled barley transcriptomics with DON measurement and symptom determination. In the first 48h after infection, there was limited fungal growth and low DON accumulation, and limited host transcriptional response. This was followed by a phase of increasing infection, DON production and increased host response. The ability of *F. graminearum* to transverse the rachis in wheat but not in barley may be reflected by the very high amount of fungal genes expressed during wheat infection at the 96 hai time point, which were identified in a study of the transcriptome of *F. graminearum* (Lysoe et al., 2011).

A crosstalk exists between the pathogen and the host during infection (Walter et al., 2010). Many of the involved metabolites are shared between both organisms and in fact, the fungus may hijack some of the signals and compounds implicated in plant defense. An example is the production of polyamines which is an early plant defense response to FHB infection (Gardiner et al., 2010a). Oxidation of polyamines by the plant's polyamine oxidase (PAO) enzyme leads to H_2O_2 production and cell death, restricting the growth of the pathogen in its biotrophic stage. Indeed, Ding et al. (2011) have shown an early activation and peaking of PAO transcription in resistant wheat cultivars. However, intermediates and end products of the polyamine pathway have been shown to be strong inducers of DON biosynthesis in *F. graminearum*, and these may thus be a cue for the pathogen to enter its fully nectrotrophic stage. Additionally, H_2O_2 which is produced by PAO also leads to increased trichothecene production (Audenaert et al., 2010). As H_2O_2 induced cell death is not an efficient defense against necrotrophs, the expression of plant PAO decreases from 12 hai, but interestingly a fungal PAO is activated in wheat (but not in barley) from 48 hai (Lysoe et al., 2011). The hijacking of the plant's primary nitrogen metabolism to the pathogen's advantage is most definitely not *Fusarium* specific, and knows many more examples (Seifi et al., 2013). However, during infection also the primary metabolism of the fungal pathogen is intricately associated with pathogenicity, as was recently demonstrated for the leucine metabolic pathway in *F. graminearum* (Subramaniam et al., 2015).

DON plays roles in the physiology of *F. graminearum* besides its demonstrated role in penetration of the rachis in wheat spikelets. It is in fact a vital part of the fungal armor against external stressors such as oxidative stress, sublethal fungicide application and increased plant defense (Audenaert et al., 2010; Audenaert et al., 2014; Ameye et al., 2015). One of the core defense mechanisms of the wheat plant is depriving the pathogen of its virulence factor. Conjugation of DON, primarily to glucose, renders it significantly less toxic to both plants and

animals (Berthiller et al., 2013). The ability of the plant to detoxify DON is correlated with its resistance against *F. graminearum* (Audenaert et al., 2013). These conjugated metabolites still end up in the food and feed chain however and may as such still pose a risk to human health (see Chapter 3 of this thesis). Indeed, reports indicate that they may be hydrolyzed in the gastrointestinal tract, releasing anew the parent toxic compound (Berthiller et al., 2011). In barley, Gardiner et al. (2010b) discovered a novel inactivation mechanism of DON dependent on glutathione conjugation.

Within the species *F. graminearum*, different trichothecene chemotypes (see **Box 2.2**) may confer competitive advantages among one another and lead to population displacement. In the Southern United States, NIV chemotypes are dominant, while a 3-ADON population diverged in several Northern states in the last decade (Liang et al., 2014). In Canada, the 3-ADON population of *F. graminearum* increased more than 14-fold between 1998 and 2004 (Ward et al., 2008).

Box 2.2 – Of chemotypes and genotypes

The chemotype of a *Fusarium* isolate or species is defined as the spectrum of different mycotoxins that it produces. The capability to produce this mycotoxin blend is determined by the genes that are present within the genome of an individual, often designated the "genotype". However, the actual production of mycotoxins is dependent on a range of environmental factors, substrate, etcetera. Within the scope of this thesis, the chemotype refers to the blend of trichothecenes that is produced. These are a family of toxins with a tricyclic 12,13-epoxytrichothec-9-ene backbone structure. Different groups of trichothecenes exist, and *Fusarium* species produce type A and type B trichothecenes, such as respectively diacetoxyscirpenol (DAS), neosolaniol (NEO), T-2, HT-2, and deoxynivalenol (DON), 3-acetyldeoxynivalenol (3-ADON) and 15-acetyldeoxynivalenol (15-ADON), fusarenone-x (FUS-X) and nivalenol (NIV) (McCormick et al., 2011). Type A trichothecenes contain either a hydroxyl group, ester function or no oxygen substitution at the C8 position, while type B trichothecenes have a keto function at C8 (see the Figure in this Box). Chapter 6 goes deeper into the genetic distinction between type A and type B trichothecenes.

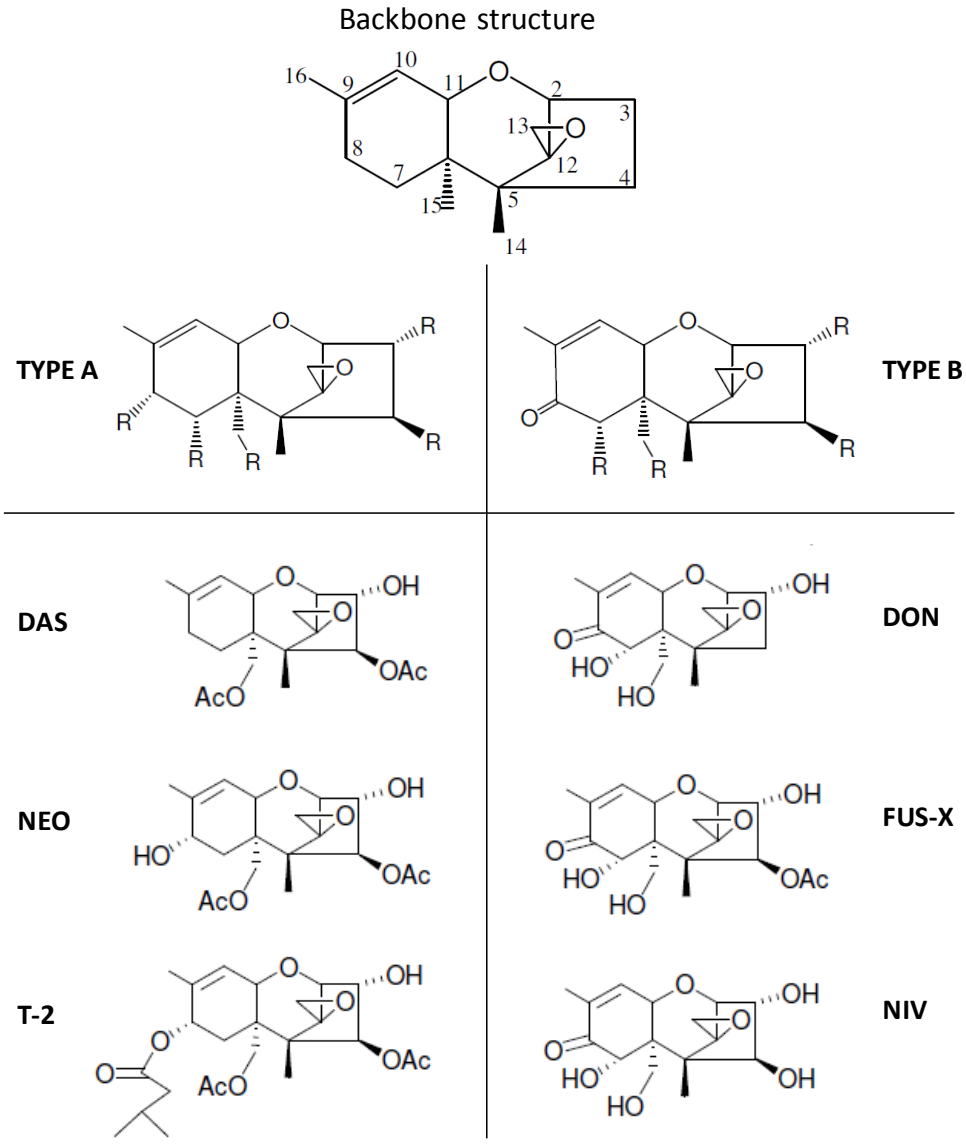

2.6 *F. poae* / *F. langsethiae* pathogenesis

The importance of *F. poae* and *F. langsethiae* within the FHB complex, at least on certain hosts or under certain conditions, is without doubt. Less is known about the epidemiology of these species when compared to *F. graminearum*. In the following paragraphs the current knowledge is reviewed, and the differences with *F. graminearum* are highlighted.

Regarding trichothecene contamination related to *F. poae*, nivalenol (NIV) is probably the primary concern. It has been determined that a correlation exists between the NIV concentration and the degree of *F. poae* infestation after artificial inoculation (Vogelgsang et al., 2008b). This may indicate that NIV plays a similar role in the biology of *F. poae* as DON does in *F. graminearum*, but knockout studies in *F. poae* are still lacking. Brennan et al. (2007) showed that two *F. poae* isolates produced NIV in three out of seven tested wheat cultivars. In a study by Covarelli et al. (2015), ten out of twelve tested *F. poae* isolates produced NIV on autoclaved rice medium. Thrane et al. (2004) found that 51 out of 52 isolates produced NIV on various *in vitro* media. While these *in vitro* studies show an unequivocal correlation between *F. poae* and NIV production, such correlations are in the field less clear. Edwards et al. (2012) found only a weak correlation between *F. poae* DNA and NIV concentration, and the same has been found in Switzerland (dr. Susanne Vogelgsang, personal communication). DON concentration and *F. graminearum* DNA are usually well-correlated (Waalwijk et al., 2004; van der Fels-Klerx et al., 2012).

F. poae has additionally been implicated as a producer of enniatins (ENNs) and beauvericin (BEAU) (Thrane et al., 2004; Kulik and Jestoi, 2009), which are cyclic hexadepsipeptide mycotoxins that are produced by a range of *Fusarium* species (Jestoi, 2008). Finally, and most surprisingly, *F. poae* is also a type A trichothecene producer, which are more toxic to the plant than type B trichothecenes (Desjardins et al., 2007). This makes it, together with *F. equiseti* (Barros et al., 2012), the only species of which isolates are able to simultaneously produce type A and type B trichothecenes. Chapters 5 and 6 of this thesis go deeper into this finding. However, it is interesting to note that the type A trichothecenes which are produced by *F. poae in vitro* (DAS and NEO) are seldom detected in relation to this species in the field. Possibly, any production of DAS goes unnoticed as it may occur in the form of scirpentriol (SCR) or other closely related derivatives, which are rarely included in standard mycotoxin analysis methods (Schollenberger et al., 2007). Indeed, Schollenberger et al. (2011) noted a decrease of DAS followed by an increase in SCR after inoculation of autoclaved oats with *F. sporotrichioides* and *F. poae*. SCR is not often included in routine analytical methods.

Much is unknown about the epidemiology of *F. poae*. It is not regularly isolated from soil samples, and reports on its saprophytic character are sometimes contradictory. Pereyra and Dill-Macky (2008) mention that *F. poae* is a strong saprophyte under competition with other species. Landschoot et al. (2011) analyzed crop residues (maize and wheat residues) in November and found for two consecutive years that *F. poae* comprised 8 and 14% of isolated *Fusarium* species, making it the fifth and third most prominent species respectively. Fernandez et al. (2008) did not regularly detect *F. poae* from crop residues in Saskatchewan, Canada. Studies investigating the epidemiology of *F. langsethiae* have shown that by far its preferred infection route is through the cereal ear (Opoku et al., 2013). Root infection and inoculation of soil samples did not lead to notable infection (Divon et al., 2012).

From the above, it seems that soil and crop residues are not particularly important overwintering niches for *F. poae* and *F. langsethiae*, in contrast to *F. graminearum*. However, they may be able to grow on weeds and other less typical *Fusarium* hosts. Landschoot et al. (2011) remarked that in November, 38% of the *Fusarium* species on gramineous weeds was made up of *F. poae*. Remarkably, Jenkinson and Parry (1994) reached the exact same conclusion and were the first to suggest that weeds may be an important overwintering niche for *F. poae*. The broad host range of *F. poae* may be a significant asset in its epidemiology. It has been isolated as a pathogen from tomato (Stenglein et al., 2009), and from residues of sunflower (Pereyra and Dill-Macky, 2008). Interestingly, it has recently been identified as the dominant *Fusarium* species on *Miscanthus* in Ireland, which the authors consider as a possible reservoir for cereal pathogens (Glynn et al., 2015). Similar studies have not been carried out for *F. langsethiae* at the time of this writing, so pinpointing the favored overwintering niche for this pathogen is troublesome. However, we argue that its specific mode of infection (see above) makes a soil-based origin unlikely, and relocation of the pathogen to non-cereal hosts outside of the cereal growing season is a plausible hypothesis.

Regardless of whether the origins of their inocula are shared, the morphological outcome of *F. poae* and *F. langsethiae* infection is similar. *F. poae* infection does not lead to a clear FHB-phenotype (Vogelgsang et al., 2008b), and instead of traditional bleaching only small necrotic lesions can be detected (**Figure 2.6**). It is frequently isolated from asymptomatic ears (Hudec and Rohacik, 2003; Kulik and Jestoi, 2009). Its effect on yield parameters has been shown to be limited in published studies (Doohan et al., 1999; Vogelgsang et al., 2008b). Nevertheless, it has been reported that on barley in Argentina *F. poae* leads to clearly distinguishable spots on the leaf sheaths, glumes and grains (Barreto et al., 2004). Xu et al. (2008) found that while

F. poae was the most dominant species in four European countries on the level of incidence, its abundance (measured as fungal DNA) was the lowest of all species. The general lack of aggressiveness by *F. poae* supports the notion that it is a secondary invader of wheat ears. Correlations between the DNA of *F. poae* and other species of the FHB complex in several studies, particularly *F. graminearum* and *F. avenaceum*, are in agreement with this hypothesis (Xu et al., 2005; Audenaert et al., 2009).

In the case of *F. langsethiae*, two symptom types have been described, on the one hand distinct glume spots (Torp and Adler, 2004) and on the other hand subtle browning of panicle structures (Divon et al., 2012), see **Figure 2.6**. These reports are unanimous in their conclusion that *F. langsethiae* produces limited symptoms and does not result in reduction of grain yield. However, even asymptomatic grains can contain elevated levels of T-2 and HT-2 toxin (Opoku et al., 2013). *F. langsethiae* is responsible for the production of a series of type A trichothecenes. It is a potent producer of NEO, DAS, T-2 and HT-2, and close derivatives thereof such as T-2 triol and T-2 tetraol (Thrane et al., 2004). In oats, these were detected as a complex closely correlating with *F. langsethiae* incidence which is detailed in Chapter 3 of this thesis.

Figure 2.6 – Symptoms of *F. langsethiae*, *F. poae* and *F. graminearum* infection. **A** and **B**: *F. langsethiae* symptoms on respectively oat (Divon et al., 2012) and wheat (Torp and Adler, 2004). **C** and **D**: *F. poae* infected wheat ears, two different isolates (Vogelgsang et al., 2008b). **E**: *F. graminearum* infected wheat ear, own work.

As indicated above, we do not know whether trichothecenes produced by *F. poae* and *F. langsethiae* perform similar roles as they do in *F. graminearum*. However, the plant's response to this toxic metabolites may be similar, as glucosylated forms of NIV, FUS-X and all type A trichothecenes have been detected in recent years in a variety of matrices (Nakagawa et al., 2011; Nakagawa et al., 2013; De Boevre et al., 2014). This does not automatically subscribe a virulence related role to these mycotoxins, as plants likely conjugate a wide range of xenobiotics.

The epidemiology of *F. poae* and *F. langsethiae* seems very different from that of *F. graminearum*, and this does not explain their prominence in the FHB complex, as they are rather weak pathogens with limited aggressiveness to their host plant. Perhaps their toxic type A trichothecenes give these species a competitive advantage against other micro-organisms occupying the ear, but information on this subject is lacking. In the next section, several hypotheses are proposed to explain the prominence of *F. poae* and *F. langsethiae* in the disease complex.

2.7 Population shifts unraveled

Fisher et al. (2012) describe emerging infectious diseases as those pathogens that are increasing in their incidence, geographic or host range, and virulence. It remains to be seen whether *F. poae* and *F. langsethiae* can truly be designated emerging fungal diseases, as *F. poae* has been a commonly detected FHB pathogens for several decades (see section 2.3), and *F. langsethiae* was only very recently described for the first time and sampling and identification may have been troublesome before then. Nevertheless, their purported lack of aggressiveness and cryptic epidemiologies are remarkable in light of their high incidence. In this section, possible causal factors for the prominence of *F. poae* and the potential emergence of *F. langsethiae* are identified, that may be shared between the two organisms. In the following sections 1) their fungicide resistance patterns and the potential link with a more toxic chemotype and 2) how they might respond to a changing climate are considered.

Tolerance of triazoles and production of type A trichothecenes

We hypothesize that the widespread occurrence of *F. langsethiae* in several (European) countries may have followed the adoption of triazoles as the preferred fungicide against *Fusarium* during the eighties of last century (Morton and Staub, 2008). **Box 2.3** gives some background and history on the use of triazoles.

Box 2.3 – Triazoles as the preferred antifungal against *Fusarium* species

Information in this Box is largely adapted from Morton and Staub (2008). Triazoles are the largest class of fungicides used worldwide, and the most important disease management tool for *Fusarium* control. They were introduced in the 1970s and started to become widely used in the 1980s. Triazoles are broad spectrum antifungals, with functionality against *Fusarium* but also mildew and *Septoria*. They function by inhibiting demethylation during sterol biosynthesis in fungi at the target enzyme C-14 demethylase, a cytochrome P450 of the CYP51 family (see Figure in this Box). Their mode of action assigns them to the group of demethylation inhibitors (DMI). Ergosterol is a vital component of the fungal cell membrane. The efficacy of triazoles has been remarkably durable, as they are still the preferred fungicide against agronomically important fungi such as powdery mildew, rust and *Fusarium* after close to four decades. Nevertheless, several mechanisms have been described that confer resistance to fungi such as sequence mutations at the P450 target site, higher expression of the P450 gene, sequence alterations at the promotor of the P450 and additional copies of the P450 gene. A combination of these may lead to the erosion of efficacy of triazole compounds. The most popular triazoles are tebuconazole, epoxiconazole, propiconazole and prothioconazole. For the treatment against *Fusarium* triazoles are generally applied from halfway heading (GS55) to mid flowering/anthesis (GS65), expressed as growth stages on the Zadoks scale (Zadoks et al., 1974).

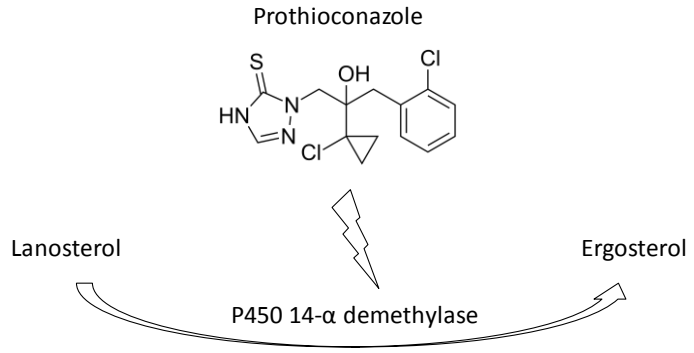

A finding in a Norwegian field study carried out by Bioforsk was that *F. langsethiae* is not consistently controlled by Proline (active ingredient prothioconazole). Unpublished data from the Norwegian field trials was kindly provided by dr. Ingerd Hofgaard (Bioforsk, Norway). Results are detailed in **Figure 2.7**. Kokkonen et al. (2014) found that tebuconazole, the most popular triazole on the market, had no effect on *F. langsethiae* in an oat based medium. **Figure 2.7** also shows that *F. poae* is not a major problem in oats in Norway, as it only rarely occurred in the control treatment, but in two instances its share increased after prothioconazole application, particularly when this was carried out at GS55 (Hedmark, Vestfold).

A similar result for *F. poae* was found in a large scale field study in Belgium (**Figure 2.8**). The results of these experiments are detailed in Audenaert et al. (2011). In a first experiment, *F. poae* appeared in the population after prothioconazole application at GS55. In a second experiment, *F. poae* was already present in the untreated control, at ~15% of total isolates

characterized to be *Fusarium*. The *F. poae* share in the population increased drastically upon triazole application at GS55. Apparently, a species displacement takes place whereby species such as *F. graminearum* and *F. culmorum* are controlled by the fungicide, and *F. poae* is not, or less so. While *F. poae* has been described as a prominent member of the FHB complex already in the eighties of last century (Haave, 1985; Clear and Patrick, 1993; Polley and Turner, 1995) and therefore its "emergence" does not necessarily correlate with the introduction of triazoles, the use of triazoles may be conducive to the perpetuation of this otherwise rather weak pathogen. Moreover, it was detected already as the predominant species in durum wheat seeds collected between 1937 and 1943 in Canada (Gordon, 2006).

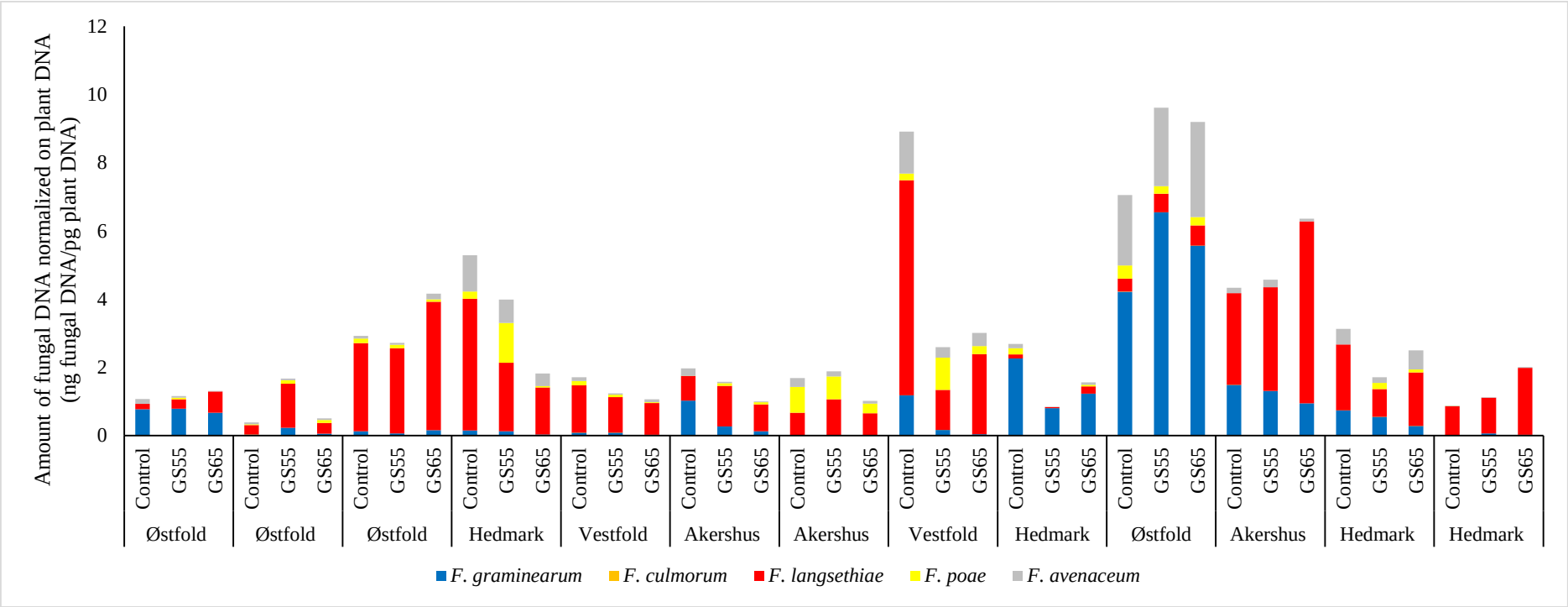

Figure 2.7 – Results of Norwegian field trials investigating fungicide efficacy on *Fusarium* species in oats, unpublished results kindly shared by dr. Ingerd Hofgaard (Bioforsk, Norway). Thirteen separate trials are shown (carried out from 2006 to 2008 over four locations). Proline (active ingredient: prothioconazole) was either not applied (control), or applied at GS55 or GS65. The major problem in oats, *F. langsethiae* (red) is in most cases not efficiently controlled by fungicide application.

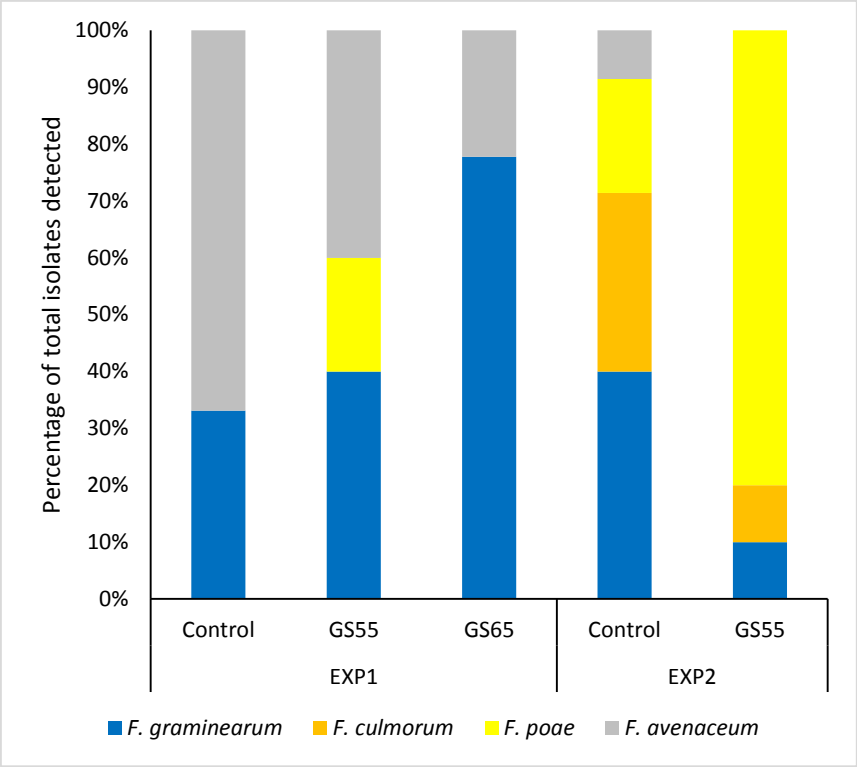

Figure 2.8 – Results of Belgian wheat field trials surveying the changes in the *Fusarium* population after prothioconazole application. Commercial wheat varieties and normal crop husbandry were used. In a first experiment (EXP1), prothioconazole was applied at GS55 or GS65 (results for one location and one year). No *F. poae* is present in the control treatment (no fungicide), but the species appears in the GS55 treatment. In a second experiment (EXP2), prothioconazole was applied at GS55 (combined results of two locations, Bottelare and Beitem, from 2008-2010). The share of *F. poae* increases dramatically after fungicide application. Source: Audenaert et al. (2011).

The results of these field studies do not necessarily agree with the results of laboratory tests. Indeed, *in vitro* studies have been published that confirm the efficacy of triazoles in the control of *F. langsethiae* and *F. poae* (Mullenborn et al., 2008; Mateo et al., 2013). However, in standard growth assays, it is unlikely that secondary metabolite production will mimic that of the field situation, where all the plant precursors and inducers are present. Where possible, *in vivo* studies in the field are strongly preferred. Conclusions from *in vitro* studies could therefore be hampered if secondary metabolite production plays a role in fungicide resistance. This conclusion was reached in the system *F. graminearum* – DON, in which a *Tri5* knockout mutant becomes completely susceptible to triazole application, even at low doses (Audenaert et al., 2010).

Information is currently lacking on why *F. poae* and *F. langsethiae* appear to deal with triazole application in the field setting better than other *Fusarium* species do. As mentioned in **Box 2.3**, the target of triazole antifungal compounds is sterol 14 alpha-demethylase, a vital enzyme in

ergosterol biosynthesis, encoded in fungi by the *CYP51* gene. In *Fusarium* species three classes of *CYP51* are present in the genome, one of which is mainly implicated as the target of triazoles (Fan et al., 2013). Mutations in the *CYP51* genes are known to confer resistance to triazoles in *Mycosphaerella graminicola* (Leroux et al., 2007) and *Blumeria graminis* (Wyand and Brown, 2005), however no such mutations have been reported for *F. graminearum*. Isolates that were adapted *in vitro* to tebuconazole did not show sequence alterations at any of the *CYP51* genes (Becher et al., 2010), and neither did resistant isolates from multiple field surveys (Yin et al., 2009; Talas and McDonald, 2015). Therefore, triazole resistance in *F. graminearum* likely depends on other mechanisms. No information is available on *CYP51* configuration for either *F. poae* and *F. langsethiae*.

Aside from at the CYP51 level (see **Box 2.3**), fungal resistance against triazoles and antifungal compounds in general is mediated by efficient efflux of these compounds from the intracellular space (Coleman and Mylonakis, 2009). According to Stergiopoulos et al. (2002), ABC transporters broadly are generally implicated in tolerance against xenobiotics as well as externally added mycotoxin (intermediates) (Seong et al., 2009; Abou Ammar et al., 2013), while MFS transporters are involved in efflux of fungal toxins or virulence factors (Menke et al., 2012). However, there are indications that this division is not absolute. In *F. graminearum,* several ABC transporters are under the direct control of TRI6, a transcription factor specifically regulating trichothecene production (Seong et al., 2009). Two ABC transporters of *M. graminicola* have been shown to simultaneously confer tolerance against exogenously added DAS and triazoles (Zwiers et al., 2003). As type A trichothecenes have been shown to be more acutely toxic than type B trichothecenes, at least to plants (Desjardins et al., 2007), it is possible that *F. poae* and *F. langsethiae* have evolved more efficient efflux systems for their mycotoxins, a system which in turn could be hijacked towards elevated triazole mediation. Significant substrate redundancy among transporters complicates research in this field, but nevertheless it should be investigated whether there is a link between a more toxic chemotype and elevated fungicide tolerance in these *Fusarium* species.

A changing climate

The worldwide effect of global warming on plant pathogens and pests was recently investigated (Bebber et al., 2013). It was determined that since the 1960s, fungi have generally migrated poleward. Two *Fusarium* species with sufficient observations and significant outcome were *F. sporotrichioides,* sister species to *F. langsethiae*, and *F. avenaceum* which have significantly moved polewards and in the direction of the equator, respectively. A high optimal growth

temperature was determined for *F. sporotrichioides* (Nazari et al., 2014). *In vitro* studies that designate optimal growth temperatures for fungal species based on vegetative growth experiments should be interpreted with caution however. These do not necessarily concur with the actual *in planta* optima, as was clearly illustrated for *F. langsethiae* (Divon et al., 2012).

Since reports exist that distinguish *F. poae* as one of the dominant FHB species since the mid-eighties of last century, it is rather unlikely that climate change has been responsible for an "emergence" of *F. poae*. It has however been described that the species prefers warm and dry conditions (Xu et al., 2008), which are the effects that global climate change is expected to have. We therefore suggest that *F. poae* predominance may even increase above its current levels in the coming decades. A general increase of FHB has been predicted as a result of wheat anthesis occurring earlier in the growing season with rising temperatures (Madgwick et al., 2011). The high minimum growth temperature of *F. poae* was previously seen as an explanation of low *F. poae* levels in Mid-Norway (Kosiak et al., 2003). In this study, *F. langsethiae* was well correlated with *F. poae*, raising the possibility that they share environmental preferences. Accordingly, Parikka et al. (2012) suggested that the prevalence of both *F. langsethiae* and *F. poae* may increase in the future.

2.8 Conclusions and perspectives

The importance of *F. poae* and *F. langsethiae* has been extensively illustrated from literature. Chapter 3 of this thesis details their incidence in the Belgian fields, and food and feed chain. *F. poae* and *F. langsethiae* produce a toxic chemotype that includes type A trichothecenes, which may be linked to their elevated resistance against triazoles in field trials. Chapters 5 and 6 go into detail on the chemotype of *F. poae* isolates. Finally, much is still unclear about the epidemiology and mode of reproduction of *F. poae* and *F. langsethiae.* Chapter 4 details the genome sequencing effort for *F. poae*, and we identified indications for a mixed reproduction system, together with dynamic genomic elements, that have previously been identified as significant threats to durable disease management. Taken together, this thesis aims to uncover potential keys to success for *F. poae*.

Chapter 3: *Fusarium* species and mycotoxins in Belgium: a one year case study

Vanheule, A, Audenaert, K, De Boevre, M, Landschoot, S, Bekaert, B, Munaut, F, Eeckhout, M, Hofte, M, De Saeger, S, Haesaert, G. (2014) The compositional mosaic of *Fusarium* species and their mycotoxins in unprocessed cereals, food and feed products in Belgium. International Journal of Food Microbiology, 181, 28-36.

3.1 Abstract

In Chapter 2, the importance of *F. poae* in agro-ecosystems was illustrated by a screening of literature. In this Chapter, we present a case study of *Fusarium* species incidence and mycotoxin contamination by analyzing field samples from a single harvest year, as well a series of food and feed samples collected throughout the cereal processing chain in Belgium. This provides a single snapshot of *Fusarium* species and mycotoxins in Belgium in 2012, without going deeper into the agronomic and environmental parameters that may influence FHB, and the agricultural background of most of the samples is unknown. Ultra performance liquid chromatograpy tandem mass spectrometry (UPLC-MS/MS) was applied to detect twelve different mycotoxins, and quantitative PCR (qPCR) was used to measure the presence of ten *Fusarium* species. We found that different cereal matrices have different characteristic contamination profiles, and correlation studies identified certain mycotoxins for future assessment (*e.g.* moniliformin (MON) produced by the *F. avenaceum*/*F. tricinctum* species group). The investigated harvest year of 2012 yielded non-processed field materials containing elevated levels of DON, while even in what is likely a so-called "DON-year" less prevalent toxins such as T-2 and HT-2 might be considered problematic due to their consistent co-occurrence with related type A mycotoxins. *F. graminearum* and *F. poae* were among the most important species in wheat, confirming earlier reports.

3.2 Introduction

In recent years, the scientific community has taken great steps towards a better understanding and surveillance of mycotoxin contamination of cereals and their derived feed and food products. Mycotoxins are produced by several toxigenic fungi, the most important of which are *Fusarium*, *Alternaria*, *Claviceps*, *Aspergillus* and *Penicillium* (Pitt, 2000). Historically, several notable instances of mycotoxin exposure in humans or animals exist, with widespread consequences. During World War II, Russian harvests heavily infected with the toxigenic species *Fusarium sporotrichioides* were contaminated with high levels of T-2 toxin, a trichothecene compound with notable toxicity (Li et al., 2011). Consumption of this harvest led to the death of thousands of people (Joffe, 1974). In 2012-2013, elevated levels of aflatoxin were detected in milk produced on several farms in the Netherlands. This particularly toxic compound is produced by *Aspergillus* species. Milk from cattle that are fed with contaminated feed lots may in turn be contaminated with aflatoxins. It was found that these maize lots were imported from South-East European countries where the harvest in the 2012-2013 season contained particularly high levels of aflatoxin. This sparked several international alerts and

significantly impacted production and import-export regulations across the continent (Verstraete, 2013). Even more recently, several lots of breakfast cereal had to be taken from shelves in Belgian supermarkets, as they were contaminated with DON (http://deredactie.be/permalink/1.2241974).

When contaminated lots are found, they can be re-orientated to a purpose where regulatory limits are lower and where the compounds exert less damage. **Table 3.1** shows which regulatory limits and guidance values are in place for *Fusarium* mycotoxins. T-2 and HT-2 toxins are not regulated at the moment, but "indicative values" have been set by the European Commission for a range of cereal commodities (European Commission, 2013). Repeated findings above this indicative level should spark investigation into causal factors. These indicative values are the Commission's response to a Scientific Opinion by the European Food Safety Authority (EFSA) on T-2 and HT-2 in 2011 (EFSA CONTAM Panel, 2011b). More Scientific Opinions are expected in the coming years, e.g. on DAS, DON and MON, and Member States of the European Union are encouraged to submit surveys of these mycotoxins to EFSA in official "call for data" requests.

Table 3.1 – Legislative values for *Fusarium* mycotoxins. These are maximum regulatory limits for deoxynivalenol, zearalenone and the sum of fumonisin B_1 and B_2 in foodstuffs, guidance values for deoxynivalenol, zearalenone and the sum of fumonisin B_1 and B_2 in feedstuffs, and indicative values for the sum of T-2 and HT-2, as detailed in Commission Regulation 1881/2006 (European Commission, 2006a), Commission Recommendation 2006/576/EC (European Commission, 2006b), and Commission Recommendation 2013/165/EU (European Commission, 2013) respectively.

Mycotoxin	Matrix	Value (µg/kg)
Deoxynivalenol	FOOD	
	Unprocessed cereals other than durum wheat, oats and maize	1250
	Unprocessed durum wheat and oats	1750
	Unprocessed maize, with the exception of unprocessed maize intended to be processed by wet milling	1750
	Cereals intended for direct human consumption, cereal flour, bran and germ as end product marketed for direct human consumption, with the exception of foodstuffs listed below	750
	Pasta (dry)	750
	Bread (including small bakery wares), pastries, biscuits, cereal snacks and breakfast cereals	500
	Processed cereal-based foods and baby foods for infants and young children	200
	FEED	
	Cereals and cereal products with the exception of maize by-products	8000
	Maize by-products	12000
	Complementary and complete feedingstuffs with exception of those below	5000
	Complementary and complete feedingstuffs for pigs	900
	Complementary and complete feedingstuffs for calves (<4 months), lambs and kids	2000
Zearalenone	FOOD	
	Unprocessed cereals other than maize	100
	Unprocessed maize with the exception of unprocessed maize intended to be processed by wet milling	350
	Cereals intended for direct human consumption, cereal flour, bran and germ as end product marketed for direct human consumption, with the exception of foodstuffs listed below	75
	Refined maize oil	400
	Bread (including small bakery wares), pastries, biscuits, cereal snacks and breakfast cereals, excluding maize-snacks and maize-based breakfast cereals	50

	Maize intended for direct human consumption, maize-based snacks and maize-based breakfast cereals	100
	Processed cereal-based foods (excluding processed maize-based foods) and baby foods for infants and young children	20
	Processed maize-based foods for infants and young children	20
	FEED	
	Cereals and cereal products with the exception of maize by-products	2000
	Maize by-products	3000
	Complementary and complete feedingstuffs for piglets and gilts (young sows)	100
	Complementary and complete feedingstuffs for sows and fattening pigs	250
	Complementary and complete feedingstuffs for calves, dairy cattle, sheep (including lamb) and goats (including kids)	500
T-2 + HT-2	UNPROCESSED CEREALS	
	Barley (including malting barley) and maize	200
	Oats (with husk)	1000
	Wheat, rye and other cereals	100
	CEREAL GRAINS FOR DIRECT HUMAN CONSUMPTION	
	Oats	200
	Maize	100
	Other cereals	50
	CEREAL PRODUCTS FOR HUMAN CONSUMPTION	
	Oat bran and flaked oats	200
	Cereal bran except oat bran, oat milling products other than oat bran and flaked oats, and maize milling products	100
	Other cereal milling products	50
	Breakfast cereals including formed cereal flakes	75
	Bread (including small bakery wares), pastries, biscuits, cereal snacks, pasta	25
	Cereal-based foods for infants and young children	15
	CEREAL PRODUCTS FOR FEED AND COMPOUND FEED	
	Oat milling products (husks)	2000
	Other cereal products	500
	Compound feed, with the exception of feed for cats	250
Fumonisin B_1 + B_2	FOOD	

Unprocessed maize	2000
Maize based foods for direct human consumption, excluding those listed below	1000
Maize flour, maize meal, maize grits, maize germ and refined maize oil	400
Processed maize-based foods and baby foods for infants and young children	200
FEED	
Feed materials: maize and maize products	60000
Complementary and complete feedingstuffs for pigs, horses (Equidae), rabbits and pet animals	5000
Complementary and complete feedingstuffs for fish	10000
Complementary and complete feedingstuffs for poultry, calves (< 4 months), lambs and kids	20000
Complementary and complete feedingstuffs for adult ruminants (> 4 months) and mink	50000

The year-to-year variability in mycotoxin contamination of small-grain cereals is large, and troublesome to interpret and predict (Landschoot et al., 2012). Logically, the population structure and disease pressure of the FHB complex play an important part (van der Fels-Klerx et al., 2012). Why *Fusarium* spp. should invest energy in the production of mycotoxins has not yet been fully elucidated, although in recent years progress has been made towards a central "oxidative stress theory" of mycotoxin biosynthesis, which states that within the conditions that are favourable for production of secondary metabolites in fungi, oxidative stress always plays a role (Reverberi et al., 2010). Indeed, studies have been published that assign an important role to DON in fusariosis of wheat (Maier et al., 2006; Audenaert et al., 2014) and the fungal response to oxidative stress (Audenaert et al., 2010).

Phytotoxicity of DON and other mycotoxins has been well established (Eudes et al., 2000; Desjardins et al., 2007), which explains why the plant has developed mechanisms to detoxify these toxins (Berthiller et al., 2013). Reports on new derivatives of previously well-described toxins have been regularly published in recent years (Gardiner et al., 2010b; Nakagawa et al., 2011), but the glucosylation of DON to DON-3-glucoside (DON-3G) is by far the best described mechanism of the "masked mycotoxin" formation. The conjugated forms of these toxins still end up in the food and feed chain however, and should not be underestimated as a potential health hazard (De Boevre et al., 2013). They are subject to potential hydrolysis after ingestion, and may thus result in an additional delivery of the toxic parent form (Berthiller et al., 2011).

The goal of this study was to get a snapshot of *Fusarium* species and mycotoxins incidence in Belgium, both on the field and in feed and food samples. Both UPLC-MS/MS and qPCR analyses were performed on 237 samples and the results were correlated in order to understand which *Fusarium* species were at the basis of the mycotoxins detected within these samples. However, it was not within the scope of the study to correlate this occurrence with agronomic or other environmental variables, and therefore only one harvest year and a limited set of food and feed products was considered.

3.3 Material and methods

3.3.1 Collection of small-grain cereals, food and feed samples

A total of 237 samples from different matrices were collected. Small-grain cereals were collected during the harvest of 2012 from fields in eight locations in Flanders, Belgium, in collaboration with the Agricultural Centre for Cereals. The locations and small-grain species

(wheat, barley, triticale) were selected based on their importance in cultivation in Flanders and are shown in **Figure 3.1**.

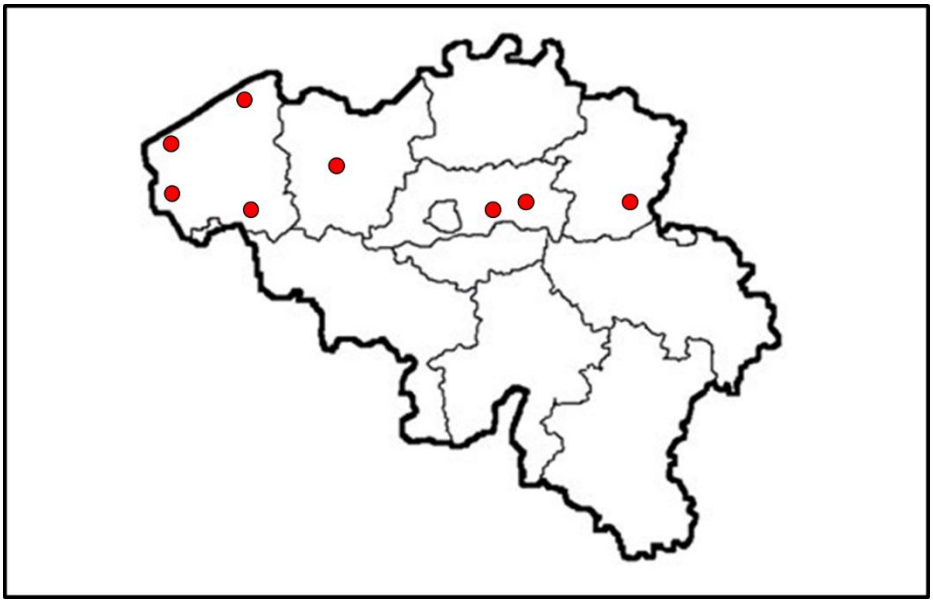

Figure 3.1 – Eight locations in Flanders where small-grain cereals were sampled from the field in the 2012 harvest year.

Feed samples were collected in November and December of 2012. Twenty-six samples were collected from several manufacturers in different geographic regions of Flanders. Ten samples consisted of processed oats, and 16 samples comprised diverse matrices, intended for pig (13) and poultry (3) feeding. The composition of these mixed feed samples reflects the investigated field materials: barley, wheat and triticale. The quantitative composition of the mixed feed samples is not known and was not considered for this study.

Forty-five cereal-derived food samples, consisting of 25 breads and 20 breakfast cereals, were collected from various retail markets during August – December 2012. Fiber contents of the food samples ranged from 2 % to 16 %. Cereal matrices present in the food samples included wheat, rye, oats, barley, soybean, corn, rice and buckwheat. The composition of the food samples (in qualitative terms) can be found in **Table S3.1**.

3.3.2 Processing of samples and LC-MS/MS procedure

An UPLC-MS/MS method was developed and validated in the framework of this study. The extraction protocol, parameters of the LC-MS/MS method and method validation can be found in the Appendix of this thesis. Due to a technical error, NIV levels could not be measured in this study.

Representative parts of each sample were obtained and ground to obtain a homogenous matrix. Small-grain cereals (wheat, barley, triticale) and feed samples were ground using a M20 grinder (Ika Werke, Staufen, Germany). Food samples were pulverized with a mortar after treatment with liquid nitrogen. After vigorous homogenization of the matrix, 2.5 g of each sample was weighed for extraction which was performed as described previously (De Boevre et al., 2012b).

3.3.3 DNA extraction and qPCR conditions

DNA was extracted from all 237 samples collected in the survey. DNA extraction was performed using the Invisorb Spin Plant mini kit (Invitek, Germany), as per the manufacturer's instructions.

qPCR primers for fungal and plant DNA based on elongation factor-1α (EF-1α) sequences were taken from literature and have been described as discriminating for ten FHB-causing *Fusarium* species most frequently encountered in Europe (Nicolaisen et al., 2009). The qPCR reactions were performed in a total reaction volume of 12.5 µl, consisting of 6.25 µl proprietary GoTaq qPCR Master Mix (Promega), 0.208 µl of CXR reference dye (Promega), 250 nM of each primer and 2.5 µl of DNA. Analysis was performed on an ABI 7000 Sequence Detection System with the following cycle settings: 50 °C during 2 min; 95 °C during 10 min; 40 cycles of 95 °C during 15 s and 63.5 °C during 1 min; followed by dissociation curve analysis from 65 °C to 95 °C. Results were analyzed with the Applied Biosystems' 7000 System SDS Software and Microsoft Excel 2010.

Fungal DNA for every species was normalized on the amount of amplified plant DNA. All primers were tested and confirmed for specificity among the 10 *Fusarium* species investigated in this study. This validation was performed with at least one Mycothèque Université catholique de Louvain (MUCL) reference isolate per species. For quantification of the plant DNA, a standard dilution series of plant DNA extracted of non-contaminated material was made and assigned concentrations after measurement with Nanodrop 1000.

3.3.4 Statistical analysis

For statistical evaluation, the R software package (version 2.15.3) was used (R Core Development Team, 2012). Since normality assumptions of parametric tests were not met, differences between groups of data were tested for significance using a non-parametric Kruskal-Wallis test with a Bonferroni correction for multiple comparisons at $\alpha = 0.05/n$ with n the number of pair-wise comparisons.

The relationship between the toxin contents, species presence and different food, feed and field samples was investigated using the Spearman correlation coefficient. These correlations are represented using a heat map with different colors corresponding to the strength of the correlation. Average linkage clustering using the Spearman distance was used to generate the heat map dendrograms. The Spearman correlations that the heat maps are based on can be found in **Table S3.2** to **Table S3.5**.

3.4 Results

3.4.1 Different categories have different characteristic contamination profiles

Figure 3.2 depicts a graphic presentation of the Spearman correlations between the amounts of DNA for all determined *Fusarium* species, mycotoxin levels, and the tested categories of field, feed and food samples.

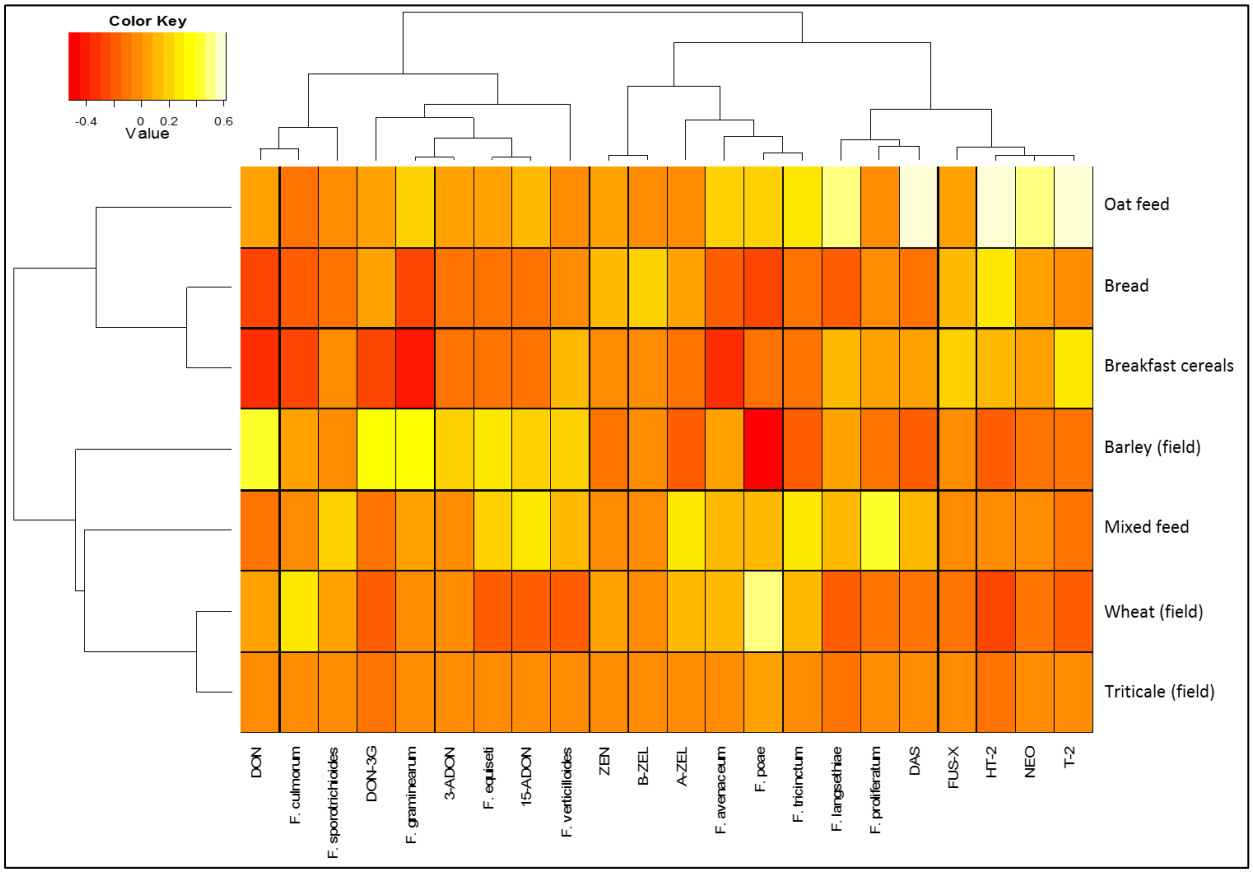

Figure 3.2 – Heat map based on the pairwise Spearman rank correlations between every class of sampled cereal matrix, and the different variables that were measured. A lighter color designates a higher correlation, as is shown in the color scale bar. The dendrogram, clustering the different classes of cereal matrices, was generated using average linkage clustering and the Spearman distance. The correlations at the basis of this heat map can be found in **Table S3.2**.

The heat map provides a general overview of contaminants characteristic for certain sample categories, but nevertheless the graph should be interpreted cautiously. A *Fusarium* species or mycotoxin can be designated as characteristic for certain sample categories, but this does not exclude it from being present in the others; it only implies that the contamination is present in the sample category *more* than expected in a random distribution of contamination levels in all 237 samples. This means that these designations are only valid when they are used in a comparative context, *e.g.* a *Fusarium* species or mycotoxin has a much higher qualitative and quantitative incidence in one category than in the other, rendering it a characteristic contaminant for the one category, but not the other. Finally, the dendrogram on the left-hand side of **Figure 3.2** clusters together those sample categories that have similar characteristic contamination profiles.

Oat feed and food samples have profiles that cluster together, with a marked presence in oat feed of NEO, DAS, T-2, HT-2 and *F. langsethiae*. The category of mixed feed samples and the categories of field samples demonstrate profiles that cluster together. For the field samples, DON, DON-3G and *F. graminearum* stand out in barley, and *F. culmorum* and *F. poae* stand out in wheat. *F. proliferatum* stands out in mixed feed. Triticale demonstrates no distinct mycotoxins or *Fusarium* species in this comparative framework.

Table 3.2 and **Table 3.3** detail the incidence of *Fusarium* species and mycotoxins for every sample category.

Table 3.2 - Results of the fungal biomass analysis on small-grain cereals, feed and food products. Values represented are the mean amount of fungal DNA present in the sample (pg fungal DNA / ng plant DNA), with the total number of positive samples between brackets. Mean values were calculated from positive samples only. In the header of the table, the number of tested samples for each sample type are reported. Within each separate *Fusarium* species, significant differences between the evaluated sample categories according to a post-hoc Kruskal-Wallis test are denoted with different letters. Only variables with more than one positive sample were included in the Kruskal-Wallis test.

	Wheat (field) (n = 93)		**Barley (field) (n = 65)**		**Triticale (field) (n = 10)**		**Oat feed (n = 10)**		**Feed (mixed) (n = 16)**		**Bread (n = 25)**		**Breakfast cereals (n = 20)**	
F. poae	0.61 ab	(81)	0.08 d	(8)	0.12 b	(9)	1.00 a	(10)	0.32 b	(13)	0.17 cd	(5)	0.67 c	(8)
F. langsethiae	0.56 c	(7)	0.10 bc	(13)	0.00	(0)	2.43 a	(10)	0.03 b	(7)	0.00	(0)	0.19 b	(6)
F. sporotrichioides	0.05 ab	(5)	0.31 ab	(3)	0.00	(0)	0.00	(0)	0.02 a	(3)	0.00	(0)	0.00	(0)
F. graminearum	1.53 c	(89)	1.52 ab	(65)	0.67 cd	(10)	4.27 a	(10)	1.20 bc	(16)	0.45 d	(21)	0.20 e	(9)
F. equiseti	0.03 b	(2)	0.03 a	(14)	0.00	(0)	0.05 a	(2)	0.04 a	(5)	0.00	(0)	0.00	(0)
F. culmorum	0.13 a	(66)	0.16 ab	(34)	0.06 abc	(6)	0.41 cd	(2)	0.05 abc	(11)	0.09 bcd	(6)	0.01 d	(2)
F. proliferatum	0.00	(0)	0.00	(0)	0.00	(0)	0.00	(0)	0.04 a	(4)	0.00	(0)	0.01	(1)
F. tricinctum	0.02 b	(36)	0.06 b	(11)	0.02 b	(2)	0.11 a	(9)	0.08 a	(11)	0.04 b	(3)	0.01 b	(4)
F. verticillioides	0.00	(0)	0.08 ab	(9)	0.00	(0)	0.00	(0)	0.01 a	(3)	0.13	(1)	7.32 ab	(3)
F. avenaceum	0.36 b	(88)	0.32 b	(58)	0.20 bc	(9)	1.23 a	(10)	1.16 ab	(16)	0.20 cd	(15)	0.11 d	(9)

Table 3.3 - Results of the multi-mycotoxin survey on small-grain cereals, feed and food products. Values represented are the mean concentration of mycotoxin present in the sample (µg / kg sample material), with the total number of positive samples between brackets. Mean values were calculated from positive samples only. In the header of the table, the number of tested samples for each sample type are reported. For each separate mycotoxin, significant differences between the evaluated sample categories according to a post-hoc Kruskal-Wallis test are denoted with different letters. Only variables with more than one positive sample were included in the Kruskal-Wallis test. NQ (not quantifiable) designates samples that were just below the decision limit, these were not included in the Kruskal-Wallis test. ND represents a non-detected compound.

	Wheat (field) (n = 93)		**Barley (field) (n = 65)**		**Triticale (field) (n = 10)**		**Oat feed (n = 10)**		**Feed (mixed) (n = 16)**		**Bread (n = 25)**		**Breakfast cereals (n = 20)**	
DON	1053 abc	(81)	2029 a	(64)	1145 bc	(8)	2385 ab	(6)	565 cd	(14)	316 de	(24)	1295 e	(5)
3-ADON	38 a	(4)	120 a	(8)	ND	(0)	135	(1)	75	(1)	ND	(0)	ND	(0)
15-ADON	87 c	(2)	97 bc	(10)	ND	(0)	49 ab	(2)	59 a	(6)	ND	(0)	ND	(0)
DON-3G	250 bc	(54)	390 a	(59)	169 cd	(6)	616 a	(7)	231 cd	(7)	490 ab	(15)	325 d	(5)
ZEN	33 a	(5)	18	(1)	ND	(0)	16	(1)	ND	(0)	22 a	(3)	ND	(0)
α-ZEL	39 b	(15)	ND	(0)	ND	(0)	136 b	(1)	62 a	(6)	64 b	(3)	ND	(0)
β-ZEL	104	(1)	ND	(0)	ND	(0)	ND	(0)	ND	(0)	19 a	(2)	ND	(0)
FUS-X	508	(1)	NQ	(1)	ND	(0)	NQ	(1)	ND	(0)	505 a	(2)	796 a	(3)
NEO	161	(1)	ND	(0)	ND	(0)	178	(5)	ND	(0)	NQ	(2)	NQ	(1)
DAS	87 b	(3)	ND	(0)	ND	(0)	32 a	(8)	NQ	(3)	ND	(0)	37 b	(2)
T-2	123	(1)	NQ	(2)	ND	(0)	77 a	(9)	ND	(0)	24 b	(2)	31 c	(7)
HT-2	70 c	(2)	NQ	(2)	ND	(0)	196 a	(10)	NQ	(2)	NQ	(12)	38 b	(6)

Some findings from **Figure 3.2** are nuanced in **Table 3.2** and **Table 3.3**. Indeed, *F. poae* is consistently an important species in wheat samples from the field. Quantitatively, oat feed samples do contain higher biomass concentration of this species, but it was not designated as particularly characteristic for this class, as from a comparative point of view the levels of *F. langsethiae*, DAS, T-2 and HT-2 are even higher. *F. proliferatum* is only marginally present in feed (four samples at low concentration), but since this is high in incidence and abundance in comparison to the other sample categories it stands out in **Figure 3.2**. This could be seen as an artefact of the heat map based approach and illustrates that caution should be exercised when interpreting these graphical representations.

A relatively high number of barley field samples contains *F. equiseti* and *F. verticillioides*, albeit in low concentration. Generally, and expectedly, low amounts of fungal DNA were detected in bread and breakfast cereal samples.

3.4.2 Different correlations are present within the different sample categories

Correlation studies were performed within every sample category. Again, caution should be exercised when interpreting these heat maps, as they inadvertently also include the correlations which are artefacts based on a very limited number of positive samples. **Figure 3.3** shows the results of the correlation study for the wheat and barley field samples.

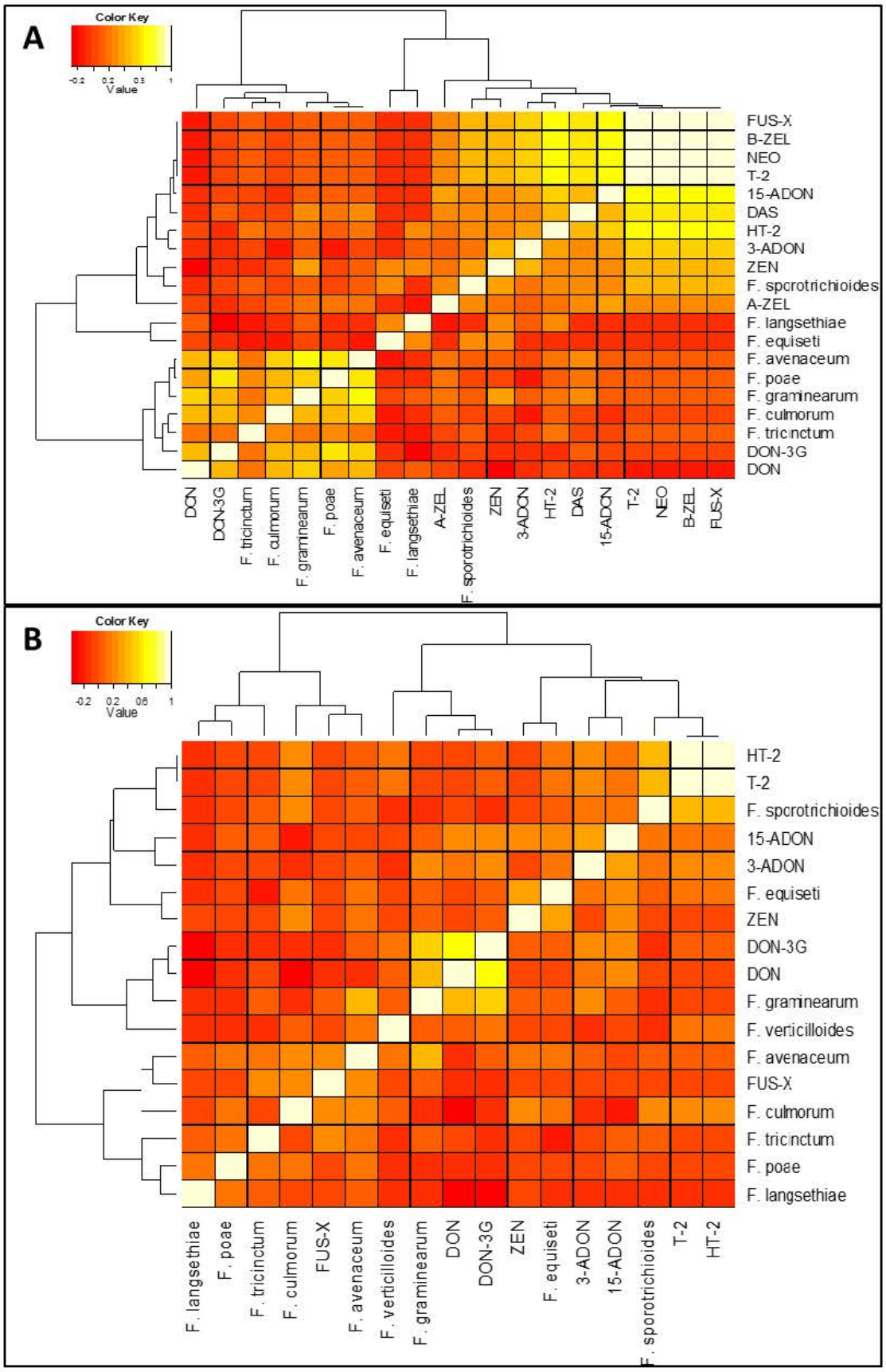

Figure 3.3 – Heat map based on the pairwise Spearman rank correlation coefficients between the measured toxin contents and *Fusarium* DNA from the different species in wheat field samples (**A**) and

barley field samples (**B**). A lighter color designates a higher correlation, as is shown in the color scale bar. Both (identical) dendrograms are generated using average linkage clustering with the Spearman distance. The correlations at the basis of these heat maps can be found in **Table S3.3** and **Table S3.4** respectively.

Some marked differences can be observed between the wheat and barley field samples. DON and DON-3G are better correlated in barley than in wheat, as **Table 3.3** already showed there are more samples with DON and no DON-3G in wheat. Aside from DON and DON-3G, all other correlations are generally weaker in barley than in wheat.

Some interesting inter-species correlations are present in the wheat samples. The weak pathogen *F. poae*, and *F. tricinctum* and *F. avenaceum*, which are closely related, are highly correlated with the aggressive species *F. graminearum* and *F. culmorum*. The inclusion of DON and its glucoside DON-3G in this cluster follows from the presence of *F. graminearum* as the main producer of DON. In wheat, but not in barley, *F. culmorum* is tightly linked with the DON – *F. graminearum* axis. Surprisingly, the acetylated forms of DON, 3-ADON and 15-ADON, are not well correlated with DON, *F. graminearum* and *F. culmorum*.

While correlations between *Fusarium* species and type A trichothecenes exist for these field samples, such as the cluster T-2, HT-2 and *F. sporotrichioides* in barley, these should be cautiously interpreted due to the very low number of positive samples and lack of quantification in the case of barley. Indeed, in one of the two T-2/HT-2 positive samples in barley, *F. sporotrichioides* but not *F. langsethiae* was detected. On the other hand, one of the two HT-2 positive samples in wheat also contained the highest load of *F. langsethiae* detected in the entire study, while the other contained *F. sporotrichioides*.

Twenty-five bread samples were fully analyzed, but performing a correlation study for this matrix was troublesome, as degradation of the DNA is likely to have occurred during processing. Indeed, **Figure 3.4** and **Table 3.2** illustrate that in bread, the lowest levels of fungal DNA were retrieved. **Figure 3.4** reveals a situation that is different for breakfast cereals than for the other analyzed matrices. *F. verticillioides* seems at first sight to be the most important species in this sample category, which is in fact a consequence of one hyper-contaminated sample of breakfast cereal. Due to the likely degradation of DNA in the food products, an intra-category correlation study is not useful for breads and breakfast cereals.

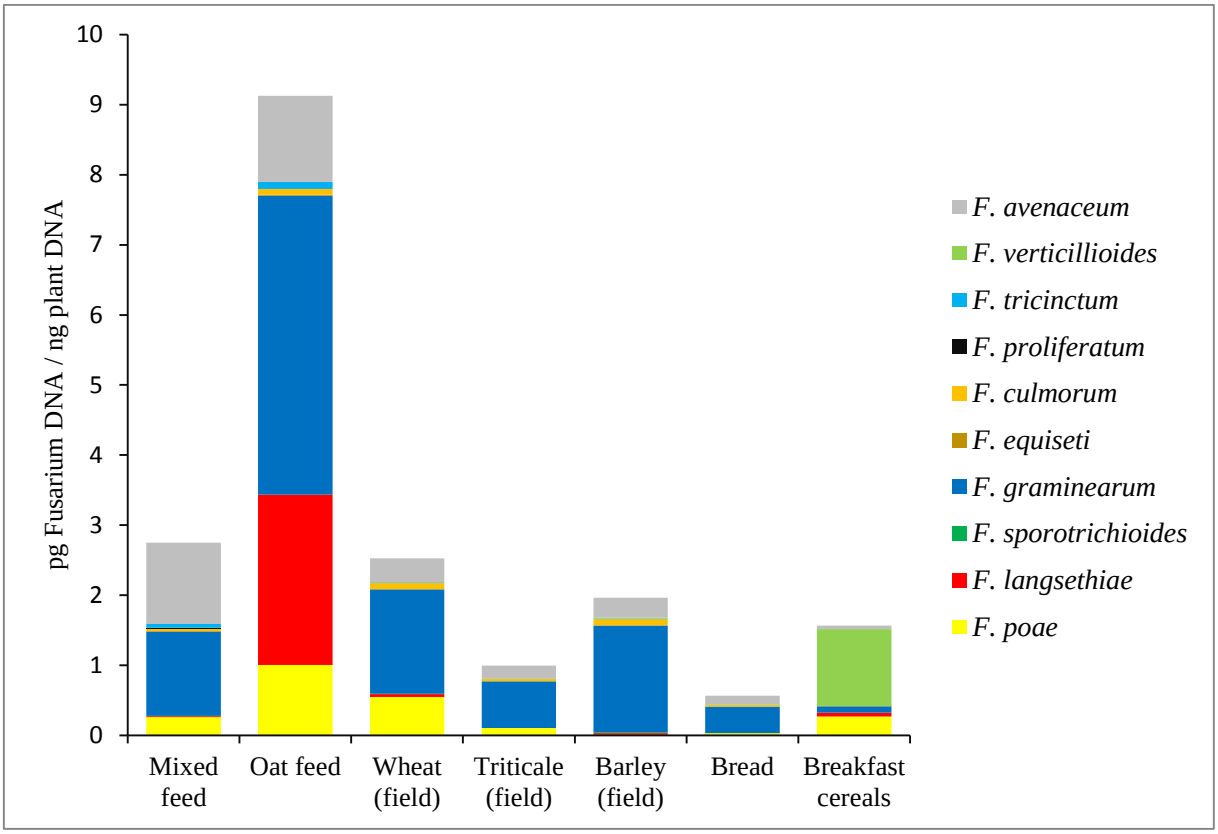

Figure 3.4 – Amount of fungal DNA (pg *Fusarium* DNA normalized on ng plant DNA) retrieved in every matrix for every species. Values depicted are the means of all samples for every matrix. A separate bar graph with standard errors can be found in **Figure S3.1**.

Finally, 26 feed samples were analyzed. Sixteen feed samples had a mixed origin and the contamination profile of this category clustered together with the profiles of the investigated field samples (**Figure 3.2**). The heat map for the mixed feed samples can be found in **Figure S3.2**. Certain correlations that were also present in the the wheat field samples are found in the mixed feed samples such as the clustering of *F. graminearum* and *F. avenaceum*. *F. poae*, *F. tricinctum* and *F. langsethiae* form a separate cluster, and *F. poae* is correlated with *F. culmorum*. One exceedance of guidance values was noted when only considering native DON levels, with two more feedstuffs containing more than 900 µg/kg for pig feed when all DON-equivalents (sum of DON, 3-ADON, 15-ADON and DON-3G) were taken into account (European Commission, 2006b).

Figure 3.5 shows the heat map calculated from the analyzed oat feed samples. From **Figure 3.2**, it is clear that the segment of "feed samples" is not uniform. Indeed, oat-based feed shows a radically different contamination profile than feed based on other small-grain cereals.

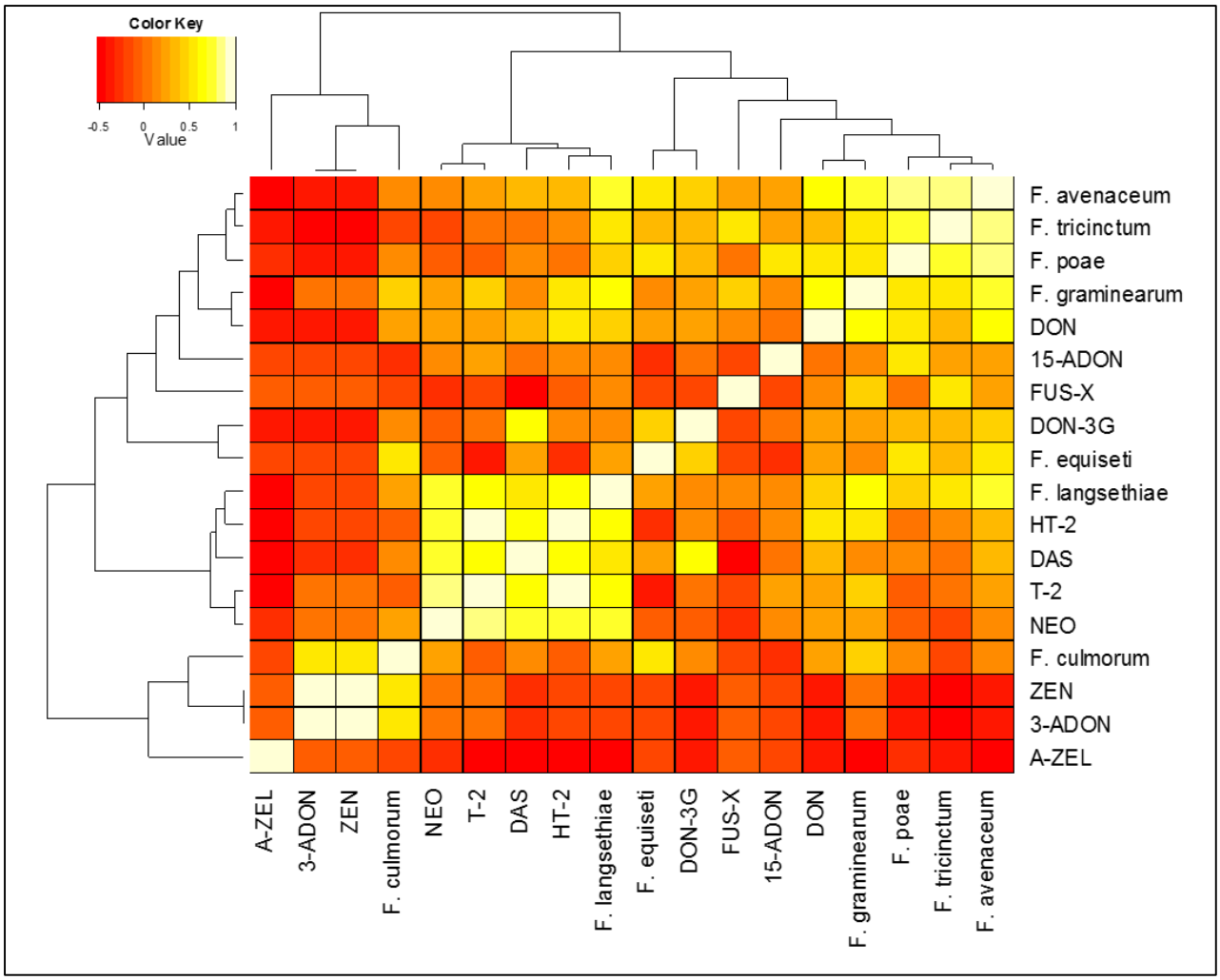

Figure 3.5 – Heat map based on the pairwise Spearman rank correlation coefficients between the measured toxin contents and *Fusarium* DNA from the different species in oat feed samples. A lighter color designates a higher correlation, as is shown in the color scale bar. Both (identical) dendrograms are generated using average linkage clustering with the Spearman distance. The correlations at the basis of this heat map can be found in **Table S3.5**.

The central cluster of *F. langsethiae* with the four type A trichothecenes, and the lack of *F. sporotrichioides* inclusion, depicts the former species as the main causal agent for these toxic compounds. It is obvious that indeed in oats, *F. langsethiae* is the undeniable causal agent of an entire complex of type A trichothecenes, contrary to the ambiguous situation in the field samples. It is noteworthy that levels of *Fusarium* infection are much higher in oats than in the other analyzed sample categories. This is not only the case for the expected *F. langsethiae*, but also for *F. graminearum*, *F. poae* and *F. avenaceum*, as can be seen in **Figure 3.4**. In oats, *F. culmorum* is correlated with ZEN and 3-ADON contamination, which was not the case in wheat and barley.

3.5 Discussion

In this study, a screening of common FHB related mycotoxins and *Fusarium* species was performed for non-processed field samples, feed samples, and food samples on the Belgian market. This results in a single snapshot of FHB related species and mycotoxins in Belgium. Throughout the following discussion it should therefore be kept in mind that the detected correlations between species and mycotoxins are valid for the considered one year case study, but these could be different in different growing seasons, as agronomic and environmental factors heavily influence FHB. Moreover, at several points a comparison is made between the contamination profiles of the field samples and the mixed feed samples (and the profiles of these classes cluster together as can be seen in **Figure 3.2**), it must be noted that the raw materials used for the considered feed samples likely do not have the same geographic origin as the considered field samples, and may even be from different harvest years.

The species that were encountered most in this study include *F. poae*, *F. graminearum*, *F. culmorum* and *F. avenaceum*. While Ioos et al. (2004) used a very different technique in a large-scale survey in France, these authors found very similar results. More recent investigations for France are lacking. In Luxemburg for 2007-2008 however, *F. poae*, *F. graminearum* and *F. avenaceum* were also the three most retrieved species (Giraud et al., 2010).

Previous correlation studies have often focused on the relation between the main causal agent of FHB, *F. graminearum*, and DON. Our results indicate a slightly stronger link in wheat than in barley ($r = 0.53$ and $r = 0.42$; respectively, correlations can be found in **Table S3.3** and **Table S3.4**). Interestingly, it has been described that DON is a virulence factor for *F. graminearum* infection in wheat, but not in barley (Maier et al., 2006). The relation between *F. culmorum* and DON is difficult to interpret. *F. culmorum* can exhibit two chemotypes, either it is a producer of NIV/FUS-X, or a producer of DON/3-ADON (Quarta et al., 2005). In 2009, 88-95% (over two sampling years) of *F. culmorum* isolates in Belgium was of the NIV chemotype (Audenaert et al., 2009). Recent efforts within the EU FP7 project MycoRed indicate that the 3-DON chemotype of *F. culmorum* may have become more important in recent years (Pasquali et al., submitted), which may explain the tight inclusion of *F. culmorum* in the DON – *F. graminearum* cluster in wheat. Unfortunately, 3-ADON could at the same time not be linked to *F. culmorum*, but it is notable that *F. culmorum* was present in much lower levels than *F. graminearum* in all matrices.

In barley, *F. graminearum* seems to be the sole causal agent of DON (**Figure 3.3**), up to levels 2-fold higher than is the case in wheat (**Table 3.3**). This finding is surprising, since a five-year study in the United Kingdom indicated that levels of DON in wheat exceeded those in barley by far (Edwards, 2009c, a).

Taking into account that field samples collected in this survey were all destined for the production of animal feed, only one barley sample exceeded the EU guidance value of 8000 µg/kg (cereals and cereal products with the expection of maize by-products, see **Table 3.1**). Nevertheless, chronic exposure to even low levels of mycotoxins could lead to economic damage by decreasing animal productivity (Bryden, 2012). The situation for the food products is slightly more worrisome, as only three breads exceeded the limit of 500 µg/kg when only considering DON, but when taking into account the sum of DON-equivalents (the sum of DON, 3-ADON, 15-ADON and DON-3G) 15 breads contained more than 500 µg/kg. Finally, one oat-based breakfast cereal was encountered with a DON content of over 5000 µg/kg, an alarming exceedance of the EU maximum 500 µg/kg limit (**Table 3.1**).

The acetylated forms of DON are usually co-occurring with DON as a certain low percentage of the total DON load, which is confirmed in this study. A dominance of 15-ADON over 3-ADON could be noted in the feed samples, but was only poorly reflected in the constituting compounds barley and wheat.

ZEN was not a major contaminant in any of the tested products, which does not concur with previous studies (De Boevre et al., 2012a). The high variability of ZEN contamination related to weather variables has however been described (Edwards, 2011). Interestingly, ZEN was well correlated with *F. graminearum* in wheat, while the one barley sample that was contaminated with ZEN, had a high *F. culmorum* load. Its derivatives α-ZEL and β-ZEL were sporadically detected, with α-ZEL detected more often and in larger amounts, confirming previous findings (De Boevre et al., 2012a). ZEN values did not exceed regulatory limits throughout the entire study. If the sum of ZEN and its derivatives is taken into account, the concentrations are higher than the maximum regulatory limit (100 µg/kg) in one unprocessed cereals sample, and higher than the limit (50 µg/kg) for three breads.

F. avenaceum is a frequently detected species in this study and in neighboring countries in Western Europe. It has been described as a slow grower and was closely correlated with the presence of *F. graminearum* ($r = 0.72$ in wheat, $r = 0.43$ in barley; correlations in **Table S3.3** and **Table S3.4**) (Yli-Mattila, 2010). In both cereal species, it clustered together with the closely

related species *F. tricinctum*. The high prominence of these moniliformin and enniatin producers dictates that future surveys should include these compounds in multi-mycotoxin methods.

In this study, only one year of harvest was analyzed for its mycotoxin contamination. It has been shown that DON and T-2/HT-2 show signs of mutual exclusion *in planta*, indicating the different climatic conditions that each *Fusarium* species favors (Edwards, 2009c, b, a). The very low levels of T-2/HT-2 in the field samples, along with the elevated DON-levels, allow us to classify the growing season of 2012 as favoring DON-producing species. Inter-genus competition between toxigenic fungi on the other hand is less well described. Müller and Korn (2013) hypothesized that depending on the year's specific weather conditions, *Alternaria* and *Fusarium* may be in competition *in planta* leading to only one genus' specific mycotoxins, or both species may co-exist and a wide range of mycotoxins originating from both species may be detected. The latter was confirmed in an extensive screening by Streit et al. (2013).

DON glucosylation to DON-3G is a well-described part of the plant's defense (Berthiller et al., 2013). In barley field samples, DON and DON-3G were better correlated than in wheat (r = 0.57 and r = 0.45; respectively; correlations in **Table S3.3** and **Table S3.4**). Possibly, this indicates the larger presence of other DON-detoxifying mechanisms in wheat.

Data on the presence of DON-3G in neighboring countries is still rather lacking. Berthiller et al. (2009) investigated the situation for wheat from Germany, Austria and Slovakia in 2005, and found mean DON and DON-3G levels of respectively 1500 µg/kg and 393 µg/kg; absolute values that are about 50% higher than those found for wheat in this study. On the other hand, Streit et al. (2013) found lower values in a large study of mixed origin samples. Vendl et al. (2010) screened a large set of food products for DON, ZEN and their conjugates, and found markedly lower mycotoxin levels than were detected in the current study. A large inter-year variability in these surveys should be pointed out, as in a 2010-2011 survey on cereal-based food products in Belgium (De Boevre et al., 2012a) mycotoxin levels that are lower than those in this 2012 study and more similar to those by Vendl et al. (2010) were reported. It is notable that all the studies listed in this paragraph mention molar ratios of DON-3G/DON of about 15%, a mean value which we also recorded for all unprocessed cereal product classes.

The occurrence of T-2 and HT-2 is usually caused by *F. langsethiae* and *F. sporotrichioides*, species with a highly similar chemotype, but different morphology and epidemiology (Thrane et al., 2004; Edwards et al., 2012). Due to the low number of T-2/HT-2 positive wheat and

barley field samples, the identification of the causal agent in those classes is troublesome. *F. langsethiae* was not a very important pathogen of wheat and barley, but nevertheless is detected in 7 respectively 13 samples. More recently other researchers also detected *F. langsethiae* from wheat in Belgium (Dedeurwaerder et al., 2014).

In oats, *F. langsethiae* was the causal agent for the presence of not only T-2 and HT-2, but an entire type A trichothecene complex, which has also been firmly established in the United Kingdom (Edwards et al., 2012). Clearly, when faced with a T-2 or HT-2 contamination in this matrix, it is likely that NEO and DAS will co-occur, possibly leading to as yet unknown additive or synergistic effects. For example, additive adverse effects of T-2 and DAS in poultry have been reported (Grenier and Oswald, 2011). It would therefore be prudent to no longer ignore these highly toxic metabolites in legislation and surveillance, however the increasing awareness in this matter is evidenced by the recent European Commission recommendations on T-2/HT-2 indicative values (European Commission, 2013), and the upcoming EFSA Scientific Opinion on DAS.

This study showed that in the single harvest year that was investigated, *F. poae* was an important part of the FHB complex on wheat. In wheat, it was detected in 87% of samples and overall stands as the second most abundant species in the wheat ear, after *F. graminearum*. Its occurrence in barley stands in marked contrast to wheat. It has been determined in infection trials that wheat cultivars are generally more susceptible to *F. poae* than barley (Stenglein et al., 2014). Still, *F. poae* has been found as one of the predominant FHB on barley in other countries such as Slovakia and the UK (Hudec and Rohacik, 2009; Nielsen et al., 2014), so the lack of *F. poae* in barley in this study is surprising.

3.6 Supporting information

Table S3.1 – Qualitative composition of the bread and breakfast cereals as indicated on the labels.

ID	Foodstuff	Wheat	Rye	Oat	Barley	Rice	Maize	Soy	Buckwheat
1	Bread	x	x						
2	Bread	x	x	x					
3	Bread	x							
4	Bread	x	x		x				
5	Bread	x							x
6	Bread	x			x				
7	Bread	x							
8	Bread	x	x						
9	Bread	x	x					x	
10	Bread	x	x						
11	Bread	x							
12	Bread	x	x					x	
13	Bread	x	x						
14	Bread	x		x					
15	Bread	x							
16	Bread	x	x						
17	Bread	x	x						
18	Bread	x	x						
19	Bread	x	x	x					
20	Bread	x							
21	Bread	x			x				
22	Bread	x							
23	Bread	x							
24	Bread	x		x	x				
25	Bread	x			x				
1	Breakfast cereal	x			x	x			
2	Breakfast cereal	x							
3	Breakfast cereal	x			x				
4	Breakfast cereal	x			x				
5	Breakfast cereal	x			x				
6	Breakfast cereal	x			x	x			
7	Breakfast cereal	x			x				
8	Breakfast cereal			x					
9	Breakfast cereal			x					
10	Breakfast cereal	x		x	x				
11	Breakfast cereal				x		x		
12	Breakfast cereal	x		x	x				
13	Breakfast cereal	x		x	x		x		
14	Breakfast cereal	x							
15	Breakfast cereal	x			x				
16	Breakfast cereal	x		x					
17	Breakfast cereal	x				x	x		

18	Breakfast cereal	x			x
19	Breakfast cereal		x		x
20	Breakfast cereal	x	x		

Table S3.2 - Table depicting the pairwise Spearman rank correlations between every class of sampled cereal matrix, and the different variables that were measured. Correlations with a value higher than |0.25| are significant at α=0.05. Some correlations may be artefacts due to low numbers of positive samples, and the relevant correlations are discussed in the text.

	Barley (field) n = 65	**Wheat (field) n = 93**	**Triticale (field) n = 10**	**Mixed feed n = 16**	**Oat feed n = 10**	**Bread n = 25**	**Breakfast cereals n = 20**
F. poae	-0.53	0.54	0.06	0.1	0.23	-0.25	-0.12
F. langsethiae	0.02	-0.21	-0.1	0.15	0.48	-0.16	0.09
F. sporotrichioides	0	0.03	-0.05	0.17	-0.05	-0.08	-0.07
F. graminearum	0.35	-0.03	-0.03	0.04	0.17	-0.23	-0.4
F. equiseti	0.25	-0.2	-0.07	0.19	0.08	-0.11	-0.1
F. culmorum	0.05	0.27	0	0	-0.12	-0.18	-0.27
F. proliferatum	-0.09	-0.12	-0.03	0.43	-0.03	-0.05	0.06
F. tricinctum	-0.18	0.09	-0.05	0.24	0.29	-0.13	-0.1
F. verticillioides	0.17	-0.21	-0.06	0.12	-0.06	-0.04	0.1
F. avenaceum	0.04	0.14	-0.01	0.14	0.17	-0.21	-0.32
DON	0.39	0.07	-0.01	-0.12	0.03	-0.27	-0.36
3-ADON	0.17	-0.06	-0.05	0	0.04	-0.09	-0.08
15-ADON	0.16	-0.18	-0.06	0.28	0.09	-0.1	-0.09
DON-3G	0.37	-0.17	-0.09	-0.12	0.08	0.06	-0.25
ZEN	-0.08	0.05	-0.04	-0.06	0.06	0.14	-0.06
A-ZEL	-0.21	0.14	-0.07	0.24	0	0.02	-0.1
B-ZEL	-0.07	-0.01	-0.02	-0.03	-0.02	0.21	-0.03
FUS-X	-0.06	-0.1	-0.04	-0.05	0.07	0.09	0.2
NEO	-0.12	-0.11	-0.04	-0.05	0.51	0.07	0.02
DAS	-0.17	-0.11	-0.06	0.13	0.61	-0.09	0.04
T-2	-0.13	-0.21	-0.07	-0.08	0.62	-0.02	0.28
HT-2	-0.2	-0.27	-0.09	-0.02	0.57	0.3	0.14

Table S3.3 - Table depicting the pairwise Spearman rank correlation coefficients between the measured toxin contents and *Fusarium* DNA from the different species in **wheat field samples** (n = 93). Correlations with a value higher than |0.18| are significant at α=0.05. *F. lang* = *F. langsethiae*; *F. spor* = *F. sporotrichioides*; *F. gram* = *F. graminearum*; *F. equi* = *F. equiseti*; *F. culm* = *F. culmorum*; *F. tric* = *F. tricinctum*; *F. avena* = *F. avenaceum*. 3-AD = 3-ADON; 15-AD = 15-ADON. Some correlations may be artefacts due to low numbers of positive samples, and the relevant correlations are discussed in the text.

	F. poae	*F. lang*	*F. spor*	*F. gram*	*F. equi*	*F. culm*	*F. tric*	*F. avena*	DON	3-AD	15-AD	DON-3G	ZEN	A-ZEL	B-ZEL	FUS-X	NEO	DAS	T-2	HT-2
F. poae	1.00	-0.06	0.05	0.54	-0.02	0.47	0.24	0.65	0.36	-0.15	0.07	0.63	0.05	0.20	0.08	0.08	0.08	0.23	0.08	0.09
F. lang		1.00	-0.07	0.12	0.25	-0.07	-0.12	-0.04	0.08	0.13	-0.04	-0.27	0.28	-0.13	-0.03	-0.03	-0.03	-0.05	-0.03	0.25
F. spor			1.00	0.14	0.27	0.04	0.07	0.07	-0.08	0.20	0.30	0.05	0.39	0.29	0.45	0.45	0.45	0.24	0.45	0.30
F. gram				1.00	0.06	0.44	0.23	0.72	0.53	0.08	0.14	0.46	0.33	0.16	0.15	0.15	0.15	0.28	0.15	0.22
F. equi					1.00	-0.15	-0.12	-0.17	-0.01	-0.03	-0.02	-0.09	0.29	-0.07	-0.02	-0.02	-0.02	-0.03	-0.02	-0.02
F. culm						1.00	0.24	0.52	0.45	-0.11	-0.05	0.46	0.03	0.07	0.06	0.06	0.06	0.05	0.06	0.15
F. tric							1.00	0.23	0.17	0.06	0.00	0.20	-0.04	0.03	0.08	0.08	0.08	0.06	0.08	0.17
F. avena								1.00	0.49	-0.01	0.15	0.54	0.11	0.18	0.13	0.13	0.13	0.26	0.13	0.16
DON									1.00	-0.07	-0.06	0.48	-0.19	0.01	-0.13	-0.13	-0.13	-0.03	-0.13	0.00
3-AD										1.00	0.35	-0.09	0.42	0.08	0.51	0.51	0.51	0.28	0.51	0.35
15-AD											1.00	-0.01	0.31	0.37	0.71	0.71	0.71	0.41	0.71	0.50
DON-3G												1.00	-0.10	-0.02	0.00	0.00	0.00	0.11	0.00	-0.08
ZEN													1.00	0.17	0.46	0.46	0.46	0.24	0.46	0.31
A-ZEL														1.00	0.28	0.28	0.28	0.26	0.28	0.17
B-ZEL															1.00	1.00	1.00	0.58	1.00	0.71
FUS-X																1.00	1.00	0.58	1.00	0.71
NEO																	1.00	0.58	1.00	0.71
DAS																		1.00	0.58	0.41
T-2																			1.00	0.71
HT-2																				1.00

Table S3.4 - Table depicting the pairwise Spearman rank correlation coefficients between the measured toxin contents and *Fusarium* DNA from the different species in **barley field samples** (n = 65). Correlations with a value higher than |0.21| are significant at α=0.05. *F. lang* = *F. langsethiae*; *F. spor* = *F. sporotrichioides*; *F. gram* = *F. graminearum*; *F. equi* = *F. equiseti*; *F. culm* = *F. culmorum*; *F. tric* = *F. tricinctum*; *F. verti* = *F. verticillioides*; *F. avena* = *F. avenaceum*. 3-AD = 3-ADON; 15-AD = 15-ADON. Some correlations may be artefacts due to low numbers of positive samples, and the relevant correlations are discussed in the text.

	F. poae	*F. lang*	*F. spor*	*F. gram*	*F. equi*	*F. culm*	*F. tric*	*F. verti*	*F. avena*	DON	3-AD	15-AD	DON-3G	ZEN	FUS-X	T-2	HT-2
F. poae	1.00	0.16	-0.08	-0.14	-0.03	0.15	0.18	-0.15	0.17	-0.14	0.00	0.08	-0.09	-0.05	-0.05	-0.07	-0.07
F. lang		1.00	-0.11	-0.13	-0.11	0.00	0.07	-0.10	0.02	-0.28	-0.09	-0.12	-0.36	-0.06	-0.06	-0.09	-0.09
F. spor			1.00	-0.10	0.06	0.24	0.07	-0.09	0.06	-0.08	0.14	0.11	-0.12	-0.03	-0.03	0.39	0.41
F. gram				1.00	0.05	-0.11	0.06	0.06	0.43	0.42	0.23	0.03	0.49	0.03	0.01	-0.08	-0.08
F. equi					1.00	0.11	-0.23	-0.02	0.15	-0.08	0.12	0.25	0.02	0.28	-0.06	0.11	0.12
F. culm						1.00	-0.05	0.03	0.26	-0.30	-0.12	-0.21	-0.17	0.22	0.20	0.25	0.25
F. tric							1.00	-0.09	0.13	-0.05	-0.05	0.03	-0.13	-0.06	0.27	-0.08	-0.08
F. verti								1.00	0.12	0.01	-0.15	-0.02	0.10	-0.05	-0.05	0.18	0.17
F. avena									1.00	-0.11	0.06	-0.02	0.03	0.13	0.21	0.06	0.06
DON										1.00	0.18	0.26	0.67	-0.08	-0.10	-0.02	-0.02
3-AD											1.00	0.36	0.20	-0.05	-0.05	0.20	0.20
15-AD												1.00	0.21	0.25	-0.05	0.16	0.16
DON-3G													1.00	0.08	-0.17	0.07	0.07
ZEN														1.00	-0.02	-0.02	-0.02
FUS-X															1.00	-0.02	-0.02
T-2																1.00	1.00
HT-2																	1.00

Table S3.5 - Table depicting the pairwise Spearman rank correlation coefficients between the measured toxin contents and *Fusarium* DNA from the different species in **oat feed samples** (n = 10). Correlations with a value higher than |0.68| are significant at α=0.05. *F. lang* = *F. langsethiae*; *F. gram* = *F. graminearum*; *F. equi* = *F. equiseti*; *F. culm* = *F. culmorum*; *F. tric* = *F. tricinctum*; *F. avena* = *F. avenaceum*. 3-AD = 3-ADON; 15-AD = 15-ADON. Some correlations may be artefacts due to low numbers of positive samples, and the relevant correlations are discussed in the text.

	F. poae	*F. lang*	*F. gram*	*F. equi*	*F. culm*	*F. tric*	*F. avena*	DON	3-AD	15-AD	DON-3G	ZEN	A-ZEL	FUS-X	NEO	DAS	T-2	HT-2
F. poae	1.00	0.42	0.52	0.54	0.16	0.71	0.82	0.51	-0.41	0.53	0.39	-0.41	-0.29	0.06	-0.06	0.11	-0.10	0.05
F. lang		1.00	0.64	0.29	0.22	0.52	0.75	0.43	-0.17	0.16	0.17	-0.17	-0.52	0.17	0.73	0.58	0.63	0.67
F. gram			1.00	0.16	0.47	0.52	0.73	0.69	0.06	0.12	0.25	0.06	-0.52	0.41	0.24	0.18	0.41	0.52
F. equi				1.00	0.50	0.34	0.54	0.20	-0.17	-0.25	0.47	-0.17	-0.17	-0.17	-0.06	0.29	-0.37	-0.22
F. culm					1.00	-0.21	0.16	0.20	0.58	-0.25	0.16	0.58	-0.17	-0.17	0.19	0.14	-0.06	-0.07
F. tric						1.00	0.87	0.31	-0.52	0.29	0.39	-0.52	-0.41	0.52	-0.15	0.05	0.05	0.16
F. avena							1.00	0.60	-0.41	0.22	0.44	-0.41	-0.52	0.29	0.16	0.33	0.22	0.39
DON								1.00	-0.36	-0.01	0.28	-0.36	-0.36	0.18	0.21	0.32	0.27	0.56
3-AD									1.00	-0.17	-0.41	1.00	-0.11	-0.11	0.06	-0.29	0.06	-0.17
15-AD										1.00	0.07	-0.17	-0.17	-0.17	0.15	0.03	0.23	0.14
DON-3G											1.00	-0.41	-0.41	-0.18	-0.03	0.61	0.04	0.15
ZEN												1.00	-0.11	-0.11	0.06	-0.29	0.06	-0.17
A-ZEL													1.00	-0.11	-0.31	-0.47	-0.52	-0.52
FUS-X														1.00	-0.31	-0.47	-0.12	-0.06
NEO															1.00	0.72	0.80	0.74
DAS																1.00	0.61	0.67
T-2																	1.00	0.94
HT-2																		1.00

Table S3.6 - Table depicting the pairwise Spearman rank correlation coefficients between the measured toxin contents and *Fusarium* DNA from the different species in **mixed feed samples** (n = 16). Correlations with a value higher than |0.43| are significant at α=0.05. *F. lang* = *F. langsethiae*; *F. spor* = *F. sporotrichioides*; *F. gram* = *F. graminearum*; *F. equi* = *F. equiseti*; *F. culm* = *F. culmorum*; *F. culm* = *F. culmorum*; *F. tric* = *F. tricinctum*; *F. verti* = *F. verticillioides*; *F. avena* = *F. avenaceum*. 3-AD = 3-ADON; 15-AD = 15-ADON. Some correlations may be artefacts due to low numbers of positive samples, and the relevant correlations are discussed in the text.

	F. poae	*F. lang*	*F. spor*	*F. gram*	*F. equi*	*F. culm*	*F. prol*	*F. tric*	*F. verti*	*F. avena*	DON	3-AD	15-AD	DON-3G	A-ZEL	DAS	HT-2
F. poae	1	0.58	0.1	-0.13	0.26	0.52	0.27	0.4	-0.07	-0.24	-0.12	-0.14	-0.24	0.07	0.06	0.17	0.03
F. lang		1	0.13	-0.15	0.07	0.06	0.1	0.59	-0.4	-0.18	-0.28	-0.22	-0.52	-0.06	-0.14	-0.1	0.02
F. spor			1	-0.31	0.24	0.07	0.07	-0.25	0.08	-0.53	-0.11	-0.12	0.01	-0.1	-0.36	0.17	-0.18
F. gram				1	0.19	0.44	-0.22	0.34	-0.26	0.77	0.69	-0.25	0.14	0.23	0.11	-0.14	-0.21
F. equi					1	0.37	0.22	-0.23	-0.09	0.19	0.03	-0.17	0.08	0.2	-0.49	-0.03	-0.25
F. culm						1	0.39	0.16	0.21	0.13	0.36	0.03	-0.12	0.14	-0.02	0.31	0.12
F. prol							1	-0.1	0.55	-0.29	-0.12	0.55	0.29	-0.07	-0.12	0.46	0.65
F. tric								1	-0.37	0.08	-0.04	-0.31	-0.2	-0.16	0.41	-0.11	-0.15
F. verti									1	-0.38	0.07	0.62	0.34	0.03	-0.06	0.53	0.39
F. avena										1	0.45	-0.2	-0.03	0.24	-0.07	-0.29	-0.13
DON											1	-0.08	0.32	0.44	0.16	0.25	0.07
3-AD												1	0.29	0.4	-0.19	-0.12	0.73
15-AD													1	0.24	0.04	0.11	0.09
DON-3G														1	-0.37	-0.4	0.16
A-ZEL															1	0.32	0.18
DAS																1	0.27
HT-2																	1

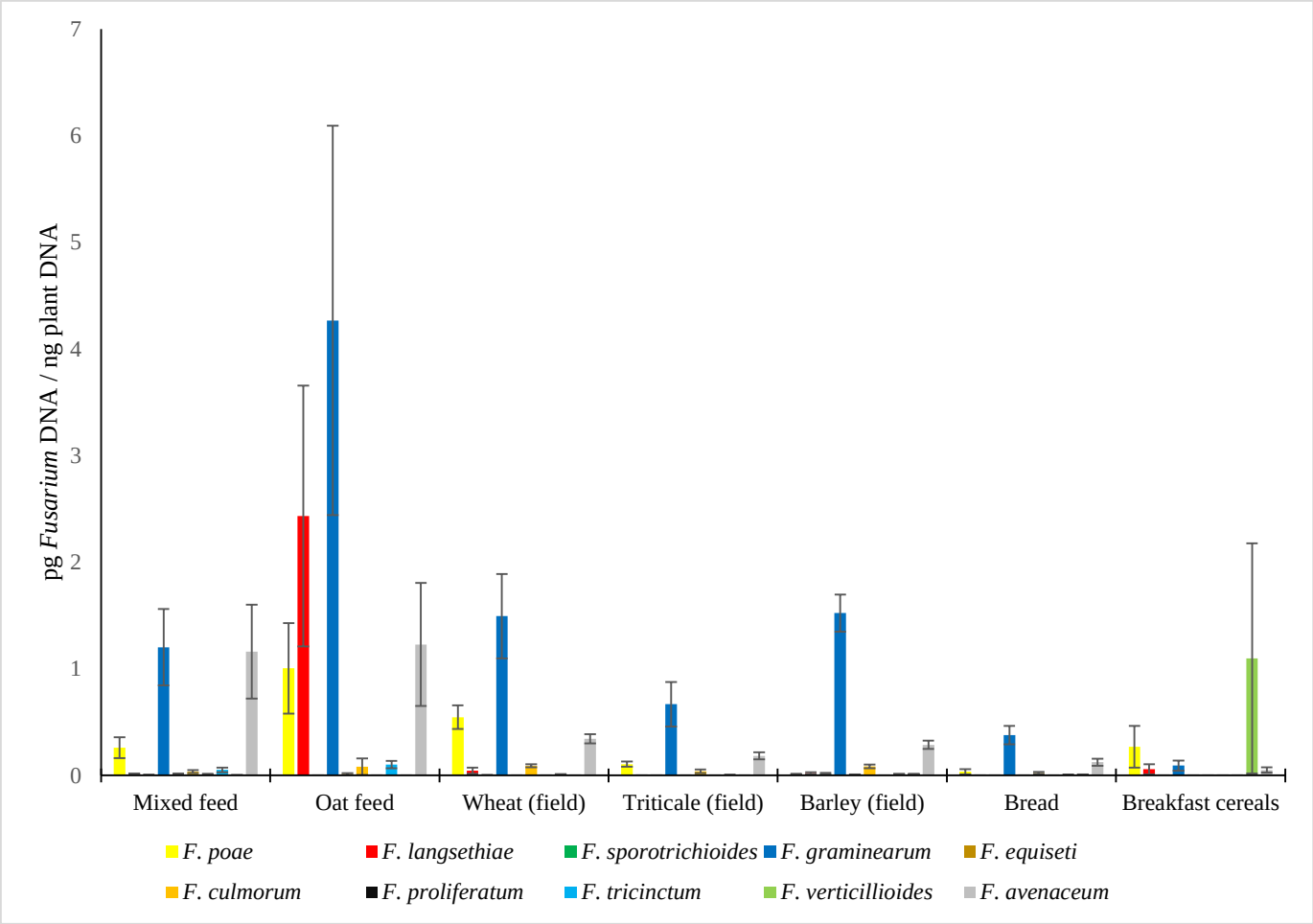

Figure S3.1 - Amount of fungal DNA (pg *Fusarium* DNA normalized on ng plant DNA) retrieved in every matrix for every species. Mean values and standard errors are calculated based on all (rather than only positive) samples of every matrix.

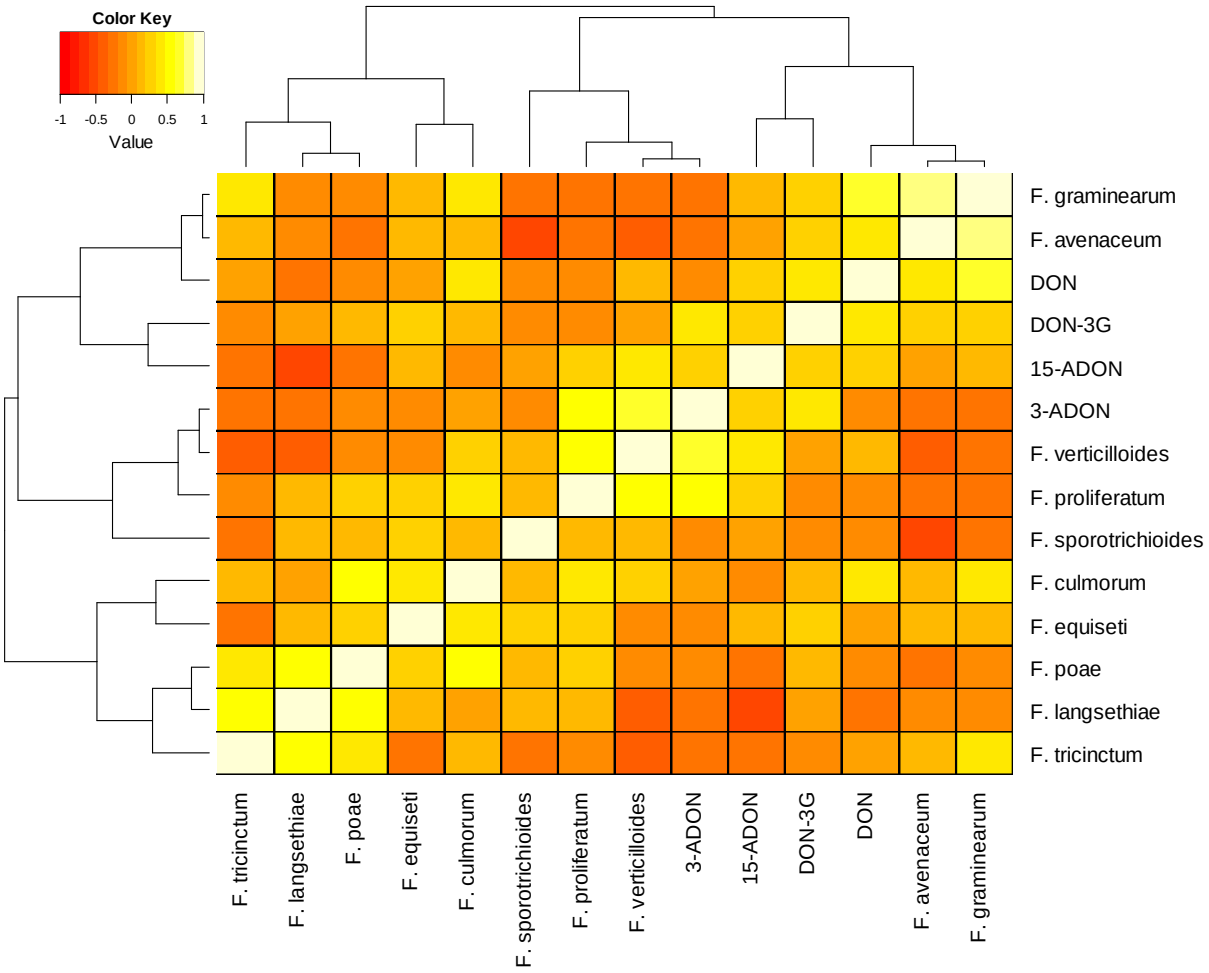

Figure S3.2 - Heat map based on the pairwise Spearman rank correlation coefficients between the measured toxin contents and *Fusarium* DNA from the different species in mixed feed samples. A lighter color designates a higher correlation, as is shown in the color scale bar. Both (identical) dendrograms are generated using average linkage clustering with the Spearman distance. The correlations at the basis of this heat map can be found in **Table S3.6**.

Chapter 4: Unique genome dynamics in *Fusarium poae*

Vanheule, A, Audenaert, K, Warris, S, van de Geest, H, Schijlen, E, Höfte, M, De Saeger, S, Haesaert, G, Waalwijk, C, van der Lee, T. (2015) Living apart together: crosstalk between the core and supernumerary genomes in a fungal plant pathogen. Submitted to BMC Genomics.

4.1 Abstract

In the previous Chapters of this thesis the prominence of *F. poae* in the FHB disease complex was detailed. In this Chapter the goal was to create a solid basis for future work on *F. poae* by delivering a high quality genome assembly and annotation. The link between genome plasticity and biology and fungal evolution and adaptation is well-documented. The presence of supernumerary chromosomes that differ markedly from the core chromosomes is a key example of fungal genome plasticity. The origin of these supernumerary chromosomes, the reason for their different characteristics, and their interactions with the core genome are still largely unknown. Throughout this Chapter, we report on the supernumerary chromosomes of *F. poae*. Using single molecule real time (SMRT) long reads, the 38 Mb core genome was assembled into four chromosomes that contain the complete genome complement of related *Fusarium* species in a highly syntenic fashion. An additional ~8 Mb of sequence was assembled into contigs that make up at least one supernumerary chromosome. Clear differences exist between the core and supernumerary genome. The core chromosomes contain 2% transposable elements (TEs) while the supernumerary genome consists of 25% TEs. The TEs on the core chromosomes show clear signs of repeat-induced point mutation (RIP), in sharp contrast no RIP was found on the supernumerary genome. Furthermore, no duplicated genes are present on the core, but at least 81 are found on the supernumerary genome. Importantly, the specific absence of RIP in the supernumerary genome accounts for the differences between the core and supernumerary genomes in *F. poae*. An exchange of genetic material occurs between the core and supernumerary genomes. Intact TEs from the supernumerary genome integrate into the core chromosomes, occasionally leading to gene disruptions. On the core chromosomes, the integrated TEs become subjected to RIP. In addition, large blocks of supernumerary sequence (>200kb) have recently been translocated to the core chromosomes. *Vice versa*, genes from the core chromosomes are duplicated to the supernumerary genome, where they may increase in copy number. This genetic exchange bestows significant opportunities for adaptation and evolution on the organism, and shows that the presence of the supernumerary genome causes novel genotypes to arise.

4.2 Introduction

Genome plasticity is one of the most important drivers of evolution in eukaryotes. This plasticity includes large scale genome duplications, rearrangements, deletions and compartmentalization (Coghlan et al., 2005; Stukenbrock and Croll, 2014). Fungi represent these dynamics better than any other kingdom. They occupy a highly diverse set of niches, and

emerging fungal diseases are considered one of the primary threats for plant health and food safety (Fisher et al., 2012). The organization of fungal genomes varies remarkably and has been described to facilitate rapid evolution and speciation (Stukenbrock, 2013). Supernumerary chromosomes are one of most radical extensions of this genome plasticity. They represent chromosomal structures that vary in size and distribution among individuals of the same species. In some cases they contain genes needed for pathogenicity and efficient colonization of the host as in *Alternaria alternata* (Hatta et al., 2002), *Fusarium solani* (formerly known as *Nectria haematococca*) (Coleman et al., 2009), and *F. oxysporum* f. sp. *lycopersici* (Ma et al., 2010). In other species, the role of supernumerary chromosomes is less clear as they do not show obvious pathogenicity related functions, as in *Zymoseptoria tritici* (formerly known as *Mycosphaerella graminicola*) (Goodwin et al., 2011). In all cases however, these chromosomes differ markedly from the core chromosomes in characteristics such as gene content, codon usage and distribution of transposable elements. The specific reasons for the differences between core and supernumerary chromosomes are for most species unknown, and speculations include different origins and evolutionary pressure (Mehrabi et al., 2011; Croll and McDonald, 2012).

TEs play an important role in fungal genome diversity and the evolutionary success of some pathogens (Stukenbrock and Croll, 2014). Examples are the vast differences in genome sizes of *Fusarium* (Ma et al., 2010) and *Phytophthora* species (Haas et al., 2009), and the shaping of pathogenicity in *Pyrenophora tritici-repentis* (Manning et al., 2013) and *Leptosphaeria maculans* (Rouxel et al., 2011). The possible deleterious effects of mobilization of TEs include gene disruption and intra- or inter-element recombination, potentially leading to gene loss. Fungi have evolved a specific genome defense mechanism against repetitive DNA, RIP, that efficiently inactivates TEs by introducing cytosine to thymidine mutations, thereby leading to a premature stop of translation (Cambareri et al., 1989). However, this process does not discriminate between TE proliferation and duplicated genes, and therefore the near-absence of paralogs has been found to be a hallmark of a RIP-active species, e.g. in *Fusarium graminearum* (Cuomo et al., 2007) and *Neurospora crassa* (Galagan et al., 2003). This finding has been termed the evolutionary cost of genome defense (Galagan and Selker, 2004). RIP functions on repetitive sequences with greater than 80% identity and exceeding +/- 1000 bp in length (Galagan and Selker, 2004). **Box 4.1** gives an impression of how RIP works.

Box 4.1 – Repeat-induced point mutation: genome defense wanted!

Repeat-induced point mutation is a defense mechanism against disruptive transposable elements, specific to fungi. During the pre-meiotic phase, repetitive DNA is detected and inactivated by multiple C→T mutations and as such premature stopcodons are likely introduced in the coding region of the TE. RIP acts on all copies of the repetitive DNA during this inactivation. However, RIP is not able to discriminate between TE proliferation (scenario on the left in the figure) and potentially beneficial gene duplications (scenario on the right in the figure), and therefore a species with efficient RIP usually does not contain any paralogs within its genome.

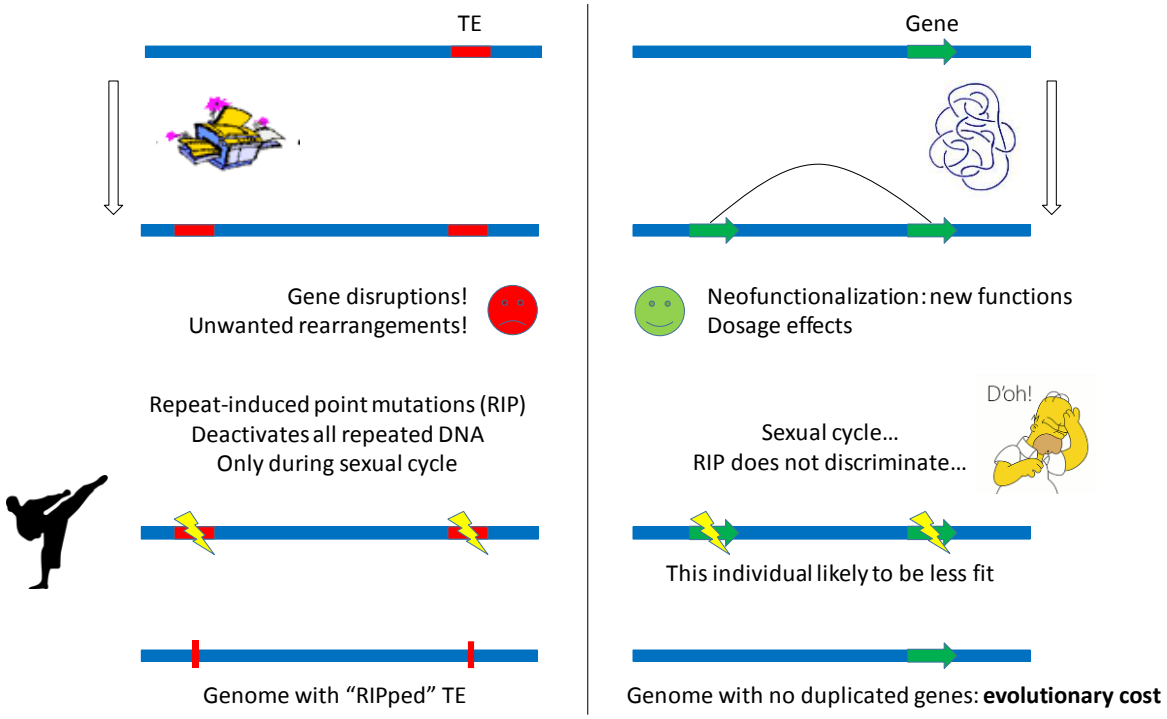

The RIP process occurs only during the di-karyotic pre-meiotic phase (after plasmogamy but preceding karyogamy) and is therefore intricately associated with the sexual cycle (Pomraning, 2012). Meiosis in fungi is partially regulated by the genes occupying the mating type locus. In heterothallic fungal species the locus is occupied by either the MAT1-1 or the MAT1-2 idiomorph (an idiomorph consists of genes that share no similarity to those of the opposing idiomorph, see **Box 2.1**), and isolates of these species require partners of the opposing mating type to enter into meiosis. For certain species, a "cryptic" sexual cycle is presumed to occur in the field, which has however never been observed (Turgeon, 1998). The presumption of active meiosis becomes substantiated when markers for a sexual mode of reproduction are considered, including recombination (Tavanti et al., 2004), RIP (Clutterbuck, 2011), distributions of the mating idiomorphs in the population (Paoletti et al., 2005), and functional constraint on the genes implicated for meiosis (Ropars et al., 2012).

Meiosis is one of the drivers of diversity in length and number of supernumerary chromosomes in fungi. It has been shown that during meiosis a process called nondisjunction is responsible for the loss of these chromosomes in *Z. tritici* offspring, even if both parents contained the supernumerary chromosome (Wittenberg et al., 2009). Importantly, the offspring of these crosses are viable, underlining the conditionally dispensable nature of this part of the genome. The birth of a new supernumerary chromosome has been experimentally shown to occur through fusion of sister chromatids during meiosis, followed by breakage-fusion-bridge cycles (Croll et al., 2013). Other proposed origins of these chromosomes include horizontal gene transfer from other fungi (Ma et al., 2010; Hu et al., 2012) and degeneration from the core genome (Galazka and Freitag, 2014). It has been argued that supernumerary chromosomes may be extreme cases of genome compartmentalization, demonstrated to occur within the core chromosomes of *Fusarium graminearum* (Galazka and Freitag, 2014; Zhao et al., 2014). These compartments may serve as evolutionary cradles with higher mutation rates and increased recombination (Cuomo et al., 2007), enriched for genes such as secondary metabolite clusters but often transcriptionally silent or only expressed under specific conditions ("cryptic" genome). How the presence of supernumerary chromosomes influences the fate of the core chromosomes and whether a genetic exchange between the two genome components exists has not been investigated.

As is evident from the examples in the paragraphs above, species of the genus *Fusarium* contain the hallmarks of fungal genome plasticity such as supernumerary chromosomes and compartmentalization of the core chromosomes. They are therefore excellent model organisms to investigate fungal genome plasticity and evolution. The genome of *F. graminearum* was recently finished to completion, making it an excellent model system for comparative genomics (King et al., 2015). Previous chapters of this thesis described the importance of *F. poae* within the FHB complex. Individuals of this species were shown to contain a highly variable set of supernumerary chromosomes (Fekete and Hornok, 1997). This is visualized in **Figure 4.1**.

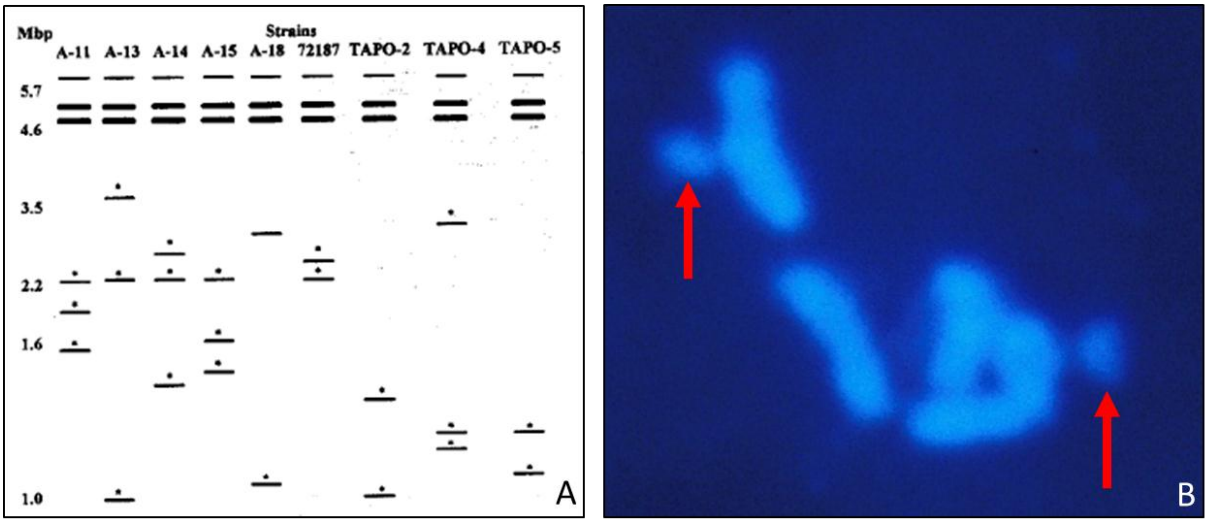

Figure 4.1 – Supernumerary chromosomes in *F. poae*. **A**: stylized result of a karyotyping experiment with nine *F. poae* isolates taken from Fekete and Hornok (1997). These authors separated chromosomes by pulsed-field gel electrophoresis. Larger chromosomes are more difficult to separate and may co-migrate (thicker bands). The asterisks represent chromosomes that gave a positive signal after hybridization with a ZIT1 probe (see further for description of this element). Aside from the conserved larger sized chromosomes (likely core chromosomes), every isolate contains 2-3 chromosomes of smaller size (likely supernumerary chromosomes). **B**: visualization of four core chromosomes and two supernumerary chromosomes (red arrows) with the "germ tube burst method" (source: dr. Cees Waalwijk, personal communication).

In this study, we sequenced the genome of one isolate of *F. poae* using SMRT long read technology. **Box 4.2** illustrates the importance of long reads in genome sequencing. Using these reads we performed a high quality genome assembly and annotation, and with HiSeq reads of three additional isolates we assessed the TE landscape over the genome. We determined that *F. poae* is likely a sexual species, with active RIP, that does not act on the supernumerary chromosomes however. This accounts for the marked differences between the two genomic components. We detected an exchange of genetic material between the core and supernumerary chromosomes, with both advantageous and deleterious consequences, and we suggest that the co-occurrence of the core and supernumerary chromosomes may confer novel opportunities for adaptation and evolution to the species.

Box 4.2 – Read length in the genomics era: size matters

The output of genome sequencing is numerous short and contiguous pieces of sequenced DNA. These can be computationally assembled to longer sequence units, and ideally to whole chromosomal structures. These longer units are callled contigs, and they are the consensus sequence of overlapping individual sequences, or "reads". The length of these individual reads is the most important determinant for genome assembly, and longer reads will make it easier to reach the "golden standard" of one chromosome = one contig (Koren and Phillippy, 2015). Short reads will not be able to span repetitive elements such as transposable elements and the rDNA tandem unit. These repetitive sequences match on multiple genomic locations and when interspersed throughout the genome lead to a fragmented assembly.

Typically, next generation sequencing methods such as Illumina sequencing have produced short reads, currently at a maximum of 2 x 300 bp. These methods are able to produce paired reads whereby two ends of a DNA fragment are sequenced in opposing directions, with an insert of known size in between. Assembly with short reads routinely leads to a large number of relatively short contigs, and for every repetitive element a "collapsed", high-coverage contig. Recently developed single molecule real time (SMRT) sequencing has made it possible to obtain reads over 10kb in length. These reads span repetitive elements and allow them to be placed within their correct genomic environment. This leads to a reduced number of contigs (no longer broken up by repetitive elements) and greater resolution to investigate chromosomal variation and biology.

4.3 Materials and methods

4.3.1 Fungal material

Table 4.1 lists the *F. poae* isolates that were used for whole genome sequencing. Three isolates originate from Belgian fields (isolates 2516, 2548 and 7555), of which two were isolated from the same field at the same time (isolate 2516 and 2548). Isolate 7555 was purchased from a culture collection and was isolated long before the others. One isolate was collected in China (bfb0173). An additional 69 *F. poae* isolates were collected from various sources (**Table S4.1**) and used for diagnostic PCRs (see further). Chapter 5 of this thesis lists more information on the source of the fungal isolates and the process that was used to make them single spore cultures.

Table 4.1 - Isolates used for whole genome sequencing. MUCL = Mycothèque de l'Université catholique de Louvain (Louvain-la-Neuve, Belgium).

ID	Sequencing	Location	Year	Host	Reference
bfb0173	HiSeq	Shayang, Hubei, China	2005	Barley	Yang et al. (2008)
2516	HiSeq + SMRT	Zwevegem, Belgium	2011	Wheat	this study
2548	HiSeq	Zwevegem, Belgium	2011	Wheat	this study
7555	HiSeq	Heverlee, Belgium	1965	Wheat	MUCL

4.3.2 Growth conditions and nucleic acid manipulation

Conidia were taken from long term storage (-80°C in 20% glycerol solution for Belgian isolates, deep frozen in liquid nitrogen for the Chinese isolate) and plated on PDA plates. For isolates 2548, 7555 and 2516 (HiSeq sequencing), mycelium was picked from the edges of the grown plates (5 days old), and cultured in liquid GPY (glucose peptone yeast, 10 g/l glucose; 1 g/l yeast extract; 1 g/l peptone, Oxoid, Belgium) medium for 5 days with 100rpm shaking at room temperature and 16h light/8h dark regime. Mycelium was collected, lyophilized and pulverized in liquid nitrogen with a pestle. DNA was extracted with the Invisorb Spin Plant Mini kit (Invitek) according to the manufacturer's instruction. Mycelium from isolate bfb0173 was inoculated in 100ml potato dextrose broth and was kept stationary for six days at room temperature and 16h light/8h dark regime. Mycelium was harvested, lyophilized and pulverized by beadbeating with 3.2mm chrome-steel beads at 2500 rpm for 20 seconds in a Hybaid Ribolyser. DNA was extracted with the Wizard Magnetic DNA Purification System for Food (Promega) according to the manufacturer's instructions. For SMRT sequencing, DNA was isolated from isolate 2516. After growth in stationary liquid GPY medium, under conditions as described above (5 days with 100rpm shaking at room temperature and 16h light/8h dark regime), mycelium was immediately crushed in liquid nitrogen with a pestle. Genomic DNA was extracted with the Wizard Magnetic DNA Purification System for Food (Promega) according to the manufacturer's instructions.

Two different RNA samples were prepared from isolate 2516 for RNA sequencing, one favoring primary metabolism (growth in complete medium (CM) (Correll et al., 1987)) and one favoring secondary metabolism (a composite of 5 conditions that are known to induce stress or secondary metabolism). For all treatments, conidia were prepared by inoculating young mycelium on PDA plates and incubating them for 7 days under conidiation inducing conditions (UV 10 hours / dark 14 hours at room temperature). Spores were harvested with Tween20 (0.01%) and gentle disruption with a spatula. After filtration through Miracloth (Merck), concentrations were determined with a Bürker chamber. All replicates were performed at 100 rpm shaking, room temperature and 16h light/8h dark regime. For the primary metabolism sample, 10^6 conidia were inoculated in 250ml CM and incubated for 30 hours. For the "secondary metabolism" sample, five different conditions were used: trichothecene biosynthesis induction, fungicide application, N starvation, C starvation, and conidiation under UV. RNA was extracted from two replicates of every condition, the two RNA extracts were

pooled for every condition, and the five resulting RNA extracts (from five conditions) were pooled again for sequencing,

Trichothecene biosynthesis inducing medium consisted of basal medium (Correll et al., 1987) without agar, but amended with L-arginine at 5mM (Gardiner et al., 2009), and was inoculated with 10^6 conidia in 250 ml for 48 hours. For prothioconazole application, N-starvation and C-starvation, 10^6 spores were inoculated in 250ml CM, and after 12 hours the mycelia were harvested on sterile filter paper, flushed with sterile water, and transferred to erlenmeyers containing 250 ml of the prothioconazole containing or starvation media for another 12 hours. Fungicide containing medium consisted of CM amended with 3 mg/kg of prothioconazole. N-starvation medium consisted of pure basal medium without added N-source, while for C-starvation $NaNO_3$ was included in this medium, and sucrose was dropped.

RNA was extracted with TRIzol (Life Technologies). Subsequently, the crude RNA was purified with the RNA cleanup protocol included in the RNeasy Plant Mini kit (Qiagen) according to the manufacturer's instructions. Quantity of DNA/RNA were assessed with respectively Picogreen or Ribogreen (Life Technologies).

4.3.3 HiSeq library preparation and sequencing

DNA from isolate bfb0173 was used for random sheared shotgun library preparation using the NEXTflex ChIP-seq Library prep kit with adaptations for low gDNA input (optimized for 1-10 ng of DNA) according to the manufacturer's instructions (Bioscientific). In short, approximately 10 ng DNA was used for fragmentation in a 50 µl volume using a Covaris E210 device targeting 400-500 bp fragment sizes. From the fragmented DNA, 40 µl was used for end repair at 22°C for 30 minutes with the enzyme provided by the manufacturer. End repaired DNA was purified using the purification column provided and eluted in 16 µl elution buffer. 3' adenylation and barcoded adapter ligation was done according to the manufacturer's instructions (Bioscientific). For all temperature incubation steps a 2720 Thermocycler (Life Technologies) was used. Adapter ligated fragments were then purified twice using 1 volume Ampure XP beads (Agencourt) and finally used in a 50 µl PCR reaction with 15 cycles for library amplification. Amplified libraries were purified using AmpureXP beads and eluted in 20 µl. Final libraries were quantified by Qubit (Life Technologies) and Bioanalyzer High Sensitivity DNA assay (Agilent technologies). The library was loaded as (part of) one lane of an Illumina Paired End flowcell for cluster generation using a cBot. Sequencing was performed

on an Illumina HiSeq2000 instrument using 101, 7, 101 flow cycles for forward, index and reverse reads respectively. De-multiplexing of resulting data was carried out using Casava 1.8.

For isolates 2516, 2548 and 7555, shotgun libraries were made using the Illumina TruSeq LT DNA sample prep kit according to the manufacturer's instructions (Illumina). Libraries were quantified by Qubit fluorescence and library fragment size was analyzed by Bioanalyzer High Sensitivity DNA assay. Libraries were then pooled equimolarly and loaded on one flowcell lane for 2x100 nt paired end sequencing on an Illumina HiSeq2000 platform as described above.

4.3.4 RNAseq library preparation and sequencing

RNAseq library preparation was carried out using the Illumina TruSeq total RNA sample preparation kit and guidelines. From 1 µg of total RNA, mRNA was isolated using oligo dT beads, fragmented thermochemically and used for first and second strand cDNA synthesis by random priming. cDNA fragments were (end) repaired, purified using AmpureXP, 3' adenylated and used for adapter ligation. Adapter ligated cDNA fragments were purified using AmpureXP beads and enriched by PCR amplification using 15 cycles. Final libraries were quantified by Qubit (Life Technologies) and fragment size distribution was determined by Bioanalyzer RNA6000 pico DNA assay (Agilent technologies). These libraries were pooled equimolarly and loaded on one Illumina HiSeq2000 flowcell lane for 2x100 nt paired end sequencing as described above.

4.3.5 SMRT library preparation and sequencing

Twenty µg DNA was used for a large (10 kb) library prep according to the manufacturer's instructions (Pacific Biosciences) with small adaptations. For all bead purifications, siliconized tubes (Sigma) and a Labquake rotator were used to homogenize DNA bead solutions and DNA was eluted for at least 30 minutes. In short, DNA was sheared using a Covaris g-tube by centrifugation two times for 1 minute at 6000 rpm. Sheared DNA was purified and concentrated using 0.45 x washed AmpureXP beads. Fragmented DNA was analyzed on a Bioanalyzer 12000 DNA chip (Agilent technologies). DNA damage repair and polishing was done according to the provided protocol. Using the enzyme provided in library prep kit, adapters were ligated over night at 25˚C, followed by heat inactivation of the enzyme at 65˚C for 10 minutes. Subsequently, ligated DNA fragments were treated with ExoIII and ExoVII to remove linear DNA molecules (i.e. those that are bound to no or only one SMRT bell(s)), and finally SMRT bells were purified with Ampure XP beads. SMRT bells were quantified using Qubit (Life Technologies) and Bioanalyzer 12000 DNA chip.

SMRT bells were size selected on a Bluepippin High-Pass v3 cassette (Sage science) with a 7000 bp minimum cutoff. After elution, DNA was left for 45 minutes in the elution port before collection and the elution port was washed once to increase the yield of recovered DNA. Size selected SMRT bells were finally purified with AmpureXP beads and eluted in 10 µl, and part was quantified and analyzed on a Bioanalyzer 12000 DNA assay.

Size selected purified SMRT bells were used for primer binding and subsequent P6 polymerase complexing in long term storage buffer for four SMRT cells according to PacBio's binding calculator version 2.3.0.0. Complex Magbead binding was done for 45 minutes at 4˚C and finally used for a 0.05 nM on plate loading concentration on a Pacbio RS II system. Sequencing was done using one cell per well, C4 chemistry and 240 minutes movie time. Magbead binding complexes for an addition twelve SMRT cells were prepared for 0.12 nM on plate loading and sequencing, with same settings as described.

4.3.6 Genome assembly

From SMRT Portal version 2.3.0.140893, the Hierarchical Genome Assembly Process (HGAP2) was initiated using data from 16 SMRT cells. Raw reads were filtered on read quality >= 0.83, polymerase read length >1000bp and subread length >1200bp. The seed read length for the error correction procedure was manually set to 6kb. After the error correction step, the data was filtered for reads >9kb. With this dataset the assembly was performed with Celera, using the default settings provided by HGAP2. The contigs from this assembly (base assembly) were taken as the basis for a hybrid assembly approach, for which the contigs were supplemented with those derived from two additional automatic HGAP2 assemblies. One assembly was performed with 10 SMRT cells using default settings, and one with 16 SMRT cells using only HQ input data (read quality >= 0.85, polymerase and subread length >4000bp).

The largest contigs, corresponding to a major part of a hypothetical chromosome were used as queries for blastn searches against the other contigs in the assemblies. Contigs were joined on the basis of their collinearity (usually excluding the very end of one contig and the very beginning of another, where the assembler presumably stalled or followed a wrong seed for a particular assembly) and their macrosynteny with other *Fusarium* species. Rightful joining of contigs was checked by evaluating SMRT long reads mapping. The resulting hybrid assembly of four chromosomes was polished using Quiver (SMRT Portal resequencing protocol) for 2 times, using HQ reads (read quality >= 0.80, polymerase and subread length >3000bp). The hybrid assembly was supplemented with the remaining contigs and the degenerate unitigs from

the base assembly (see above). Nine contigs that only contained rDNA tandem repeats, and 66 contigs that contained mitochondrial sequence were removed. The remaining contigs were added to the four-chromosome assembly and the entire assembly was error corrected in 1 pass using quiver (read quality >= 0.84, polymerase and subread length >1000bp). After this quiver run, 13 contigs were removed from the assembly because of overall base quality scores close to zero, compared to an average base quality of 50 for the rest of the assembly.

The mitochondrial genome was assembled with GRABb using standard settings and with the PH-1 mitochondrion (NCBI accession HG970331.1) as bait (Brankovics et al., submitted). One mitochondrial plasmid was assembled in SMRT assembly A. Two additional mitochondrial plasmids were taken from the HiSeq assembly (see below), that were not present in the SMRT assembly. This may result from the fragment size selection that was performed, as the plasmids are <3kb in size. The final assembly therefore contains four chromosomes, 172 unplaced contigs, one mitochondrial genome and three mitochondrial plasmids. For the four chromosomes, the error rate of the SMRT assembly was checked by mapping the HiSeq reads of isolate 2516 to the SMRT assembly with CLC Genomics Workbench 7.5 (length and similarity fraction = 0.8). Basic variant detection was run with minimum coverage = 50, minimum count = 10 and minimum frequency = 70%, and other settings at standard value. A *de novo* assembly of Illumina HiSeq reads for isolate 2516 was performed with CLC Genomics Workbench 7.5 using standard settings.

4.3.7 Annotation of the reference genome

The Illumina HiSeq RNAseq paired-end reads (combined from both "primary metabolism" and "secondary metabolism" samples) were cleaned and trimmed using Trimmomatic (Bolger et al., 2014). Tophat2 (Kim et al., 2013) was used to map the trimmed reads to the SMRT assembly of isolate 2516. The mapping results were used in the genome annotation pipeline BRAKER1 (Hoff et al., 2015) for training GeneMark (Lukashin and Borodovsky, 1998) and Augustus (Stanke et al., 2006). BRAKER1 uses the introns parsed from the TopHat2 mapping as extrinsic evidence for the final gene models predicted by Augustus. The annotation was outputted as a GFF file with genes, introns, exons and the protein sequences predicted to be encoded by these genes. A short Python script was used to extract the protein sequences from the GFF.

4.3.8 Repeat identification, localization, structural and functional characterization

RepeatModeler (Smit and Hubley, 2008-2015) was run on the genome of isolate 2516 with standard settings. RepeatModeler output was manually curated to obtain complete elements.

These elements were then subjected to functional and structural characterization. When possible, terminal inverted repeats (TIR) and long terminal repeats (LTR) were identified. Bowtie2/TopHat2 read mapping as well as related NCBI accessions were examined to find intron/exon boundaries. The translations of the predicted ORF for every TE were used as blastp queries against the NCBI non-redundant protein sequences database. The 15 best hits were aligned with the TE query using ClustalO (Sievers et al., 2011) implemented in CLC Genomics Workbench 7.5. The resulting neighbor-joining phylogenetic trees are included in the TE data sheets. The elements were divided into superfamilies based on their domain similarities to described TEs. For RIP analysis, all copies from every family were identified with blastn in CLC Genomics Workbench 7.5, and exported by using the getfasta functionality of BEDtools (Quinlan and Hall, 2010). They were aligned with ClustalO (Sievers et al., 2011) and subjected to alignment-based repeat-induced point mutation analysis using RIPcal (Hane and Oliver, 2008).

4.3.9 Analysis of transposable element integration sites

Blastn (expect value < $1e^{-10}$) was used to obtain genomic coordinates of all intact and RIPped copies of TEs. RIPped copies are easily distinguishable from intact copies, as they are still picked up by blastn but their identity is as low as 60% and nearly all mutations are C→T or G→A transitions. Using the getfasta utility of BEDtools (Quinlan and Hall, 2010) these hits, including their flanking regions were extracted. HiSeq reads from all isolates in this study were subsequently mapped to the extracted reference sequences at high stringency (minimum length fraction 0.95, minimum similarity fraction 0.95) in CLC Genomics Workbench 7.5. Results were manually inspected to find identical genomic environments. Elements with read support for only one flank were also considered to be identically inserted.

For synteny of the MITE, a prototype of the element was used as a blastn query against the entire genome (expect value < $1e^{-10}$), hits were extracted including 500bp upstream and downstream flanking sequence with the getfasta utility of BEDtools (Quinlan and Hall, 2010). This was done for the assembly with long reads of isolate 2516 and the short read *de novo* assemblies of isolates 2548, 7555 and bfb0173. For every isolate, the resulting sequence list was queried against the genome assemblies of the other isolates with blastn, and the matches longer than 640bp were counted (indicating instances where the localization of the MITE coincides between isolates: at least one flank of 500bp and the 140bp element are shared).

4.3.10 Divergence estimates of TE copies

Intact (not RIPped) copies were extracted as described above from the core and unplaced sequence separately. Only families containing five or more copies were retained. ClustalO alignments (Sievers et al., 2011) were fed to PhyML (Guindon and Gascuel, 2003) and maximum-likelihood phylogenies were built for every family with settings retrieved from literature (Rouxel et al., 2011). Specifically, a neighborhood joining tree was used as starting tree, the transition/transversion ratio was 4, the HKY85 evolution model was used and distribution parameters were allowed to optimize. In the resulting phylogenies, terminal branch lengths represent the relative age of every separate element. These branch lengths were extracted from the Newick files with Newick Utilities (Junier and Zdobnov, 2010). Using the substitution rate determined for protein-coding genes in fungi ($1.05 * 10^{-9}$ (Kasuga et al., 2002)), divergence time estimates were calculated from the branch lengths. These were then visualized as Box-Whisker plots using SPSS22.

4.3.11 Paralogs and gene duplications

All genes from the repeat masked core genome and all genes from the repeat masked supernumerary genome were extracted separately. The genes from the supernumerary genome were queried against those from the core genome with blastn (expect value < $1e^{-5}$). Results were filtererd to hits > 80% nucleotide identity and length above the RIP threshold of +/- 1000 nucleotides (Watters et al., 1999). This resulted in 81 instances of a gene on the supernumerary genome having a hit with a gene from the core genome above the RIP thresholds, indicating a likely duplicated gene. These were formatted for Circos visualization. When the genes from the core genome were queried against themselves, there were no such hits other than self hits. Using the gff2sequence tool (Camiolo and Porceddu, 2013) the 81 genes in the supernumerary genome and their 31 paralogs on the core chromosomes were extracted, including 500bp up- and downstream. These sequences were aligned all-vs-all with Smith-Waterman using a python application based on PaSWAS (Warris et al., 2015), which produced local alignments in SAM (Li et al., 2009) format.

For phylogeny of paralogs, the predicted protein of paralog on the core genome was used as blastp query against the NCBI non-redundant protein sequences database. The 15 best hits were aligned with the query and the predicted proteins of the paralogs on the supernumerary genome using ClustalO (Sievers et al., 2011) implemented in CLC Genomics Workbench 7.5. The resulting neighbor-joining phylogenetic trees was constructed using midpoint rooting.

4.3.12 Genome visualization

Circos (Krzywinski et al., 2009) was used for circular genome visualization. Locations of TEs were extracted from blastn output (expect value < $1e^{-10}$). Duplicated genes above the RIP threshold were parsed from the blastn output as detailed above.

4.3.13 Diagnostic PCRs

To determine the MAT1-1 and MAT1-2 distribution in the collection of 69 *F. poae* isolates, primer pairs POA-1-F/POA-1-R and POA-2-F/POA-2-R were used (Kerenyi et al., 2004). For the two insertions of supernumerary sequence into the core chromosomes, primers were designed flanking insertion site as well as covering the extremes of the inserted block (visualized in **Figure 4.12**). All primers used in this study can be found in **Table 4.2**. PCR reactions were carried out with Promega GoTaq G2 Polymerase according to the manufacturer's instructions (Promega, Leiden, the Netherlands). Annealing temperatures were calculated based on Promega's Biomath Calculator. PCR was performed in an Applied Biosystems GeneAmp PCR System 9700. PCR products were separated on 1.5% (wt/vol) agarose gels stained with 0.1 μg/ml ethidium bromide, and visualized with a Biorad Gel Doc XR+.

Table 4.2 – Primers used in this study.

ID	Sequence (5' → 3')	Reference	Target
POA-1-F	GCCTCACACTTTTTTCCTTCTTC	Kerenyi et al. (2004)	MAT1-1
POA-1-R	CAGTAAACCGGAATCATCAACG	Kerenyi et al. (2004)	MAT1-1
POA-2-F	ACGTACCATCTGACACTTGCTCG	Kerenyi et al. (2004)	MAT1-2
POA-2-R	AGTCGAGGAGGTCGTCAATCAAT	Kerenyi et al. (2004)	MAT1-2
Fp82F	CAAGCAAACAGGCTCTTCACC	Parry and Nicholson (1996)	EF-1α
Fp82R	TGTTCCACCTCAGTGACAGGTT	Parry and Nicholson (1996)	EF-1α
INS1-FLANK-fwd	CAGCGACTTGGTTCCGTATG	this study	Insertion 1
INS1-BLOCK-rev	GAAGCTTGTGACCACCCAAG	this study	Insertion 1
INS1-BLOCK-fwd	AGGTTCCGTCTTACTGGGTG	this study	Insertion 1
INS1-FLANK-rev	TCAACCAAGGCGTCGAAAAG	this study	Insertion 1
INS2-FLANK-fwd	GCATTGTGACGGATGGTACC	this study	Insertion 2
INS2-BLOCK-rev	GGTCTCACGATTTTCAGGCG	this study	Insertion 2
INS2-BLOCK-fwd	AGGTTCCGTCTTACTGGGTG	this study	Insertion 2
INS2-FLANK-rev	GCAGTACAAGCTACGATGGC	this study	Insertion 2

4.3.14 Comparative genomics intra- and inter-species

To estimate the number of intact copies for every family in the isolates that were sequenced with only Illumina technology, reads were mapped to the curated library of repeats (see above),

and the resulting coverage was normalized against the mean coverage of the single-copy genome for each isolate. To estimate the coverage across the four largest supernumerary contigs, HiSeq reads from every isolate were mapped with CLC Genomics Workbench 7.5 (length and similarity fraction = 0.8) to the reference assembly which was masked for TEs with RepeatMasker. BAM files were processed with the coverage utility of BEDtools (Quinlan and Hall, 2010) to find the fraction of bases covered by reads in a 1kb sliding window. For whole-genome alignment, the genome of the reference isolate was masked using the curated repeat library with RepeatMasker. The masked genome was aligned with the completed genome of *F. graminearum* PH-1 using MUMmer (Kurtz et al., 2004).

4.4 Results

4.4.1 The genome is composed of a core and supernumerary component

The genome of *F. poae* isolate 2516 was assembled from the SMRT reads using a hybrid approach, based on macrosynteny with related *Fusarium* species as well as support from different assemblies using different parameters. The general statistics of the assembly can be found in **Table 4.3**, and are compared with a *de novo* assembly of the HiSeq reads for this isolate. The SMRT assembly contains an additional 7.28Mb of sequence, significantly reduces the total number of contigs and has a much larger representation of bases in large contigs. In the SMRT assembly, four chromosomes were built from 9 contigs (two, three, three and one respectively), accounting for a total 38.13Mb of sequence. They contain one, two, two and one telomere caps respectively. The long arm of chromosome 1 misses the telomere in this assembly. The short arm of chromosome 4 ends in the ribosomal DNA tandem repeat. The long arm of chromosome 3 contains a series of 5000 "N"s at 150kb into the sequence. At this junction a 150kb contig was joined to the rest of the assembly on the basis of its collinearity with *F. graminearum* and other *F. poae* isolates.

Table 4.3 - Assembly statistics of the assembly with SMRT long reads and the assembly with HiSeq reads for isolate 2516. The statistics for the SMRT assembly are based on the manually refined final assembly: 4 core chromosomes (originally built from 9 contigs) and 172 supernumerary contigs.

Parameter	SMRT assembly	HiSeq assembly
Number of contigs	176	1 253
Average coverage over all contigs	20.2	111.5
Total assembly sequence size (bp)	46 309 701	39 020 932
Average contig sequence length (bp)	263 123	31 142
Minimum contig length (bp)	10 816	1 004
Maximum contig length (bp)	11 790 407	701 709
N50 sequence index (# of contigs)	2	62
N50 sequence length (bp)	8 783 590	170 721

The base quality of the assembly of the four core chromosomes was checked by mapping the HiSeq reads of isolate 2516 to the reference assembly. Over these 38.13 Mb, only one single nucleotide polymorphism (SNP) was detected between the HiSeq and SMRT reads. Two hundred and twenty-two variants were detected in homopolymeric stretches of nucleotides and low complexity (low GC%) regions (219 and 3 respectively). For these variants, read mapping was inconclusive for both HiSeq and SMRT reads.

Figure 4.2 shows the result of a whole genome alignment of the four core chromosomes of *F. poae* 2516 and *F. graminearum* PH-1. The latter was recently assembled to the chromosomal level (King et al., 2015). Aside from two major chromosomal inversions and several smaller ones, the core chromosomes show extensive macrosynteny among the species. Moreover, the entire *F. graminearum* sequence complement is present in our assembly, with a 1.4 Mb series of rDNA tandem repeats at the end of chromosome 4 as the exception. Two blocks of 204 and 464kb in chromosome 3 of *F. poae* 2516 do not show synteny with *F. graminearum* (black arrows in **Figure 4.2**) and are described in detail further below.

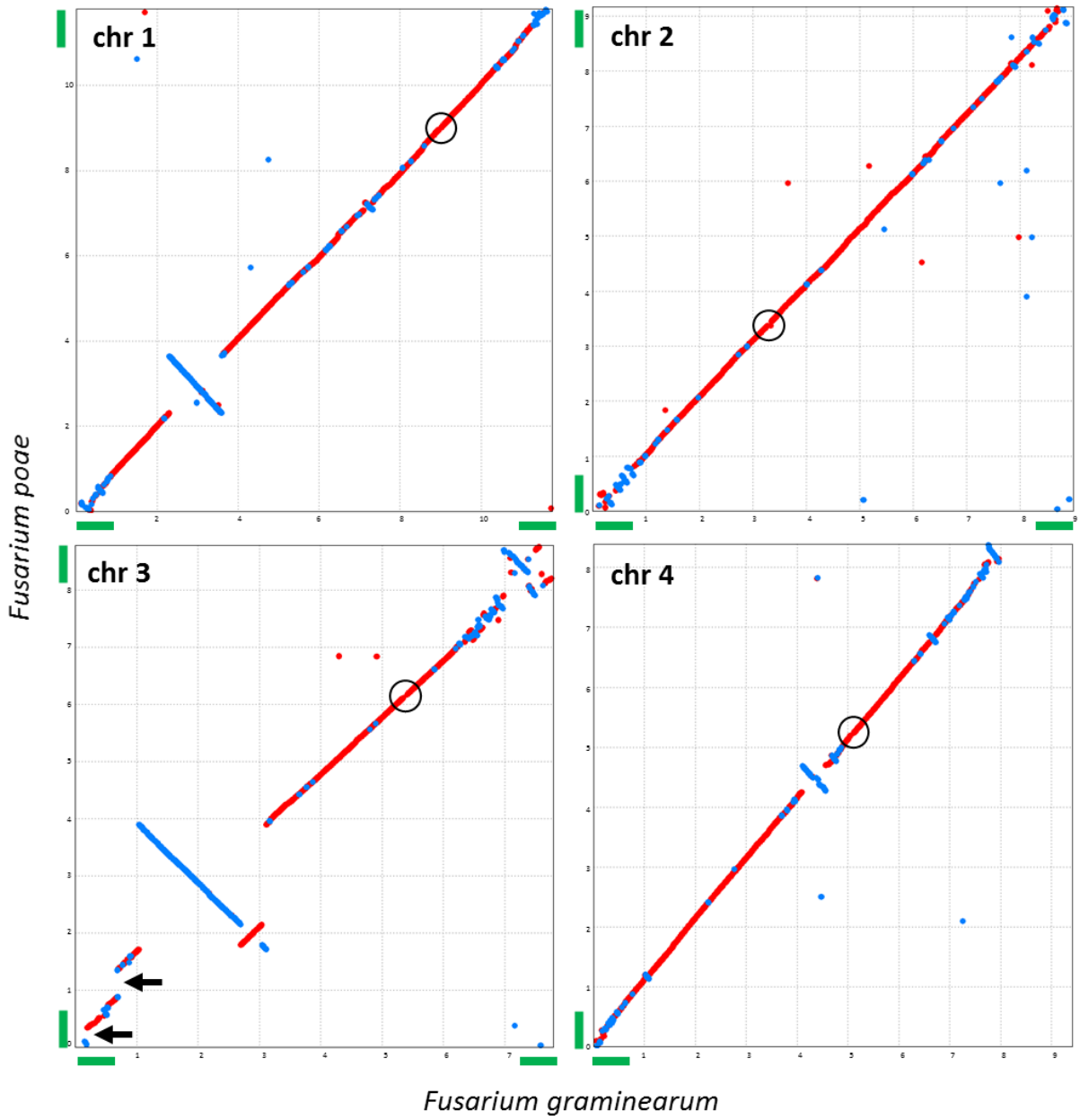

Figure 4.2 – Chromosome alignments between *F. graminearum* (x axis; NCBI accessions HG970332 to HG970335) and *F. poae* (y axis). The best 1:1 alignment is shown between the four chromosomes of *F. graminearum* and the four core chromosomes of *F. poae*. Red indicates best hits in the same orientation while blue indicates inversions. The short arm of *F. graminearum* chromosome four ends in ~1.4Mb of rDNA repeats that are not assembled in *F. poae*. All *F. graminearum* telomeres except the telomere of the short arm of chromosome 4 are assembled. For *F. poae*, the same telomere is lacking as well as the one on the long arm of chromosome 1. Telomeres that are assembled are shown with green bars on the arms of the chromosomes. Two insertions into *F. poae* chromosome 3 are denoted with black arrows. Approximate locations of the centromeres are shown with black circles.

The remaining 172 contigs (8.18Mb) do not show any synteny with closely related species *F. graminearum*. These 172 contigs contain eight copies of the ZIT1 TE described earlier as a specific marker for supernumerary chromosomes in *F. poae* (Fekete and Hornok, 1997); this

element was not found on the four core chromosomes. Not only ZIT1, but all TEs show an unequal distribution between the core chromosomes and supernumerary contigs, which is described in detail further below. The most striking difference in TE distribution comes from a Miniature Inverted–Repeat Transposable Element (MITE) that is the most abundant repetitive element in the genome. All 712 copies (with expect value < e^{-10}) were found dispersed over the core chromosomes. In sharp contrast no MITE was found on the 172 supernumerary contigs. Its positional conservation among *F. poae* isolates was investigated, and for all four isolates the localization of the vast majority of MITE instances (97.7-99.8%) was identical to at least one other isolate.

Taken together, the 172 contigs are likely to make up one or more supernumerary chromosomes, and they are designated as the "supernumerary genome" for the purpose of this study. The 8.18 Mb that the 172 contigs contain is likely a slight overestimation, as in some instances the end of one contig (contig x) is collinear and identical to the start of the contig that follows in the assembly (contig x+1), potentially indicating a (partial) double assembly (see **Figure 4.13** for an example). These are likely instances where the assembly algorithm "stalled" or followed a wrong seed, leading to the termination of contigs which should otherwise be joined/overlap. Besides the four core chromosomes and 172 supernumerary contigs, the assembly contains the mitochondrial genome of 138kb, and three mitochondrial plasmids. These plasmids were confirmed to be mitochondrial as their ORFs encode a reverse transcriptase only with the mold mitochondrial genetic code.

4.4.2 A high quality machine annotation

Isolate 2516 was grown in six diverse conditions (one favouring primary metabolism and five favouring secondary metabolism) to stimulate transcription of as many genes as possible. RNA was extracted and sequenced, and 659 076 900 RNAseq sequence reads were obtained from all conditions combined. These were quality trimmed and the resulting 562 136 710 reads were used in the BRAKER1 pipeline (Hoff et al., 2015). This is a novel annotation method that uses RNAseq reads as extrinsic evidence, to annotate the genome in a rapid and automated way without any manual curation steps. In total 14817 genes were predicted for isolate 2516. **Table 4.4** lists core features of the machine annotation of *F. poae* 2516 compared to the annotation of *F. graminearum* PH-1 (King et al., 2015). **Figure 4.3** shows an example of a BRAKER1 annotation based on a TopHat mapping of the RNAseq reads.

Table 4.4 - General features of the machine annotation of *F. poae* 2516 compared to the published annotation of *F. graminearum* PH-1.

	F. poae			
Parameter	**Total**	**Core**	**Supernumerary**	***F. graminearum***
Genome size (bp)	46 309 701	38 129 297	8 180 404	37 958 956
GC%	46.30%	46.00%	47.60%	48.20%
# of genes	14 817	12 097	2 720	14 160
Mean gene density (per Mb)	320	317	332	373
Median gene length (bp)	1 391	1 406	1 309	1 257
Avg introns/gene	1.82	1.88	1.57	1.72
Median intron length (bp)	54	54	57	55

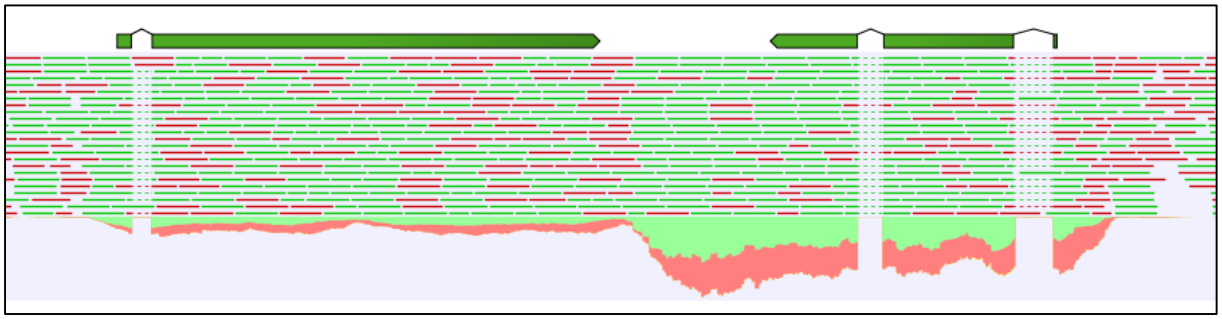

Figure 4.3 – Mapping of the RNAseq reads with TopHat, and BRAKER1 annotation. Red and green represent reads in different directions (as paired reads get broken up through the import of the TopHat mapping to CLC Genomics Workbench for visualization). Below the individual reads, the peaks give an impression of the overall read coverage. Note that untranslated regions (UTRs) of the two genes overlap, a significant issue for annotation efforts in gene-dense fungal genomes.

The BUSCO (Benchmarking Universal Single-Copy Orthologs) data set for fungi was used to assess whether the annotation can be considered complete (Simão et al., 2015). This set comprises proteins that are very likely to be present in a queried genome, based on an analysis of other genomes within a particular kingdom. The predicted proteins from *F. poae* 2516 as well as the proteins from the most recent annotation of *F. graminearum* PH-1 (King et al., 2015) were analyzed by comparing them to the BUSCO data set. **Table 4.5** shows the output for both species. The *F. poae* protein set is assessed at equally high quality as the *F. graminearum* set, indicating that the *F. poae* genome annotation is as accurate and complete as the *F. graminearum* annotation.

Table 4.5 - BUSCO analyses of *F. poae* and *F. graminearum*.

Organism	Complete	Fragmented	Missing	Total
F. poae	1431	7	0	1438
F. graminearum	1432	6	0	1438

Fragmented BUSCOs are proteins that are only partially recovered (Simão et al., 2015). These were analyzed manually with RNAseq data. For *F. graminearum* an RNAseq data set described before was used (Zhao et al., 2013). Three of the fragmented BUSCOs were shared between *F. poae* and *F. graminearum*, and examination of the RNAseq data did not provide conclusive evidence that the genes are miss-annotated. The remaining four and three proteins of *F. poae* and *F. graminearum* represent gene models that are likely to be miss-annotated in these species. In all four cases of *F. poae* and in one case of *F. graminearum*, a hybrid gene model was built from two separate genes. The remaining two *F. graminearum* gene models respectively lack two exons and contain two exons in excess. The BUSCO analysis suggests that the annotation of *F. poae* 2516 did not miss any conserved genes, and within the conserved genes, <0.5% is miss-annotated.

4.4.3 The ingredients for meiosis and RIP are present in the genome

RIP only functions during the sexual cycle, which has not been definitively shown in *F. poae*. Therefore the conservation of the necessary ingredients for meiosis was investigated for isolate 2516. The MAT1-1 locus was extracted from the assembly, and its architecture is presented in **Figure 4.4**. As all four isolates in this study have the MAT1-1 mating type, the architecture of the MAT1-2 locus could not be investigated. The number, order and direction of the genes occupying the MAT1-1 locus is identical to that in other *Fusarium* species (Ma et al., 2013). The *MAT1-1-1*, *MAT1-1-2* and *MAT1-1-3* genes have a predicted ORF with high similarity to those found in related species (85%, 86% and 92% similarity to proteins from *F. graminearum*). The *MAT1-1-1* gene was previously identified for *F. poae* (Kerenyi et al., 2004) and has 99% protein similarity with the gene model in this study. Transcription of the genes within the MAT1-1 idiomorph was noted in the RNAseq data, and the predicted splice forms lead to functional proteins (**Figure 4.4**). A collection of 69 isolates was screened for the presence of MAT1-1 and MAT1-2 and both idiomorphs were detected, albeit in heavily skewed distribution (81% MAT1-1, 19% MAT1-2; 1 undetermined; **Table S4.1**).

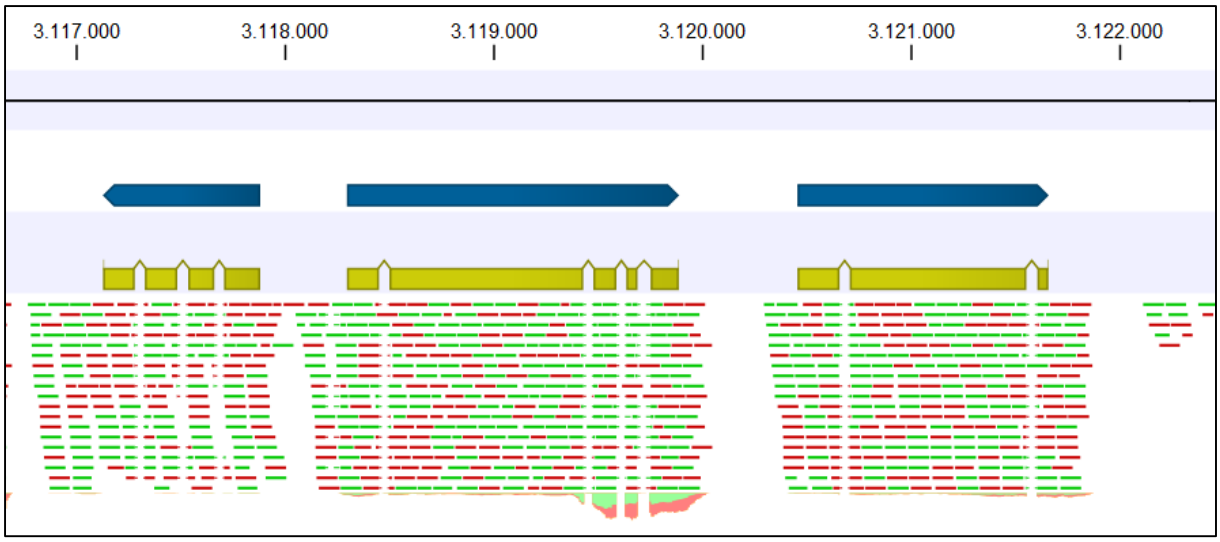

Figure 4.4 - Architecture of the MAT1 locus in *F. poae* isolate 2516, located at 3 120 000 bp into chromosome 2. The top track represents the predicted gene model, the second track represents the predicted coding features and the bottom track shows the TopHat mapping of the RNAseq reads. Red and green represent reads in different directions (as paired reads get broken up through the import of the TopHat mapping to CLC Genomics Workbench for visualization). Below the individual reads, the peaks give an impression of overall read coverage. Note the correct splicing of introns for all three alleles.

The KEGG pathway for meiosis in *F. graminearum* (fgr04113) was examined to identify proteins involved in a putative sexual cycle. The conservation of this 'meiotic toolbox' was investigated in *F. poae*. All fifty-one entries in fgr01443 give best reciprocal protein hits with *F. poae* at expect values below 10^{-150}, indicating that all ingredients of the meiotic toolbox are present in *F. poae*.

The *rid* (RIP defective) gene has been described to be essential for RIP, initially in *Neurospora crassa* (Freitag et al., 2002) and recently also in *F. graminearum* (Pomraning, 2012). A homolog of this gene is present, intact and transcribed in *F. poae* (**Figure 4.5**). However, the expected intron was not spliced in the RNAseq data and the splice variant that was observed encodes a protein with a premature termination of translation.

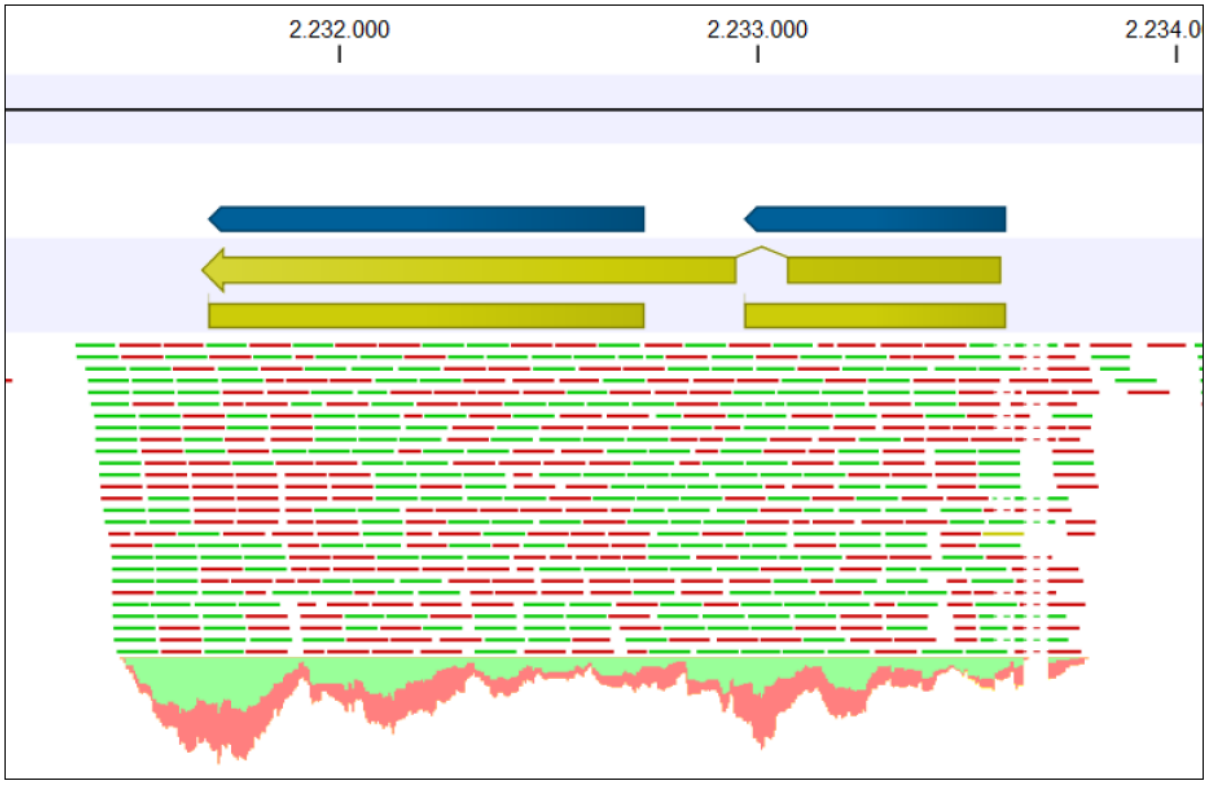

Figure 4.5 - The *rid* (RIP defective) gene in *F. poae* isolate 2516, located at 2 232 000 bp into chromosome 2. The top track represents the predicted gene models, the second track represents the predicted coding features and the bottom track shows the TopHat mapping of the RNAseq reads. Red and green represent reads in different directions (as paired reads get broken up through the import of the TopHat mapping to CLC Genomics Workbench for visualization). Below the individual reads, the peaks give an impression of overall read coverage. Two separate genes were predicted by the BRAKER1 pipeline. The *F. pseudograminearum* like gene model is superimposed as the single long coding feature. There is no splicing that supports this model under the conditions tested in this study.

4.4.4 Distribution of transposable elements differs markedly between core and supernumerary genome

The distribution of TEs throughout the genome is listed in **Table 4.6**. **Figure 4.6** visualizes the chromosomal distribution of TEs. Twenty-four out of thirty-three TE families only contain intact copies on the supernumerary component of the genome. RepeatMasker analysis with the identified TEs classified 2.1% of the core genome and 25.6% of the supernumerary genome as TEs.

Table 4.6 - Classification and key characteristics of TE families in the genome of *F. poae* 2516. Elements below the length threshold for RIP (1000bp) are not included (MITE, ZIT1). Repetitive elements such as the rDNA tandem and two families of telomere linked RecQ helicases are not included. Nomenclature of TEs is as recommended in literature (Wicker et al., 2007). Each TE is assigned a three letter code for its class, order and superfamily. Class: R = retrotransposon; D = DNA transposon. Order: L = long terminal repeat (LTR); T = terminal inverted repeat (TIR). Superfamily: G =

Gypsy; C = Copia; F = Fot1/Pogo; T = Tc1/mariner; M = Mutator; A = hAT; x = unknown. n/a designates instances where a TIR/LTR could not be detected for a specific element.

	Core		Supernumerary				
	Intact	**RIP**	**Intact**	**RIP**	**Size (bp)**	**LTR/TIR (bp)**	**Family**
Retrotransposons							
RLG_*Maggy*	27	25	11	-	5684	240	Gypsy/Ty3 like
RLG_*Skippy*	5	7	13	-	6561	379	Gypsy/Ty3 like
RLC_*Ghost*	-	1	14	-	4900	195	Copia/Ty1 like
Rxx_*marsu*	-	-	30	-	2234	n/a	unknown
DNA transposons							
DTF_*Fot4*	1	-	-	-	1852	48	Pogo
DTF_*Fot8*	-	-	1	-	2133	43	Pogo
DTF_*Fot2*	-	2	41	-	2220	90	Pogo
DTF_*Fot3-A*	-	1	7	-	2212	75	Pogo
DTF_*Fot3-B*	-	1	20	-	2200	73	Pogo
DTF_*Fot3-C*	-	-	9	-	2203	73	Pogo
DTF_*Fot5-A*	40	10	9	-	1865	51	Pogo
DTF_*Fot5-C*	-	15	7	-	1865	51	Pogo
DTF_*ESP4-A*	-	-	21	-	2909	98	Pogo
DTF_*ESP4-B*	12	11	24	-	2868	90	Pogo
DTF_*Drogon*	33	-	24	-	1934	51	Pogo
DTF_*Viserion*	8	6	8	-	2885	84	Pogo
DTF_*Rhaegal*	-	1	10	-	1854	36	Pogo
DTF_*Balerion*	-	-	12	-	2749	79	Pogo
DTA_*RLT1*	-	-	17	-	2912	27	hAT-like
DTA_*RLT2*	-	-	11	-	2975	22	hAT-like
DTA_*RLT3*	-	-	12	-	2954	n/a	hAT-like
DTA_*Hornet1*	-	1	10	-	2613	n/a	hAT-like
DTA_*Hornet2*	-	-	22	-	2739	n/a	hAT-like
DTA_*Hornet3*	-	-	11	-	2965	n/a	hAT-like
DTA_*Tfo1*	-	-	20	-	2852	28	hAT-like
DTA_*Tfo2*	-	-	15	-	2838	26	hAT-like
DTA_*Drifter*	-	-	23	-	2779	n/a	hAT-like
DTA_*Obara*	-	-	13	-	3867	19	hAT-like
DTA_*Nymeria*	-	-	36	-	2850	30	hAT-like
DTA_*Obella*	-	-	5	-	2480	29	hAT-like
DTA_*Sarella*	-	-	12	-	4236	n/a	hAT-like
DTM_*Hop7*	8	10	2	-	3449	81	Mutator
DTM_*Hop4*	1	-	7	-	2825	97	Mutator
Sum	**135**	**91**	**477**	**0**			

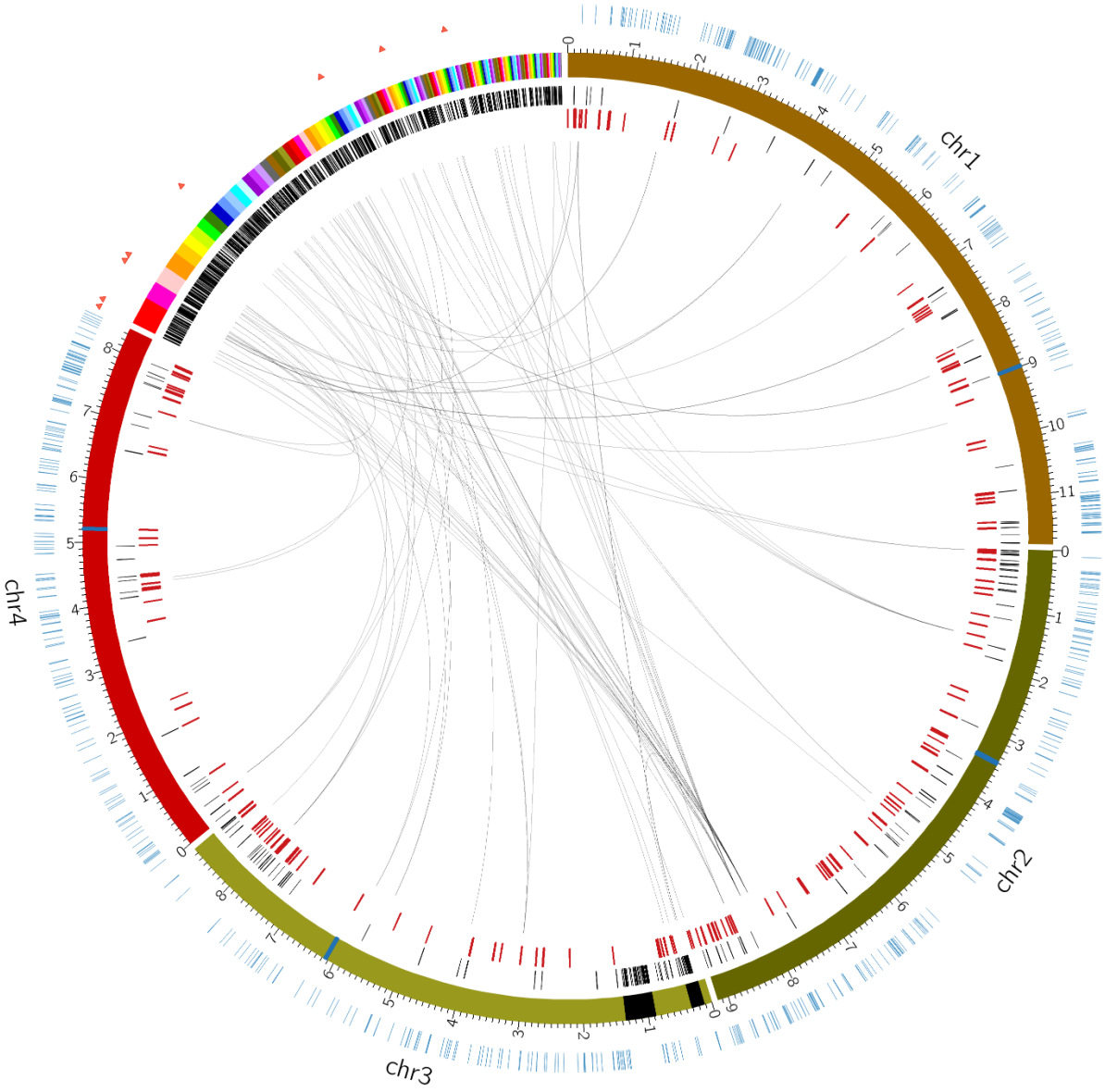

Figure 4.6 - Circos plot showing differences between the core and supernumerary components of the genome. Outer circle: blue lines denote the distribution of a MITE, red triangles denote ZIT1 copies. Second circle: core chromosomes and supernumerary contigs are colored, blue blocks on the chromosomes indicate the centromeres, black blocks show the two insertions of supernumerary sequence into the core chromosomes. Third circle: black lines represent intact (not RIPped) copies of TEs. Fourth circle: red lines represent RIPped copies of TEs. At the center of the plot, black lines connect likely duplicated genes between the core genome and the supernumerary genome. Only those pairs of genes with blastn hits exceeding 80% nucleotide identity and 1000bp length are shown, as these values have been described as the thresholds for RIP (Galagan and Selker, 2004). Duplicated genes within the supernumerary genome are not mapped.

Transcription and splicing of the predicted introns were noted for all intact TE families. Single nucleotide polymorphisms (SNPs) in the RNAseq reads allowed for the specific copy/copies of TEs that were transcribed to be identified. Two examples of the resulting data sheets are given

in **Figure 4.7** and **Figure 4.8**. The functional and structural features of every TE were used for the classification into superfamilies (**Table 4.6**). Phylogenetic trees were made for every element for which a protein coding sequence could be determined. In most cases, TE phylogeny lines up well with species phylogeny (example DTF_*Fot-3A* in **Figure 4.7**). Exceptions are the TEs DTA_*Nymeria* (item C in **Figure 4.8**) and DTM_*Hop7*, that show higher similarity to elements from unrelated fungi than to elements from related *Fusarium* species.

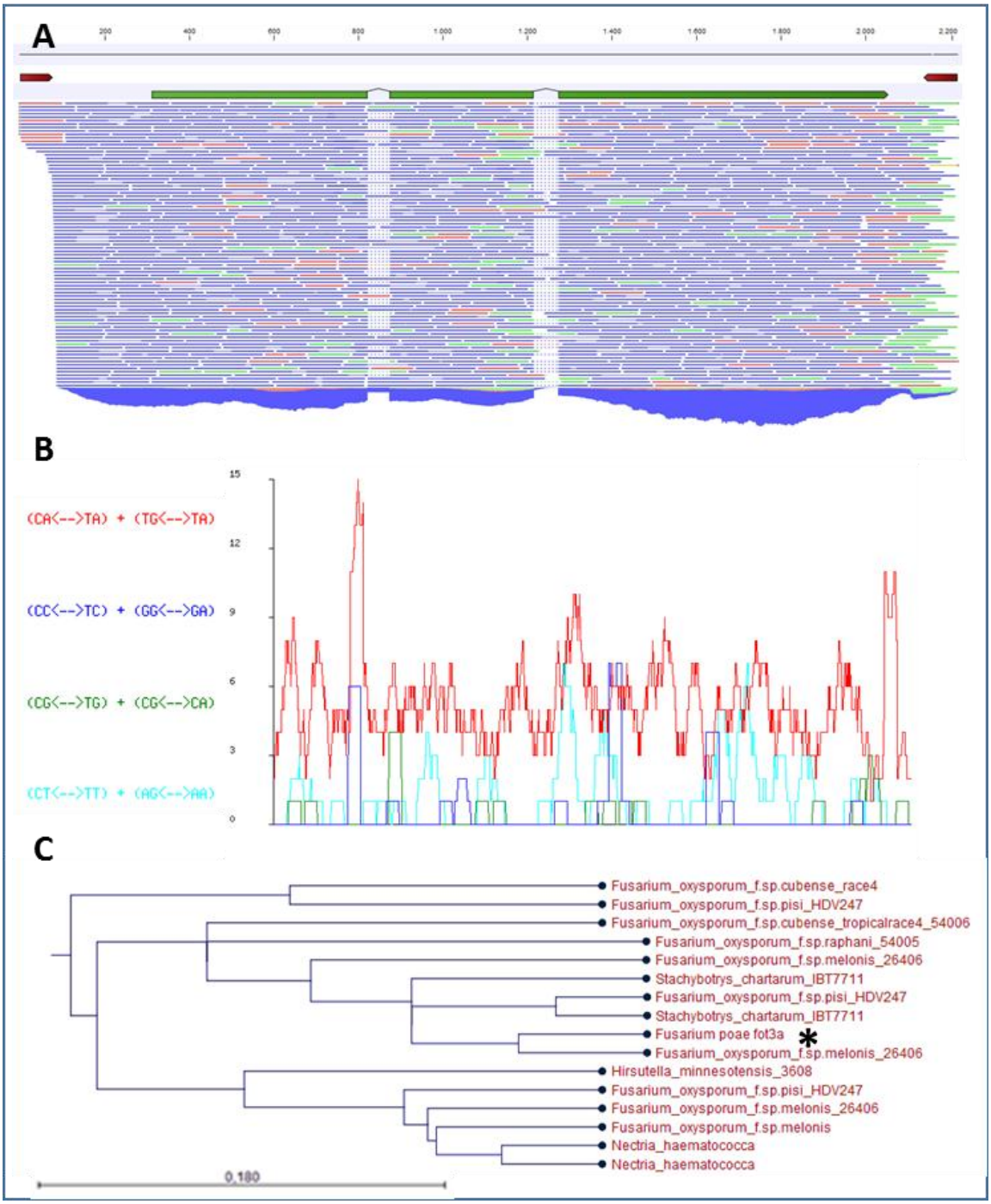

Figure 4.7 - Example information sheet on DTF_*Fot-3A*. **A**: Tracks from top to bottom: annotation of the LTR/TIR, annotation of the coding region, mapping of individual RNAseq reads (blue for paired reads; red and green for broken pairs) and total reads coverage (blue). **B**: RIP calculation with the RIPcal package after alignment of all copies with ClustalO. Each color represents the frequency of RIP-like mutations (C→T mutations or conversely G→A mutations) according to type (different dinucleotide environment) across the length of the TE (x-axis) in a 50bp sliding window. **C**: Neighbour-joining phylogenetic tree based on alignment of the predicted protein of every TE (denoted by an asterisk in the tree) and its 15 best blastp hits. No outgroup was set and the trees are mid-point rooted. The predicted protein was determined from an expressed copy of the TE (as determined by inspecting the RNAseq read mapping).

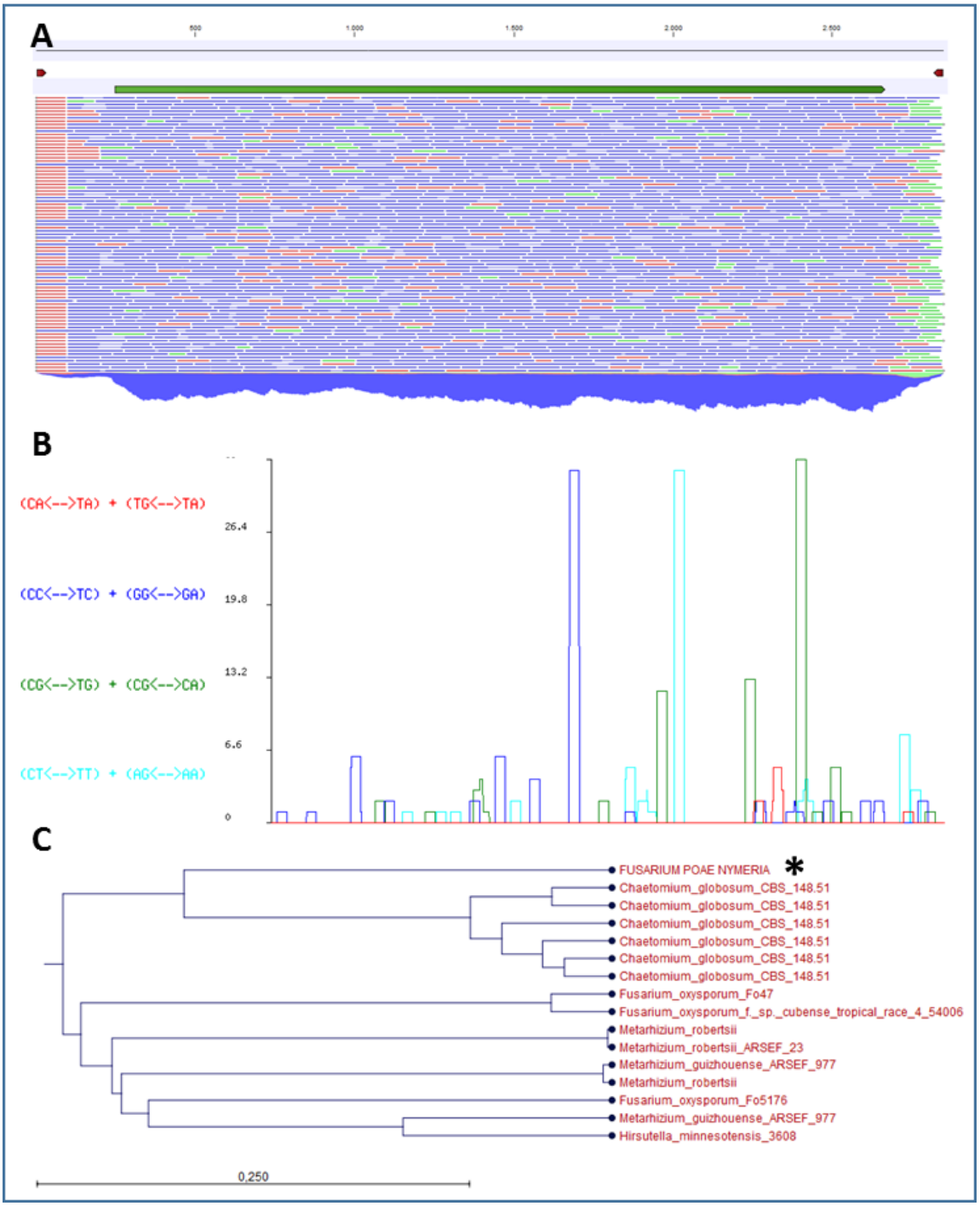

Figure 4.8 – Example information sheet on DTA_*Nymeria*. **A**: Tracks from top to bottom: annotation of the LTR/TIR, annotation of the coding region, mapping of individual RNAseq reads (blue for paired reads; red and green for broken pairs) and total reads coverage (blue). **B**: RIP calculation with the RIPcal package after alignment of all copies with ClustalO. Each color represents the frequency of RIP-like mutations (C→T mutations or conversely G→A mutations) according to type (different dinucleotide environment) across the length of the TE (x-axis) in a 50bp sliding window. **C**: Neighbour-joining phylogenetic tree based on alignment of the predicted protein of every TE (denoted by an asterisk in the tree) and its 15 best blastp hits. No outgroup was set and the trees are mid-point rooted. The predicted protein was determined from an expressed copy of the TE (as determined by inspecting the RNAseq read mapping).

4.4.5 Unbalanced RIP between core and supernumerary genome

RIPped copies of TEs were only detected on the core genome (**Figure 4.6** and **Table 4.6**). RIPcal profiles as exemplified in **Figure 4.8** showed that for 13 out of 34 TE families CpA → TpA mutations are predominant, which is characteristic for RIP, while also the CpT → TpT dinucleotide is a preferred secondary target for RIP.

In three cases, low complexity regions on the supernumerary genome resembled RIP of intact elements. These also contained most transversions when compared to genuinely RIPped copies. An example is given in **Table 4.7**.

Table 4.7 - RIP-like mutations in RLG_*Maggy* on the supernumerary genome. The intact element (not RIPped, located on the core genome) is compared with RIPped copies on the core chromosomes, and "RIP-like copies" (unknown) on the supernumerary genome. The total number of transitions and transversions compared to the intact reference (ref) is given, as well as the transition/transversion ratio, which is lower for the "RIP-like copies" on the supernumerary genome.

Sequence	Location	Length	GC%	Transitions	Transversions	Transition/ transversion ratio
Intact (ref)	Core	5684	55,2	0	0	
Intact	Core	5683	55,2	0	2	0,0
Intact	Core	5681	55,2	1	0	
Intact	Core	5677	55,2	0	0	
RIPped	Core	5992	16,4	2165	11	196,8
RIPped	Core	5762	15,4	2258	9	250,9
RIPped	Core	6022	12,2	2427	12	202,3
unknown	Supernumerary	3454	14,5	1340	112	12,0
unknown	Supernumerary	1157	16,7	445	51	8,7
unknown	Supernumerary	3455	14,5	1340	112	12,0
unknown	Supernumerary	1534	14,2	595	36	16,5
unknown	Supernumerary	1332	17,0	513	38	13,5
unknown	Supernumerary	1057	14,9	430	27	15,9

4.4.6 Transposable elements copy number is dynamic between isolates of the same species

The TE copy number variation among the isolates in this study is shown in **Table 4.8**. Based on genome coverage the most abundant element in isolate 2516 (DTM_*Drogon*) occurs only once in isolate bfb0173, a strain originating from China. As its ORF and TIRs are intact, it remains unknown why this element has not proliferated in isolate bfb0173. Isolates 2516 and 2548 were isolated from the same Belgian field at the same time, but show sharp differences in TE copy number. Two families that contain multiple copies in the Belgian isolates, are not

present as intact copies in the Chinese isolate (RLG_*Maggy*, DTM_*Hop7*). However, RIPped copies present in the genome of bfb0173 indicate that during the evolution of the lineage that isolate bfb0173 belongs to, intact copies of these families have been present but were effectively eradicated from the genome.

Table 4.8 - Prediction of TE numbers in the different *F. poae* isolates used in the study, as determined by a coverage-based method. Repeat families are classified in decreasing order of incidence in the genome of *F. poae* 2516; only class I and II transposable elements that are intact in *F. poae* 2516 are included, therefore elements such as the rDNA tandem and two families of telomere linked RecQ helicases are not in the table. X denotes families for which RIP was detected. It should be noted that average read coverage does not account for possible truncations and therefore the numbers in this table should be considered an estimate. For this reason, they do not completely line up with the figures in **Table 4.6** (which also separates the TEs according to their localization, something that is not possible with this coverage based method). The darker the grey shading of the isolate-TE combination, the more copies of this TE were detected with this coverage based method.

TE (down) / isolate (right)	2516		2548		7555		bfb0173	
DTF_*Drogon*	54		18		45		1	
DTF_*Fot5-A*	48	x	63	x	5	x	38	x
DTF_*Fot2*	37	x	21	x	28	x	17	x
RLG_*Maggy*	32	x	44	x	28	x	0	x
DTF_*ESP4-B*	32	x	58	x	76	x	34	x
DTA_*Nymeria*	25		19		35		9	
Rxx_*Marsu*	21		13		20		11	
DTF_*Fot3-B*	20	x	5		15		8	x
DTA_*Tfo1*	19		16		20		10	
DTF_*ESP4-A*	18		9		17		13	
DTA_*Hornet2*	18		12		19		16	
RLG_*Skippy*	17	x	6	x	7	x	9	x
DTA_*Drifter*	16		7		6		16	
DTF_*Viserion*	15	x	9	x	9	x	9	x
DTA_*Sarella*	14		8		12		8	
DTA_*Hornet3*	13		11		15		6	x
RLC_*Ghost*	12	x	7		16		8	
DTA_*RLT2*	12		6		8		5	
DTA_*Tfo2*	12		4		9		10	
DTA_*RLT1*	11		5		12		5	x
DTA_*RLT3*	10		10		13		9	
DTF_*Balerion*	10		7		11		4	
DTM_*Hop7*	10	x	14	x	16	x	0	x
DTA_*Obara*	9		12		7		8	
DTF_*Fot3-C*	9		7		9		8	
DTF_*Fot5-C*	8	x	89	x	63	x	4	x
DTA_*Obella*	7		6		5		7	
DTF_*Rhaegal*	7	x	6	x	7	x	2	x
DTM_*Hop4*	7		2		7		6	
DTA_*Hornet1*	6	x	23		10		6	x
DTF_*Fot5-B*	6		5		6		5	x
DTF_*Fot3-A*	6	x	4		4		3	
DTF_*Fot4*	1		0		1		1	
DTF_*Fot8*	1		1		1		0	
Total # of TEs	544		527		561		294	

Interestingly, RIP of certain elements seems isolate-specific, such as DTA_*RLT1* in isolate bfb0173 and RLC_*Ghost* in isolate 2516. A process similar to the loss of DTM_*Hop7* and RLG_*Maggy* in isolate bfb0173 may have occurred species-wide, as RIPped elements in isolate 2516 were detected of up to 14 families that no longer contain any intact copies in this isolate, or any other isolate in this study. For a retrotransposon of the Gypsy family, RIPped copies are present in all isolates, but only isolate 2548 contains intact copies.

4.4.7 Localization and divergence of transposable elements differs between the core and supernumerary genome

The localization and divergence of the intact TEs was investigated. One hundred and thirty-five intact TEs are present on the core chromosomes of isolate 2516 (**Table 4.6**). **Table 4.8** shows that elements of these families are often, but not always, present in multiple copies in the genomes of the other isolates in this study. However, read mapping shows that none of the 135 elements on the core chromosomes of isolate 2516 are present in the same location in isolates

2548, 7555 and bfb0173. An example is given in **Figure 4.9**. The integration of these elements therefore seems to have happened recently.

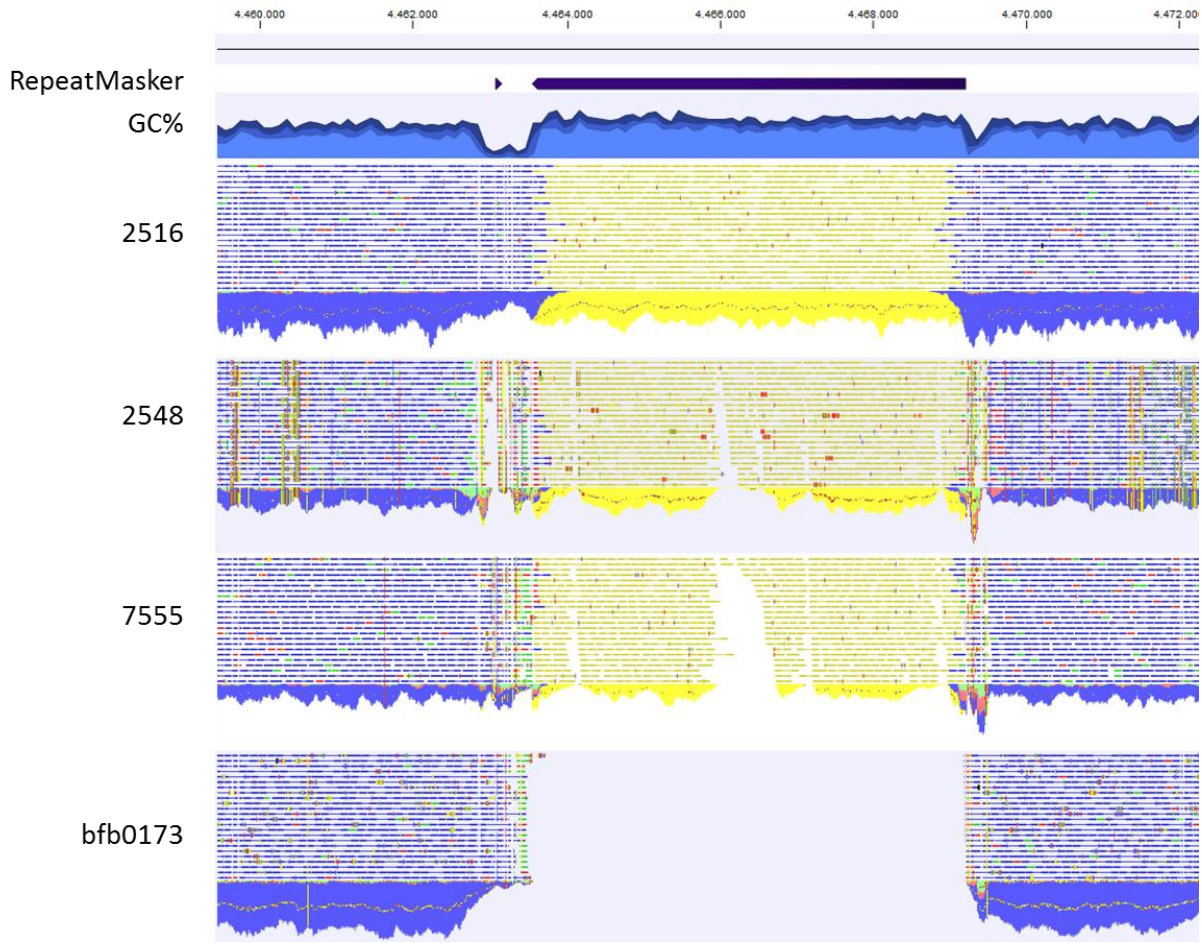

Figure 4.9 - Integration of a RLG_*Maggy* element in chromosome 4 of isolate 2516. Location of the TE is shown in the RepeatMasker track. Mapping of the HiSeq reads of isolates 2516, 2548, 7555 and bfb0173 is shown. This TE is not present at the same location in the other isolates. In isolate 2548 and 7555, no reads span the borders of the element (but the element is present in other locations in the genomes of isolates 2548 and 7555, and therefore reads for this sequence do exist). In isolate bfb0173, RLG_*Maggy* is not present at all. Yellow indicates that the reads could have mapped to other places in the genome of isolate 2516 as well.

In contrast, on the supernumerary genome of isolate 2516 elements can be found that show identical integration in isolate 2516 and one or more of the other isolates. **Figure 4.10** illustrates this for supernumerary contig 308. The four tracks show the TE presence (yellow diamonds) and genome coverage (lines) for every isolate. Several elements have identical flanks in all isolates, indicating that they are ancestral integrations (yellow diamonds that line up vertically in **Figure 4.10**). **Figure S4.1** shows the profile for supernumerary contigs 668, 561 and 550. Together these four contigs are the largest supernumerary contigs, totaling 1.26Mb. Whole blocks of sequence are absent from some isolates: most of contig 550 in isolate bfb0173, parts

of contig 561 in isolates 2548 and bfb0173. This absence/presence of sequence on the supernumerary genome is not cumulative for any one isolate or contig investigated. Moreover, the integration of TEs on the supernumerary genome is also not concordant with vertical inheritance. This is illustrated in **Figure S4.2**. The recombination-like picture of sequence absence/presence and TE integration, may reflect the dynamics the supernumerary chromosomes undergo during crossing.

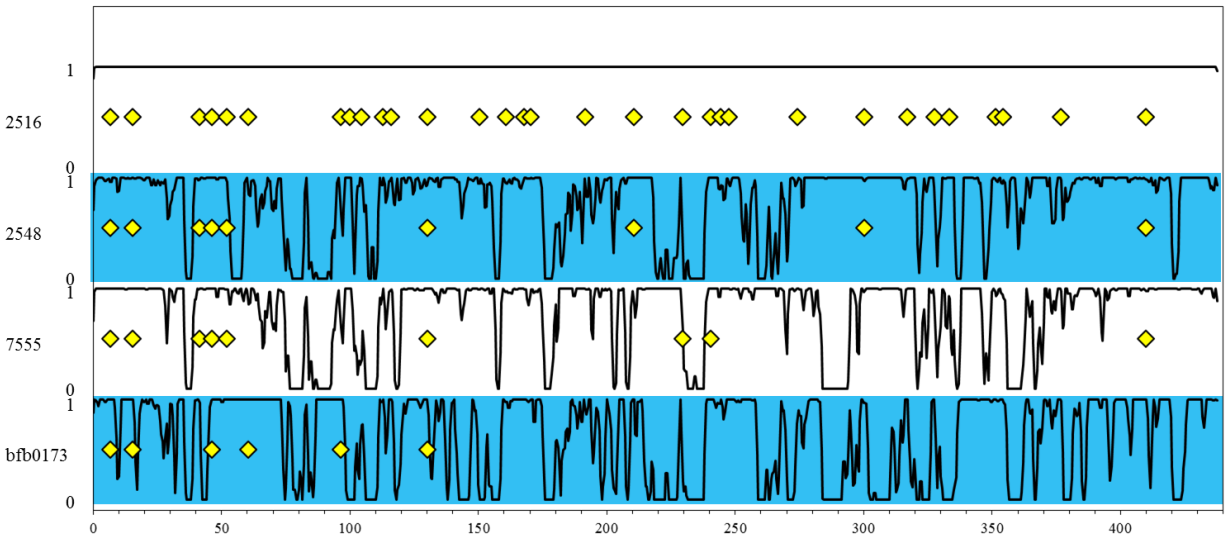

Figure 4.10 - Integration of intact TEs on supernumerary contig 308. The graphs shows in a sliding 1kb window the fraction of bases from the reference contig that is covered by HiSeq reads of every isolate (value between 0 and 1). The upper track shows all TEs on contig 308 of isolate 2516 that are >1kb and >90% identity to the element prototype with yellow diamonds. This TE landscape was used for comparison with isolates 2548, 7555 and bfb0173. Yellow diamonds for these three isolates indicate elements for which there is read mapping that an element has integrated in the exact same location as the element in isolate 2516 (and is therefore ancestral). Yellow diamonds that align vertically are conserved in multiple isolates.

A comparison was made between the estimated divergence time of TEs in the core genome and those in the supernumerary genome of isolate 2516. This is based on the principle that when TEs are present at a certain location for a longer period of time, they gradually accumulate more SNPs, which can be used to calculate the time elapsed since their insertion. As can be seen in **Figure 4.11**, TEs in the supernumerary genome are more divergent and are therefore presumed to result from more ancient transposition events.

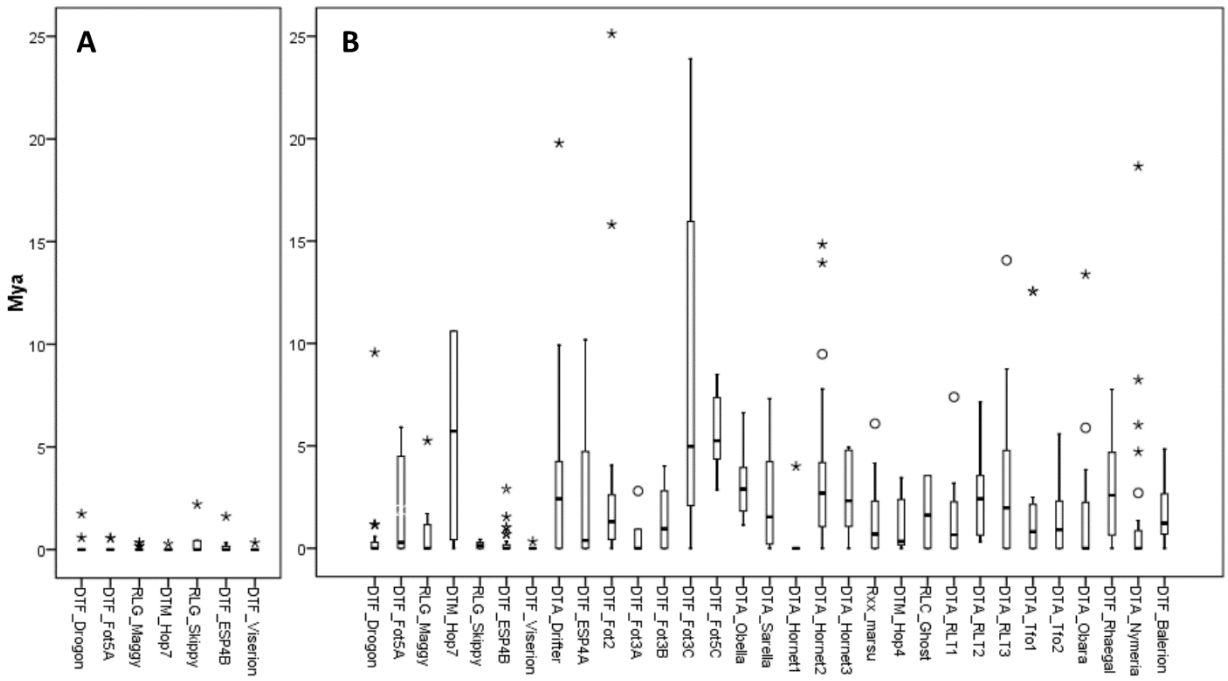

Figure 4.11 - Divergence estimation of intact (not RIPped) TE copies on the core (**A**) and supernumerary (**B**) genomes. Copies were aligned and branch lengths extracted from a maximum-likelihood phylogenetic tree. Branch lengths were used to calculate divergence times with a fixed substitution rate ($1.05 * 10^{-9}$ substitutions per site per year (Kasuga et al., 2002)). Y axis scale was cut off at 25 Mya, but for the supernumerary genome several extreme values are above this value (1 for DTF_*Fot5-A*, 1 for RLG_*Skippy*, 1 for DTF_*ESP4-B*, 3 for DTF_*Fot2*, 1 fot DTF_*Fot3-C*, 1 for DTF_*Fot5-C*, 1 for DTA_*Sarella*, 1 for DTA_*Hornet1*, 2 for DTA_*RLT1*, 1 for DTA_*RLT2*, 1 for DTA_*Tfo1* and 1 for DTA_*Tfo2*, all of them ranging between 25 Mya and 120 Mya). The boxes for every TE show the lower and upper quartile of the divergence estimates and the median (thick line within the boxes). The whiskers represent the minimum and maximum values. Circles and asterisks are outliers and extreme values which fall respectively outside of one-and-a-half additional box lengths and three additional box lengths counted from the upper quartile limit.

4.4.8 The core genome is invaded by transposable elements from the supernumerary genome

TEs on the supernumerary genome are more divergent than TEs on the core chromosomes (**Figure 4.11**) and some are present at identical sites in at least two isolates (**Figure 4.10**). We therefore wanted to test whether TEs in the core genome may originate from the supernumerary genome. This directionality was best illustrated by one element of RLG_*Skippy* located on the short arm of chromosome 3. This TE has recently integrated into the genome of isolate 2516 and contains 23 SNPs compared to the other copies on the core genome of this isolate. These 23 SNPs, together with one additional SNP, are also present in a copy on the supernumerary genome, that is at the exact same location for all isolates and therefore is an ancestral insertion.

The recent integration of TEs into the core genome of isolate 2516 has sometimes occurred within the coding region of genes. The environment of all 135 recent integrations in the core genome was investigated. Ten instances were found where integration disrupted a gene. Notably, DTF_*Drogon* integrations account for nine of these. Remarkable differences can be detected between the environments of the different TE families. DTF_*Fot5-A* elements consistently integrate within RIPped or low complexity (low GC%) environments, while DTF_*Drogon* elements have integrated within regions of average GC% (46.00% averaged over the entire core genome).

An extreme case of core genome invasion is found near the telomere of the long arm of chromosome 3. Two sequence blocks do not show any synteny with *F. graminearum*, with coordinates 115 073-319 336 bp (204kb) and 883 738-1 348 064 bp (464kb). Analysis of the flanking sequences of these two regions shows that they are continuous in isolates 2548, 7555 and bfb0173. Therefore, these regions represent translocations of supernumerary sequence to the core genome of isolate 2516. All parameters that were used to compare the core and supernumerary genome in this study, support the classification of these sequence blocks as supernumerary sequence (they contain no RIPped TEs, a high concentration of TEs and several gene paralogs). For the purpose of this study they have been regarded as part of the "supernumerary genome". The 204kb insertion is an underestimate as a stretch of 5000 "N"s was inserted at 150kb into chromosome 3 during the assembly phase, where presumably one or more of the 172 supernumerary contigs belong – all of which are larger than 5000 bp.

These insertions into the core genome, both of single TEs and whole blocks of supernumerary sequence, may have large implications for the organism such as respectively gene disruptions (as illustrated above for 10 TE insertions) and hampered meiotic alignment (as parts of chromosome 3 of an isolate with the supernumerary sequence insertions will not be able to align with the chromosome 3 of an isolate that does not have the insertions). We investigated how common the two supernumerary sequence translocations are in a population of 69 *F. poae* isolates and found that eight isolates contain the first insertion, closest to the telomere. These eight isolates were isolated from three different locations in Belgium. Three of these eight isolates also contain the second insertion, at 883 738 bp into chromosome 3 (**Table S4.1**). Isolate 2516 is one of these three isolates. Isolates 2548, 7555 and bfb0173 were confirmed not to have any of the insertions. **Figure 4.12** shows the strategy and gel electrophoresis for the detection of the two insertions.

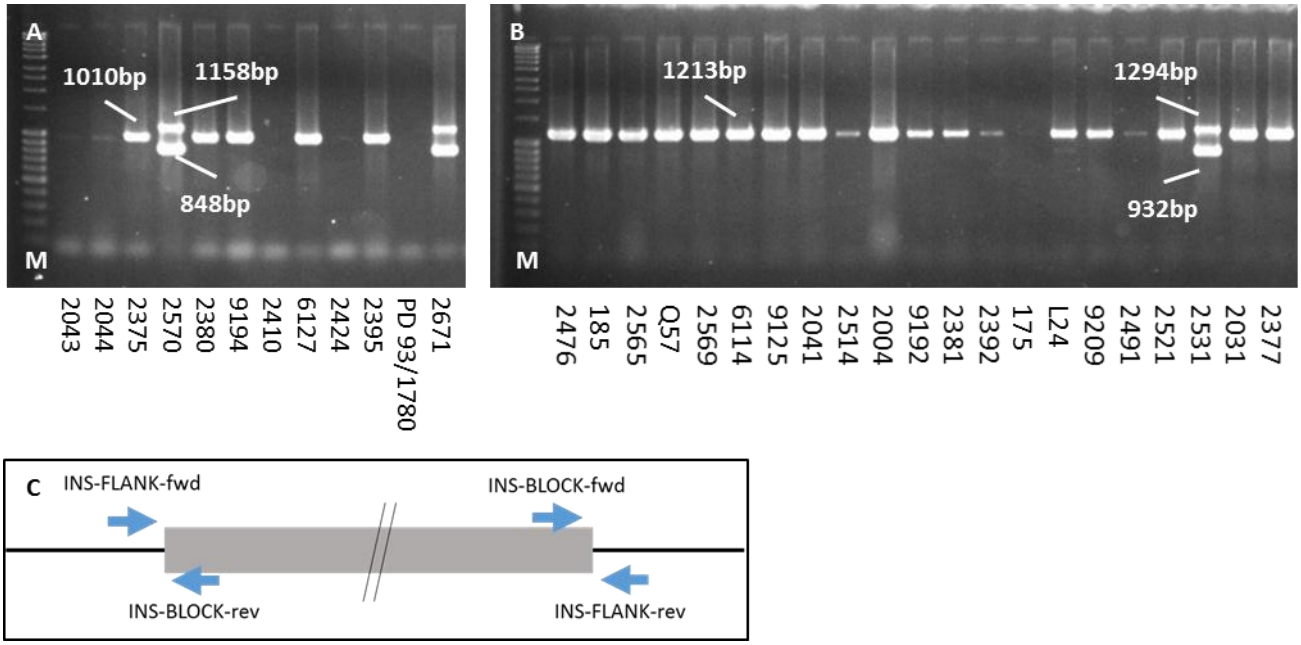

Figure 4.12 - Gel electrophoresis and PCR schematic for two major insertions into chromosome 3. **A**: insertion 1 at 115-319kb of chromosome 3. A single amplicon of 1010 bp is formed in the absence of the insertion (primers INS1-FLANK-fwd + INS1-FLANK-rev), for example isolates 2375 and 2380. When the insertion is present, two amplicons of 848 bp (INS1-FLANK-fwd + INS1-BLOCK-rev) and 1158 bp (INS1-BLOCK-fwd + INS1-FLANK-rev) are formed, for example isolates 2570 and 2671. M is for the molecular weight marker (Thermofisher's Massruler DNA Ladder Mix). **B**: insertion 2 at 883-1.348 kb of chromosome 3. A single amplicon of 1213 bp is formed in the absence of the insertion (primers INS2-FLANK-fwd + INS2-FLANK-rev), for example isolates 2476 and 185. When the insertion is present, two amplicons of 932 bp (INS2-FLANK-fwd + INS2-BLOCK-rev) and 1294 bp (INS2-BLOCK-fwd + INS2-FLANK-rev) are formed, for example isolate 2531. M is for the molecular weight marker (Thermofisher's Massruler DNA Ladder Mix). **C**: An impression of the PCR schematic is given, the principle is the same for both insertions. It is not certain what caused the PCR reaction to fail repeatedly for certain isolates, and divergence at the sequence level may be one explanation.

4.4.9 The supernumerary genome is a refuge for duplicated genes

The absence of paralogs is a hallmark of a RIP-active species (Cuomo et al., 2007). In a blastn (expect value < $1e^{-5}$) of all genes on the core chromosomes against themselves, no hits with nucleotide identity >80% and lengths above the RIP length threshold (+/- 1000 nucleotides; Watters et al. (1999)) were found. This confirms that the core chromosomes are subjected to RIP. Subsequently, all genes on the supernumerary genome were queried against those on the core genome with blastn (expect value < $1e^{-5}$). Eighty-one hits above the RIP length threshold show nucleotide identity exceeding 80% and represent paralogs that have not been inactivated by RIP. A total of 31 genes on the core chromosomes have one or more duplicates in the supernumerary genome, totaling 81 hits on the latter. **Figure 4.6** visualizes these paralogs as

lines connecting both the gene on one of the four core chromosomes and its paralog(s) on the supernumerary genome.

Table S4.2 lists the functional annotation of these duplicated genes. Notable instances include key component of the RNA silencing machinery *Dicer2* (Segers et al., 2007) and secondary metabolite backbone gene *PKS8* (Hansen et al., 2015). To ascertain that these paralogs are not artefacts from the assembly, the duplicated sequences and their 500bp flanking regions were aligned. Potential assembly artefacts are identified by sequence alignments with nearly 100% sequence identity across the entire region. Four of the 81 paralogs on the supernumerary genome were identified as potential double assemblies at the extremes of contigs which follow each other in the assembly, as is explained in section 4.4.3 (asterisks in **Table S4.2**). **Figure 4.13** shows examples of both a genuine paralog and an instance of two identical genes that is likely caused by double assembly.

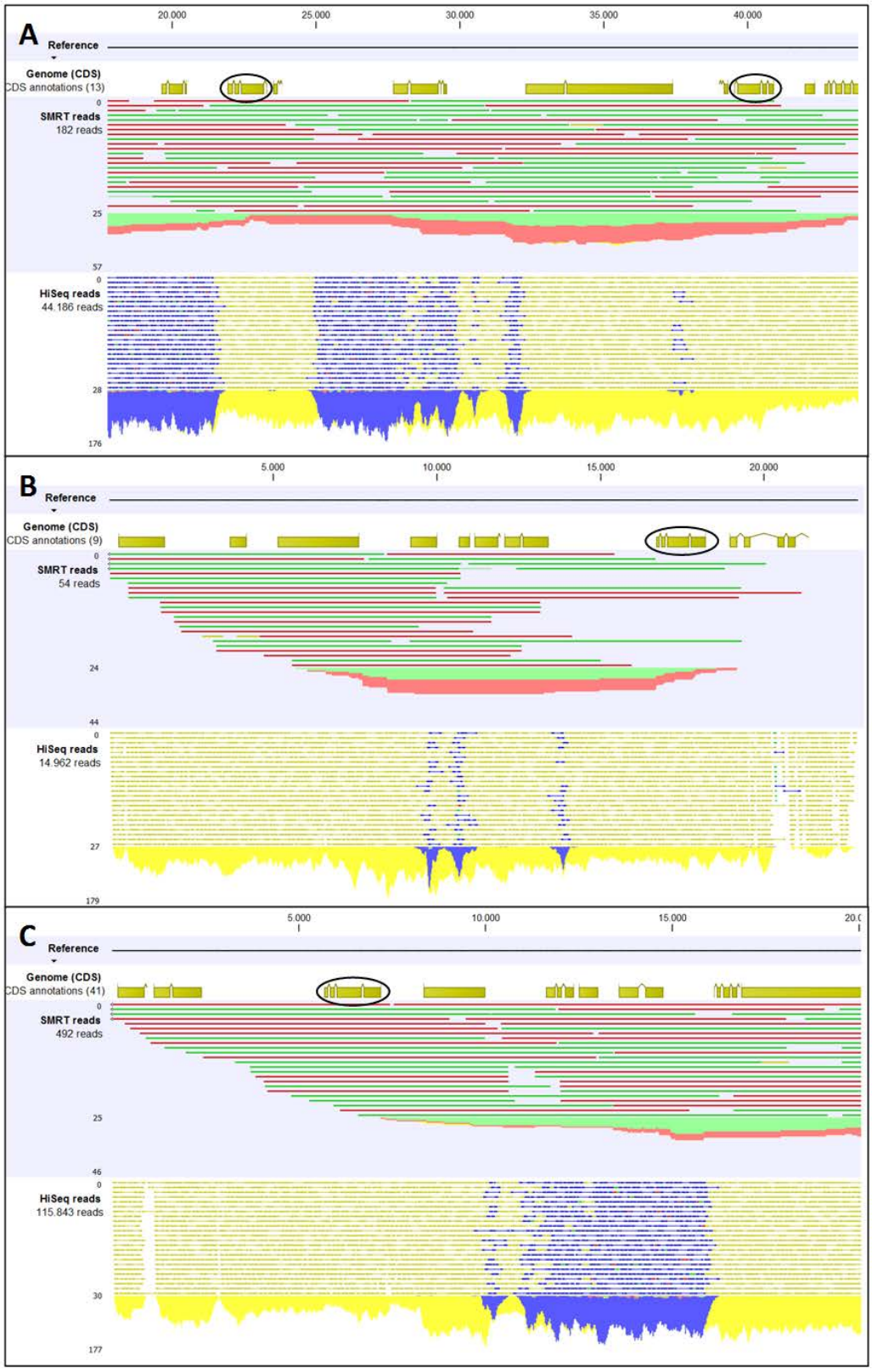

Figure 4.13 - Genuine duplicated gene (**A**) and likely double assembly (**B** and **C**). Upper track in every panel: CDS annotations. Second track: mapping of the SMRT reads; green and red represent forward and reverse reads respectively. Lower track: mapping of the HiSeq reads of isolate 2516. Yellow reads represent reads that could have fit equally well on another place of the genome (repetitive sequence). Blue reads represent paired reads. The peaks below the reads give an impression of overall read

coverage. **A**: two identical genes (circled in black, g12962 and g12967) on contig 459, separated by 20kb of sequence. SMRT read mapping shows contiguous sequence without assembly mistakes. **B** and **C**: identical genes (circled in black) are present at respectively the end of contig 440 (g12779 at 17kb of the 23kb contig) and the beginning of contig 441 (g12783 at 6kb into the contig). Note the untangling of the SMRT reads near the end of the contig 440, where the assembler presumably stalled. The environment of the "duplicated genes" is identical in both instances. This is likely a case of double assembly.

While duplication from a gene on the core genome is the most likely origin of the detected paralogs on the supernumerary genome, there are other potential origins such as horizontal gene transfer. The detected paralogs of an aspartic peptidase, *PKS8* and *Dicer2* were investigated for their phylogeny. The result can be found in **Figure 4.14**. For the aspartic peptidase (**A**) the paralog on the supernumerary genome may be older than its paralog on the core genome of *F. poae* and its homologs in related *Fusarium* species. For *PKS8*, phylogeny supports the notion that the paralogs on the supernumerary genome are duplications from the gene on the core genome. For *Dicer2* (**C**), phylogeny is inconclusive for one copy on the supernumerary genome (g14523 on contig 658), but for the other paralogs duplication and divergence from the gene on the core genome is most plausible. The inclusion of *Dicer2* from *F. langsethiae* within the clade of paralogs on the supernumerary genome of *F. poae* is unexpected.

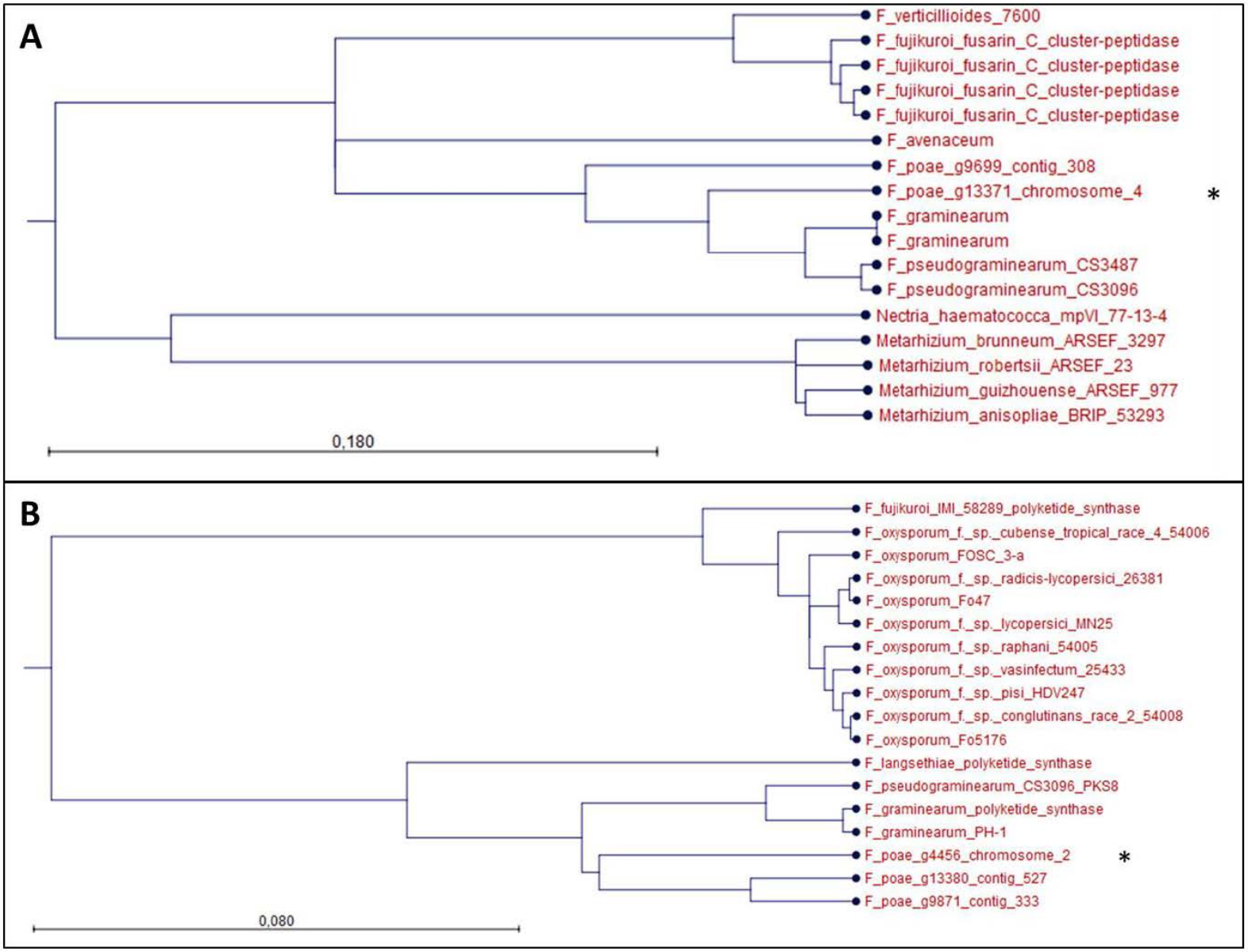
A
F_verticillioides_7600
F_fujikuroi_fusarin_C_cluster-peptidase
F_fujikuroi_fusarin_C_cluster-peptidase
F_fujikuroi_fusarin_C_cluster-peptidase
F_fujikuroi_fusarin_C_cluster-peptidase
F_avenaceum
F_poae_g9699_contig_308
F_poae_g13371_chromosome_4
*
F_graminearum
F_graminearum
F_pseudograminearum_CS3487
F_pseudograminearum_CS3096
Nectria_haematococca_mpVI_77-13-4
Metarhizium_brunneum_ARSEF_3297
Metarhizium_robertsii_ARSEF_23
Metarhizium_guizhouense_ARSEF_977
Metarhizium_anisopliae_BRIP_53293
0,180
B
F_fujikuroi_IMI_58289_polyketide_synthase
F_oxysporum_f._sp._cubense_tropical_race_4_54006
F_oxysporum_FOSC_3-a
F_oxysporum_f._sp._radicis-lycopersici_26381
F_oxysporum_Fo47
F_oxysporum_f._sp._lycopersici_MN25
F_oxysporum_f._sp._raphani_54005
F_oxysporum_f._sp._vasinfectum_25433
F_oxysporum_f._sp._pisi_HDV247
F_oxysporum_f._sp._conglutinans_race_2_54008
F_oxysporum_Fo5176
F_langsethiae_polyketide_synthase
F_pseudograminearum_CS3096_PKS8
F_graminearum_polyketide_synthase
F_graminearum_PH-1
F_poae_g4456_chromosome_2
*
F_poae_g13380_contig_527
F_poae_g9871_contig_333
0,080

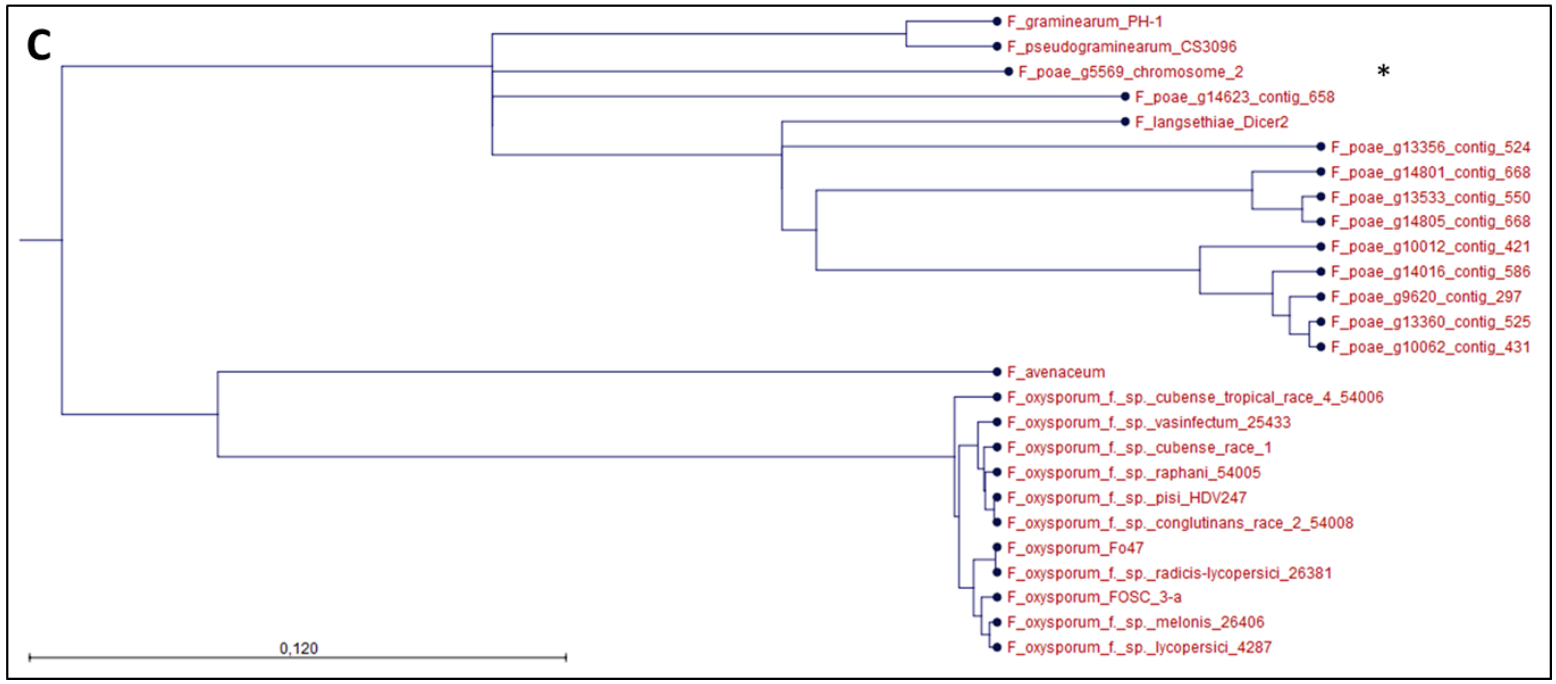

Figure 4.14 – Phylogenetic tree based on the detected paralogs of three genes. For every case, the potentially duplicated gene on the core genome was queried against the nonredundant NCBI protein database and the 15 best hits were used together with the query and the paralogs in the supernumerary genome for alignment with ClustalO. The resulting neighbor joining tree is shown, for which midpoint rooting was used. The *F. poae* gene on the core genome is denoted with an asterisk. If any annotation of the 15 hits was included, this was added to the labels in the tree. **A**: aspartic peptidase (core g13371, one paralog on the supernumereary genome g9699). **B**: *PKS8* (core g4456; two paralogs on the supernumerary genome g9871 and g13380). **C**: *Dicer2* (core g5569; 10 paralogs on the supernumerary genome included in the analysis).

4.5 Discussion

Chromosomes that vary in both size and number, and have an uneven distribution among individuals of the same species, have been described in animals (Vujosevic and Blagojevic, 2004), plants (Jones and Houben, 2003) and fungi (Galazka and Freitag, 2014). Throughout these kingdoms they are identified as supernumerary, accessory, dispensable or B chromosomes, in contrast to the core or A chromosomes. These supernumerary chromosomes show distinct features compared to the core chromosomes: they can be high in repeats and transposable elements (Coleman et al., 2009), have different gene density and function (Jones, 1995) and/or GC-content (Goodwin et al., 2011), can be transmitted by horizontal transfer (Ma et al., 2010) and are unstable in meiosis (Wittenberg et al., 2009). This sharp contrast between the two sets of chromosomes can be explained by different evolutionary pressure, different origins, or a combination of both (Mehrabi et al., 2011; Croll and McDonald, 2012). The functions of the supernumerary chromosomes are unclear. Speculations range from selfish DNA fragments without benefit to the host (Nur et al., 1988) to components that are critical for pathogenicity and survival (Ma et al., 2010). As they occur in the same nucleus, this raises questions how the different sub-genomes are managed within the organism and if there are potential conflicts and interactions. The dynamics between the core genome of an organism and its extra-chromosomal DNA have been studied for plasmids in bacteria (Godfrey et al., 2011), and mitochondrial DNA insertions into the nuclear genome of many eukaryotes (Hazkani-Covo et al., 2010). In this study we aimed to elucidate the differences between the two genomic components, to identify a cause for these differences, and to investigate any resulting genetic exchange that occurs between the core and supernumerary chromosomes.

We analyzed the genome of *Fusarium poae*, a species previously shown to contain supernumerary chromosomes based on pulse field gel electrophoresis (Fekete and Hornok, 1997), and compared it to its well-studied related species *F. graminearum* that only contains four core chromosomes. For this comparison a high quality genome assembly and annotation of *F. poae* was generated. The assembly using SMRT long reads allowed the division of the genome into a core and supernumerary component, a feature that was not possible with the assembly using short reads due to the presence of highly repetitive DNA. A novel genome annotation pipeline was used to annotate the genome of *F. poae* (Hoff et al., 2015). This method uses RNAseq data as extrinsic evidence, and is particularly suited for gene-dense genomes as it extracts only intron information from the RNAseq data, and therefore hybrid gene models

due to overlapping UTRs become less of a concern (Yandell and Ence, 2012). The BUSCO analysis showed that the machine annotation of the *F. poae* genome is of a high quality.

The core chromosomes of *F. poae* showed a high level of macrosynteny with *F. graminearum* and cover the entire *F. graminearum* sequence complement. They showed characteristics of chromosomes under the control of RIP, such as inactivated TEs and no gene paralogs with high sequence identity. The opposite is true for the supernumerary chromosomes, and the absence of RIP on the supernumerary genome is responsible for the differences between the core and supernumerary genome in *F. poae*. Indeed, on the supernumerary chromosomes, no RIPped TE copies are found, and at least 81 duplicated genes are present. This is the first time a clear reason is identified for the sharp contrast between the core and supernumerary chromosomes in a fungal pathogen.

The different rules that govern the core and supernumerary chromosomes make it possible for a genetic exchange to occur between them. We found several cases of exchange of genetic material between the core and supernumerary genomes. Thirty-one genes from the core chromosomes have been duplicated to the supernumerary genome, where some of these genes have undergone further copy number expansion (leading to 81 paralogs on the supernumerary genome). *Vice versa*, transposable elements originating from the supernumerary genome have integrated into the core chromosomes and, in 10 instances have led to gene disruptions. Most drastically, large sequence blocks (>200 kb) have been translocated from the supernumerary genome to the core chromosomes. Translocation of whole regions from supernumerary chromosomes to core chromosomes is not restricted to *F. poae*. A region of core chromosome 1 of *F. oxysporum* f. sp. *lycopersici* has all the characteristics of supernumerary sequence (Ma et al., 2010; Galazka and Freitag, 2014). It has been shown that this region is highly syntenic with one of its supernumerary chromosomes (Zhao et al., 2014). This situation may have arisen from ancient translocation followed by chromosome gain, or by duplication and integration of the supernumerary sequence into the core chromosome. Our results show that unique events such as large insertions into the core chromosomes give rise to novel genotypes in *F. poae*, which may be able to rapidly spread as they were recovered from three different locations. Interestingly, both in *F. poae* and *F. oxysporum* f. sp. *lycopersici*, insertion of blocks of supernumerary sequence has occurred close to a telomere of core chromosomes, which supports the finding that core chromosomes in *Fusarium* species may be divided into distinct chromosomal regions on both structural and functional levels (Connolly et al., 2013; Zhao et al., 2014).

The evolutionary advantage of a genomic region not burdened by RIP defense is evident from the duplicated genes occurring specifically on that region. In *Metarhizium*, it has been hypothesized that an arrest of RIP was instrumental in the evolution to generalist infection agents (Hu et al., 2014), and the advantages of a temporary RIP relaxation or arrest may include accelerated evolution and divergence between related species (Stukenbrock and Croll, 2014). The mechanism that gave rise to the existence of supernumerary chromosomes in *F. poae* is unknown. In *Z. tritici*, it has been suggested that supernumerary chromosomes may have originated from core chromosomes and subsequently degenerated and evolved separately (Croll et al., 2013). A recent large scale duplication seems unlikely for *F. poae*, as an ancient MITE (occurring in the same genomic locations for the four isolates in this study) that characterizes the core chromosomes is completely absent from the supernumerary chromosomes. The contribution of horizontal chromosome transfer remains to be investigated, but has likely contributed to the supernumerary chromosome diversity in other species (Ma et al., 2010; Hu et al., 2012). **Figure 4.14** showed that phylogeny of paralogs on the supernumerary genome does not necessarily line up with duplication and divergence from the counterpart on the core genome. It will be interesting to investigate whether horizontal gene transfer from related *Fusarium* species has played a role in the occurrence of paralogs on the supernumerary genome, but regardless, these paralogs have not been inactivated by RIP.

Specific exclusion of duplicated genes from RIP has been observed before in *F. solani* (formerly known as *N. haematococca*) (Coleman et al., 2009). Similar to those in *F. poae*, its supernumerary chromosomes are rich in TEs and duplicated genes. It was experimentally determined that progeny, of which one of the parents contained two copies of the hygromycin phosphotransferase marker gene, contained both an intact and a RIPped copy of that gene (Coleman et al., 2009), contrary to the standard *modus operandi* of RIP wherein all copies are inactivated. Apparently, a region in the genome of *N. haematococca* is excluded from RIP, but it is not known whether this coincides with the supernumerary chromosome(s). The regional variability of RIP extends beyond supernumerary chromosomes however. Nucleolus organizer regions (NORs) contain the rDNA tandem repeats in many fungal species, and within this region they are protected from RIP (Galagan and Selker, 2004). Either this is an active form of protection, which may be similar to what is happening on the supernumerary chromosomes of *F. poae*, or rDNA is mutated by RIP and mutated copies subsequently undergo reduced intrachromosomal recombination to give rise to a full-length rDNA tandem during meiosis (Pomraning, 2012).

As is described above, *F. poae* is not the only *Fusarium* species with supernumerary chromosomes. Analyses similar to those in this study have not been carried out for *F. solani* and *F. oxysporum*. In the former, RIP was experimentally demonstrated but localization of RIPped TEs has not been investigated, and potential paralogs occur on all chromosomes (Coleman et al., 2009). *F. oxysporum* is considered an asexual species and therefore likely does not have active RIP. Several other *Fusarium* have been shown to contain supernumerary chromosomes, such as *F. asiaticum* (Galazka and Freitag, 2014), *F. sporotrichioides* (Fekete et al., 1993) and *F. langsethiae* (Lysoe et al., 2015), but contiguous assemblies are lacking for these species. It is therefore difficult to assess whether or not our findings in *F. poae* are directly applicable to other *Fusarium* species or not.

Balancing clonal propagation with intermittent sexual reproduction is a key trait of a successful pathogen system (Li et al., 2012; Wicker et al., 2013). The sexual cycle has never been shown for *F. poae*, but in light of the findings in this study is highly likely to occur. Indeed, RIPped copies in isolate 2516 are not shared with the other sequenced isolates and therefore were independently inactivated in this isolate or its ancestors. Additionally, several isolates contain RIPped copies of families that are not RIPped in the other isolates. Since RIP is isolate-specific, we conclude that in *F. poae* RIP is an active process that periodically inactivates TEs that have integrated in the core chromosomes since the last sexual cycle. This also confirms that *F. poae* should be a sexual species, which has been speculated in the past (Kerenyi et al., 2004). The tight correlation between RIP and meiosis should offer opportunities for understanding the balance between clonal and sexual reproduction, by using TE insertions as markers for "track and trace" studies and monitoring when/if they become RIPped. Species capable of combining both sexual and asexual reproduction, and containing an active arsenal of transposable elements, are considered to be the biggest challenges for durable disease management (McDonald and Linde, 2002). In this study, the clonal spread of novel genotypes and indications for an active sexual cycle were found for *F. poae*.

Meiosis and RIP may not have happened for isolate 2516 very recently, allowing for the modest accumulation of intact TEs on the core genome during asexual propagation. The demonstrated gene disruptions that these TE insertions caused, may account for the instability of single spore cultures previously reported for *F. poae* (Kerenyi et al., 1997). Isolate bfb0173 generally had lower numbers of TEs and several families have become completely extinct in this isolate (with only RIPped copies still present). Frequent meiosis, associated with frequent RIP and the possibility for loss of supernumerary chromosomes and the reservoir of TEs that they contain,

could account for such extinction events. Whether bfb0173, a Chinese isolate, is indeed part of a sexually more active population is unknown. Geographical differences in sexual activity have been demonstrated before in *Magnaporthe oryzae* (Saleh et al., 2012). The skewed mating type distribution within a set of Belgian *F. poae* isolates may indicate that meiosis does not occur at high frequency in that population.

The occurrence of both recently integrated intact TEs as well as recently RIPped copies, side by side in the genome has not been observed before. Most of the previously sequenced fungi verge towards either extinction of TEs (*F. graminearum, F. solani, Z. tritici* (Cuomo et al., 2007; Coleman et al., 2009; Dhillon et al., 2014)), or heavy proliferation with little to no genome defense (*F. oxysporum* f. sp. *lycopersici, P. tritici-repentis* (Ma et al., 2010; Manning et al., 2013)). A recent study investigated the TE/RIP landscape for 49 ascomycete fungi (Clutterbuck, 2011). For many of these species, signatures of RIP could be ancient and therefore may not indicate active RIP. In *F. oxysporum*, the RIP signatures investigated were specifically found on the core rather than the supernumerary chromosomes. In *Aspergillus oryzae*, fragments of AT-rich TEs were attributed to an ancient wave of TE amplification and RIP, with intact elements constituting a more recent wave (Clutterbuck, 2011). In *F. poae* three low complexity alleles on the supernumerary chromosomes resemble RIP, but these also contain high levels of transversions, and they may therefore be ancient RIPped copies that have since diverged.

It is thought that RIP functions after plasmogamy but before the final pre-meiotic DNA replication and karyogamy. It works multiple times during the rounds of nuclear division that occur at this point, presumably during G1 or near the replication fork during the S phase (Pomraning, 2012). It functions only in the nucleus, or nuclei, that contain(s) DNA duplications and does so on a single DNA strand. Mis-pairing of duplicated DNA has been hypothesized to deliver the substrate for RIP (Pomraning, 2012). Why supernumerary chromosomes in *F. poae* escape RIP is unknown. While physical alignment of duplicated copies is presumed to be important, the exact scanning mechanism for homology is unknown. Clutterbuck (2011) proposed two hypotheses for the function of RIP that implicate either the temporal or the spatial proximity of haploid nuclei in dikaryotic cells, where RIP acts, to diploid cells undergoing meiotic pairing. This pairing was previously shown to be hampered for supernumerary chromosomes through their high variability (Wittenberg et al., 2009). The splice form of the *rid* gene, shown to be vital for RIP, that was detected in this study does not lead to a functional protein. One explanation for this may be that the gene model constitutes a case of crucial alternative splicing, and the *rid* gene is only correctly spliced in the pre-meiotic phase.

Supernumerary or extra-chromosomal structures are considered to be evolutionary cradles for pathogenicity in viruses, bacteria and fungi, as they often contain the determinants for successful infection of the host (Croll and McDonald, 2012). In our study, we determined that the supernumerary genome in the prominent plant pathogen *F. poae* is governed by different rules than the core chromosomes. Whether the regional selectivity of RIP explains the differences between the core and supernumerary genomes in other pathogenic fungi remains to be seen. Regardless, the co-occurrence of the core and the supernumerary genome within the same nucleus, "living apart together" as they are separate entities but with significant interaction, bestows the organism with unique tools for rapid adaptation and evolution. Future investigation will also have to show whether this gives *F. poae* a competitive advantage over other species in the FHB complex, and whether any parallels can be drawn with related species. Moreover, a functional characterization of the duplicated genes will shed light on any advantages such as gene dosage effects or neofunctionalization that *F. poae* may have due to its supernumerary genome.

4.6 Supporting information

Table S4.1 – List of 69 *F. poae* isolates used in this study. Chapter 5 of this thesis includes more information on the source of the isolates and the way that they were single spored. For one isolate (isolate 2547), no mating type could be determined. Insertion 1 and insertion 2 are the two insertions of supernumerary sequence into chromosome 3 of eight respectively three *F. poae* isolates (insertion 1 closest to the telomere: 115-319kb into the chromosome; insertion 2: 883-1348kb into the chromosome).

ID	Location	Host	Year	Reference	Mating type	Insertion 1	Insertion 2
175	Aas, Norway	Barley	1996	CBS	MAT1-2	no amplicon	no
177	Aas, Norway	Wheat	1996	CBS	MAT1-1	no	no
182	Aas, Norway	Barley	1996	CBS	MAT1-1	no	no
185	Aas, Norway	Barley	1996	CBS	MAT1-1	no	no
1879	Bottelare, Belgium	Wheat	2010	this study	MAT1-1	no amplicon	no
2004	Zwevegem, Belgium	Wheat	2010	this study	MAT1-1	no	no
2019	Zwevegem, Belgium	Wheat	2010	this study	MAT1-1	no	no
2022	Zwevegem, Belgium	Wheat	2010	this study	MAT1-1	no	no
2023	Zwevegem, Belgium	Wheat	2010	this study	MAT1-1	no amplicon	no
2028	Zwevegem, Belgium	Wheat	2010	this study	MAT1-1	no	no
2031	Zwevegem, Belgium	Wheat	2010	this study	MAT1-1	no	no
2033	Zwevegem, Belgium	Wheat	2010	this study	MAT1-1	no	no
2041	Zwevegem, Belgium	Wheat	2010	this study	MAT1-2	no	no
2043	Zwevegem, Belgium	Wheat	2010	this study	MAT1-1	no	no
2044	Zwevegem, Belgium	Wheat	2010	this study	MAT1-2	no	no
2056	Zwevegem, Belgium	Wheat	2010	this study	MAT1-1	no	no
2371	Bottelare, Belgium	Wheat	2011	this study	MAT1-2	no	no
2375	Bottelare, Belgium	Wheat	2011	this study	MAT1-1	no	no
2377	Bottelare, Belgium	Wheat	2011	this study	MAT1-1	no amplicon	no
2380	Bottelare, Belgium	Wheat	2011	this study	MAT1-1	no	no
2381	Bottelare, Belgium	Wheat	2011	this study	MAT1-1	no amplicon	no
2390	Bottelare, Belgium	Wheat	2011	this study	MAT1-1	no	no
2392	Bottelare, Belgium	Wheat	2011	this study	MAT1-1	no	no

2395	Bottelare, Belgium	Wheat	2011	this study	MAT1-1	no	no
2410	Bottelare, Belgium	Wheat	2011	this study	MAT1-1	no amplicon	no
2411	Bottelare, Belgium	Wheat	2011	this study	MAT1-1	no	no
2424	Koksijde, Belgium	Wheat	2011	this study	MAT1-1	no amplicon	no
2476	Poperinge, Belgium	Wheat	2011	this study	MAT1-1	no amplicon	no
2491	Poperinge, Belgium	Wheat	2011	this study	MAT1-2	no amplicon	no
2514	Zwevegem, Belgium	Wheat	2011	this study	MAT1-1	no	no
2516	Zwevegem, Belgium	Wheat	2011	this study	MAT1-1	yes	yes
2517	Zwevegem, Belgium	Wheat	2011	this study	MAT1-1	no	no
2519	Zwevegem, Belgium	Wheat	2011	this study	MAT1-2	no	no
2521	Zwevegem, Belgium	Wheat	2011	this study	MAT1-1	yes	no
2524	Zwevegem, Belgium	Wheat	2011	this study	MAT1-1	no amplicon	no
2525	Zwevegem, Belgium	Wheat	2011	this study	MAT1-1	no	no
2531	Zwevegem, Belgium	Wheat	2011	this study	MAT1-1	yes	yes
2532	Zwevegem, Belgium	Wheat	2011	this study	MAT1-1	no amplicon	no
2547	Zwevegem, Belgium	Wheat	2011	this study	no amplicon	no	no
2548	Zwevegem, Belgium	Wheat	2011	this study	MAT1-1	no	no
2565	Zuienkerke, Belgium	Wheat	2011	this study	MAT1-1	yes	no
2569	Zuienkerke, Belgium	Wheat	2011	this study	MAT1-1	yes	no
2570	Zuienkerke, Belgium	Wheat	2011	this study	MAT1-1	yes	no
2571	Zuienkerke, Belgium	Wheat	2011	this study	MAT1-1	yes	no
2671	Linter, Belgium	Wheat	2011	this study	MAT1-1	yes	yes
6114	Denmark	Barley	1964	MUCL	MAT1-2	no amplicon	no
6127	Wageningen, the Netherlands	Wheat	1964	MUCL	MAT1-2	no	no
7555	Heverlee, Belgium	Wheat	1965	MUCL	MAT1-1	no amplicon	no
9125	Ferrara, Italy	Wheat	2005	Somma et al. (2010)	MAT1-1	no	no
9139	Ferrara, Italy	Wheat	2005	Somma et al. (2010)	MAT1-2	no amplicon	no
9181	Ferrara, Italy	Wheat	2005	Somma et al. (2010)	MAT1-2	no	no
9186	Ferrara, Italy	Wheat	2005	Somma et al. (2010)	MAT1-1	no	no
9189	Ferrara, Italy	Wheat	2005	Somma et al. (2010)	MAT1-1	no amplicon	no

9192	Ferrara, Italy	Wheat	2005	Somma et al. (2010)	MAT1-1	no	no
9194	Ferrara, Italy	Wheat	2005	Somma et al. (2010)	MAT1-1	no	no
9196	Ferrara, Italy	Wheat	2005	Somma et al. (2010)	MAT1-2	no amplicon	no
9203	Ferrara, Italy	Wheat	2005	Somma et al. (2010)	MAT1-1	no	no
9209	Ferrara, Italy	Wheat	2005	Somma et al. (2010)	MAT1-1	no amplicon	no
11456	Heverlee, Belgium	Barley	1968	MUCL	MAT1-2	no amplicon	no
15926	Quebec, Canada	Wheat	1970	MUCL	MAT1-1	no	no
30702	unknown	*In vitro* ornamental plant	1990	MUCL	MAT1-2	no	no
42824	Belgium	Wheat	2000	MUCL	MAT1-1	no	no
bfb0173	Shayang, Hubei, China	Barley	2005	Yang et al. (2008)	MAT1-1	no	no
PD 93/1780	The Netherlands	carnation	1993	dr. Cees Waalwijk	MAT1-1	no	no
F49	Ath, Belgium	Maize	2007	MUCL	MAT1-1	no amplicon	no
K46	Ath, Belgium	Maize	2007	MUCL	MAT1-1	no	no
L24	Buissenal, Belgium	Maize	2007	MUCL	MAT1-1	no amplicon	no
Q57	Buissenal, Belgium	Maize	2007	MUCL	MAT1-1	no amplicon	no
S46	Villeroux, Belgium	Maize	2007	MUCL	MAT1-1	no	no

Table S4.2 - Genes from the core that have been duplicated to the supernumerary chromosomes. Gene identifier for the core and supernumerary gene(s) are given as well as the blastn hit length and nucleotide similarity. Locations of the duplicated genes on the supernumerary genome are given. Finally the functional annotation of the gene on the core that was duplicated is detailed. Likely double assemblies are denoted by an asterisk.

Core ID	Supernumerary ID	Paralog location	%ID (nt)	Hit length (nt)	Functional annotation
g10194	g13851	Contig 566	89.49	2606	Peptidase C2, calpain family
g10194	g14036	Contig 587	90.73	1693	Peptidase C2, calpain family
g10194	g14344	Contig 640	91.48	1045	Peptidase C2, calpain family
g1026	g14359	Contig 640	87.05	1151	Hypothetical protein
g1026	g9930	Contig 415	86.94	1141	Hypothetical protein
g1026	g14362	Contig 641	87.09	1139	Hypothetical protein
g113	g13770	Contig 563	87.06	2287	Alpha-L-rhamnosidase

g11371	g9699	Contig 308	92.49	1118	Aspartic peptidase
g11386	g13752	Contig 563	88.32	1139	Hypothetical protein
g12303	g13087	Contig 475	90.08	1945	Kinetochore protein Ndc80
g12303	g14699	Contig 668	89.92	1945	Kinetochore protein Ndc80
g1343	g9986	Contig 419	92.67	1679	Hypothetical protein
g14	g13753	Contig 563	82.27	1190	P-loop containing nucleoside triphosphate hydrolase, exonuclease
g158	g14572	Contig 650	82.84	1795	Zn(2)-C6 fungal-type transcription factor
g1866	g14009	Contig 586	88.19	1745	Hypothetical protein; unintegrated signatures
g1866	g14550	Contig 649	87.99	1441	Hypothetical protein; unintegrated signatures
g1991	g9761	Contig 308	93.49	1244	Protein kinase
g1991	g14564	Contig 650	93.56	1243	Protein kinase
g2589	g14007	Contig 586	98.39	1868	Acyl-CoA dehydrogenase
g2589	g12736	Contig 439	98.39	1868	Acyl-CoA dehydrogenase
g2589	g9693	Contig 308	98.29	1868	Acyl-CoA dehydrogenase
g2589	g12964	Contig 459	98.18	1868	Acyl-CoA dehydrogenase
g2760	g13489	Contig 550	85.38	1881	DUF3468; Zn(2)-C6 fungal-type transcription factor
g2869	g9741	Contig 308	100	1457	S-adenosyl-L-methionine-dependent methyltransferase
g2869	g13637	Contig 561	98.76	1456	S-adenosyl-L-methionine-dependent methyltransferase
g3381	g13938	Contig 581	84.94	1720	Protein of unknown function DUF3468
g3381	g9962	Contig 417	84.94	1720	Protein of unknown function DUF3468
g3381	g9967	Contig 418	84.83	1720	Protein of unknown function DUF3468
g3381	g9960	Contig 416	84.89	1588	Protein of unknown function DUF3468
g3381	g14167	Contig 628	84.62	1443	Protein of unknown function DUF3468
g4456	g13380	Contig 527	86.68	8553	Polyketide synthase
g4456	g9871	Contig 333	85.72	2703	Polyketide synthase
g4537	g9765	Contig 308	90.17	1984	Zn(2)-C6 fungal-type transcription factor
g5515	g13454	Contig 550	84.58	1323	Hypothetical protein
g5515	g14578	Contig 650	84.43	1323	Hypothetical protein
g5515	g14662	Contig 668	84.43	1323	Hypothetical protein
g5515	g9814	Contig 315	84.43	1323	Hypothetical protein

g5515	g9578	Contig 293	84.2	1323	Hypothetical protein
g5515	g13063	Contig 475	84.13	1323	Hypothetical protein
g5515	g10071	Contig 431	84.57	1322	Hypothetical protein
g5515	g13672	Contig 561	84.42	1322	Hypothetical protein
g5515	g9582	Contig 293	84.42	1322	Hypothetical protein
g5515	g70	Chromosome 3	84.51	1278	Hypothetical protein
g5515	g14722	Contig 668	84.43	1278	Hypothetical protein
g5515	g14324	Contig 639	84.19	1278	Hypothetical protein
g5515	g13675	Contig 561	84.42	1271	Hypothetical protein
g5515	g13221	Contig 496	83.86	1270	Hypothetical protein
g5515	g13487	Contig 550	84.15	1243	Hypothetical protein
g5569	g13533	Contig 550	82.75	4619	Dicer2
g5569	g14805	Contig 669	82.57	3643	Dicer2
g5569	g9620	Contig 297	82.54	3609	Dicer2
g5569	g13360 *	Contig 525	82.57	3608	Dicer2
g5569	g13363 *	Contig 526	82.57	3608	Dicer2
g5569	g10062	Contig 431	82.48	3608	Dicer2
g5569	g14016	Contig 586	82.6	3574	Dicer2
g5569	g14801	Contig 668	81.46	2249	Dicer2
g5569	g13356	Contig 524	81.81	2012	Dicer2
g5569	g10012	Contig 421	83.3	1976	Dicer2
g5569	g14623	Contig 658	84.26	1703	Dicer2
g5569	g9601	Contig 293	83.71	1467	Dicer2
g5670	g9948	Contig 415	81.96	1386	CFEM superfamily
g5670	g12779 *	Contig 440	81.82	1386	CFEM superfamily
g5670	g12783 *	Contig 441	81.82	1386	CFEM superfamily
g5670	g13668	Contig 561	81.92	1372	CFEM superfamily
g5893	g13233	Contig 496	93.41	1442	Hypothetical protein
g5941	g57	Chromosome 3	94.46	2437	Hypothetical protein
g5941	g14743	Contig 668	95.29	1295	Hypothetical protein

g5941	g14744	Contig 668	93.59	1138	Hypothetical protein
g5942	g58	Chromosome 3	94.66	1218	Aminoglycoside 3-phosphotransferase
g6413	g12840	Contig 443	89.5	1362	Taurine catabolism dioxygenase TauD/TfdA
g6413	g12790	Contig 441	89.43	1353	Taurine catabolism dioxygenase TauD/TfdA
g7188	g9701	Contig 308	93.22	3185	P-type ATPase, subfamily IIA, SERCA-type
g7188	g13640	Contig 561	93.37	1433	P-type ATPase, subfamily IIA, SERCA-type
g7188	g13646	Contig 561	93.37	1433	P-type ATPase, subfamily IIA, SERCA-type
g7680	g9717	Contig 308	82.54	1329	Epoxide hydrolase-like
g8238	g13621	Contig 561	86.92	1713	Cytochrome P450
g8239	g13622	Contig 561	81.04	1271	Ankyrin repeat containing
g8240	g13623	Contig 561	88.91	1560	Ergosterol biosynthesis ERG4/ERG24
g8552	g14207	Contig 630	91.21	1354	Alfa/beta hydrolase fold
g8553	g14206	Contig 630	92.94	3653	Haem peroxidase; cytochrome P450
g8824	g13651	Contig 561	85.71	1001	Transketolase, bacterial-like

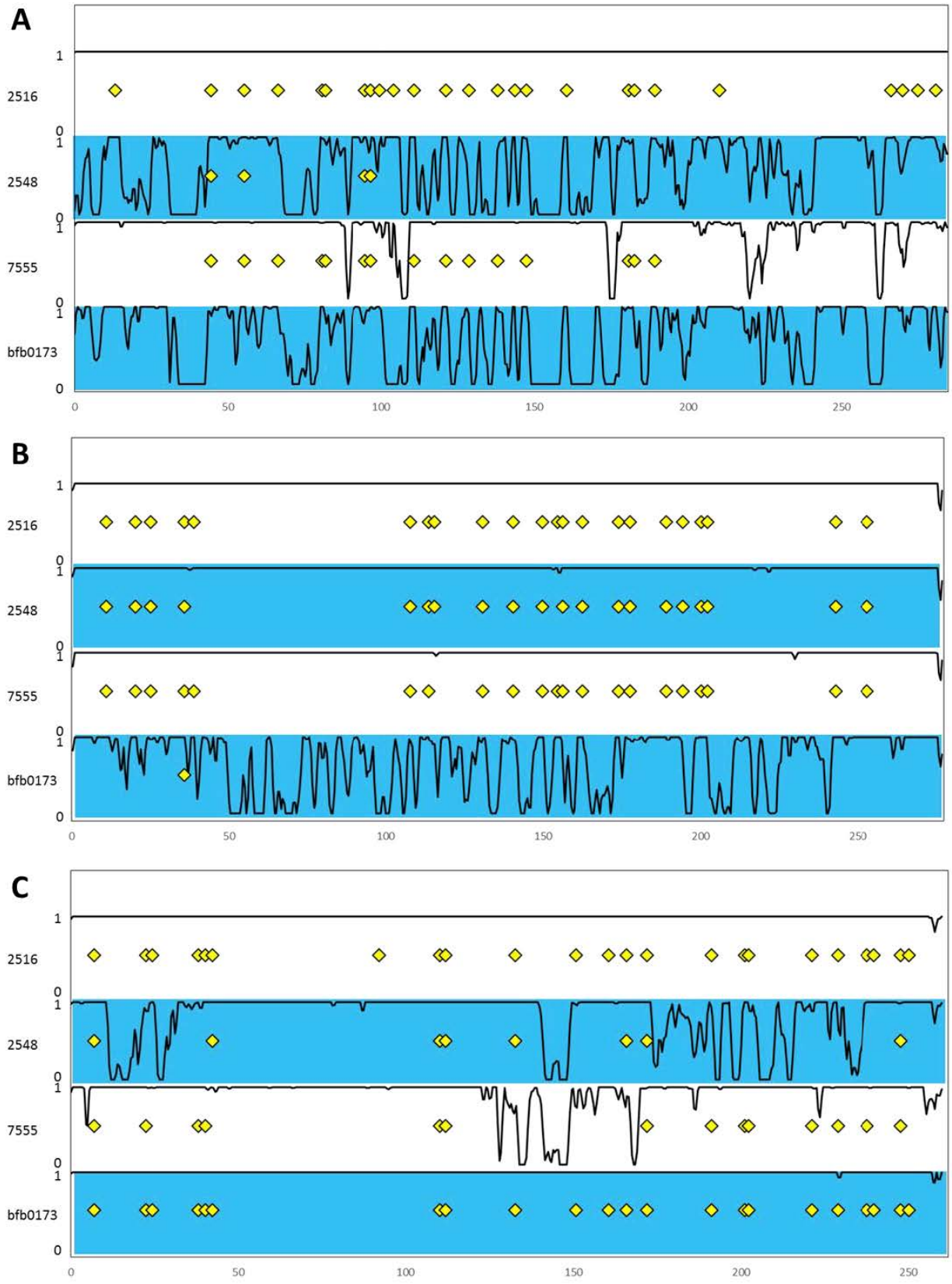

Figure S4.1 - Integration of intact TEs on supernumerary contigs 668 (**A**), 561 (**B**) and 550 (**C**). The graphs shows in a sliding 1kb window the fraction of bases from the reference contig that is covered by HiSeq reads of every isolate (value between 0 and 1). The upper track shows all TEs on contig 668,

561 and 550 of isolate 2516 that are >1kb and >90% identity to the element prototype with yellow diamonds. This TE landscape was used for comparison with isolates 2548, 7555 and bfb0173. Diamonds for these three isolates indicate elements for which there is read mapping that an element has integrated in the exact same location as the element in isolate 2516 (and is therefore ancestral). Diamonds that align vertically are conserved in multiple isolates.

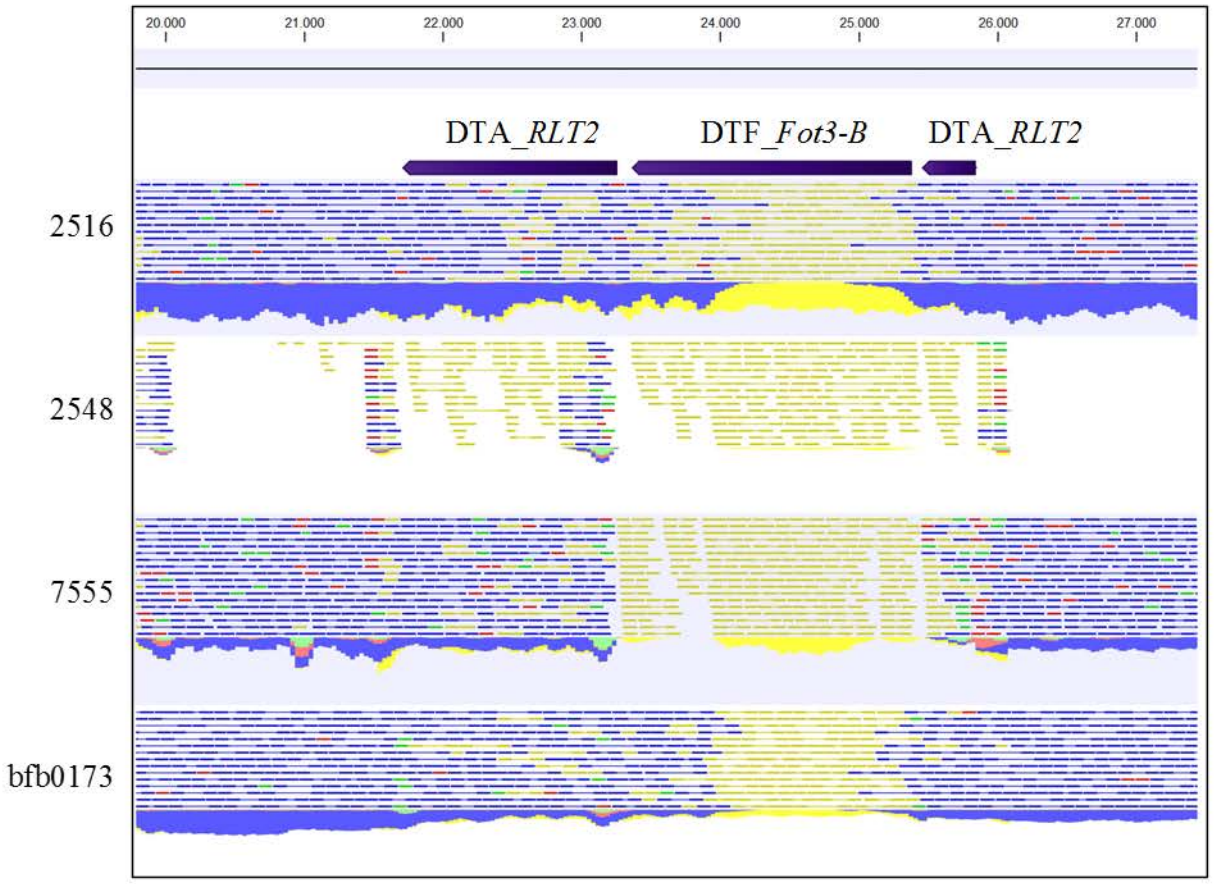
20.000
21.000
22.000
23.000
24.000
25.000
26.000
27.000
DTA_RLT2
DTF_Fot3-B
DTA_RLT2
2516
2548
7555
bfb0173

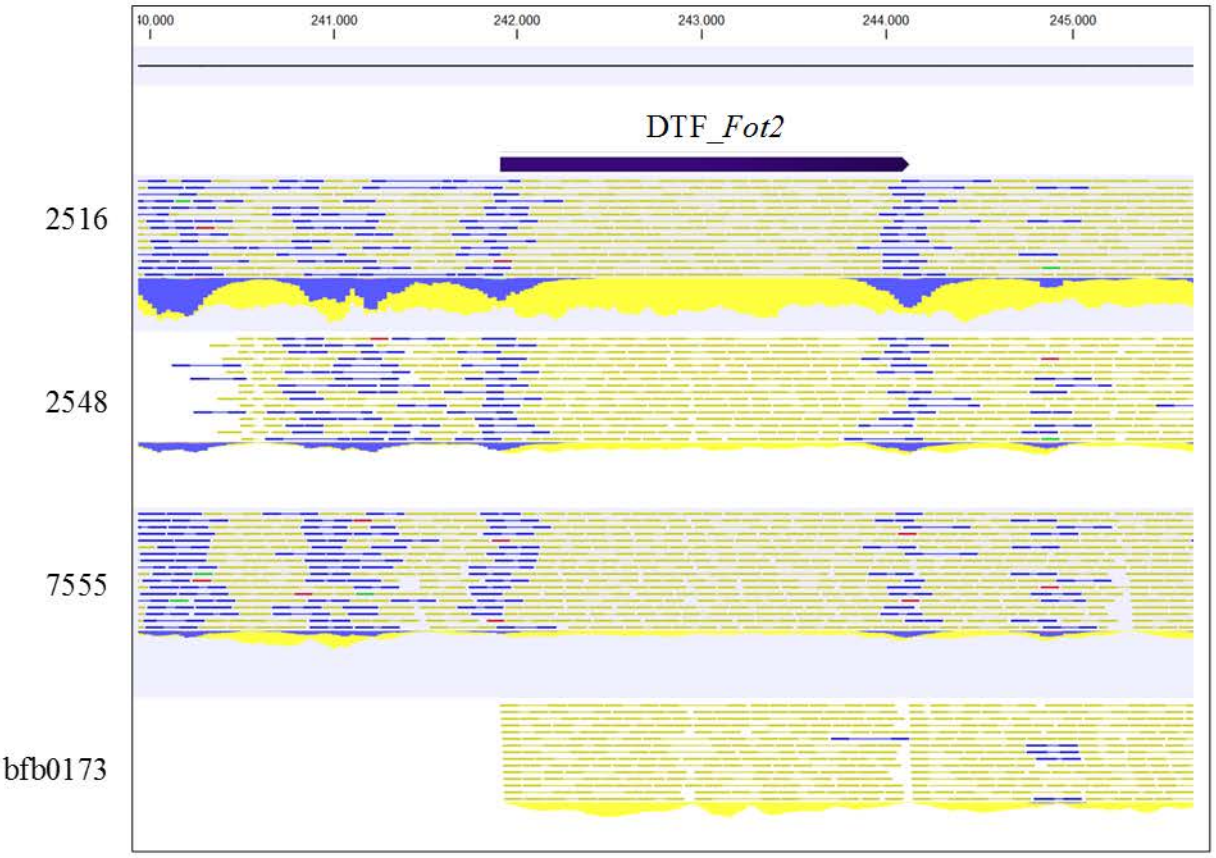
10.000
241.000
242.000
243.000
244.000
245.000
DTF_Fot2
2516
2548
7555
bfb0173

Figure S4.2 - Synteny of transposable elements on the supernumerary genome. Two instances are shown where a transposable element is in the same location for isolate 2516 and one or more other isolates. Tracks from top to bottom: RepeatMasker output, HiSeq reads from isolate 2516, HiSeq reads from isolate 2548, HiSeq reads from isolate 7555, and HiSeq reads from isolate bfb0173. Reads that can map to more than one location in the genome are automatically colored yellow in CLC Genomics Workbench.First screenshot: A DTF_*Fot3-B* element has inserted into a DTA_*RLT2* element on contig 308. The DTA_*RLT2* element is shared between 2516, 7555 and bfb0173. The insertion of DTF_*Fot3-B* is shared between 2516 and bfb0173. Second screenshot: a DTF_*Fot2* element is shared between 2516, 2548 and 7555 on contig 550.

Chapter 5: *In vitro* characterization of a *Fusarium poae* population: (un)linking genotype and chemotype

Vanheule, A, De Boevre, M, Bekaert, B, Moretti, A, Scauflaire, J, Munaut, F, Waalwijk, C, van der Lee, T, Höfte, M, De Saeger, S, Audenaert, K, Haesaert, G. Large genetic variation and trichothecene chemotype instability in a sexual *Fusarium* species. In preparation to be submitted.

5.1 Abstract

In this Chapter, the goal was to determine the genetic diversity and trichothecene chemotype of *F. poae*. In addition to the 69 isolates of *F. poae* that are already described in Chapter 4, isolates from related species were collected. Genetic diversity was assessed with AFLP, which showed a high intra-species variability, potentially explained by the active genome dynamics described in Chapter 4. Trichothecene biosynthesis inducing medium was used to stimulate trichothecene production, and was analyzed with LC-MS/MS to identify the produced compounds. Isolates of *F. poae* were found to produce both type A and type B trichothecenes, with the former likely being the first to be produced in the biosynthetic pathway. Indeed, a strictly sequential scheme of trichothecenes was consistently detected, consisting of DAS, NEO, FUS-X and NIV. DAS was produced in by far the highest concentration with this approach. Opposed to the well-described situation in the FGSC, the chemotype was not fixed *in vitro*, and especially type B production was variable. The genotype of the isolates was determined by diagnostic PCR and all were found to have the NIV genotype. The troublesome link between the genotype and chemotype in *F. poae* is discussed. We conclude that likely all *F. poae* isolates have the potential to produce both type A and type B trichothecenes, up to NIV, but yet unknown environmental or epigenetic cues determine to which stage the sequential chemotype is followed.

5.2 Introduction

An increasing number of studies has shown the importance of *Fusarium poae* within the FHB complex on small grain cereals (Xu et al., 2005; Audenaert et al., 2009). Within the last decade, this has sparked a number of studies that aimed to elucidate the intricacies of *F. poae* populations and the genetic diversity it contains. Additionally, a lot of attention has gone out to identifying the set of mycotoxins (chemotype) that isolates of the species produce *in vitro* and *in vivo*.

Several studies have been carried out that investigate the population composition of *F. poae*. Kerenyi et al. (1997) detected a large number of vegetative compatibility groups (VCGs) in 50 geographically diverse isolates. Somma et al. (2010) found in a geographically narrow population a high level of intra-species variability with AFLP, which was also found for worldwide *F. poae* collections by a number of techniques (AFLP, ISSR, RAPD) in a series of studies from an Argentinian research group (Dinolfo et al., 2010; Dinolfo et al., 2014). Consistently, geography can only partially explain for this large diversity at best, supporting the notion that *F. poae* isolates are generally part of one global population. Moreover, the broad

host range of *F. poae* isolates and their nature as secondary attackers within the FHB complex have been suggested as reasons for the lack of pathogenic subgroups associated with host specific specialization, in contrast to for example *F. oxysporum*.

Contrary to the results in genome-wide approaches, multi-locus barcoding consistently leads to the detection of rather low intra-species variability (Stenglein et al., 2010; Kulik and Pszczolkowska, 2011). Possibly, this discrepancy may be in part explained by the specific genome composition of *F. poae*. Isolates of this species have a highly variable set of supernumerary chromosomes, differing in size and number between individuals (Fekete and Hornok, 1997). Chapter 4 of this thesis has shown that sequence absence/presence is frequent on these chromosomes, and moreover their presence leads to significant rearrangements within the core chromosomes as well. The dynamics mediated by the supernumerary chromosomes, and transposable elements in particular, may lead to significant genotype diversity on a short evolutionary timescale, not picked up with a multi-locus analysis of barcoding genes.

Similarly, it is plausible that VCG compatibility may be quickly distorted by these genome dynamics. Moreover, at the time of the VCG studies, *F. poae* was thought of as a strictly asexual fungus, and recombination was not one of the causal factors considered for the highly complicated VCG pattern. Since then, we know that *F. poae* contains all the ingredients necessary for meiosis and it likely has an active, though perhaps infrequent, sexual cycle (Kerenyi et al., 2004 and Chapter 4 of this thesis).

Investigations into the mycotoxin production profile of *F. poae* isolates have focused primarily on the trichothecenes. Trichothecenes are produced by a large number of *Fusarium* species and can be divided mainly into type A (DAS, NEO, T-2, HT-2) and type B trichothecenes (NIV, FUS-X, DON), differing at the functional group occupying the carbon 8 position (McCormick et al., 2011 and Box 2.2). The precise structure of the end products of the trichothecene biosynthesis depends on whichever enzymes are encoded by genes in the genome of the *Fusarium* species. Genes for trichothecene biosynthesis are organized in clusters at up to three different loci and homologues with different functionality may occupy the same locus in different *Fusarium* species (Kimura et al., 2007). For the case of type A versus type B production, different alleles of the *Tri1* gene have been found to be the main determinant (McCormick et al., 2006).

The mycotoxin production potential of *F. poae* has been the subject of debate. Roughly two decades ago with a first report in 1999 (Torp and Langseth, 1999), the highly toxigenic species

F. langsethiae emerged in Scandinavian countries, which is morphologically similar to *F. poae* (Torp and Nirenberg, 2004). The production of T-2 and HT-2 toxin was at that time sometimes erroneously attributed to *F. poae* isolates. Presently it is generally accepted that most isolates of *F. poae* are not able to produce these highly toxic trichothecenes, as they lack the functional *Tri16* gene that is necessary for their biosynthesis (Proctor et al., 2009). Surprisingly, many authors have detected production of both type A and type B trichothecenes simultaneously by isolates of *F. poae* (Sugiura et al., 1993; Thrane et al., 2004; Vogelgsang et al., 2008a; Somma et al., 2010).

In this study we have set up a *Fusarium poae* collection and analyzed the genetic diversity among the isolates with both a single locus barcoding and whole genome approach. Using an *in vitro* method and a validated LC-MS/MS, the chemotype of every isolate was determined.

5.3 Material and methods

5.3.1 *Fusarium* collection

Chapter 4 of this thesis described the characteristics of 69 *F. poae* isolates (**Table S4.1**). Of these 69 *F. poae* isolates, ten isolates were kindly donated by dr. Antonio Moretti and are of Italian origin (Somma et al., 2010). Four isolates were donated by dr. Anne van Diepeningen from the CBS collection. Two isolates were donated from the *Fusarium* collection at Wageningen University and Research Centre. Five isolates originating from maize were donated by dr. Jonathan Scauflaire. Six isolates were purchased from the MUCL collection. Finally, forty-one isolates were collected from fields all over Flanders, Belgium.

Table 5.1 – Isolates from additional *Fusarium* species collected for this study. "-" indicates that the year of isolation is unknown.

ID	Species	Location	Host	Year	Reference
1070	*F. culmorum*	Verrebroek, Belgium	soil	2011	this study
2702	*F. culmorum*	Zwalm, Belgium	wheat	2011	this study
2799	*F. culmorum*	Scy, Belgium	wheat	2011	this study
861	*F. culmorum*	Koksijde, Belgium	soil	2011	this study
888	*F. culmorum*	Poperinge, Belgium	soil	2011	this study
2321	*F. graminearum*	Ciney, Belgium	wheat	2010	this study
2322	*F. graminearum*	Ciney, Belgium	wheat	2010	this study
2415	*F. graminearum*	Bottelare, Belgium	wheat	2011	this study
2471	*F. graminearum*	Poperinge, Belgium	wheat	2011	this study
2472	*F. graminearum*	Poperinge, Belgium	wheat	2011	this study
2475	*F. graminearum*	Poperinge, Belgium	wheat	2011	this study
2598	*F. graminearum*	Zuienkerke, Belgium	wheat	2011	this study
2715	*F. graminearum*	Verrebroek, Belgium	wheat	2011	this study

8/1	*F. graminearum*	Germany	unknown	-	Jansen et al. (2005)
6133	*F. sporotrichioides*	Heverlee, Belgium	tobacco	1964	MUCL
113234	*F. langsethiae*	Norway	oats	-	CBS
2004/170	*F. langsethiae*	United Kingdom	wheat	2004	Imathiu et al. (2009)
2004/171	*F. langsethiae*	United Kingdom	wheat	2004	Imathiu et al. (2009)
041/11	*F. langsethiae*	United Kingdom	oats	2004	Imathiu et al. (2009)
2004/59	*F. langsethiae*	United Kingdom	oats	2004	Imathiu et al. (2009)
201086	*F. langsethiae*	Roverud, Norway	oats	2011	dr. Ingerd Hofgaard
201087	*F. langsethiae*	Roverud, Norway	oats	2011	dr. Ingerd Hofgaard
NRRL54940	*F. langsethiae*	Norway	oats	2011	dr. Ingerd Hofgaard
34988	*F. langsethiae*	Unknown	wheat	1992	MUCL

Field isolates, presumed to consist of a mix of species and genotypes, were obtained and confirmed to contain *F. poae* as described in Audenaert et al. (2009). These were single spored according to a method developed by dr. Susanne Vogelgsang (Agroscope, Zürich, Switzerland, personal communication). Briefly, composite isolates were sporulated by incubating a mycelium plug on a PDA plate for 7 days under a light regime of UV/darkness (12h (365 nm 10W)/12h). With a cork borer, a piece of agar and sporulated mycelium was taken from the plate and added to 9 ml of distilled water. After vortexing and diluting the resulting conidial suspension six and thirty-six times, three suspensions (including the undiluted suspension) were obtained which were poured on plates containing water agar. Conidia were allowed to settle briefly after which the suspension was poured off. Plates were incubated for 16 h in the dark in a slanted position. Finally, with a light microscope germinating conidia with the typical *F. poae* shape were identified. These were extracted with a sterile Pasteur pipette tip and positioned on a fresh PDA plate.

Eight *F. graminearum* isolates and five *F. culmorum* isolates were obtained from Belgian fields as described above. The *F. graminearum* 8/1 isolate was kindly provided by dr. Karl-Heinz Kogel. The *F. sporotrichioides* isolate and one *F. langsethiae* isolate were purchased from the MUCL collection. One *F. langsethiae* isolate was purchased from the CBS collection. Four and three *F. langsethiae* isolates were kindly donated by dr. Simon Edwards (Harper Adams College, UK) and dr. Ingerd Hofgaard (Bioforsk, Norway) respectively. These isolates are described in **Table 5.1**. The geographic origins of the isolates for the four major species in this study are given in **Figure 5.1**.

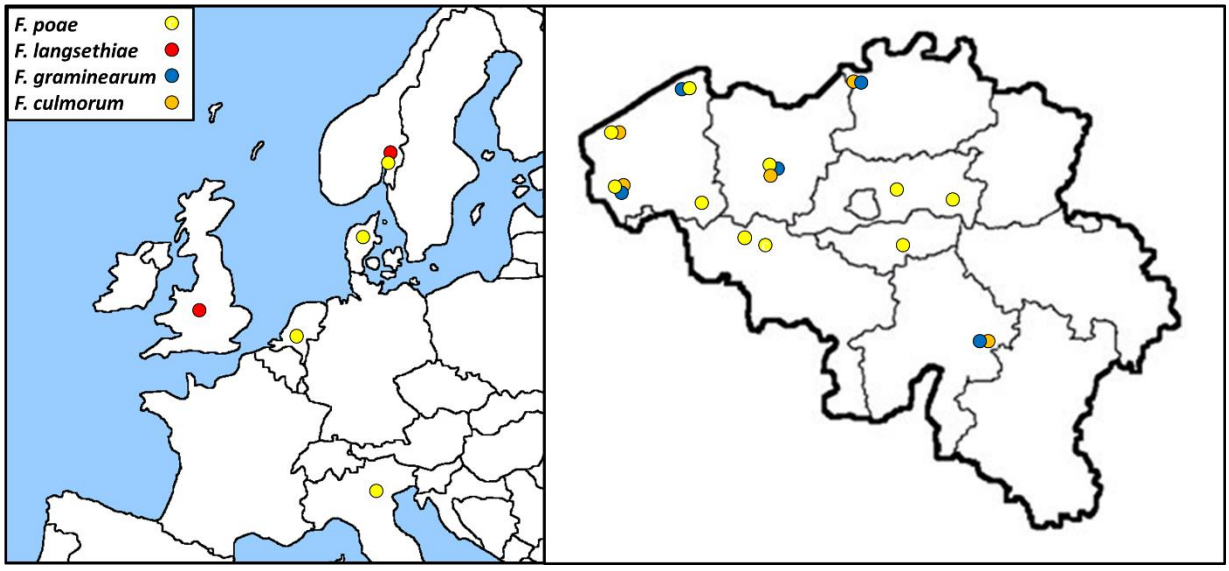

Figure 5.1 – Geographic origins of isolates for *F. poae* (yellow), *F. langsethiae* (red), *F. culmorum* (orange) and *F. graminearum* (blue). Circles are not scaled to the number of isolates collected at every location.

DNA extraction of single spored isolates was performed as described by Audenaert et al. (2009). Isolates confirmed to be *F. poae* with primers Fp82F/R (Parry and Nicholson, 1996) were preserved at -80°C as spores in a 20% glycerol solution.

5.3.2 Phylogenetic analyses

DNA for AFLP was extracted with the Invisorb Spin Plant MiniKit (Invitek, Berlin, Germany) according to the manufacturer's instructions and quantified with the Nanodrop 1000 system. Broadly, AFLP analysis was performed as described in Scauflaire et al. (2011). Restriction and ligation of genomic DNA was performed with EcoRI and MseI enzymes and reagents from the AFLP Core reagent kit (Invitrogen, now Life Technologies, USA). Pre-amplification was performed with the Amplification Core mix from the AFLP Microbial Fingerprinting kit of Applied Biosystems (now Life Technologies, USA). For the selective amplification, four primer pairs based on literature were used: EcoRI-AC – MseI-CC, EcoRI-AC – MseI-CA, EcoRI-AC – EcoRI-CG and EcoRI-GG – MseI-CA. Fragments were analyzed on a CEQ 2000 Genetic Analysis System (Beckman Coulter, Fullerton, California) and were visualized with the Genographer 1.6.0 software (Benham, Montana State University, Bozeman, Montana). Bands were scored visually and data was processed as described in Scauflaire et al. (2011). From the visual scoring, a binary matrix was constructed and UPGMA cluster analysis was performed based on the Dice similarity coefficients between the isolates. To determine the AFLP profile of a clonal isolate, and to determine the genotyping error rate, DNA from one isolate was included three times in the experiment.

For EF-1α phylogeny, PCR was performed with primers EF1 and EF2 (Geiser et al., 2004). PCR conditions were as described in Chapter 4 of this thesis. PCR products were purified with the EZNA Cycle-Pure kit (VWR Chemicals, Haasrode, Belgium) and sequenced in both directions by Macrogen Inc. (Amsterdam, the Netherlands). Forward and reverse sequences were manually curated for phylogeny. Sequences were aligned with ClustalO (Sievers et al., 2011). Maximum parsimony analysis was performed with PAUP version 4.0b10 (Swofford, 2003). *F. langsethiae* (NCBI accession AJ420822), *F. sporotrichioides* (NCBI accession AJ420818) and *F. kyushuense* (NCBI accession AJ427274) were included to be used as outgroup, however for construction of the tree mid-point rooting was used. Bootstrapping was performed with PAUP 4.0b10 based on 1000 replicates.

5.3.3 Chemical analyses

A trichothecene biosynthesis inducing medium described by Gardiner et al. (2009) was used. The general composition of the medium was identical as described in their study, but Phytagel was excluded and $NaNO_3$ was exchanged with L-arginine (Duchefa Biochemie, Haarlem, the Netherlands) at 5 mM, as Gardiner et al. (2009) showed that this nitrogen source induces trichothecene biosynthesis in *F. graminearum*. Medium was prepared in double concentration so that the final medium+conidia was 1x concentrated. Conidia were harvested by adding distilled water amended with 0.01% Tween80 (Merck, Germany) to the fully grown PDA plates and by rubbing the sporulated mycelium with a spatula. Conidia were counted with a Bürker counting chamber and diluted to a final concentration of $2x10^6$ conidia/ml. Finally, 0.5 ml of double concentrated medium and 0.5 ml of double concentrated conidial suspension were added together in 24 well plates (leading to 1x concentration of medium and 1x concentration of conidia) and grown in stationary phase under 16h light / 8h dark regime at 22°C. After seven days, supernatant was extracted from the cultures by centrifugation and immediately processed for LC-MS/MS analysis.

Sample preparation and LC-MS/MS followed an "evap and shoot" principle, without extensive sample cleanup. Individual mycotoxin solid standards (1 mg) of DON, NIV, 3-ADON, 15-ADON, NEO, FUS-X, T-2, HT-2, DAS and deepoxydeoxynivalenol (DOM) were supplied by Coring System Diagnostics (Gernsheim, Germany) as certified solutions. All mycotoxin solid standards were dissolved in acetonitrile (1 mg/ml), and were storable for a minimum of 1 year at -18 °C (Spanjer et al., 2008). Working solutions of 10 ng/µl for DON, NIV, 3-ADON, 15-ADON, NEO, FUS-X, T-2, HT-2, DAS and DOM were prepared in methanol and stored at -18 °C. From the individual working solutions, a mixture was prepared in methanol, stored at -18°C

and renewed monthly with the following concentrations: the mycotoxin mix (mycotoxins, 10 ng/µl) and the internal standard (DOM, 10 ng/µl).

An aliquot of the trichothecene biosynthesis inducing medium (1.0 ml) was transferred in a 10 ml glass tube and the internal standard was added (DOM, 10 µl, final concentration 100 ng/ml). For the construction of a calibration curve, five blank aliquots were spiked with the mycotoxin mix in an increasing concentration range (2 µl (20 ng/ml), 5 µl (50 ng/ml), 10 µl (100 ng/ml), 15 µl (150 ng/ml) and 20 µl (200 ng/ml), respectively). The sample was vortexed for 2 minutes (Labinco, Breda, The Netherlands). Then, the spiked medium was evaporated to dryness under a gentle N_2-stream at 60 °C using the Turbovap® LV Evaporator (Biotage, Uppsala, Sweden). The dried residue was redissolved in 100 µl injection solvent, which consisted of 70% mobile phase A (water/methanol (95/5, v/v) + 5 mM ammonium acetate, 0.1% glacial acetic acid) and 30% mobile phase B (water/methanol (95/5, v/v) + 5 mM ammonium acetate, 0.1% glacial acetic acid). Prior to injection, the sample was vigorously vortexed for 2 minutes, collected in a 0.22 µm Ultrafree-MC centrifugal device (Millipore, Bedford, MA, USA) and centrifuged for 10 minutes at 10 000 g. LC-MS/MS methodology was as detailed in the Appendix of this thesis. LODs and LOQs for the trichothecenes produced by *F. poae* were respectively 30 and 61 ng/ml (NIV), 31 and 63 ng/ml (FUS-X), 39 and 78 ng/ml (NEO) and 41 and 82 ng/ml (DAS). Certain analyzed samples showed peaks which according to the calibration curve corresponded to concentrations between the LOD and the LOQ for DAS, NEO and FUS-X. These samples were assigned the LOD concentration as they could not be reliable quantified.

Pearson correlations between the levels of trichothecenes were determined with Microsoft Excel 2013. The concentration range of the trichothecenes was visualized in Box-Whiskers plots, constructed with SPSS22.

5.3.4 Diagnostic PCR

The NIV genotype of the *F. poae* isolates was investigated with primers designed by Dinolfo et al. (2012). These primers amplify a 300 bp portion of the *Tri7*. PCR conditions were as described earlier in this thesis.

5.4 Results

5.4.1 *Fusarium poae* is a monophyletic species with high intra-species variability

Figure 5.2 shows the result of the AFLP analysis. Over all isolates (n = 88), 423 markers were scored of which 421 were polymorphic. Considering only the *F. poae* isolates (n = 64), 247 markers were scored of which 201 were polymorphic. All isolates of *F. poae* described in **Table S4.1** (n = 69)

were used for the AFLP analysis except five: isolates 175, 2521, 6127, 7555 and 42824. *F. graminearum* and *F. culmorum*, and *F. langsethiae* and *F. sporotrichioides*, cluster into separate clusters and are separated as species. This confirms the power of the analysis to discriminate between closely related species. Isolate 9125 was included three times in the analysis. The clustering of these three repetitions shows what a perfectly clonal isolate looks like and can serve as a reference for the rest of the tree. Finally, the genotyping error rate was only 3.3 to 3.8% over different primer pairs, similar to levels that have been described in literature (2-5%) (Mueller and Wolfenbarger, 1999; Bonin et al., 2004).

The *F. poae* isolates are divided into subclusters that do not correspond to host or geographic origin. Indeed, isolates from maize (L24, K46, S46, Q57, F49), and isolates from Italy (designation 9###), are spread throughout the tree. However, the one Chinese isolate in the study (bfb0173) clusters apart from the other *F. poae* isolates. The ten Italian isolates were included in an AFLP analysis before (Somma et al., 2010). In this study, isolates 9181 and 9196 clustered closely together as they do in our AFLP. Three of the four Italian isolates (9186, 9192, 9203, 9194) that cluster together tightly in our study, also clustered together in the Italian study, but the fourth is in a different group.

Figure 5.3 shows a maximum parsimony phylogenetic tree based on an alignment of the EF-1α sequences, with *F. langsethiae*, *F. sporotrichioides* and *F. kyushuense* as outgroups. The twenty three *F. poae* isolates were aligned over a 651 bp EF-1α fragment, and 4 parsimony informative sites were retrieved. These cluster the isolates into three sets that consist of identical sequences. Isolates 2410 and 2524 are in the same AFLP subcluster. Isolates 9189 and 9209, and 2043 and 2377 are very tightly clustered as well, but these pairs of isolates do not cluster with each other or isolate 177 in the AFLP analysis.

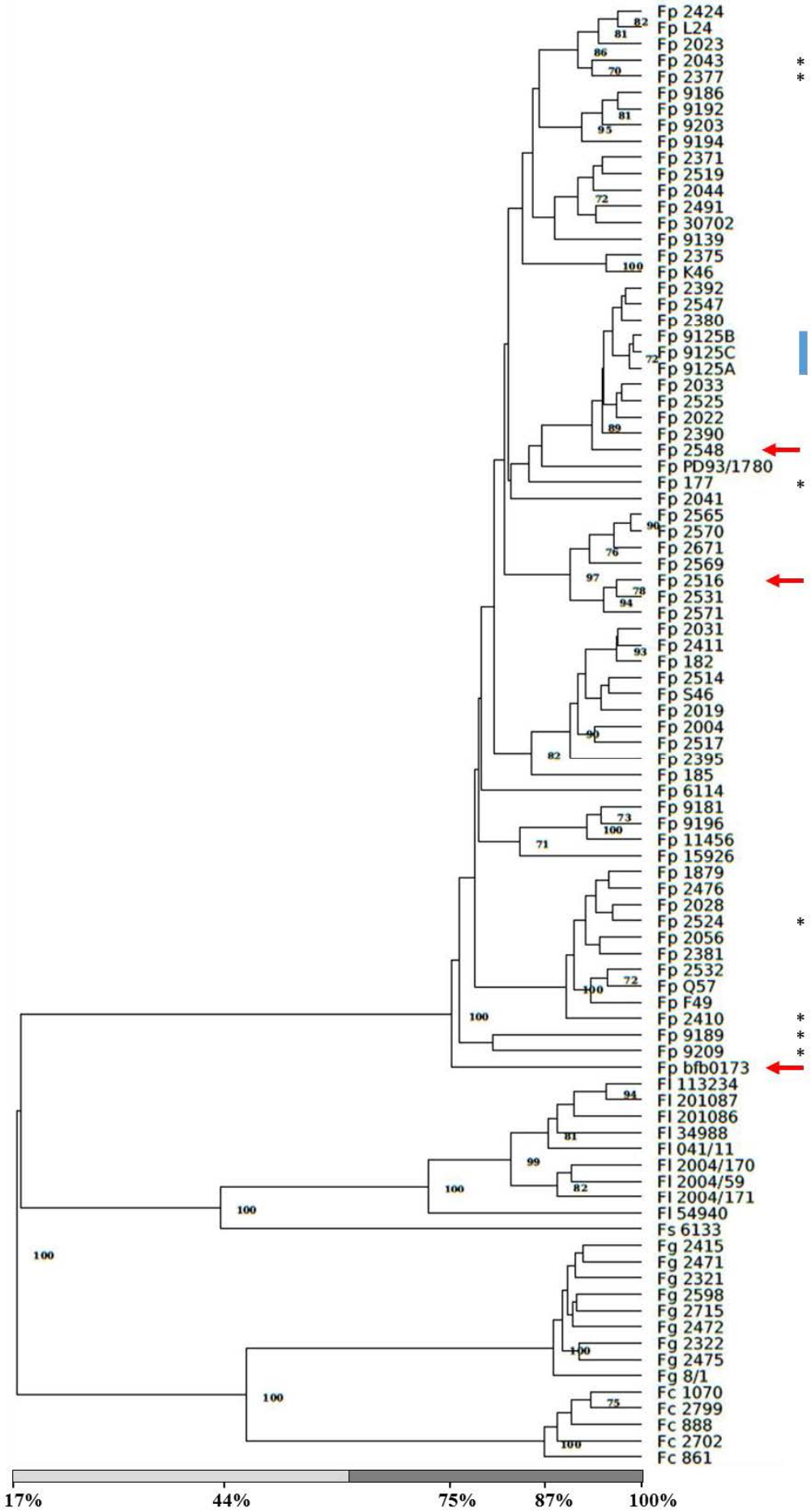
Fp 2424
Fp L24
Fp 2023
Fp 2043
Fp 2377
Fp 9186
Fp 9192
Fp 9203
Fp 9194
Fp 2371
Fp 2519
Fp 2044
Fp 2491
Fp 30702
Fp 9139
Fp 2375
Fp K46
Fp 2392
Fp 2547
Fp 2380
Fp 9125B
Fp 9125C
Fp 9125A
Fp 2033
Fp 2525
Fp 2022
Fp 2390
Fp 2548
Fp PD93/1780
Fp 177
Fp 2041
Fp 2565
Fp 2570
Fp 2671
Fp 2569
Fp 2516
Fp 2531
Fp 2571
Fp 2031
Fp 2411
Fp 182
Fp 2514
Fp S46
Fp 2019
Fp 2004
Fp 2517
Fp 2395
Fp 185
Fp 6114
Fp 9181
Fp 9196
Fp 11456
Fp 15926
Fp 1879
Fp 2476
Fp 2028
Fp 2524
Fp 2056
Fp 2381
Fp 2532
Fp Q57
Fp F49
Fp 2410
Fp 9189
Fp 9209
Fp bfb0173
Fl 113234
Fl 201087
Fl 201086
Fl 34988
Fl 041/11
Fl 2004/170
Fl 2004/59
Fl 2004/171
Fl 54940
Fs 6133
Fg 2415
Fg 2471
Fg 2321
Fg 2598
Fg 2715
Fg 2472
Fg 2322
Fg 2475
Fg 8/1
Fc 1070
Fc 2799
Fc 888
Fc 2702
Fc 861
17%
44%
75%
87%
100%

Figure 5.2 – Result of the AFLP analysis on 65 *F. poae* isolates, and isolates from *F. langsethiae*, *F. sporotrichioides*, *F. culmorum* and *F. graminearum* as outgroups. All *F. poae* isolates described in **Table S4.1** (n = 69) were included in the AFLP analysis except isolates 175, 2521, 6127, 7555 and 42824. UPGMA cluster analysis was performed based on the Dice similarity coefficients between the isolates. Over all isolates (n = 88), 423 markers were scored of which 421 were polymorphic. Considering only the *F. poae* isolates (n = 64), 247 markers were scored of which 201 were polymorphic. Bootstrap values exceeding 70% are given at the nodes, based on 1000 replications. Fp = *F. poae*; Fl = *F. langsethiae*; Fs = *F. sporotrichioides*; Fg = *F. graminearum*; Fc = *F. culmorum*. The scale bar at the bottom gives the genetic similarity based on the Dice coefficient, with a change in color at the 60% boundary. Three technical replicates of isolate 9125 are shown with a blue bar. Three isolates used for genome sequencing in Chapter 4 are indicated with a red arrow (isolate 7555 was not included in the AFLP analysis). Isolates that are discussed in the text in relation to the EF-1α phylogeny in **Figure 5.3** are denoted with asterisks.

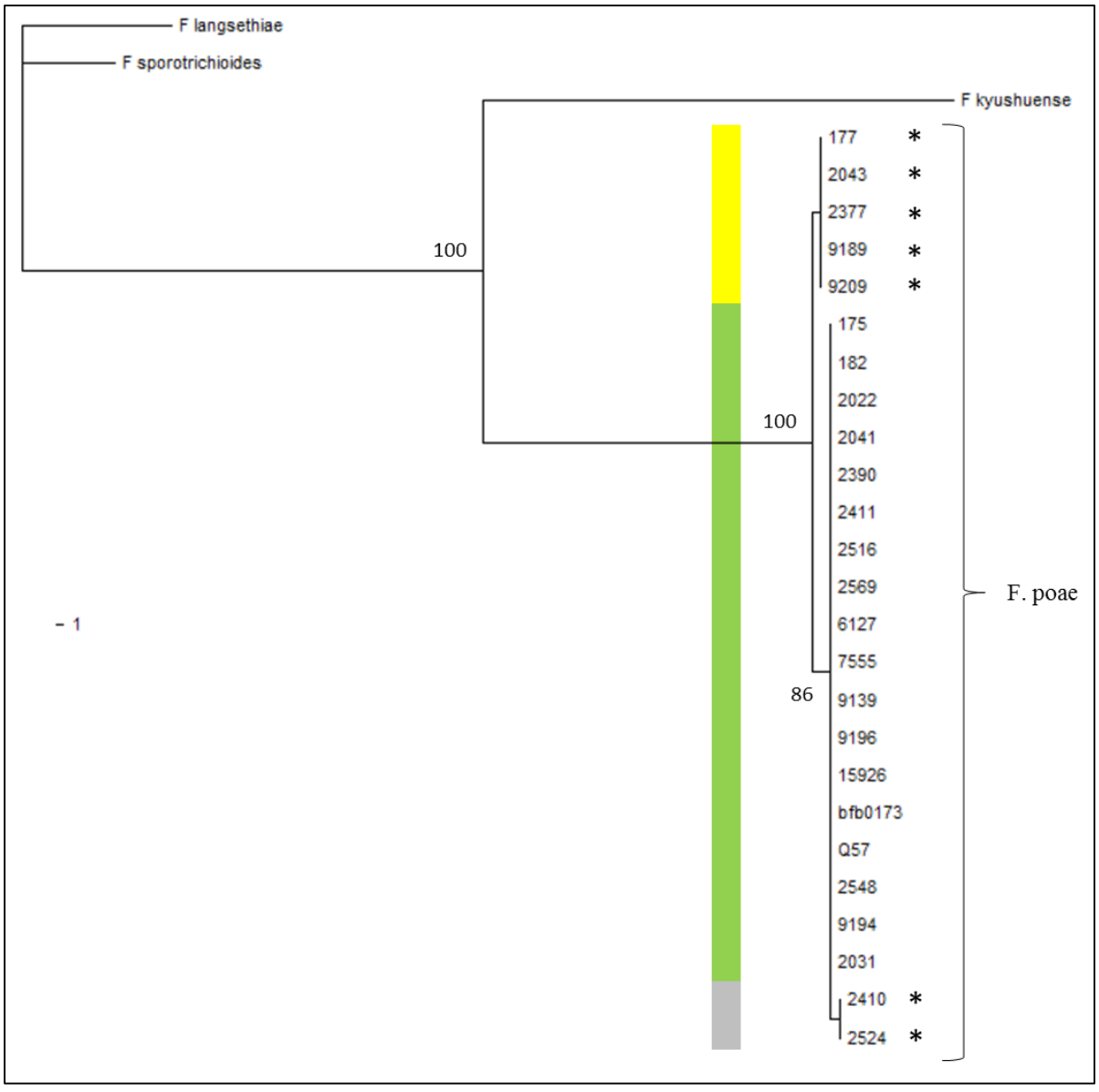

Figure 5.3 – Maximum parsimony phylogenetic tree for *F. poae* isolates based on partial *EF-1α* sequence, construed with PAUP* 4.0b10. *F. langsethiae* (NCBI accession AJ420822), *F. sporotrichioides*

(NCBI accession AJ420818) and *F. kyushuense* (NCBI accession AJ427274) were included in the analysis as outgroups, however these were not forced on to the tree and mid-point rooting was used. Bootstrap values exceeding 70% are given at the nodes based on 1000 replicates. Isolates designated with an asterisk are discussed explicitly in the text, in relation to the AFLP analysis in **Figure 5.2**. Three types of *EF-1α* were detected (marked by yellow, green and grey).

5.4.2 Isolates of *F. poae* produce both type A and type B trichothecenes

The chemotyping method, including the culturing on liquid medium and LC-MS/MS analysis without prior sample-cleanup, was biologically validated by analyzing a number of isolates from different species with known chemotype. *F. langsethiae* and *F. sporotrichioides* isolates produced abundant DAS, NEO, T-2 and HT-2. Two *F. culmorum* isolates with NIV genotype produced NIV, FUS-X and small amounts of 15-ADON. Three *F. culmorum* isolates with 3-ADON genotype produced DON, 3-ADON and limited 15-ADON. Five isolates with *F. graminearum* 15-ADON genotype produced DON, 3-ADON and 15-ADON. Conversion between 3-ADON and 15-ADON is known to occur under certain conditions (Alexander et al., 2011).

Figure 5.4 shows for 61 *F. poae* isolates the trichothecenes that were detected in the trichothecene biosynthesis inducing medium. The values were log transformed as the amounts of DAS were several orders of magnitude larger than those of the other toxins. It is also at the highest incidence, with 59 of 61 isolates being positive for DAS, ranging from the LOD to 22 300 ng/ml. Of these 59 isolates, 55 produced NEO in the range of the LOD to 375 ng/ml. Of this set, 24 isolates produced FUS-X in the range of the LOD to 171 ng/ml. Finally, of the FUS-X producers, 14 isolates also produced NIV in the range of 88 ng/ml to 122 ng/ml. The sequential nature of the chemotype is visualized in **Figure 5.5**A.

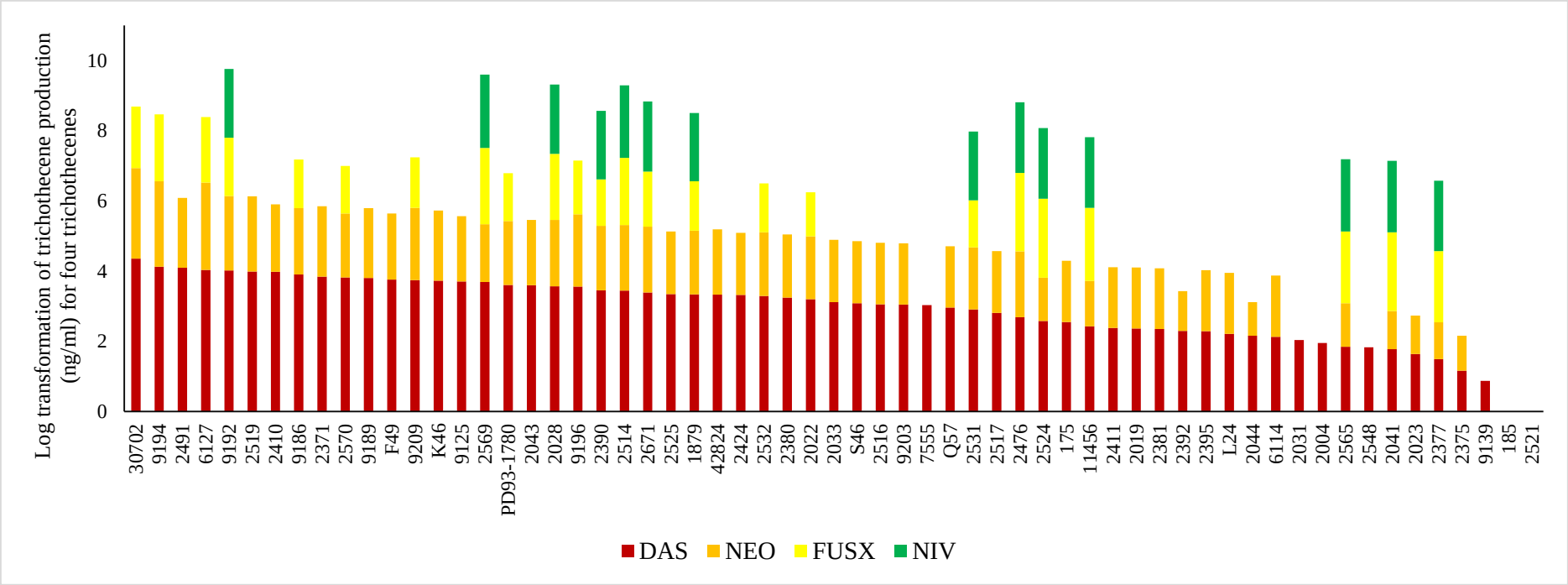

Figure 5.4 – Detailed representation of the trichothecene production profile of 61 *F. poae* isolates. Isolates are ordered from highest DAS production to lowest DAS production (two isolates with no DAS detected). The y axis shows the log transformation of the amount of trichothecenes detected. DAS was produced by most isolates and in the highest concentrations, as can be seen in **Figure 5.5**A and C.

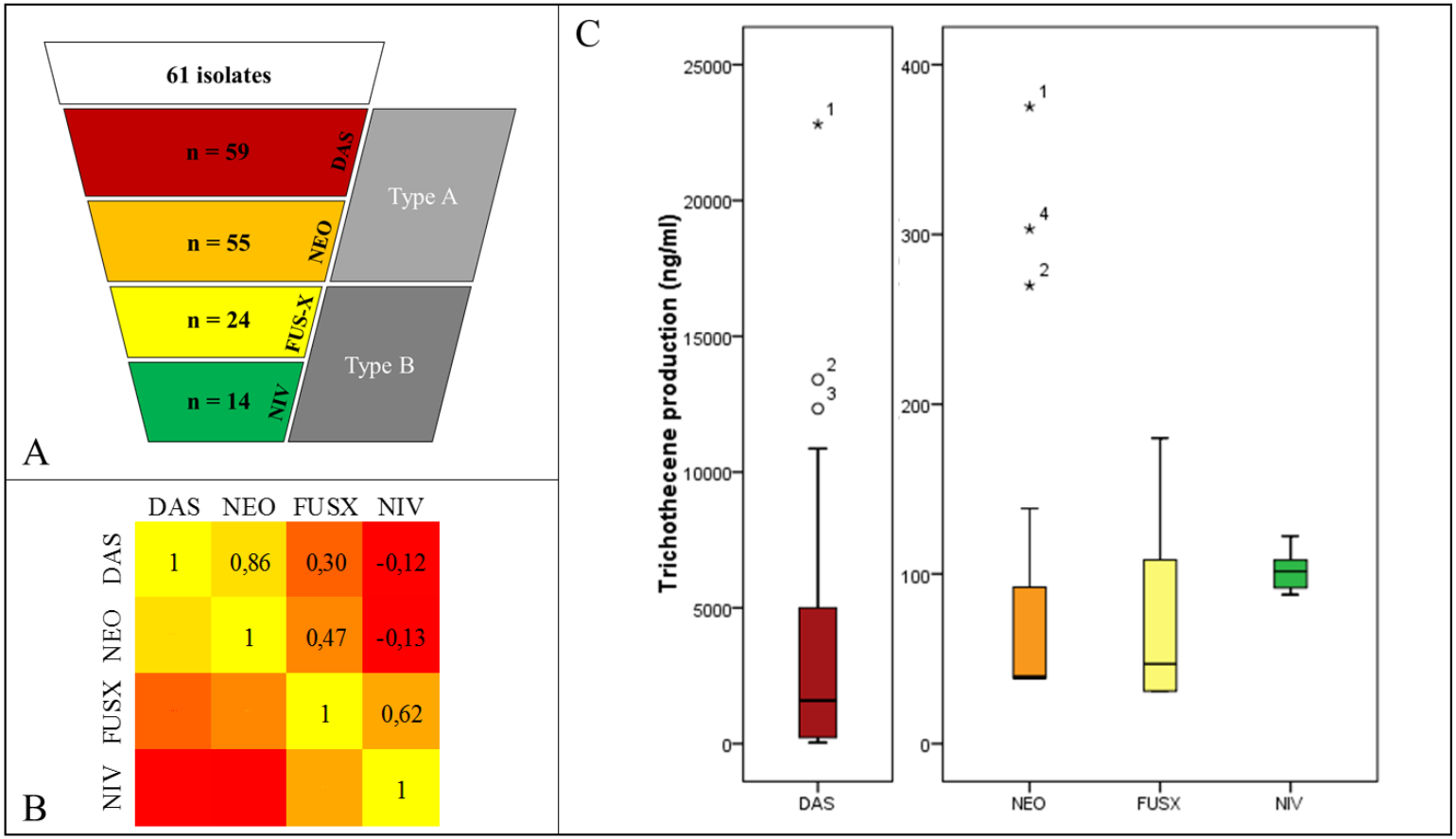

Figure 5.5 – **A**: simplified representation of the chemotype of 61 *F. poae* isolates. The chemotypes detected were strictly sequential, i.e. when compounds lower on the scheme are detected, the compounds higher on the scheme have also been produced. **B**: Pearson correlations between the four trichothecenes that are produced by *F. poae* isolates. A lighter color corresponds with a higher correlation. **C**: overview as Box-Whisker plots of the concentration ranges within which the four trichothecenes were detected. Note that the range of the y axis for DAS is two orders of magnitude higher than the range for NEO, FUS-X and NIV concentrations. The boxes for every mycotoxin show the lower and upper quartile (delineating the boxes) of the measured concentrations (ng/ml) and the median (thick line within the boxes). The whiskers represent the minimum and maximum values. Circles and asterisks are outliers and extreme values which fall respectively outside of one-and-a-half additional box lengths and three additional box lengths counted from the upper quartile limit.

Figure 5.5C summarizes the trichothecene production *in vitro* for all isolates combined. DAS production is higher by several orders of magnitude compared to production of NEO, FUS-X and NIV. Note that two outliers/extreme values for DAS and NEO overlap, e.g. number 1 (isolate 30702) and 2 (isolate 9194). Concordantly, **Figure 5.5**B shows that production of DAS and NEO is correlated.

5.4.3 The type A+B trichothecene chemotype is not fixed *in vitro*

Table 5.2 shows the result of two biological repetitions of the chemotyping experiment for 28 isolates. Compounds with a plus sign were detected consistently, while compounds with a red "o" were only detected in one of the repetitions. For 20 of the isolates in this experiment, the sequential chemotype as it is illustrated in **Figure 5.5**A, could sometimes be expanded to move "further downstream", with FUS-X or even NIV production where there was none in another iteration. The chemotype of seven isolates was identical in the different repetitions: for example isolate 7555 only produced DAS, and isolate 2569 produced all four compounds. Finally, isolate 2521 did not produce any toxins in one of the repetitions (one of the two such isolates depicted in **Figure 5.4**). It should be noted that with only two biological repetitions, it is difficult to assign a definitive chemotype for every isolate, particularly as the chemotype appears to be variable *in vitro*. However, importantly, the sequential nature of the detected chemotype was never violated.

Table 5.2 – Result of two biological chemotype repetitions for 28 *F. poae* isolates. Black "+" marks denote compounds that were consistently detected, red "o" represent compounds that were detected only in one of the repetitions, "-" is not detected. Note that sample 2521 has only "o", since in one interation no trichothecenes were detected from this isolate (see **Figure 5.4**).

Isolate	DAS	NEO	FUS-X	NIV
2371	+	+	o	-
2375	+	+	o	-
2377	+	+	+	o
2381	+	+	o	-
2390	+	+	o	o
2392	+	+	o	-
2395	+	+	o	-
2411	+	+	-	-
2491	+	+	o	-
2514	+	+	+	o
2516	+	+	o	o
2517	+	+	o	-
2519	+	+	o	-
2521	o	o	-	-
2524	+	+	o	-
2525	+	+	o	-
2531	+	+	o	o
2532	+	+	+	-
2548	+	o	o	-
2569	+	+	+	+
S46	+	+	-	-
F49	+	+	o	-
6114	+	+	-	-
6127	+	+	+	-
7555	+	-	-	-
11456	+	+	+	o
30702	+	+	+	o
42824	+	+	o	-

5.4.4 All *F. poae* isolates have a NIV genotype

The same 61 isolates that were used in the *in vitro* chemotyping were also used for genotyping. This is the process wherein a diagnostic PCR is used to predict the "chemotype" of an isolate based on the presence of some genetic marker, previously identified to be specific for the production of (a) certain compound(s). For all *F. poae* isolates, this PCR gave a positive result and therefore all isolates can be considered to have a NIV genotype and should have the genetic machinery for NIV production (**Figure 5.6**).

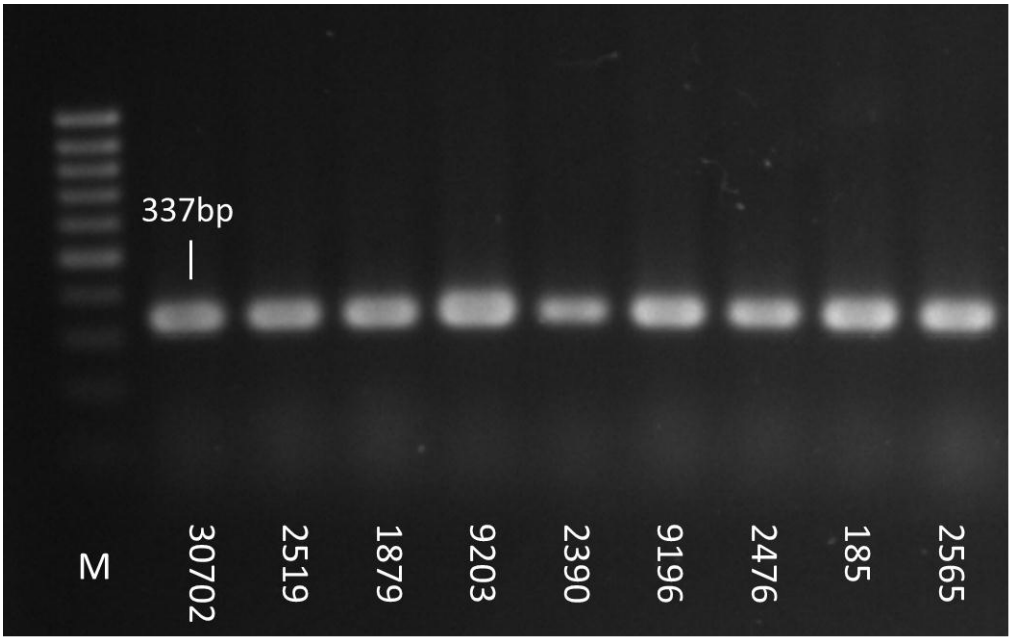

Figure 5.6 – Gel electrophoresis of diagnostic PCR targeting the NIV genotype in *F. poae*. According to Dinolfo et al. (2012), a ~300bp fragment indicates a NIV genotype, which was present for all isolates tested. M is for the molecular weight marker (Thermofisher's Massruler DNA Ladder, Low range).

5.5 Discussion

The high intraspecies variability of *F. poae* when analyzed with genome wide methods has been noted before, as studies with VCGs (Liu and Sundheim, 1996), RAPD (Kerenyi et al., 1997), AFLP (Somma et al., 2010) and ISSR (Dinolfo et al., 2010). This is in sharp contrast to multilocus barcoding analyses, which consistently pick up only low genetic variability (Stenglein et al., 2010; Kulik and Pszczolkowska, 2011). The phylogenetic analyses carried out in this study fit with what has been described previously. EF-1α sequencing is the preferred barcoding approach for *Fusarium* species (Geiser et al., 2004), but is also used for phylogeny (Kristensen et al., 2005; Somma et al., 2010). AFLP is not generally usable for determining evolutionary phylogeny between species, and has higher resolution at the refined level of isolates from the same species (Baayen et al., 2000). Nevertheless, the clustering in the AFLP tree of *F. sporotrichioides* and *F. langsethiae* with *F. poae* fits with phylogeny and matches earlier observations by Schmidt et al. (2004a).

The active genome dynamics within this species may partially account for the high intra-species variability in *F. poae*. A subcluster of the AFLP tree is made up of isolates that have a specific genome insertion of several 100kb of sequence (Chapter 4 of this thesis). The power of AFLP to discriminate *Fusarium* species to the clonal level has been shown before (Chulze et al., 2000). Chapter 4 of this thesis shows that both sexual and clonal reproduction is likely occurring in the *F. poae* population. Taking the technical repetition of isolate 9125 as the reference for a

clonal isolate, at most seven instances of two clonal isolates are present in the collection. Isolates 2516 and 2531 are one set of such likely clonal isolates. As TE-mediated disruptions and rearrangements occur on evolutionary very short timescales, this could be one of the factors explaining the discrepancy in intra-species variability between genome-wide and multi-locus barcoding approaches. Therefore, it is possible that transposable element proliferation is obscuring the similar or even clonal nature of some (sets of) isolates.

Five isolates from maize are included in the study, aside from primarily isolates from wheat. The maize isolates cluster throughout the tree, suggesting that no significant host specialization has occurred within *F. poae*. This is in agreement with literature reports that suggest that most isolates have a broad host range (Kerenyi et al., 1997). No clear geographic subclustering was observed, which is in accordance with previous studies (Dinolfo et al., 2010; Dinolfo et al., 2014). Nevertheless, isolate bfb0173 from China clustered separate from all other isolates, and Kerenyi et al. (1997) reported a partial correlation between geographic origin and VCG/RAPD. All isolates in the study share >75% similarity, suggesting that they are part of a single monophyletic lineage, which is similar to what was found before for *F. poae* (Schmidt et al., 2004b; Kristensen et al., 2005).

This study represents the first time an effective trichothecene biosynthesis inducing medium has been used for *F. poae*. Previous studies have utilized autoclaved cereal substrates (Vogelgsang et al., 2008a; Somma et al., 2010) and *in planta* inoculations (Vogelgsang et al., 2008b). Notably, the genetically unusual chemotype of both type A and type B trichothecene production holds in both approaches. Inoculations in cereal matrices seemingly shift the balance more towards type B production, while the *in vitro* trichothecene biosynthesis induction medium mainly stimulated DAS production. The reason for this is unknown, however the sequential chemotype demonstrated here makes it highly likely that DAS is the first trichothecene produced. It is plausible that the cues for further progress down the metabolic grid are not present *in vitro*. MAS and NIV have been detected together from *F. poae* in several studies, however, there are some discrepancies as to which compound of the two is produced at the highest level (Liu et al., 1998; Vogelgsang et al., 2008b). Trichothecenes of the DAS-related group such as MAS and SCR are often overlooked in mycotoxin surveys, while they may be important compounds in nature, particularly associated with *F. poae* (Liu et al., 1998; Schollenberger et al., 2011). NEO, the other type A trichothecene produced by *F. poae* in our *in vitro* setup has been detected in small amounts from *F. poae* infected cereal matrices (Liu et al., 1998; Thrane et al., 2004).

The discrepancies in chemotype depending on the matrix or medium that is used, may lead to an underestimation of certain toxicological aspects of *F. poae*. The Italian isolates in this study were previously chemotyped by growth on autoclaved wheat. Three that were found to produce no type A trichothecenes, produced both DAS and NEO in the trichothecene biosynthesis induction medium. This may be an important point to make, as reports exist stating that at least *in planta* type A trichothecenes are more toxic than type B trichothecenes (Desjardins et al., 2007). The situation is less clear when toxicity to animals is considered. While it is generally stated that again type A trichothecenes are more toxic than type B trichothecenes (Placinta et al., 1999), big differences between trichothecenes belonging to the same class make it difficult to make such an unequivocal distinction (Ueno, 1983). The instability of the *F. poae* chemotype with respect to type B trichothecene production and the strictly sequential chemotype pattern dictate that type A trichothecenes should be the first to be produced in *F. poae* (see Chapter 6 of this thesis).

The production of T-2 and HT-2 toxin, while contentious in the past, is not regularly found for *F. poae* isolates at present. Thrane et al. (2004) found T-2 and/or HT-2 production in five out of 49 investigated isolates, the genotype of which is not known. We found trace amounts of T-2 for one isolate in our study (isolate 2548; data not shown). The *Tri16* gene is not functional in this isolate (determined from the genome sequence obtained in Chapter 4), and T-2 was not detected again upon multiple repetitions. We argue that in certain media T-2 may be metabolized from closely related type A trichothecenes, whether enzymatically or by chemical equilibrium, but *F. poae* is likely not an active producer of the compound. Due to the close correlation between DAS and NEO found in the liquid medium (**Figure 5.5**B), we set out to determine whether a chemical equilibrium may be at play between these compounds. Incubation experiments with DAS at 10 and 20 mg/kg did not yield detectable NEO however. We found no correlation between the type A and the type B trichothecenes in our study, contrary to Liu et al. (1998) and Vogelgsang et al. (2008a) who saw a correlation between MAS and NIV.

Within the type B producing FGSC, it is common to define the chemotype of an isolate by its genotype, determined by a diagnostic PCR of a differential trichothecene biosynthesis gene (Pasquali and Migheli, 2014). A similar method has been developed for the NIV chemotype in *F. poae*, which is based on the *Tri7* gene (Dinolfo et al., 2012). However, the functionality of the acetyltransferase encoded by the *Tri7* gene is required for the production of all trichothecenes produced by *F. poae*, DAS, NEO, FUS-X and NIV (McCormick et al., 2011),

and therefore the test based on the *Tri7* gene may not be very selective. All *F. poae* isolates in the study of the research group that developed the diagnostic PCR, all *F. poae* isolates in the study by Covarelli et al. (2015), and all *F. poae* isolates in our study were determined to have the NIV genotype with this test.

We conclude that likely all *F. poae* isolates have the genetic machinery to produce NIV, and defining the chemotype in this way may be rather uninformative. Instead of a separate chemotype on its own, NIV is the end product of a strictly sequential type A + type B trichothecene chemotype (**Figure 5.5**A), the production of which is heavily dependent on the environmental conditions. This sequential nature of the chemotype and the lack of cues *in vitro* that lead production all the way to NIV is likely the reason for the detected instability in this study. The absence of these cues could lead to the production of only marginal amounts of NIV *in vitro,* and inconsistently over repetitions. Therefore, the link between a diagnostic genotype and the chemical chemotype in *F. poae* may not be straightforward, and as Desjardins (2008) argued more generally, it should be treated with caution.

Chapter 6: Identifying the cause of the type A + B trichothecene chemotype in *Fusarium poae*

Vanheule, A, De Boevre, M, Bekaert, B, Moretti, A, Scauflaire, J, Munaut, F, Waalwijk, C, van der Lee, T, Höfte, M, De Saeger, S, Audenaert, K, Haesaert, G. (2015) Large genetic variation and trichothecene chemotype instability in a sexual *Fusarium* species. In preparation to be submitted.

Vanheule, A, Audenaert, K, De Boevre, M, Bekaert, B, De Saeger, S, Höfte, M, Wirsel, S, Haesaert, G. (2015) TRI13 mediates different paths along the trichothecene biosynthesis grid in *Fusarium* species. In preparation to be submitted.

6.1 Abstract

In this study, we set out to identify how the unique and sequential type A + type B trichothecene chemotype that was identified in Chapter 5 can be explained at the genetic level. Moreover, we wanted to uncover whether any genomic determinants may be responsible for the instability of the chemotype. Using the genome sequences obtained in Chapter 4, the composition of the trichothecene biosynthesis loci was investigated. As expected, these are highly syntenic with other toxigenic *Fusarium* species. Notably, the locus containing 12 of the 14 genes required for trichothecene biosynthesis in *F. poae* (hereafter referred to as the *Tri* cluster) and its environment are invaded by TEs, and using these elements as markers a recombination event in the *Tri* cluster was uncovered. A *pogo* TE in the middle of the *Tri* cluster, which occurs in more than half of the *F. poae* isolates, was however not correlated with the unstable chemotype determined in Chapter 5 of this thesis. As *Tri1* is one of the molecular switches determining type A and type B trichothecene production in other fusaria, the allelic variation at this locus was assessed. Two major types of the gene were uncovered with 3% divergence, but nearly all SNPs were found to be synonymous, therefore chemotype variability could also not be explained by variability at the *Tri1* locus. Comparative *in silico* homology modelling indicated that TRI1 function in *F. poae* may not be different from that in *F. graminearum*. However, based on overall similarity of the trichothecene clusters between species, the function of FpTRI13 is likely similar to that in *F. sporotrichioides*, with a broader substrate range than in *F. graminearum*. We argue that the combination of the *F. sporotrichioides*-like TRI13 and the *F. graminearum*-like TRI1 leads to the type A + type B trichothecene chemotype in *F. poae*. This hypothesis was confirmed by *Tri13* gene swap transformations in *F. poae*.

6.2 Introduction

The ability of *F. poae* to produce both type A and type B trichothecenes was first described over 20 years ago (Sugiura et al., 1993). Since then, several researchers have seen the same chemotype associated with *F. poae* (Thrane et al., 2004; Somma et al., 2010). Chapter 5 of this thesis analyzed the trichothecene production of 61 isolates and described that most if not all isolates are able to produce type A and type B trichothecene under trichothecene biosynthesis inducing conditions. Moreover, a genetic chemotyping method identified all isolates as having a NIV chemotype. *In planta*, the most important factors determining trichothecene biosynthesis include the host and environmental conditions. However, in Chapter 5, an unstable type A + type B trichothecene chemotype was detected under controlled *in vitro* conditions. The nature

of the trichothecene combinations detected *in vitro* indicated that type A trichothecenes are likely the first to be produced in the biosynthetic pathway.

It is believed that rather than a linear series of enzymatic conversions, trichothecene biosynthesis is accomplished by a molecular grid, wherein different routes can lead to the same end product, and minor and major pathways coexist (Kimura et al., 2007). Broadly, the biosynthesis starts with the cyclization of trichodiene out of farnesyl pyrophosphate by the TRI5 enzyme. It is the first metabolic step that is specific to the trichothecene biosynthesis and is therefore a knockout target for physiological studies investigating the function of trichothecenes in different species (Jansen et al., 2005). The first steps of trichothecene biosynthesis are given in **Figure 6.1**.

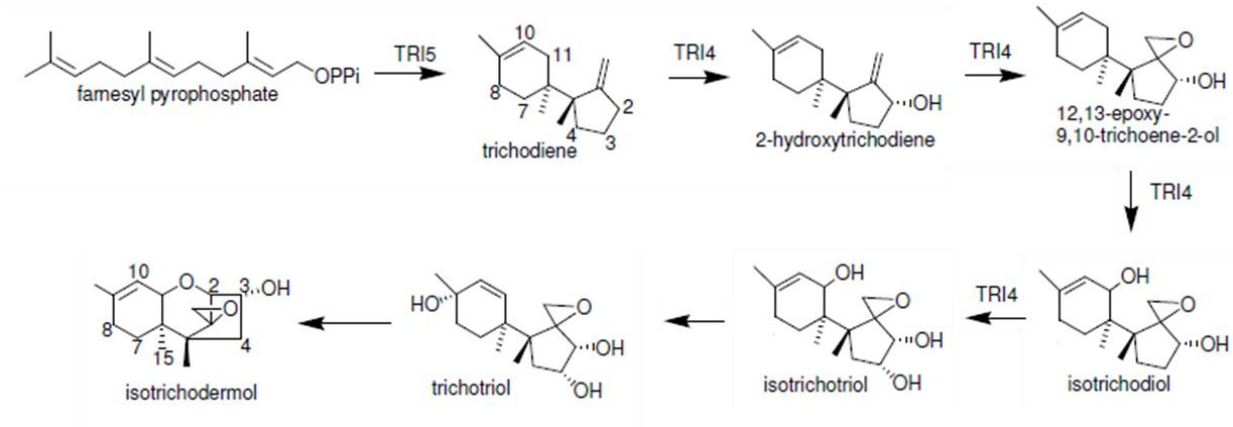

Figure 6.1 – First steps of trichothecene biosynthesis, leading to the backbone structure of the trichothecene molecule with the carbon positions for further substitutions numbered. Source: McCormick et al. (2011).

McCormick et al. (2011) recently reviewed the trichothecene biosynthesis (see **Figure 6.1** and **Figure 6.2**). Trichodiene undergoes a series of enzymatic and non-enzymatic modifications, including some for which no mechanism has been elucidated. The first step is mediated by *Tri4* which encodes a cytochrome P450 monooxygenase that catalyzes the addition of four hydroxyl groups to trichodiene. The resulting isotrichotriol is non-enzymatically converted to isotrichodermol. This intermediate is subsequently processed by an acetyltransferase encoded by *Tri101*, which has been proven to reduce the toxicity of the metabolite and can be seen as a form of self-protection for the organism (Kimura et al., 1998). A monooxygenase encoded by *Tri11* adds another hydroxyl group which is then acetylated by the enzyme encoded by *Tri3*. These steps are shared between isolates of different *Fusarium* species or chemotypes. The steps that follow have different outcomes depending on whichever homologue of a certain gene is

present in the genome of an individual. They are "molecular switches" that define the chemotype of the organism (see **Figure 6.2** and **Table 6.1**).

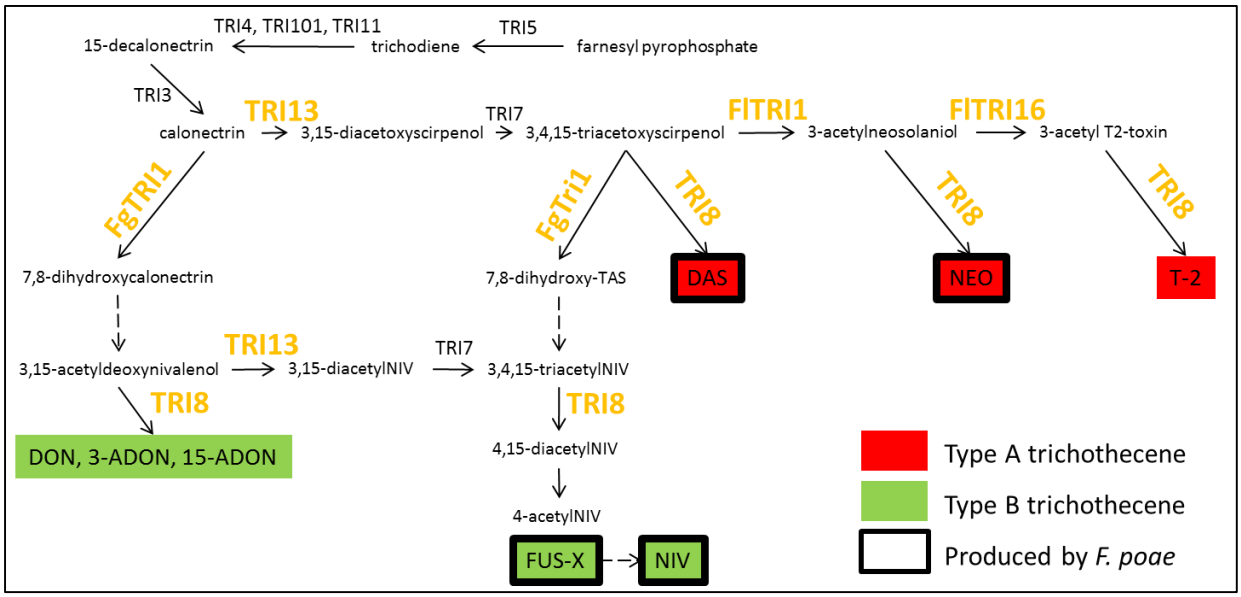

Figure 6.2 – Trichothecene biosynthesis pathway in *Fusarium* species (adapted from McCormick et al. (2011)). Enzymatic steps in orange print are the molecular switches of trichothecene biosynthesis: the presence of specific homologues of these genes will lead to a particular chemotype in the individual. For steps in dashed lines, no enzyme has been identified. Toxins in red are type A trichothecenes, green represents type B trichothecenes. Finally, the four compounds produced in *F. poae* are identified with black boxes.

The four molecular switches of trichothecene biosynthesis in *Fusarium* are listed in **Table 6.1** along with their respective functions. The most important determinant of type A versus type B trichothecene production is TRI1. Depending on whichever homologue is present within the genome, this P450 monooxygenase enzyme catalyzes the addition of one or two hydroxyl groups on its substrate (see **Figure 6.3**). FgTRI1 catalyzes the addition of two hydroxyl groups on its substrate calonectrin, which is not a substrate for FgTRI13 according to Kimura et al. (2007). The hydroxyl group at C8 is converted to a keto group by an unknown mechanism. The resulting 7,8 acetyl deoxynivalenol is a substrate for FgTRI13 and is hydroxylated in strains that have a NIV chemotype. In *F. graminearum* strains that have a DON chemotype, TRI8 converts the diacetylated substrate to mono-acetylated compounds, removing an acetyl moiety at C3 or C15 depending on the specific ADON chemotype of the isolate. The final step of ADON to DON is genetically not yet understood. The role of TRI1 as a molecular switch for trichothecene biosynthesis in *F. graminearum* was confirmed recently, when mutations at the *Tri1* locus in a subpopulation of this species led to novel trichothecene chemotypes (Varga et al., 2015).

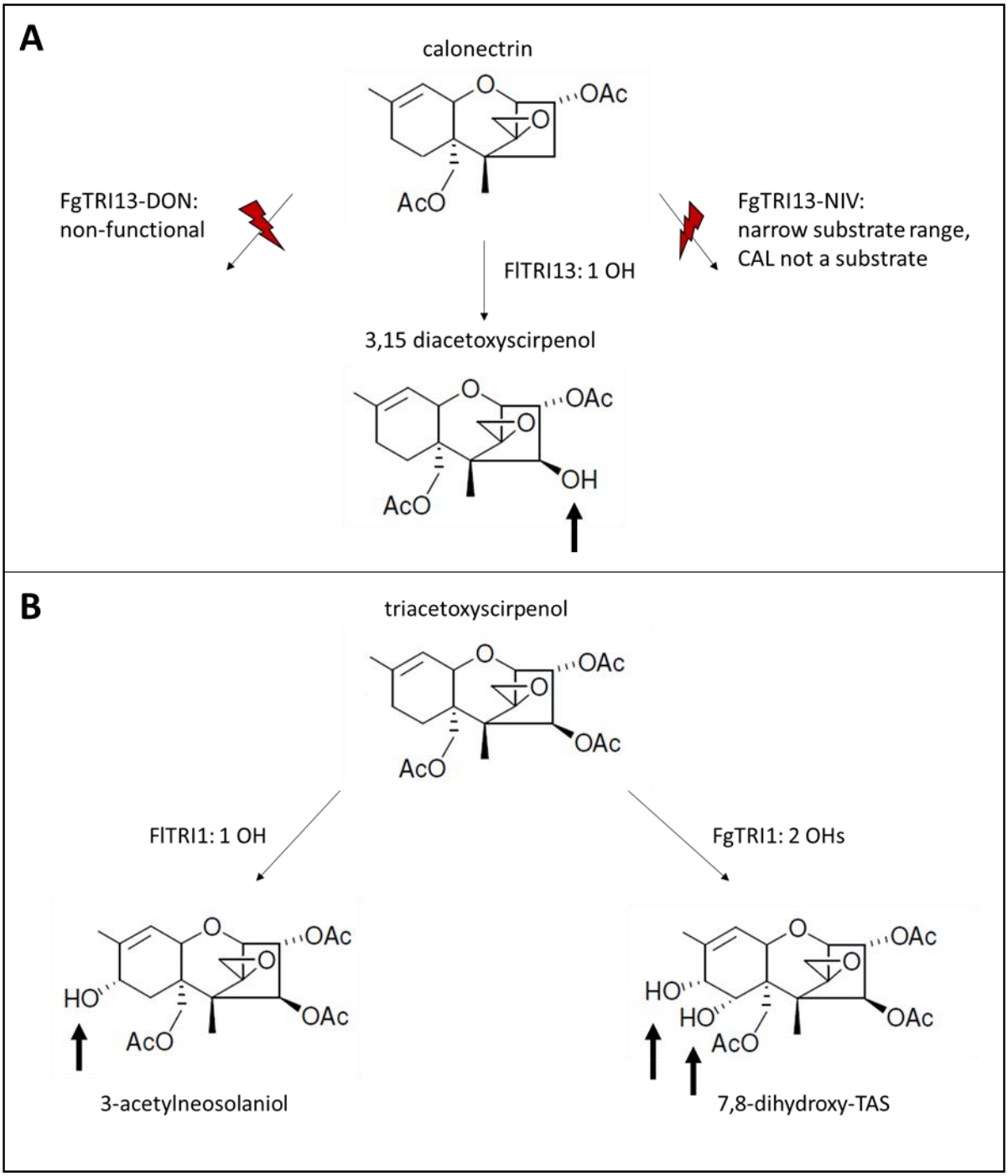

Figure 6.3 – Functional characterization of two important molecular switches of trichothecene biosynthesis. **A**: TRI13 mediates hydroxylation at the C4 position. FlTRI13 has a broad substrate range, opposed to FgTRI13-NIV which has a narrow substrate range and can only hydroxylate the substrate after it has been hydroxylated at C7 and C8 (Kimura et al., 2007). **B**: FgTRI1 catalyzes hydroxylation at C7 and C8, while FlTRI1 catalyzes hydroxylation only at C8 (McCormick et al., 2006).

The function of TRI1 is different in type A trichothecene producers. Most research into type A producers has been performed in *F. sporotrichioides*. This species is closely related to *F. langsethiae* and produces the same trichothecenes (Schmidt et al., 2004a), therefore it is

reasonable to assume that trichothecene biosynthesis should be similar, and the rest of this description will focus on *F. langsethiae*. In *F. langsethiae*, addition of only one hydroxyl group is catalyzed by FlTRI1. Biochemically this is possible with calonectrin as the substrate, as occurs in *F. graminearum* by FgTRI1. However, this is not the major pathway. Rather, calonectrin is a good substrate for FlTRI13 (in contrast to FgTRI13), and is hydroxylated by TRI13 and subsequently acetylated by TRI7 at C4. The resulting triacetoxyscirpenol is hydroxylated once at C8, giving rise to 3-acetylneosolaniol (3-ANEO). In *F. langsethiae*, a functional TRI16 enzyme is encoded, which subsequently acetylates 3-ANEO at C8, leading to 3-acetyl T-2 toxin (3-AT-2). Both 3-ANEO and 3-AT-2 are good substrates for TRI8 which converts them to respectively neosolaniol and T-2 toxin. Finally in *F. langsethiae*, triacetoxyscirpenol may also be converted to a type A trichothecene without the intervention of TRI1, depending on the esterification by TRI8 to 4,15 diacetoxyscirpenol. **Table 6.1** shows that depending on the species or chemotype, certain molecular switches may be non-functional due to mutations or deletions. The trichothecene producing *Fusarium* ancestor likely had functional *Tri13* and *Tri16* genes, as it is more likely for a functional gene to become non-functional than *vice versa* (Lee et al., 2002; Proctor et al., 2009).

Table 6.1 – Molecular switches of trichothecene biosynthesis in *Fusarium* species.

Species (chemotype)	Enzyme	Function	Reference
***F. langsethiae* (type A)**	TRI1	one hydroxylation at C8	McCormick et al. (2006)
	TRI8	deacetylation at C3	Alexander et al. (2011)
	TRI13	hydroxylation at C4, broad substrate range	Kimura et al. (2007)
	TRI16	esterification of C8	Peplow et al. (2003)
***F. poae* (type A+B)**	TRI1	hydroxylation at C7 and C8	
	TRI8	deacetylation at C3	
	TRI13	hydroxylation at C4, broad substrate range	
	TRI16	absent/truncated	Proctor et al. (2009)
***F. graminearum* NIV (type B)**	TRI1	hydroxylation at C7 and C8	McCormick et al. (2006)
	TRI8	deacetylation at C3	Alexander et al. (2011)
	TRI13	hydroxylation at C4, narrow substrate range	Kimura et al. (2007)
	TRI16	Nonfunctional	Proctor et al. (2009)
***F. graminearum* DON (type B)**	TRI1	hydroxylation at C7 and C8	McCormick et al. (2006)
	TRI8	deacetylation at C3 or C15	Alexander et al. (2011)
	TRI13	Nonfunctional	Lee et al. (2002)
	TRI16	Nonfunctional	Proctor et al. (2009)

The genes that code for the proteins that are described above are located together in clusters within the genome. It is thought that maintaining the genes for secondary metabolism together may confer an evolutionary advantage to pathogens, as epigenetic co-regulation becomes easier and genes have less chance of being separated during recombination events (Keller et al., 2005). Indeed, transcription factors tasked with the specific regulation of genes involved in the production of one secondary metabolite are often included within the secondary metabolite cluster. In the case of trichothecene biosynthesis, TRI6 and TRI10 are such transcription factors (Seong et al., 2009). Secondary metabolites are often classified by the nature of their chemical backbone structure, the formation of which is mediated by the first enzyme in the biochemical pathway. In the case of trichothecenes, this enzyme is TRI5. Beside the backbone gene, transcription factors and various tailoring enzymes (mediating hydroxylation, acetylation, etc.), efflux pumps may be encoded within the cluster that export the mycotoxins out of the hyphae, such as TRI12 in *Fusarium* (Menke et al., 2012). It was recently shown in *Fusarium graminearum* that during trichothecene metabolism, the involved enzymes are located in each other's proximity in the cytoplasm of the cell in so-called toxisomes (Broz and Kistler, 2014).

Rather unusual for secondary metabolite biosynthesis, the genes for trichothecene biosynthesis are located at 3 loci in *Fusarium* species. They are the *Tri* cluster, containing the *Tri5* backbone gene, various tailoring enzymes (*Tri11*, *Tri4*, *Tri13*, *Tri8*), two transcription factors (*Tri6*, *Tri10*) and an efflux pump (*Tri12*). A second locus consists of the *Tri1* gene, and in some species additionally the *Tri16* gene. Finally the third locus only contains one gene implicated in trichothecene biosynthesis, namely *Tri101*. Phylogeny of the trichothecene genes included in the *Tri* cluster, and *Tri101*, follow species phylogeny (Proctor et al., 2009). The phylogeny of the *Tri1* locus however is not concordant with species phylogeny, as alleles of *Tri1* are more similar to their homologues in distantly related species than to those in more closely related species (Proctor et al., 2009). This is illustrated in **Figure 6.4**. It was concluded that the four alleles of *Tri1* found within *Fusarium* species were likely to already have been present in the ancestral trichothecene producing *Fusarium*. The non-concordant phylogeny of *Tri1* when compared to species phylogeny is similar to the principle of trans-species polymorphism, which may be found within the type B trichothecene producing species. In that case, features of genes in the *Tri* cluster are shared between chemotypes, transcending species boundaries, and species may have different versions of *Tri* genes depending on their chemotype (Ward et al., 2002).

Surprisingly, in the *F. equiseti* clade, the *Tri* cluster has grown by relocation of the *Tri1* and *Tri101* genes, that have moved from their ancestral separate loci into the *Tri* cluster. Moreover,

regulation of *F. equiseti* trichothecene production may be different than in other *Fusarium* species, as an additional Zn2Cys6 transcription factor is present between *Tri5* and *Tri6* in the cluster (Proctor et al., 2009). The *F. equiseti* clade diverged from a trichothecene producing ancestor early in the evolution of trichothecene producing species. This can be seen in **Figure 2.1** (*F. equiseti* clade designated as the *incarnatum-equiseti* species complex, shaded grey). It has been described that *F. equiseti* isolates may also produce type A and type B trichothecenes simultaneously (Barros et al., 2012; Marin et al., 2012).

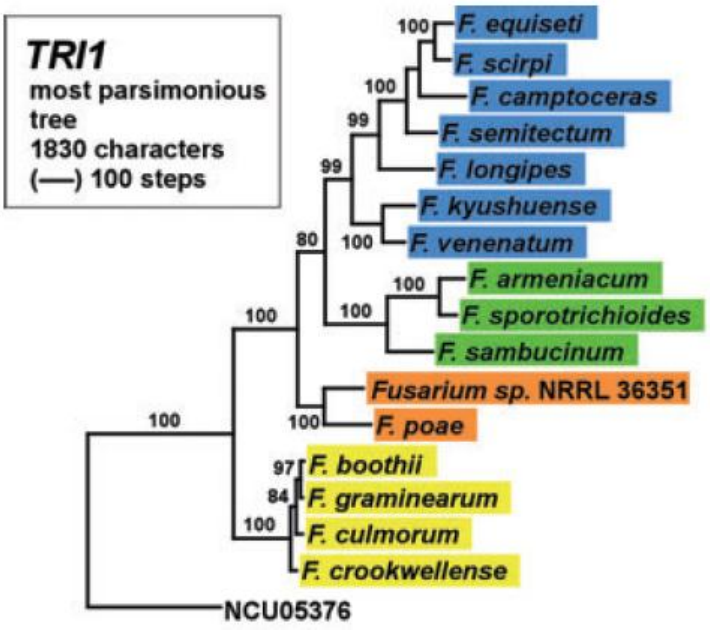

Figure 6.4 – Four alleles of the *Tri1* gene as described by Proctor et al. (2009).

How the molecular switches that mediate type A and type B trichothecene production work together to allow simultaneous production of both trichothecene types is unknown. Both *F. poae* and *F. equiseti* individuals have been described to produce both types simultaneously. Regulation of trichothecene production in *F. equiseti* may be particularly divergent however (Proctor et al., 2009). *Fusarium poae* isolates may therefore be a better fitting model to investigate the unusual chemotype. In Chapter 5 of this thesis, we showed that the link between the genotype and the detected chemotype may be tenuous in this species, and likely all isolates have the potential to produce both type A and type B trichothecenes. In this Chapter, we took the genome sequence of one such isolate and characterized the nature and function of the molecular switches. We compared the build-up of the trichothecene loci with other whole

genome sequenced isolates and screened the population for diversity at the *Tri1* locus. Finally, we propose a biosynthetic grid that explains the *F. poae* chemotype.

6.3 Material and methods

6.3.1 Sequence analysis

The genome sequences described in Chapter 4 of this thesis were used to extract the sequence of the trichothecene loci in isolates 2516, bfb0173, 2548 and 7555. The machine annotation of isolate 2516 was checked to ascertain that genes were correctly annotated, in accordance with literature on related *Fusarium* species. Similarities between amino acid sequence of the predicted proteins, and between nucleotide sequence of the intergenic regions, were determined with ClustalW2 (Larkin et al., 2007).

To visualize differences between *Tri1* alleles, the HiSeq reads of isolates bfb0173 and 2548 (see Chapter 4 of this thesis) were mapped to the only *Tri1* allele already published (NCBI accession GQ915520) with CLC Genomics Workbench 7.5. Reads were mapped at 0.5 length fraction and 0.8 similarity fraction.

A 1100 bp fragment of the *Tri1* gene was sequenced for a set of 34 isolates selected from different backgrounds and characteristics (see Chapters 4 and 5 of this thesis). Primers are shown in **Table 6.2**. PCR and sequencing were performed as described in Chapter 4 and 5 of this thesis. Maximum parsimony analysis was performed with PAUP version 4.0b10 (Swofford, 2003). The *Tri1* fragment from *Fusarium sp.* NRRL 36351 (NCBI accession GQ915523.1) was used as the outgroup, however for construction of the phylogenetic tree mid-point rooting was used. Bootstrapping was performed with PHYLIP based on 1000 replicates (Plotree and Plotgram, 1989).

The presence of a *pogo* TE in the *Tri* cluster was investigated with three primers as detailed in **Table 6.2**. Diagnostic PCR was performed as described earlier in this thesis.

Table 6.2 – Diagnostic primers used in this Chapter.

ID	Sequence (5' → 3')	Reference	Target
1285	GCGTCTCAGCTTCATCAAGGCAKCKAMTGAWTCG	Proctor et al. (2009)	*Tri1*
1292	CTTGACTTSMTTGGCKGCAAAGAARCGACCA	Proctor et al. (2009)	*Tri1*
pogo.fwd	AGACTCCGTACTGCCTTCAC	this study	*pogo* insertion
pogoabsent.rev	CTCCCCTGCAAAACATAGCC	this study	*pogo* insertion
pogopresent.rev	TATAGGGCTCTTTCAGGGGC	this study	*pogo* insertion

6.3.2 Fungal transformation

Isolate 2516 was selected for further analysis. A strategy was set up to first make a knockout of the *Tri1* and *Tri13* genes in this isolate, followed by integration of their counterparts from *F. graminearum* (NIV chemotype) and *F. langsethiae* (T-2 chemotype) into the knockout, restoring the trichothecene pathway back to functionality but with proteins with a described differential function at key points in the pathway, similar to an approach carried out before for *Tri1* alleles in *F. graminearum* (Varga et al., 2015).

The general outline of the transformation was carried out as described by Abou Ammar et al. (2013) with minor adaptations. For protoplasting, conidia were harvested from UV-exposed plates as described in Chapter 4 of this thesis. $5x10^6$ conidia were inoculated into 100 ml trichothecene biosynthesis inducting medium (see Chapter 5) to induce transcription of trichothecene genes and therefore obtain less densely wound DNA in the later stages. Growth was allowed for 16 hours at 150 rpm and 26°C. Mycelium was harvested with sterile one layer filter paper and transferred with a spatula into a sterile 100 ml Erlenmeyer. 20 ml protoplasting enzyme mix was added, which consists of 500 mg driselase, 1 mg chitinase and 100 mg lysing enzyme of *Trichoderma harzianum* (all obtained from Sigma, Diegem, Belgium) in 1.2 M KCl. Before addition to the mycelium, the protoplasting mix was stirred at room temperature and 20 rpm for 30 minutes, and subsequently filtersterilized with a 0.45 µm Millex-HA filter and 15 ml syringe (VWR). Protoplasting was allowed to proceed for four hours at 30°C and 100 rpm shaking. Protoplasts were separated from undegraded mycelium with four layers of sterile Miracloth (Merck, Overijse, Belgium) into a 50 ml Falcon tube (VWR). The protoplasts were pelleted at 1500g for 10 minutes and resuspended in 0.5 ml STC buffer (1.2 M sorbitol, 50 mM CaCl and 10 mM Tris/HCl to pH 7.5, and autoclaved). Protoplasts were quantified with a Bürker counting chamber and adjusted to $2x10^7$ protoplasts per ml.

Transformation reactions were set up in 1.5 ml tubes containing 100 µl STC buffer, $2x10^6$ protoplasts in another 100 µl STC buffer, 50 µl PEG buffer (30% PEG8000, 0.5 mM CaCl, 10 mM and 10 mM Tris/HCl to pH 8.0, and filtersterilized with a 0.45 µm Millex-HA filter) and ~7.5 µg of the DNA construct (see further). The transformation reaction was gently shaken at room temperature for 20 minutes and 50 rpm and was subsequently transferred into a 15 ml Falcon tube containing 2 ml of the PEG buffer. After another 5 minutes of shaking at the same conditions, 4 ml STC buffer was added to the tube and carefully homogenized. Aliquots of 600 µl were added to 15 ml of regeneration medium (0.5 g yeast extract, 0.5 g casein hydrolysate, 275 g saccharose and 5 g agar per 1 l distilled water), carefully homogenized and left in

petridishes for 20 hours at 26°C. 15 ml of regeneration medium containing 200 µg/ml hygromycin (Sigma, Diegem, Belgium) was added to the Petri dishes and transformants that emerged after 6 days were transferred to Petri dishes containing PDA medium amended with 100 µg/ml of the selective marker.

A representative and confirmed knockout was selected for *Tri1* and *Tri13*, and used for a second round of transformations. This was performed exactly as described above, but with different DNA constructs and selective agent. Beside the DNA construct carrying the *Tri1* or *Tri13* gene from *F. graminearum* or *F. langsethiae* between the flanks of *FpTri13*, a construct carrying a constitutively expressed resistance gene against G418 (geneticin) was used to enable selection of transformants in a co-transformation setup. Co-transformation entails that the desired transformant has two independent integration events: the *Tri* gene has integrated at the native locus, and the G418 cassette has integrated randomly in the genome. Geneticin (Sigma) was added to regeneration medium overlay at 200 µg/ml and to PDA plates for maintenance at 100 µg/ml. Successful gene swap transformants have integrated the *Tri1* or *Tri13* construct at the native locus, removing hygromycin resistance and enabling negative selection on hygromycin containing media. **Figure 6.5** visualizes the gene swap strategy.

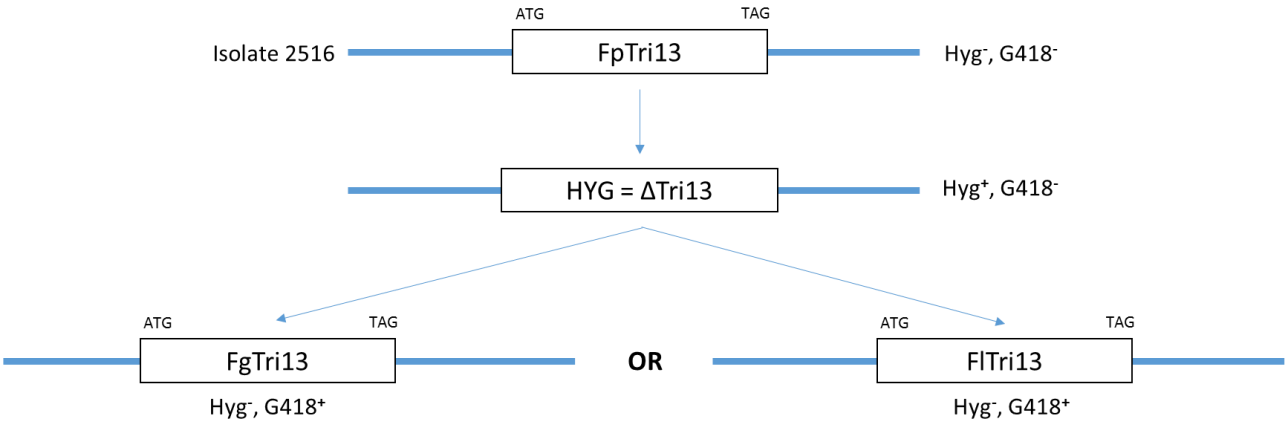

Figure 6.5 – Gene swap strategy. WT isolate 2516 is transformed with a hygromycine cassette to knockout *FpTri13*. A successful knockout has lost *FpTri13* and has gained the hygromycine cassette, and is hygromycin resistant (Hyg^+). This knockout is transformed simultaneously (co-transformation) with a G418 cassette and constructs carrying the *FgTri13* or *FlTri13* allele enclosed between the flanks of the *FpTri13* gene, introducing G418 resistance and removing hygromycin resistance in co-transformants (Hyg^- $G418^+$). The hygromycin cassette is removed as the *FgTri13* or *FlTri13* cassette has come in its place. It is therefore possible to perform negative selection on hygromycin containing medium: successful gene swaps (derived from the knockout) will not be resistant to hygromycin anymore.

6.3.3 DNA construct synthesis

All primers that were used for DNA construct synthesis can be found in **Table 6.3**. DNA constructs for knockout transformation were made using two approaches: triple crossover, also referred to as the split-marker approach (Catlett et al., 2003) and the double crossover approach (Szewczyk et al., 2006) (see **Box 6.1**). All PCR reactions involving construct synthesis were carried out with Phusion High-Fidelity DNA Polymerase (Thermo Scientific) according to the manufacturer's instructions, with minor adaptations for the amplification of construct fragments: the denaturation step of the PCR cycles was raised to 30 seconds and the final extension step was shortened to 1 minute. Broadly, for both approaches, flanks were amplified from genomic DNA of isolate 2516. Resistance cassettes were amplified from plasmid pAN7-1, containing the *hph* gene; hygromycin phosphotransferase, conferring resistance to hygromycin; including a constitutive promotor (Punt et al., 1987). Primers were designed to function in fusion PCR (Szewczyk et al., 2006) without added primers. Several *hph* primers were taken from Abou Ammar et al. (2013). The amplicons were purified with the QIAquick PCR Purification Kit (Qiagen) according to the manufacturer's instructions and were quantified with the Quantus fluorometer (Promega). Following fusion and double strand gap filling during 10 PCR cycles, another 25 cycles were run after nested primers were added, during which bulk production of the complete construct is assured. Fusion protocols were carried out as outlined by Yu et al. (2004), with some adaptations. Only a combined ~2ng of fragment DNA was used as input for the fusion PCR. Fusion PCRs were performed with the following PCR cycle parameters: initial denaturation of 30 seconds at 98°C, 10 cycles of denaturation (98°C, 15 seconds), annealing (60°C, 20 seconds) and extension (72°C, duration dependent on amplicon length), followed by a cooling down to 4°C. After nested primers were added, another 25 cycles of denaturation (98°C, 15 seconds), annealing (63°C, 20 seconds) and extension (72°C, duration dependent on amplicon length) were run, followed by a final extension period of 2 minutes (72°C) and cooling down to 4°C.

Box 6.1: double crossover versus triple crossover knockouts

Two different approaches were taken to obtain *Tri1* and *Tri13* knockouts: the double crossover approach and the triple crossover approach. In the triple crossover approach, two overlapping segments of the marker gene (i.e. a gene conferring resistance to hygromycin) are fused to respectively the upstream or downstream flank of *FpTri1* and *FpTri13*. Through triple crossover, a functional marker is obtained at the desired locus (see Figure in this Box). Crossover is shown with a dashed line. In the double crossover strategy, a functional marker gene is included within the DNA construct, requiring one less crossover event to have resistant colonies. This method has a higher chance of false positives, as simple ectopic integrations will lead to resistant colonies; ectopic integrations occur when after a naturally occurring strand break the DNA construct is included between the two ends during repair. The fusing of DNA fragments for both approaches is similar, i.e. tailed primers are used that add complementary pieces of sequence to each separate fragment, and which can be used for fusion PCR.

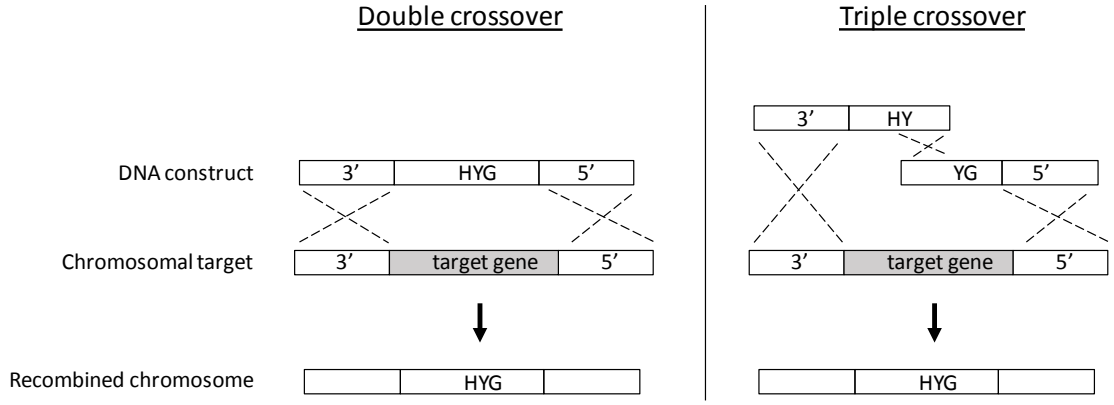

Table 6.3 - List of primers used for knockouts and gene swaps in this study. BSC = bulk synthesis of construct; KO = knockout; GS = gene swap.

Name	Sequence (5' → 3')	Target	Amplicon
FpTRI1_KO_LF5pr.F1	TGCTAACGTACCAAGGGAAAC	Fp2516	5' flank of *Tri1* for KO and GS
FpTRI1_KO_LF5pr_nest.F2	CGAGACCGTATCACGAAACATAG	fusion PCR	5' flank of *Tri1*, nested for BSC in KO and GS
FpTRI1_KO_RF3pr.R1	GCTGATGGTGCCTCAGTG	Fp2516	3' flank of *Tri1* for KO and GS
FpTRI1_KO_RF3pr_nest.R2	GGTAGAAAGAATTTCAGTCGTGG	fusion PCR	3' flank of *Tri1*, nested for BSC in KO and GS
FpTRI1_KO_LF5pr_fus_uni.R1	GTGCAACTGACAGTCGTACAGACAGCCATGATGTTGAGATG	Fp2516	5' flank of *Tri1* for KO
FpTRI1_KO_RF3pr_fus_uni.F1	GTCTGGAGTCTCACTAGCTTGGAGTCGTTGACACCTCATTACTAC	Fp2516	3' flank of *Tri1* for KO
Fp_LF_GS13_FWD	ATGTAGAAGATCCAACGC	Fp2516	5' flank of *Tri13* for KO and GS
		fusion PCR	5' flank of Tri3, nested for BSC in KO DJ-PCR and GS
Fp_LF_GS13_NEST	CTGAGACGCTGACCAAAGTAG	fusion PCR	5' flank of *Tri13*, nested for BSC
Fp_RF_GS13_REV	GTTCGGGCTGGCTGAATT	Fp2516	3' flank of *Tri13* for KO and GS
Fp_RF_GS13_fwd.2	GACCTGGAAAATGAATGGTGTC	fusion PCR	3' flank of *Tri13*, nested for BSC in split marker
Fp_RF_GS13_NEST.2	GGCATTGTGTGGTAGAGCTG	fusion PCR	3' flank of *Tri13*, nested for BSC in KO DJ-PCR and GS
FpTri13_KO_LF_uni.F1	GTCTGGAGTCTCACTAGCTTTCTTTGTAGCGTCAACCACC	Fp2516	5' flank of *Tri13* for KO
FpTri13_KO_RF_uni.R1	GTGCAACTGACAGTCGTACAGTTGCCATAGGACAAAAGAGTG	Fp2516	3' flank of *Tri13* for KO
uni-hyg.F1	TGTACGACTGTCAGTTGCACTGACCGGTGCCTGGATCTTC	pAN7-1	hyg cassette
uni-hyg.R1	AAGCTAGTGAGACTCCAGACGGTCGGCATCTACTCTATTCC	pAN7-1	hyg cassette
hyg.sm.rev	AATCGCGCATATGAAATCAC	pAN7-1	part of hyg cassette (construct A)
hyg.sm.nest.rev	TATTGACCGATTCCTTGCG	fusion PCR	nested for BSC
hyg.sm.fwd	TTGACTAACAGCTACCCCGC	pAN7-1	part of hyg cassette (construct B)
hyg.sm.nest.fwd.2	GTCTCCGACCTGATGCAG	fusion PCR	nested for BSC
hyg.sm.nx2.rev	AGCCGCGGCGATCCTGCAAG	pAN7-1	part of hyg cassette (construct C)
		fusion PCR	BSC
hyg.sm.nx2.fwd	CTGTTCTGCAGCCGGTCGC	pAN7-1	part of hyg cassette (construct D)
		fusion PCR	BSC
FpTRI1_GS_LFfp_Rev2	GACAGCCATGATGTTGAGATG	Fp2516	5' flank of *Tri1* for GS

FpTRI1_GS_RFfp_Fwd2	GCTTTCATTGGAGTCGTTGAC	Fp2516	3’ flank of *Tri1* for GS
Fp_LF_GS13_Rev2	TAGACTTGATATATATTATAAACTAGTTC	Fp2516	5’ flank of *Tri13* for GS
Fp_RF_GS13_Fgram_Fwd2	AGAAACATGATGGCTGCTTCG	Fp2516	3’ flank of *Tri13* for GS, *F. graminearum* tail
Fp_RF_GS13_Flang_Fwd2	CAGAGAGAGAGAAACATGATGGCTG	Fp2516	3’ flank of *Tri13* for GS, *F. langsethiae* tail
Fg_CDS13_Fwd2	GAACTAGTTTATAATATATATCAAGTCTATGCCCTTGTCAAGTCGAC	FgMBC-7728	coding region of *FgTri13*
Fg_CDS13_Rev2	GAAGCAGCCATCATGTTTCTCTCTATCGG	FgMBC-7728	coding region of *FgTri13*
Fl_CDS13_Fwd2	GAACTAGTTTATAATATATATCAAGTCTATGTCGTTGTTAAATCGACC	Fl202063	coding region of *FlTri13*
Fl_CDS13_Rev2	CATGTTTCTCTCTCTCTGTCTAATG	Fl202063	coding region of *FlTri13*
FpTRI1_GS_CDSFG_F1	CTCAACATCATGGCTGTCATGGCTCTCATCAC	FgPH-1	coding region of *FgTri1*
FpTRI1_GS_CDSFG_R1	GTCAACGACTCCAATGAAAGCCTAGTCATCCTGTACCAATTCC	FgPH-1	coding region of *FgTri1*
FpTRI1_GS_CDSFL_F1	CTCAACATCATGGCTGTCATGTCAAAAGTTGATAAAACTGG	Fl202063	coding region of *FlTri1*
FpTRI1_GS_CDSFL_R1	GTCAACGACTCCAATGAAAGCTTAGGACTCTGACTCCCTACTG	Fl202063	coding region of *FlTri1*

In the triple crossover approach, two overlapping segments of the *hph* gene were joined to respectively the upstream and downstream flank of the gene to be knocked out (see **Box 6.1**). Joining of the fragments occurred through the principle of double joint PCR and employed tailed primers for amplicon generation, followed by a PCR step without primers and a PCR step with nested primers (Yu et al., 2004). The two resulting constructs were used for transformation, during which triple crossover takes place at the native locus which renders the resistance gene functional and deletes the target gene. Four constructs were made: two that overlap with 368 bp (A+B) and two that overlap with 457 bp (C+D). Primers targeting the *hph* gene for constructs C and D were taken from Varga et al. (2015). In the double crossover approach, the complete constitutive promotor + *hph* gene was amplified from pAN7-1 and joined to the upstream and downstream flank of the target gene by double joint PCR (Yu et al., 2004).

Constructs for gene swaps were made that join the *Tri1* and *Tri13* genes of both *F. graminearum* and *F. langsethiae* to the upstream and downstream flanks of *FpTri1* and *FpTri13*. Flanks were amplified from genomic DNA of isolate 2516. Coding regions of *Tri1* were amplified from *F. graminearum* PH1 (kindly donated by dr. Stefan Wirsel, MLU Halle-Wittenberg, Germany) and *F. langsethiae* 202063 (kindly donated by dr. Ingerd Hofgaard, Bioforsk, Norway) genomic DNA. The *FgTri13* coding region was amplified from isolate MBC-7728, a NIV producing *F. graminearum* (therefore, with a functional *Tri13* allele) kindly donated by Pierre Hellin (UCL, Belgium). Finally, the *FlTri13* coding region was amplified from *F. langsethiae* isolate 202063. Chimeric primers were developed to synthesize constructs that are identical to the *F. poae* locus with only the exact region from start to stop codon replaced (for primers see **Table 6.3**). The double joint PCR protocols as outlined above were followed. As a separate construct for co-transformation, the G418 resistance cassette was amplified from plasmid pII99 (Namiki et al., 2001), containing a constitutive promotor, the *npt* gene (neomycin phosphotransferase; conferring resistance to G418) and a transcription termination site.

The obtained constructs were purified with the QIAquick PCR Purification Kit (Qiagen) according to the manufacturer's instructions and quantified using the Quantus fluorometer (Promega). Approximately 7.5 µg of construct was used for the double crossover approach, and approximately 5 µg of every construct in the triple crossover approach.

6.3.4 Confirmation of transformants

Freshly grown mycelium was scraped from the PDA plates and transferred to 1.5 ml centrifuge tubes, in which the mycelium were crushed using disposable Entogen inoculation loops that

were exposed to liquid nitrogen. 500 µl of lysis buffer (200 mM Tris/HCl, 50 mM EDTA, 200 mM NaCl, 1% n-lauroylsarcosin, pH = 8.0) was added and microwaved at maximum intensity (800W) to the point of boiling (+/- 1 minute). Debris was pelleted by centrifuging for 15 minutes at 13 200 rpm and room temperature, and 300 µl of supernatant was treated with 300 µl of ice-cold isopropanol. DNA was pelleted by centrifuging for 15 minutes at 13.200 rpm and room temperature. The pellet was washed with ice-cold 70 % EtOH, was allowed to dry for 30 minutes and was finally re-dissolved in 25 µl TE buffer. Correct integration of the selective marker gene was verified with triplex PCR. One amplicon spanned the left integration site, one amplicon spanned the right integration site and one amplicon was specific to the wild type gene. PCR was performed as described before. Primers used for confirmation of transformants can be found in **Table 6.4**. Transformants for which only the first two amplicons were obtained were selected for single sporing, by plating dilutions of conidial suspensions on PDA plates containing 100 µg/ml of the selective agent. Single outgrowing colonies were transferred to PDA containing the marker, and DNA was extracted using the CTAB method. Quantification was performed with the Quantus fluorometer (Promega).

Table 6.4 - List of primers used to confirm successful knockouts of *Tri1* and *Tri13*.

Name	Sequence (5' → 3')	Target	Amplicon
FpTri13.probe.fwd	CCAGGAGTCCATACGCTAGG	Fp2516-ΔTri13	wild type *Tri13*
FpTri13WT.rev1	GTTTCTCAGCCCGTTACACC	Fp2516-ΔTri13	wild type *Tri13*
FL.Tri13.contr.Fw	ACGCCATTACCATAGAATTGTCG	Fp2516-ΔTri13	confirmation integration of upstream flank *Tri13*
hyg.Fw2	GACATCACCATGCCTGAACTC	Fp2516-ΔTri13, ΔTri1	confirmation integration of upstream flank *Tri1* and *Tri13* KO
FR.Tri13.contr.rv	GCGTCAGGTCTCAGGATGAT	Fp2516-ΔTri13	confirmation integration of downstream flank of *Tri13*
hyg.conf.rev2	CCGGTGATTCGATGAAGCTC	Fp2516-ΔTri13, ΔTri1	confirmation integration of downstream flank *Tri1* and *Tri13* KO
Tri1.FL.contr.fwd	CGTGCAACTGTAGTCTTCCAG	Fp2516-ΔTri1	confirmation integration of upstream flank *Tri1*
Tri1.FR.contr.Rev2	GTAGAGTAATGCCAGCAACCG	Fp2516-ΔTri1	confirmation integration of downstream flank *Tri1*
FpTri1WT.fwd2	CTTAACCCCAAGCGCTGGTA	Fp2516-ΔTri1	wild type *Tri1*
FpTri1WT.rev2	GGCGGACTGTTCTCTCTCAC	Fp2516-ΔTri1	wild type *Tri1*

To screen for ectopic integrations, beside the correct integrations identified by the triplex PCR, Southern blotting was performed. To this end, DIG labelled hygromycin probes were generated from plasmid pAN7-1 using the PCR DIG Labeling Mix^{PLUS} (Roche) protocol according to the manufacturer's instructions. Five µg of gDNA of the transformants was restricted with XhoI in the case of *Tri13* knockouts, and SacI in the case of *Tri1* knockouts (restriction enzymes purchased from Thermo Scientific). Blotting of the restriction digest on a positively charged nylon membrane and hybridization with the DIG labelled probe occurred as described in the "DIG Application Manual for Filter Hybrization" (Roche). Subsequent binding with DIG-specific antibody and detection of chemiluminescence with CSPD were performed with the DIG Luminescent Detection Kit (Roche) according to the manufacturer's instructions.

6.3.5 Comparative homology modelling

The protein sequences of *F. kyushuense* Tri1 (FkTRI1), *F. graminearum* Tri1 (FpTRI1), *F. langsethiae* Tri1 (FlTRI1) and *F. poae* Tri1 (FpTRI1) were taken from NCBI (accessions ACZ63276.1; AAQ02672.1; AEB26549.1 and ACZ63280.1 respectively). Protein alignment was performed with ClustalO (Sievers et al., 2011). Protein sequences were used as queries for the Phyre2 algorithm (Kelley et al., 2015), which predicts a 3D structure for the protein based on local similarity with proteins that have been crystallized to determine their structure. DFire was used to assess the model quality (Zhou and Zhou, 2002) and select the top-ranking model for further analysis. Autodock VINA was used to dock selected substrates (calonectrin, 8-hydroxycalonectrin, dihydrocalonectrin, triacetoxyscirpenol, 3-acetylneosolaniol) to the best ranking model for every species (Trott and Olson, 2010). Substrate structures were downloaded from PubChem. Binding affinities were extracted from the docking results. Docking results were visualized in PyMOL.

6.3.6 Chemical analysis

Methods for the induction of trichothecene biosynthesis and analytical procedures for measurement were identical to those described in Chapter 5 of this thesis.

6.4 Results

6.4.1 The organization of the trichothecene clusters in *F. poae*

The configuration of the *Tri* cluster in *F. poae* isolate 2516 was extracted from its genome sequence and compared with those of *F. sporotrichioides* (NCBI accession AF359360.3) and *F. graminearum* (NIV chemotype, NCBI accession AF336365.2); the result can be seen in **Figure 6.6**. The overall organization of the *Tri* cluster is highly similar to what was described

previously for *F. sporotrichioides* and *F. graminearum*. The largest difference comes from the intergenic distance between *Tri5* and *Tri6*, that is expanded in isolate 2516. A low complexity region with blastx hits for a *pogo* transposable element accounts for an additional 2.1 kb of sequence in this region. No intact copies of this element could be found in the genome, and it was likely RIPped to extinction in isolate 2516 (see Chapter 4 of this thesis). The best blastx hit for the *pogo* element is "*pogo* transposable element with KRAB domain from *Fusarium oxysporum* f. sp. *cubense* race 1" (NCBI accession ENH68388.1). Brown et al. (2004) described the flanking ORFs of *F. sporotrichioides* and *F. graminearum*. The flanking ORFs of *F. poae* isolate 2516 are similar in organization to those described in their study (data not shown). The organization of the *Tri1* region in isolate 2516 is identical to what was described before by Proctor et al. (2009).

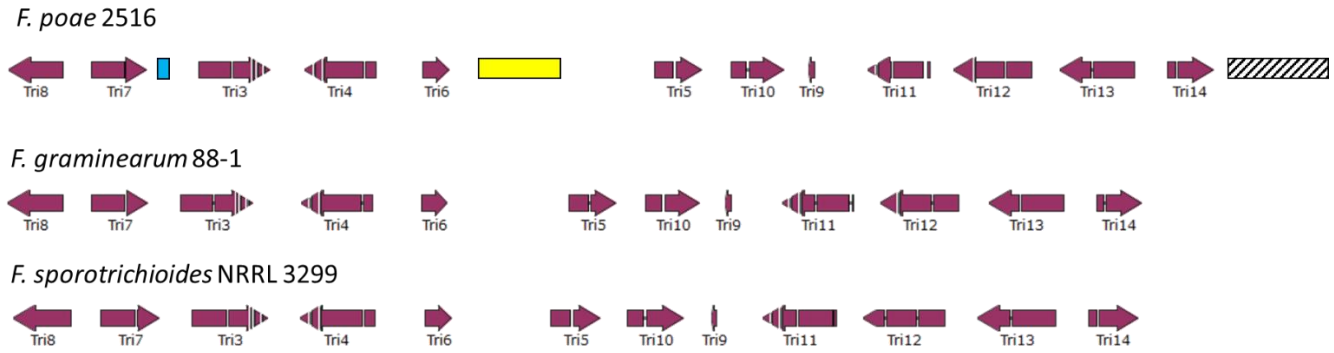

Figure 6.6 – Organization of the *Tri* cluster in *F. poae* (isolate 2516), which is identical to the organization in *F. graminearum* (isolate 88-1, NIV chemotype, NCBI accession AF336365) and *F. sporotrichioides* (isolate NRRL 3299, NCBI accession AF359360). The difference in *Tri6-Tri5* intergenic region between *F. poae* and *F. graminearum*/*F. sporotrichioides* is explained by the presence of a RIPped *pogo* transposable element (yellow). This element is also present at the same location in isolate bfb0173. In isolates 2516 and bfb0173, there is a 400bp repetitive element between *Tri7* and *Tri3* (blue). Finally, in isolates 2548 and bfb0173, there is a RIPped retrotransposon downstream of *Tri14*. It is illustrated as a shaded box in this figure, but it should be stressed that this element is in fact not present at that location in isolate 2516.

The highly contiguous assembly of *F. poae* isolate 2516 (see Chapter 4 of this thesis) allowed for the three loci to be positioned within their exact genomic coordinates. The *Tri1* gene lies at 55 207 – 56 959 bp into chromosome 1, the *Tri* cluster including *Tri5* lies at 5 545 692 – 5 575 616 bp into chromosome 2, and finally the *Tri101* gene can be found at 4 906 101 – 4 907 486 bp into chromosome 4. These positions are similar to those for the three loci in *F. graminearum*. **Figure 6.7** visualizes the three loci on the *F. poae* core chromosomes.

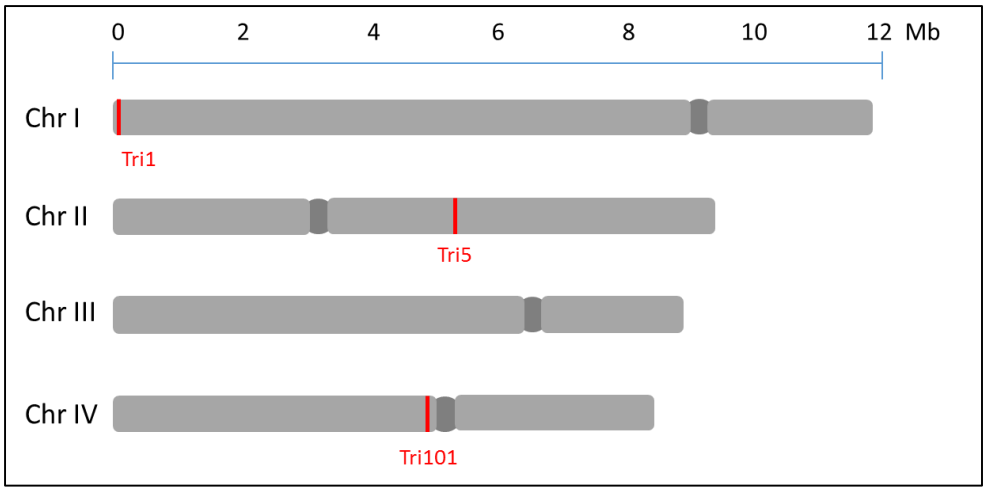

Figure 6.7 – Position on the chromosomes of *F. poae* where the three loci of trichothecene production are situated. These are similar to the loci determined for *F. graminearum*. Chromosome numbering is consistent with literature and Chapter 4 of this thesis. The scale bar shows the size of the chromosomes in Mb.

The genome sequence of isolates 2548, 7555 and bfb0173 were examined to find differences in the organization of the trichothecene clusters between these isolates and isolate 2516. The RIPped *pogo* TE that lies between *Tri5* and *Tri6* is also present in isolate bfb0173 and is highly conserved (three SNPs). It is not present in isolates 2548 and 7555. Because of its location in the middle of the trichothecene biosynthesis cluster, we set out to determine its incidence in the *F. poae* population (see **Figure 6.8**). Thirty-eight out of sixty-six isolates were confirmed to contain the insertion at the same location as isolates 2516 and bfb0173. For three isolates (isolates 2033, 2392 and 2491), the PCR did not deliver a result. There is no correlation with the chemotype, quantitatively nor qualitatively (**Figure 6.9**).

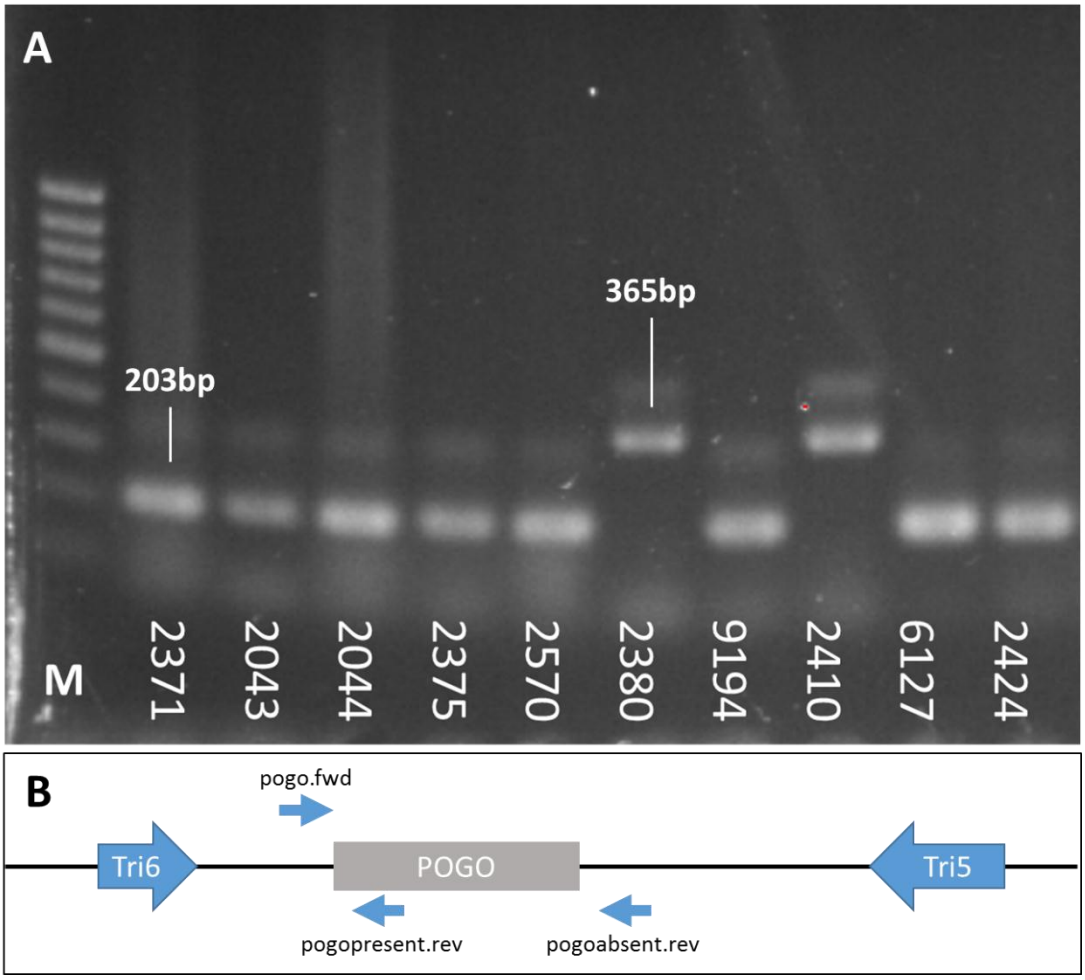

Figure 6.8 – Diagnostic PCR of the *pogo* insertion between *Tri5* and *Tri6*. **A**: Gel electrophoresis of the diagnostic PCR. **B**: Primers *pogo.fwd* and *pogopresent.rev* result in an amplicon of 203 bp (isolates 2371, 2043, 2044, 2375, 2570, 9194, 6127 and 2524), primers *pogo.fwd* and *pogoabsent.rev* result in an amplicon of 365 bp (isolates 2380 and 2410). M represents the molecular weight marker (Thermofisher's Massruler DNA Ladder Mix, Low range).

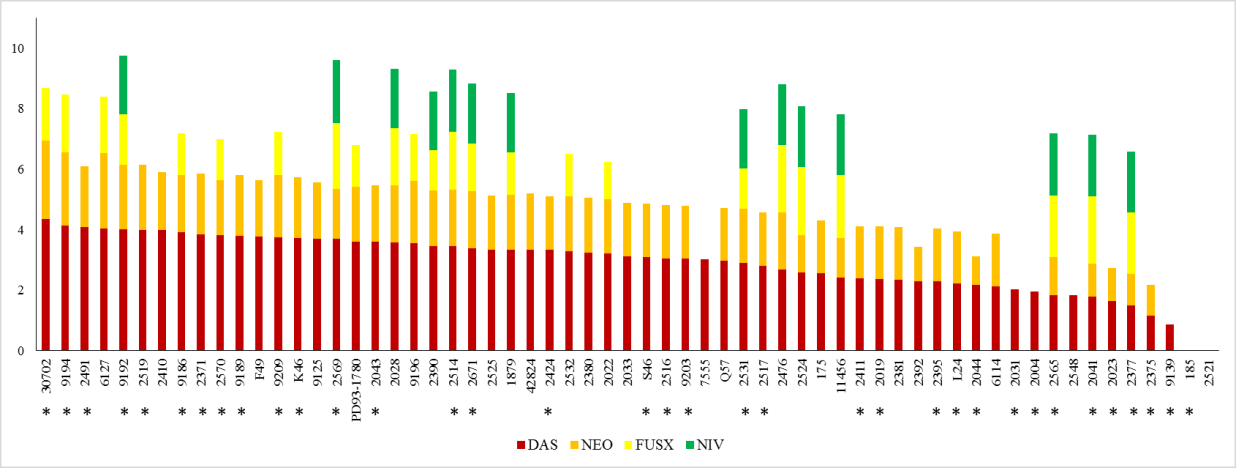

Figure 6.9 – Trichothecene chemotype of 61 *F. poae* isolates (see Chapter 5 for scales and details), and the presence of a *pogo* element between *Tri5* and *Tri6* in the *Tri* cluster (asterisks).

Downstream of *Tri14*, the outermost gene of the trichothecene cluster, a RIPped retrotransposon occurs in isolates 2548 and bfb0173. In isolate bfb0173 it consists of 3.7 kb of low complexity sequence (after which the contig ends), while in isolate 2548 1.2 kb of sequence that is highly identical to bfb0173 (10 SNPs) can be found before the contig ends. The best blastx hit for this retrotransposon is a protein from *Claviceps purpurea* (NCBI accession CCE29311.1). In isolates 2516 and bfb0173, there is a 400 bp repetitive element without blastx hits between *Tri7* and *Tri3* that is not present in isolates 2548 and 7555.

The genes in the *Tri* cluster are more closely related to *F. sporotrichioides* than to *F. graminearum* (**Table 6.5**). The same is true for *Tri101*.

Table 6.5 – Overall similarity (%) of all trichothecene biosynthesis genes between *F. poae* and *F. sporotrichioides / F. graminearum*. For the genes, protein similarity is given, while similarities of the intervening sequences (IVS) were determined on the nucleotide level. For *F. poae*, sequences were extracted from the genome of isolate 2516. For *F. graminearum*, information from the *Tri* cluster was extracted from NCBI accession AF336365 and TRI1 and TRI101 protein sequences were taken from NCBI accessions AAQ02672 and BAA33768 respectively. For *F. sporotrichioides* information from the *Tri* cluster was extracted from NCBI accession AF359360 and TRI1 and TRI101 protein sequences were taken from NCBI accessions AEB26547 and ADQ52715 respectively. There is no *Tri16* in *F. poae*.

	F. poae	
	- F. sporotrichioides	***- F. graminearum***
TRI8	85	74
IVS	73	63
TRI7	81	73
IVS	72	67
TRI3	86	84
IVS	64	62
TRI4	91	86
IVS	75	74
TRI6	88	89
IVS	73	70
TRI5	96	90
IVS	81	74
TRI10	89	89
IVS	74	72
TRI9	97	95
IVS	72	62
TRI11	94	91
IVS	72	68
TRI12	82	74
IVS	68	66
TRI13	88	78
IVS	71	67
TRI14	94	91
TRI1	68	69
TRI101	84	76

6.4.2 Different *Tri1* types in the *F. poae* population

The genome sequence of isolates 2516, bfb0173, 2548 and 7555 was examined to uncover variability at the *Tri1* locus, which is the most important determinant for type A versus type B trichothecene production. We found that the *Tri1* alleles in isolates 2516 and bfb0173 are identical to one another and the published sequence for *FpTri1* (NCBI accession GQ915520), and these have 97 % sequence identity to the *Tri1* alleles of isolates 2548 and 7555 (respectively

51 and 52 (=51+1) SNPs over the 1753 bp gene). Respectively 24 and 25 of these SNPs occur in the exons of the gene, while 87% of the gene is exonic (1527 bp). Remarkably, only respectively 2 and 3 of these SNPs are non-synonymous mutations. Two of these amino acid substitutions occur at the N-terminal end of the protein within the first 14 amino acids. **Figure 6.10** shows the read mapping of reads from isolate bfb0173 and isolate 2548 on the published *FpTri1* allele, and shows that a disproportionate amount of SNPs occurs in the introns of the genes.

A subset of 34 isolates of the *F. poae* collection (see Chapters 4 and 5 of this thesis) was selected for sequencing of a 1100 bp fragment of *Tri1*. The existence of two major *Tri1* types within the collection was confirmed, with additional variation at individual isolates' level (**Figure 6.11**). There is no clear link between the chemotype and the *Tri1* type determined here.

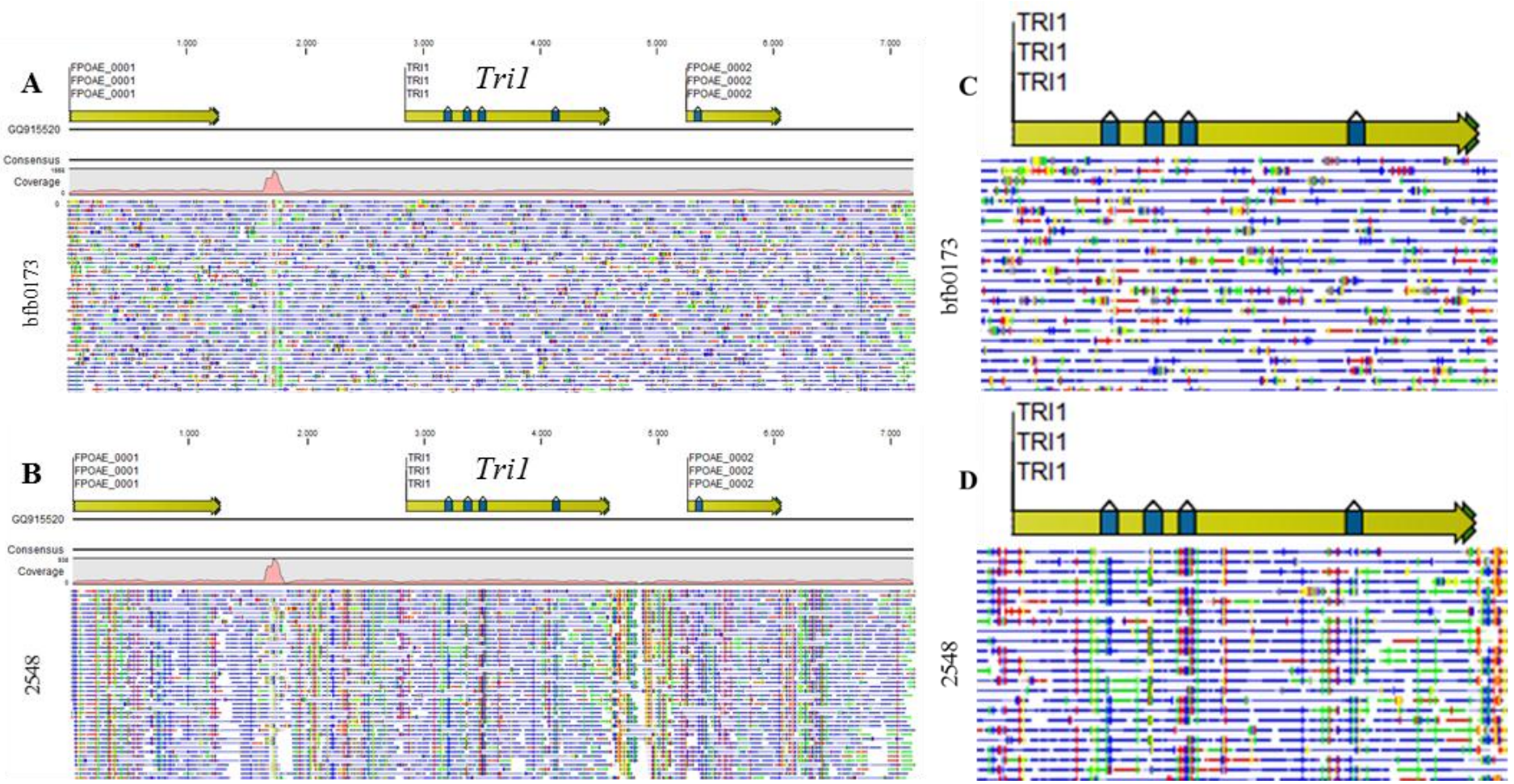

Figure 6.10 – Read mapping of reads from isolate bfb0173 (**A and C**) and isolate 2548 (**B and D**) on NCBI accession GQ915520, which is the only sequence of *FpTri1* available (Proctor et al., 2009). The published allele is identical to the one in isolate 2516 and bfb0173. Paired reads are mapped as blue and they do not show any consistent SNPs (which are designated with divergent non-blue colour). A second *FpTri1* type was identified in our study, occurring in isolates 2548 and 7555. Most SNPs (a divergent nucleotide in a read is shown with a colour different than blue, when this occurs in all reads at a certain location it is very likely a SNP) are located in introns and intergenic regions, and SNPs in the exons are predominantly synonymous by far.

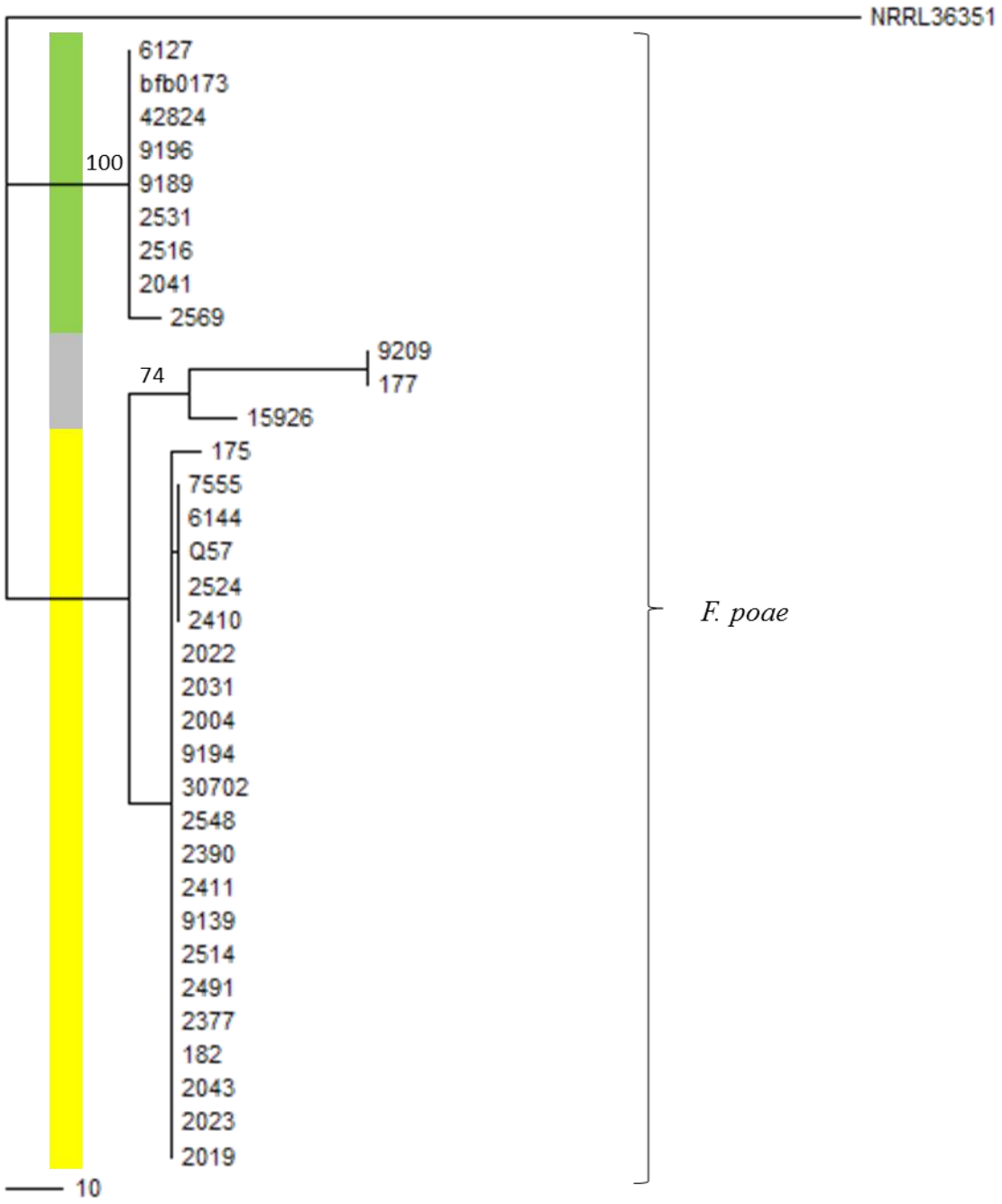

Figure 6.11 – Maximum parsimony phylogenetic tree that was built from the 1100 bp fragments of the *Tri1* gene with PAUP* 4.0b10. The tree is based on 74 parsimony informative characters. Bootstrap values were calculated with the PHYLIP package and those exceeding 70% are shown on the tree. Three major types of *Tri1* are designated with yellow, green and grey. *Fusarium sp.* NRRL 36351 (NCBI accession GQ915523.1) was used as the outgroup, however for construction of the phylogenetic tree mid-point rooting was used.

6.4.3 *Tri13* gene mutants show altered chemotypes

Transformation of *F. poae* isolate 2516 with a hygromycin cassette designed to replace the *Tri1* gene delivered 60 resistant colonies, picked from triple crossover approaches with an overlap

of 368 and 457 bp (16 and 34 transformants respectively), and the double crossover approach (10 transformants). Triplex PCR showed that only three of these had lost the WT gene (**Figure 6.12**). These were picked from the split marker transformation with 457 bp overlap. Overall integration efficiency is therefore at 5% (3/60). However, Southern blotting showed that each of these three transformants contained multiple ectopic integrations (**Figure 6.14**).Obtaining a *Tri1* knockout was attempted multiple times with the double crossover strategy. Fifty-five additional hygromycin transformants were obtained, none of which contained a correct integration at the desired locus.

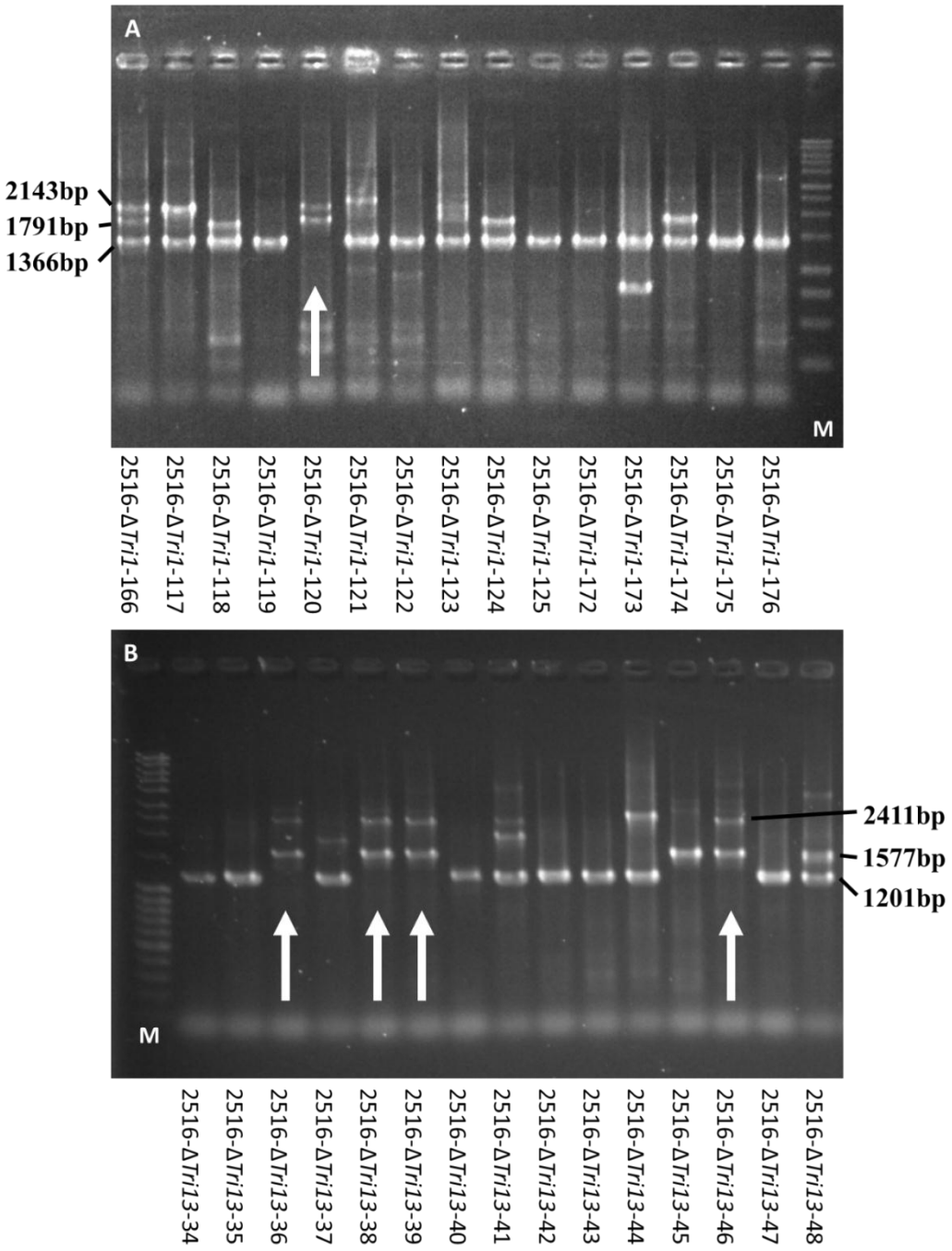

Figure 6.12 – Results of PCR analyses to confirm deletion of *Tri1* and *Tri13* in *F. poae*. The transformants marked with white arrows have lost the WT gene and show two amplicons indicative of correct integration (spanning the left and right integration sites). Triplex PCR was carried out for all hygromycin resistant colonies. **A**: *Tri1* locus. Sample 2516-ΔTri1-120 shows two amplicons indicative of correct integration (1791 and 2143 bp). All other samples still show the WT band (1366 bp). M is for the molecular weight marker (Promega's BenchTop 1kb DNA ladder). **B**: *Tri13* locus. Samples 2516-ΔTri13-36, 2516-ΔTri13-38, 2516-ΔTri13-39 and 2516-ΔTri13-46 show the two amplicons indicative of correct integration (1577 and 2411 bp). Samples such as 2516-ΔTri13-34 and 2516-ΔTri13-35 still have the WT amplicon (1201 bp). Note that sample 2516-ΔTri13-45 has lost the WT gene but does not show correct integration for both flanks. M is for the molecular weight marker (Thermofisher's Massruler DNA Ladder Mix).

The strategy that was used in the triplex PCRs is illustrated in **Figure 6.13**.

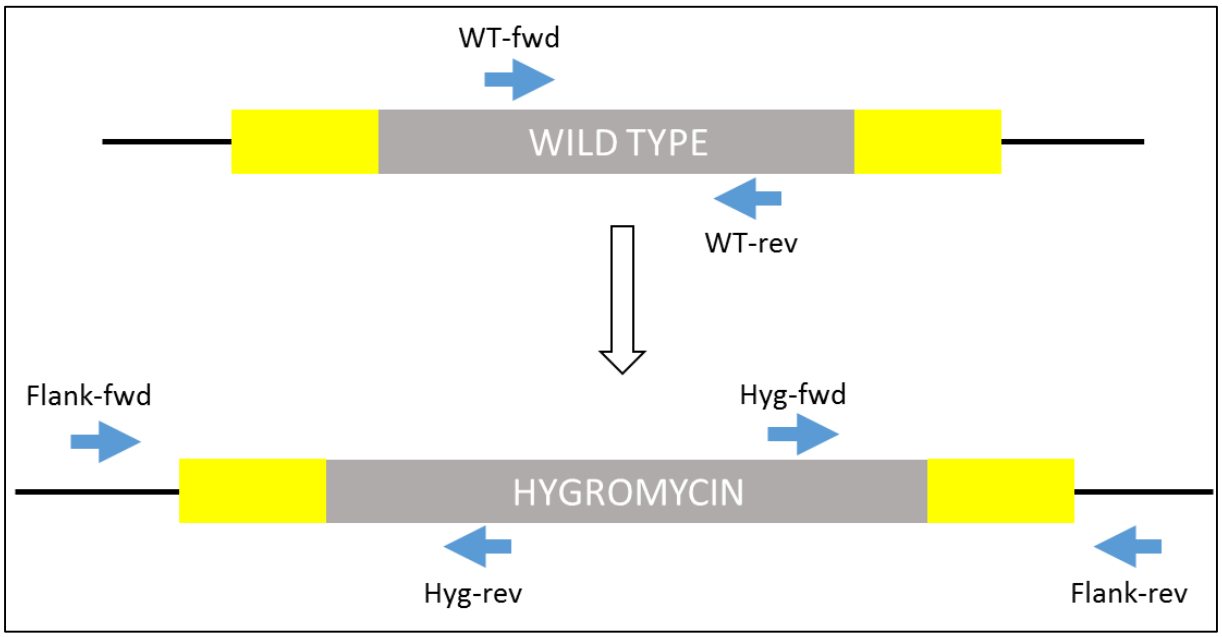

Figure 6.13 - Schematic of the triplex PCR strategy (not to scale). If the wild type gene is still present, primers FpTri1WT.fwd2 and FpTri1WT.rev2 form an amplicon of 1366 bp in the case of *Tri1*, and primers FpTri13.probe.fwd and FpTri13WT.rev1 form an amplicon of 1201 bp in the case of *Tri13*. If the wild type gene has been replaced by the hygromycin cassette, the wild type primers do not lead to an amplicon, while two amplicons will be obtained that span the integration site (external primers lie outside the flanks used for crossover (yellow)). Primers matching the hygromycin cassette are hyg.Fw2 and hyg.conf.rev2. Primers outside the site of integration are Tri1.FL.contr.fwd and Tri1.FR.contr.Rev2 in the case of *Tri1*, and FL.Tri13.contr.Fw and FR.Tri13.contr.rv for *Tri13*.

The frequency of correct integrations was higher for the *Tri13* locus. One hundred and twenty-one hygromycin resistant colonies were picked (39 for the triple crossover approach with an overlap of 368 bp; 71 for the triple crossover approach with an overlap of 457 bp; 11 for the double crossover approach), of which 28 showed an integration at the correct locus with corresponding loss of the WT gene (**Figure 6.12**). Integration efficiency is at 23%. Eighteen desired transformants were obtained from the triple crossover approach with 457 bp overlap, eight from the triple crossover approach with 368 bp overlap and 2 from the double crossover approach. Southern blotting showed that 10 of the 28 transformants did not contain additional ectopic integrations (**Figure 6.14**). Nine of these originated from triple crossover transformation with 457 bp overlap, and one from the triple crossover approach with shorter overlap. The final transformation efficiency is 10/128 or 7.8%.

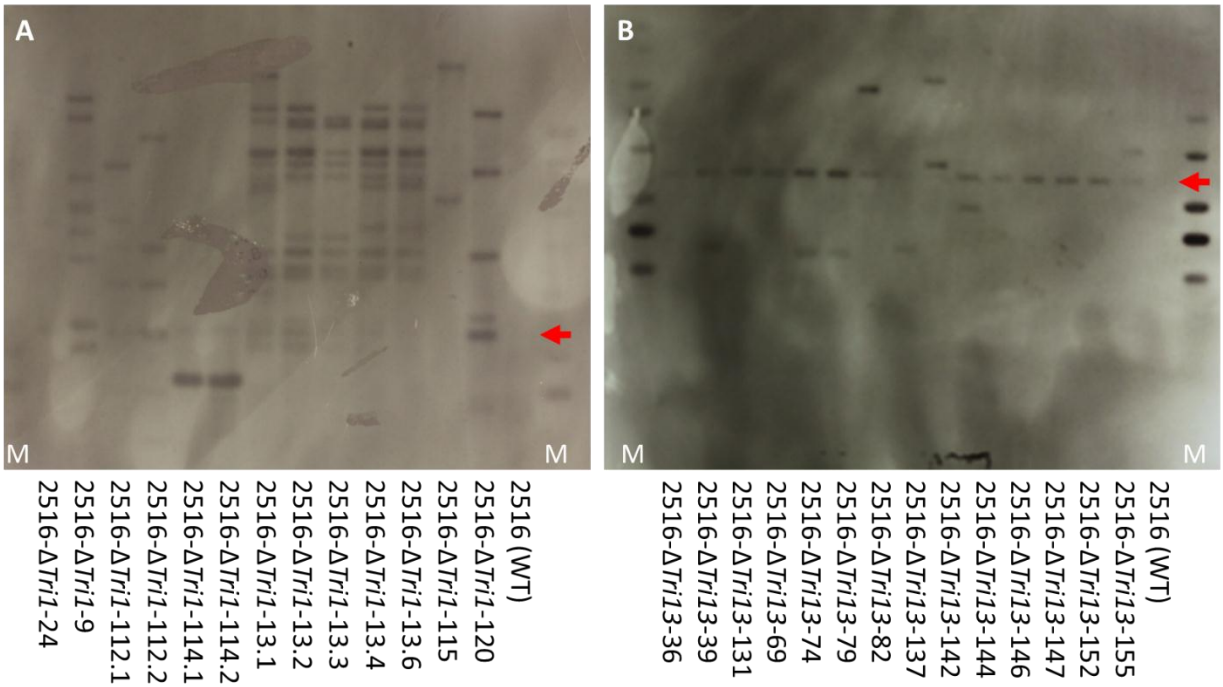

Figure 6.14 – Hybridization with a probe targeting the hygromycin gene against gDNA of candidate knockout transformants. Genomic DNA of single spored transformants was digested with SacI in the case of *Tri1* (target fragment size for hybridization: 3293 bp) and with XhoI in the case of *Tri13* (target fragment size for hybridization: 6407 bp). Transformants that show hybridization only at the expected height are clean knockouts, others have also integrated the hygromycin cassette at ectopic locations (leading to hybridization of the hygromycin probe against other fragments of the restriction digest). (**A**) For the *Tri1* gene, no transformants with an integration event only at the desired locus were obtained. Since only three transformants were confirmed to have lost the WT gene in the triplex PCR (see earlier), multiple separate single spore isolations were blotted from transformants 2516-Δ*Tri1*-112, 2516-Δ*Tri1*-114 and 2516-Δ*Tri1*-14. These led to similar hybridization profiles. (**B**) For the *Tri13* gene, multiple good transformants were obtained, including 2516-Δ*Tri13*-69 which was selected for further transformations. The red arrows show the size of the expected fragment. M denotes the lane containing the molecular weight marker (Promega's 1kb Benchtop ladder), wildtype (WT) is isolate 2516.

Tri1 knockout mutants that also contain multiple ectopic insertions were not considered fit for the gene swap experiment, and therefore the *Tri1* gene swap was abandoned. A Δ*Tri13* transformant was selected for the *Tri13* gene swap (2516-Δ*Tri13*-69). In this approach, the *FgTri13* or *FlTri13* gene should replace the hygromycin cassette, and a construct carrying a *G418* resistance gene is used in a co-transformation approach. This resulted in 11 *FlTri13*-transformants and 6 *FgTri13* transformants. Three *FlTri13* (2516-Δ*Tri13*-69-*FlTri13*-2, 2516-Δ*Tri13*-69-*FlTri13*-6 and 2516-Δ*Tri13*-69-*FlTri13*-10), and two *FgTri13* (2516-Δ*Tri13*-69-*FgTri13*-3 and 2516-Δ*Tri13*-69-*FgTri13*-5) transformants showed no growth on hygromycin-containing medium. These showed a highly divergent phenotype when grown in trichothecene

biosynthesis inducing medium, compared to those that showed normal growth on hygromycin-containing medium (**Figure 6.15**).

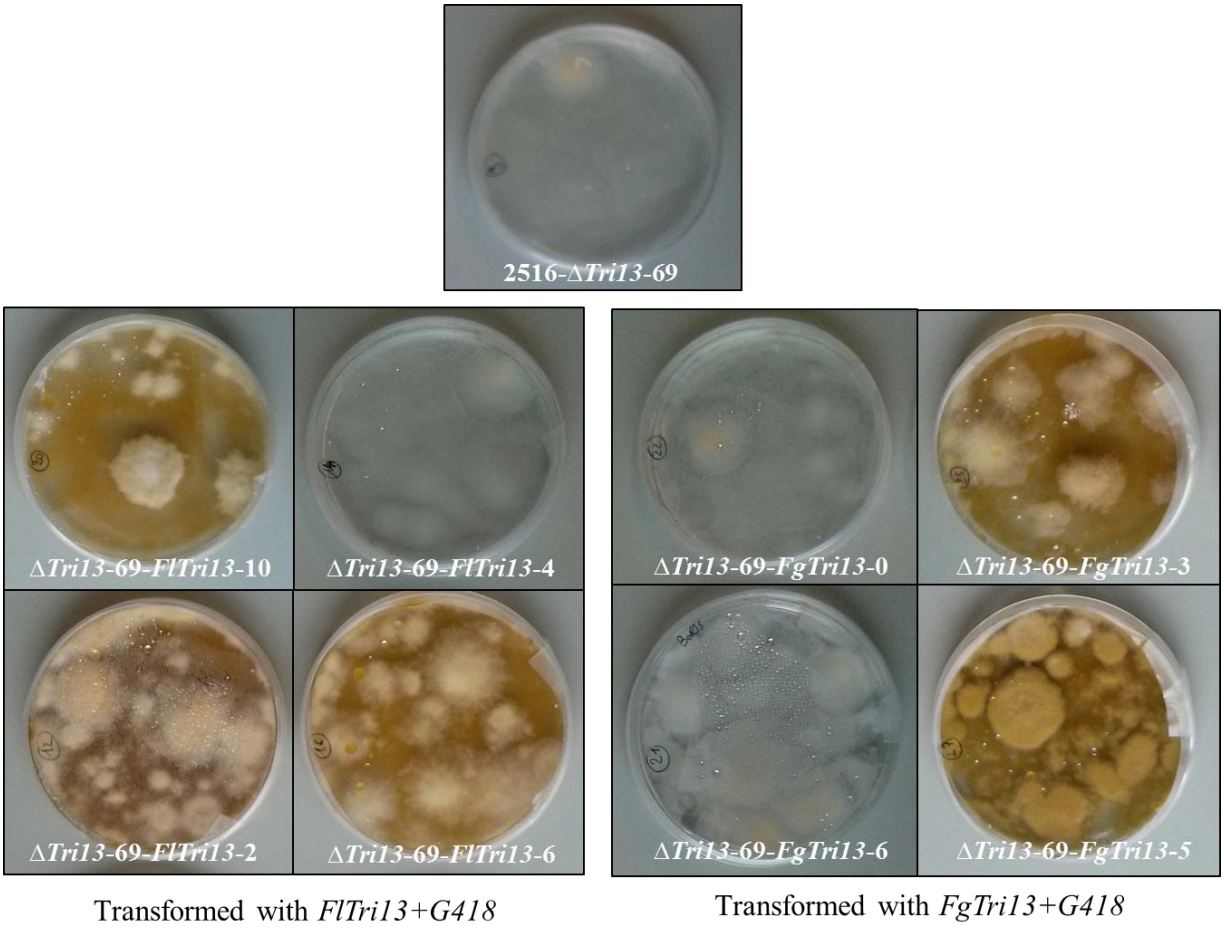

Figure 6.15 – Phenotype of *Tri13* transformants when grown on trichothecene biosynthesis inducing medium. For *FlTri13* and *FgTri13* transformations, three and two transformants respectively showed strongly inhibited growth on hygromycin-containing medium, indicating that they may have lost the hygromycin resistance cassette, and may have integrated the *FlTri13/FgTri13* gene. These showed a divergent phenotype on trichothecene biosynthesis inducing medium when compared to the *Tri13* knockout (KO) (colorless), and transformants growing normally on hygromycin-containing medium (colorless).

Confirmation of the putative gene swap transformants with PCR, and chemical profiling of the confirmed transformants is currently ongoing. The expected chemotypes in the transformants are as follows: a *FlTri13*-transformant is expected to produce the WT chemotype (DAS, NEO, FUS-X, NIV), while a *FgTri13*-transformant is expected to produce only FUS-X and NIV, as FgTRI13 has a more narrow substrate range. In this way, TRI13 mediates different paths along the biosynthesis grid.

6.4.4 Comparative homology modelling TRI1

Proctor et al. (2009) described four alleles of the *Tri1* gene in trichothecene producing *Fusarium* species (**Figure 6.4**). Two of these have been functionally characterized: the *F. graminearum* TRI1 catalyzes hydroxylation of the trichothecene skeleton at C7 and C8, and the *F. sporotrichioides*/*F. langsethiae* TRI1 does so only at C8 (McCormick et al., 2006). The two remaining alleles have not been functionally characterized, but species containing these alleles have been described to produce trichothecenes containing both OH groups. Indeed, *F. poae* isolates are *per se* able to produce FUS-X and NIV (Chapter 4 of this thesis), and *F. kyushuense* has been described to produce (trace amounts of) NIV (Thrane et al., 2004) and the novel trichothecene compound pentahydroxyscirpene (Fruhmann et al., 2014). Another species containing a *Tri1* allele similar to the one in *F. kyushuense* is *F. equiseti* which has also been described to produce compounds with two hydroxyl groups, as was described above. The genetic manipulation of *Tri1* alleles in *F. poae* proved very difficult (Section 6.4.3). For this reason, an *in silico* approach was undertaken to address the functionality of the two remaining alleles in *Fusarium* species.

Homology modelling with the Phyre2 server was used to build 3D models of the four alleles (Kelley et al., 2015). Twenty models are built for every allele, based on different Protein Data Bank (PDB) entries. While sequence identity was low for all models (approximately 15% for the top ranking models), coverage was close to 100% for the top ranking models and confidence was at 100%. As long as the confidence is high, the core of such models may still be very informative. The 20 proposed models were evaluated with DFire (Zhou and Zhou, 2002), which identified the model based on PDB entry 4lxj as the best model for all homologues, which is also the model that the Phyre2 algorithm favored. For this comparative homology framework, further analyses were performed based on the four models based on 4lxj. This is a P450 with a 14-lanosterol demethylase function from *Saccharomyces cerevisiae*, with the first step of the demethylation process being a monooxygenation of a saturated C-H bond (Monk et al., 2014).

Autodock VINA (Trott and Olson, 2010) was used to perform ligand docking to the selected models. The P450 type enzymes that TRI1 belongs to, CYP68C1 (Meek et al., 2003), contain a heme cofactor in their active site. During a series of electron transfers, in microbial P450s mediated by NADPH, and formation of a complex adduct between the iron atom and molecular oxygen, the unsaturated C-H bond is mono-oxygenated. The heme cofactor + molecular oxygen was docked to the four models first, and the best docking configuration (represented by the highest binding affinity as calculated by Autodock VINA) was retained for every model. The

heme group is primarily bound by a universally conserved cysteine residue and several flanking residues (Mestres, 2005). In the amino acid alignment of the four protein alleles and the representation of the FpTRI1 docking, these are marked blue (**Figure 6.16**).

A second round of docking was performed, using the result from the previous docking round (P450 + heme + molecular oxygen) as the receptor and several trichothecene intermediates as ligands. The binding affinities that were found in this docking experiment can be found in **Table 6.6**. The Autodock VINA algorithm delivers multiple possible docking configurations for every substrate-model combination. These differ inter- and intra-species by the hydrogen bonds that they are able to form, by the potential steric hindrance of residues in the active cavity that are different between species, etcetera. As there is not enough additional information to make an informed, and unbiased, choice on which docking configurations are most plausible, the two highest binding affinities are given as-is in **Table 6.6**, where possible. In two cases of FlTRI1 docking, only one possible configuration was found. An example of the docking results is given in **Figure 6.17** with the FpTRI1 model and TAS as a substrate.

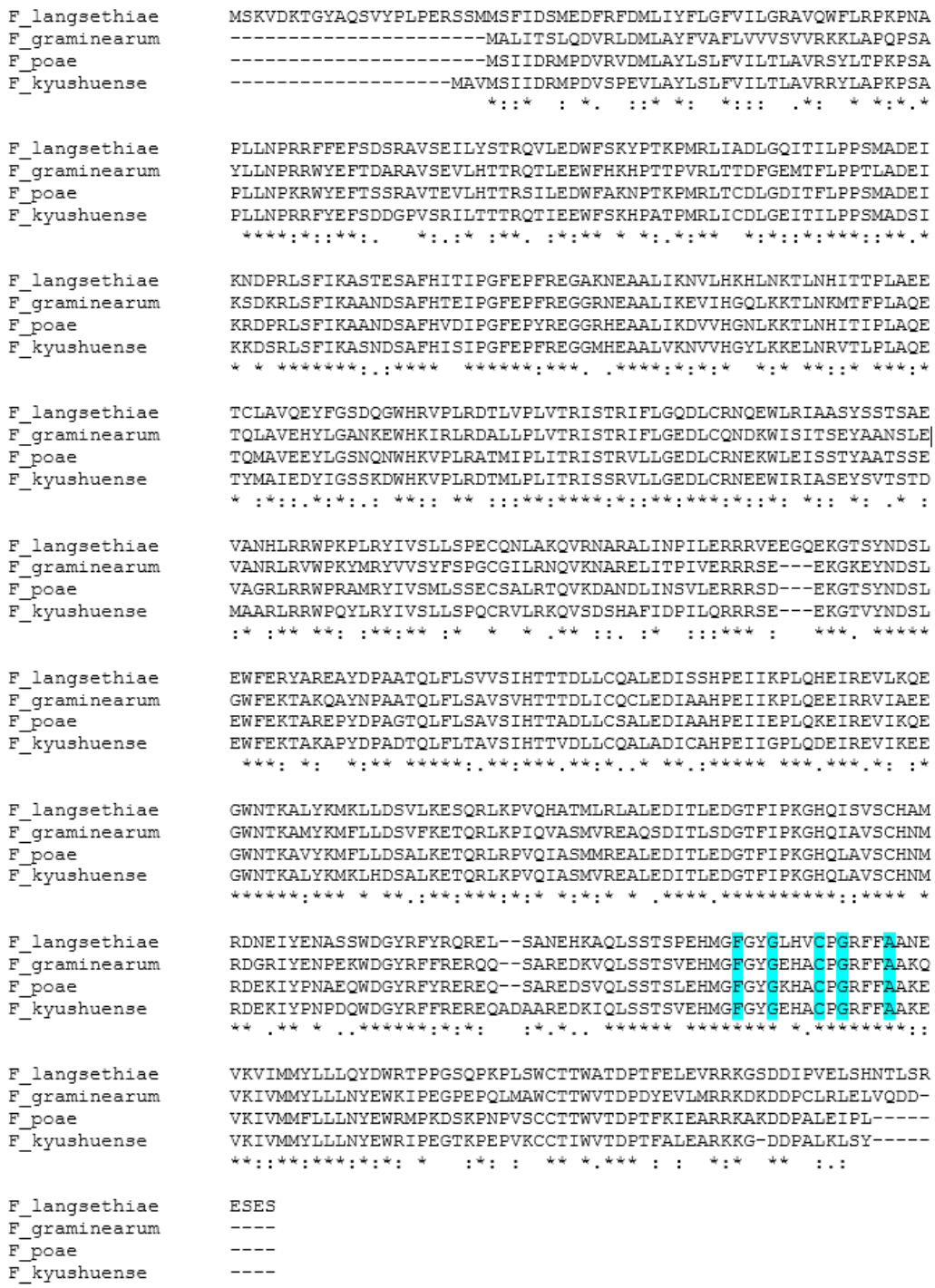

Figure 6.16 – Amino acid alignment of TRI1 of four *Fusarium* species, belonging to the four different *Tri1* alleles determined by Proctor et al. (2009). Conserved residues involved in heme binding are colored blue. Asterisks represent conserved amino acids, colons represent conservation between groups of strongly similar properties, points represent conservation between groups of weakly similar properties.

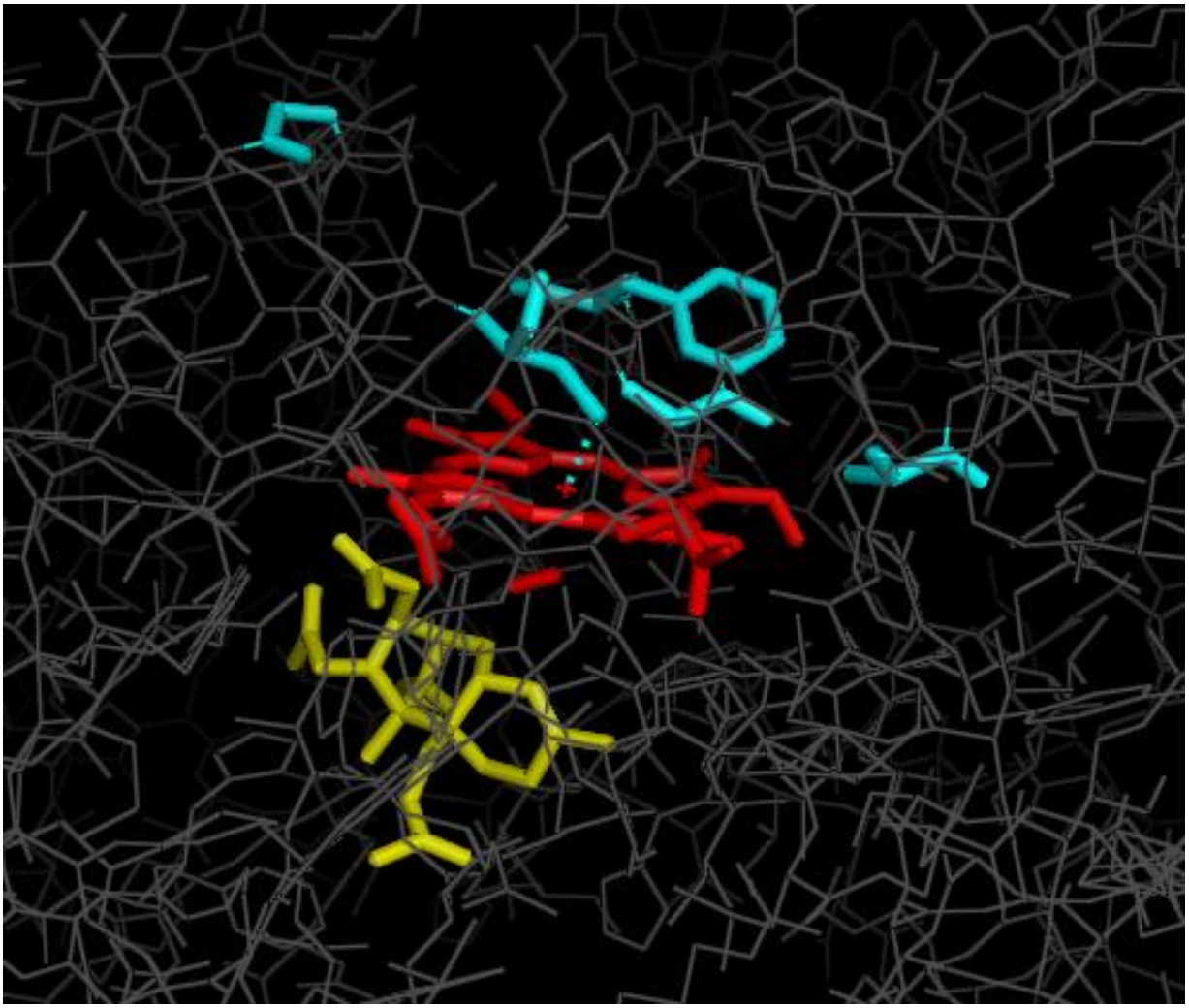

Figure 6.17 – Docking of the heme cofactor and molecular oxygen (red) and triacetoxyscirpenol (yellow) to an *in silico* predicted model of FpTRI1 (model residues as gray lines). Five conserved residues involved in heme binding are colored blue, the cysteine thiolate – iron binding is shown with a dashed line. Only one of the possible docking configurations is shown for TAS, and there is no guarantee that this configuration should take precedent over any others.

With this unbiased approach, binding affinities are consistently lowest for the model of FlTRI1 (**Table 6.6**), the only of the four homologues that can certainly not place a second OH group. Binding affinities for the FgTRI1 and FpTRI1 model are very similar, and are somewhat lower for the FkTRI1 model. This may indicate that at least FgTRI1 and FpTRI1, and perhaps also FkTRI1, are similar in function, and are different from FlTRI1.

Table 6.6 – Binding affinities for the different ligand – receptor docking simulations, expressed in kcal/mol. The two highest (most negative) binding affinities are shown for every substrate-ligand combination, except for TAS-FlTRI1 and 8-OHCAL-FlTRI1 for which only one possible docking was obtained. The top rated model for every protein was used as a receptor, with the heme cofactor and molecular oxygen docked to the active site. Five intermediates from the trichothecene biosynthesis pathway were docked as ligands: CAL = calonectrin; TAS = triacetoxyscirpenol; 8-OHCAL = 8-hydroxycalonectrin; 3-ANEO = 3-acetylneosolaniol; DI-OHCAL = dihydroxycalonectrin. The importance of these substrates can be seen in **Figure 6.2**. Binding affinities for the FlTRI1 model are lowest.

	FgTRI1	**FpTRI1**	**FkTRI1**	**FlTRI1**
0 OH				
CAL	-6.2 / -5.8	-6.6 / -6.1	-7.1 / -6.8	-5.5 / -5.0
TAS	-6.6 / -6.2	-7.1 / -6.8	-6.4 / -5.8	-5.1
1 OH (C-8)				
8-OHCAL	-7.1 / -5.9	-7.3 / -6.4	-6.0 / -6.0	-5.4
3-ANEO	-7.1 / -5.5	-7.5 / -5.9	-6.1 / -5.7	-4.0 / -3.6
2 OH				
DI-OHCAL	-6.6 / -6.6	-6.6 / -6.2	-6.0 / -5.5	-5.5 / -5.3

6.5 Discussion

Genetically unlinked from the *Tri* cluster locus, the *Tri1* gene in *F. poae* is one of four major alleles in *Fusarium* species. Functionally, only two alleles have been characterized, namely the *F. sporotrichioides*-like allele which catalyzes the addition of one OH group on its substrate, and the *F. graminearum*-like allele which catalyzes the addition of two OH groups. Species containing one of the other two alleles, e.g. *F. poae*-like and *F. kyushuense*-like, produce trichothecenes that are hydroxylated at C7 and C8, but also trichothecenes that are only hydroxylated at C8. Two explanations could account for this. Either the *F. kyushuense* – *F. poae* alleles are fundamentally different and less efficient in the hydroxylation at C7, or they enter in competition with other enzymes, which sequester part of the substrate away with only one OH group placed. Based on this study, it is not possible to conclusively decide either way. Modelling the four alleles with the same structure as a template (4lxj), and using those models for molecular docking, indicated that FpTRI1 and FgTRI1 may be distinct from FlTRI1. In both scenarios, TRI1 has the biochemical capability to catalyze hydroxylation at both C7 and C8, and we hypothesize that the difference with *F. graminearum* is that it does so on a substrate that does not occur in *F. graminearum*, due to the different *Tri13* allele. The pathway shown in **Figure 6.18** indicates that a consequence of this shift in direction, mediated by the different *Tri13* allele, leads to a competition between FpTRI1 and FpTRI8. This figure also includes all the recently described novel trichothecenes such as NX2/NX3/NX4, produced by a

subpopulation of *F. graminearum* (Varga et al., 2015) and pentahydroxyscirpene (PHS) produced by *F. kyushuense* (Fruhmann et al., 2014).

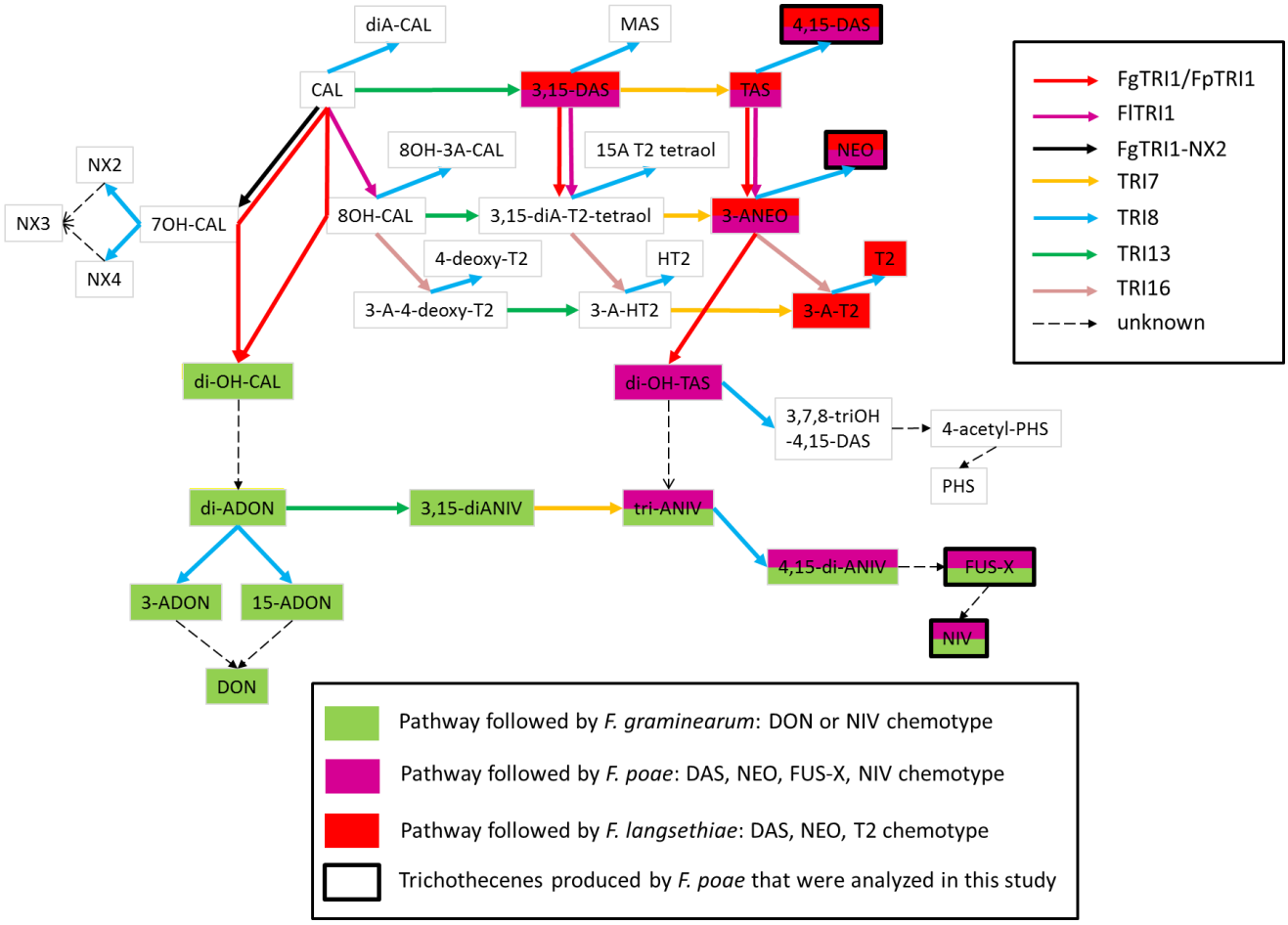

Figure 6.18 – Proposed biosynthetic grid responsible for trichothecene production in *Fusarium* species. Steps mediated by different enzymes are depicted with different colours. The major biosynthesis route of *F. graminearum* (either DON or NIV) is shown in green compounds, the major biosynthesis route of *F. langsethiae* (leading to T2 toxin) is shown in red compounds. The proposed biosynthesis scheme for *F. poae* is shown in purple compounds: initially similar to *F. langsethiae*, but continuing all the down to NIV because of a TRI1 enzyme which catalyzes the addition of two OH groups. Dashed lines represent reactions for which no genetic component has been elucidated. This figure was adapted from Kimura et al. (2007) and McCormick et al. (2011).

The type A + type B trichothecene chemotype in *F. poae* is best explained by the combination of "contrasting" TRI1 and TRI13 functions (**Figure 6.18**). FpTRI1 has a *F. graminearum*-like function with possible hydroxylation at both C7 and C8, and FpTRI13 has a *F. sporotrichioides*-like function with a broad substrate range compared to FgTRI13.

Several of the genes for trichothecene biosynthesis in *F. poae* have been investigated before by Proctor et al. (2009). They found that the phylogeny of three genes belonging to the *Tri* cluster (*Tri4*, *Tri5* and *Tri11*), along with *Tri101*, followed species phylogeny. As expected this was

confirmed in our study for the rest of the genes in the *Tri* cluster, which are more closely related to *F. sporotrichioides* than to *F. graminearum* (**Table 6.5**). Since regulation of trichothecene biosynthesis by TRI6 and TRI10 is not the same between *F. sporotrichioides* and *F. graminearum*, this may indicate that regulation in *F. poae* is also more *F. sporotrichioides*-like (Tag et al., 2001; Seong et al., 2009). Phylogeny of *Tri* genes should not be regarded as a reliable indicator for the genetic identity of an individual however. Ward et al. (2002) showed conclusively that within the type B trichothecene (NIV, 3-ADON, 15-ADON) producing species, chemotype differentiation shows signs of trans-species polymorphism which has been maintained over multiple speciation events. This genotype polymorphism has originated after the divergence of type A and type B producing species.

The variability of the *Tri1* region in *F. graminearum* is responsible for recent shifts in trichothecene production within this species (Varga et al., 2015). A subpopulation of *F. graminearum* contains a *Tri1* allele encoding for an enzyme with 14 AA substitutions when compared to the typical TRI1 e.g. in PH-1. By gene swap experiments it was confirmed that this TRI1 hydroxylates calonectrin only at C7, finally leading to a novel trichothecene compound, termed NX2. It is hypothesized that future outcrossing between populations carrying different chemotypes, determined by polymorphism in the *Tri* cluster (NIV versus 3-ADON versus 15-ADON) will allow more novel trichothecene compounds to be produced in nature (Liang et al., 2014). Like in *F. graminearum*, different types of the *FpTri1* gene can also be found in the population (**Figure 6.11**). It would appear that strong purifying selection acts on the *Tri1* gene, as most of the SNPs are synonymous mutations. An untapped pool of diversity at the *Tri1* locus exists in *F. poae*, but contrary to (the subpopulation of) *F. graminearum*, in this pathosystem TRI1 function is clearly heavily constrained.

Several steps in the trichothecene biosynthesis pathway have not yet been genetically elucidated. Examples are the conversion of the OH group on C8 to a keto group, and the final conversions of the acetyl group of ADON and ANIV to an OH group in respectively DON and NIV. This has sparked multiple investigations to try and expand the trichothecene clusters to include genes that could fulfill these hypothesized functions. Brown et al. (2004) identified 12 ORFs flanking the *Tri* cluster with similarity between *F. graminearum* and *F. sporotrichioides*. Some of the predicted functions of these genes matched biochemical reactions in trichothecene biosynthesis without assigned genes, but functional analysis showed that none of the ORFs were necessary for trichothecene production. Moreover, none of the ORFs had the TRI6 binding motif in their promotor regions. Sieber et al. (2014) included three additional genes downstream

of *Tri8* in the *F. graminearum* isolate PH-1 trichothecene cluster, based on co-expression analysis. Functional analysis of these genes, with promising predicted functions, did not confirm their importance for trichothecene production.

The genomes of the four isolates that were sequenced in Chapter 4, were mined for their trichothecene biosynthesis loci. In isolate 2516, the trichothecene cluster, and the neighboring genes, are similar in organization to the *Tri* cluster in *F. graminearum* and *F. sporotrichioides* (Brown et al., 2004). However, uniquely in *F. poae*, the cluster and its environment are invaded by TEs, in accordance with its genome dynamics. In isolates bfb0173 and 2516, the intergenic region between *Tri6* and *Tri5* is expanded by the insertion of a *pogo* transposable element that was deactivated by RIP. Also in isolates bfb0173 and 2516, a 400 bp repetitive element is present between *Tri7* and *Tri3*. Finally, for isolates 2548 and bfb0173, the *Tri* cluster at the *Tri14* side is bordered by a RIPped retrotransposon of the Ty1/Copia family, which is not present in the other isolates at this location (see **Figure 6.6**). Five RIPped copies of this TE are present throughout the genome of isolate 2516. The presence of a TE at the border of the cluster may support the demarcation of the *Tri* cluster with *Tri14*.

Chapter 4 of this thesis illustrated that the insertion of repetitive sequence into the genome is a useful tool for track and trace studies in fungal populations, as every such insertion can be considered a unique event. The three insertions in and around the *Tri* cluster (between *Tri7* and *Tri3*, between *Tri6* and *Tri5* and bordering *Tri14*) are not cumulative over the four isolates, which is best explained by a recombination event that occurred over (part of) the cluster. In Chapter 4 of this thesis indications were uncovered that *F. poae* is a sexual species. In *F. graminearum*, it was shown that the *Tri* cluster, with similar genomic coordinates as in *F. poae*, is situated in a region of the genome with elevated recombination rate (Cuomo et al., 2007). Ward et al. (2002) have shown that the composition of the *Tri* cluster the FGSC is the result of multiple recombination events. The *Tri* cluster is the result of recombination between different haplotypes in several species independently, but it remains to be seen what the functional consequences have been for trichothecene biosynthesis in either species.

The localization of a RIPped *pogo* element between *Tri6* and *Tri5* in isolates 2516 and bfb0173 is remarkable. In the *F. equiseti* complex, this space is occupied by an additional Zn2Cys6 transcription factor. There is a strong link between transposable elements and transcription factors (TF). Many TF-associated DNA binding sites are derived from ancient transposable elements and TEs have played a defining role in the formation of complex regulatory networks (Feschotte, 2008). Moreover, some TF families are derived from ancient TE domestication

(Sinzelle et al., 2009). There is no similarity between the *pogo* element in *F. poae* and the Zn2Cys6 TF in *F. equiseti*, so an evolutionary link between the two seems unlikely. Nevertheless, the *Tri6-Tri5* intergenic region is the centre of the trichothecene cluster and insertions into this region have been shown to influence trichothecene production (Tag et al., 2001). It is remarkable that a disruption of this central region of the cluster apparently does not have an effect on the trichothecene chemotype of the isolates (**Figure 6.8**).

It was not possible to obtain a *Tri1* knockout without ectopic integrations in this study. The frequency of correct insertion of the selective marker was reduced when compared to *Tri13* knockouts. For *F. graminearum*, several researchers have been successful in making *Tri1* knockouts (McCormick et al., 2004; Varga et al., 2015). We hypothesize that the proximity of the *Tri1* gene to the telomere in *F. poae* is the cause of this difficulty. In *F. graminearum*, the gene is at 292 kb of the telomere, and in this subtelomeric region the frequency of cross-over and double strand breaks is expected to be higher than in the rest of the genome (Cuomo et al., 2007). On the other hand, in *F. poae*, *Tri1* is at 55 kb of the telomere. In *Saccharomyces cerevisiae*, it was shown that the region at 0-20 kb from the telomere is particularly low in double strand breaks and cross-over events. Hotspots in such events were at 100 kb from the telomere (Blitzblau et al., 2007). The region closest to the telomere is subjected to extensive telomeric silencing, which may hamper the accessibility of the region for genomic rearrangements (Mitchell and Boeke, 2014).

Chapter 5 of this thesis illustrated that a sequential chemotype is produced *in vitro* by isolates of *F. poae*, and the nature of the chemotype dictates that type A trichothecenes should be produced first, followed by FUS-X and NIV. The pathway that we propose in this Chapter (**Figure 6.18**) explains this chemotype, should be applicable to all trichothecene chemotypes described up to now, and trichothecene chemotypes that emerge in the future.

Chapter 7: General discussion and perspectives

7.1 Introduction

The research in this PhD thesis was undertaken as a response to Belgian field surveys that showed *F. poae* as an important species within the FHB complex (Audenaert et al., 2009). In a first part, the body of knowledge on *F. poae* was reviewed and the prevalence of *F. poae* and other FHB species was assessed in a one year case study. Within this case study, *F. poae* was the second most occurring FHB species in wheat, after *F. graminearum*. A second part of the research was aimed at improving our understanding of *F. poae* by a genomics approach. The genome of one isolate was assembled to a highly contiguous state and this made it possible to describe genome dynamics for *F. poae* which have not been found in fungi before. Moreover, lessons regarding the mode of reproduction could be drawn from the genome assembly. A final part of the research focused on the production of both type A and type B trichothecenes by *F. poae*. Chemical and genetic investigations were aimed at thoroughly describing this combined chemotype and uncovering how it is produced.

7.2 Strong indications of both sexual and asexual reproduction in *F. poae*

McDonald and Linde (2002) detailed the characteristics of fungal pathogens that should pose the greatest challenge to durable disease management. These include a high mutation rate coupled with active transposable elements, high propensity for gene/genotype flow by sporulation and dispersal, and a mixed reproduction system wherein clonal and sexual reproduction can alternate. This thesis provides indications that *F. poae* fulfills all these criteria. Its genomic biology is potentially unique in the sense that the specific evasion of RIP on supernumerary chromosomes has not been described before. This allows for the retention of active transposable elements, that have the possibility of both positive and deleterious effects. Moreover, the generation of novel genotypes was demonstrated by the large translocation of sequence from the supernumerary to the core genome (Chapter 4).

Indications are offered in this research that *F. poae* reproduces both clonally and sexually. Indications for a sexual mode of reproduction include RIP of transposable elements (Chapter 4) and recombinations events (Chapter 6). Chapter 4 illustrated that a novel genotype could spread country-wide, and ready dispersal of genotypes is a key feature of a clonal mode of reproduction (see also **Figure 7.2**). Additionally, in Chapter 5 multiple instances of potentially clonal isolates were identified by AFLP. We took the *F. poae* set of the AFLP tree, and superimposed on to it the different genetic markers that were investigated throughout this thesis (*MAT1*, *pogo*, *EF-1α*, *Tri1*, translocation of supernumerary sequence). The markers are taken from **Table S4.1**, **Figure 5.3** and **Figure 6.11**. The result can be found in **Figure 7.1**. With this

very limited set of markers, it can be seen that the different combinations of these markers have likely originated through recombination. At a smaller scale, the uneven distribution of the second supernumerary translocation could be explained by a recombination event. Finally, the recombination event over the *Tri* cluster described in Chapter 6 is an indication of past meiosis.

Isolates that share >90% genetic similarity as determined by the Dice coefficient are grouped by the same color in **Figure 7.1**. With the same colors, the genetic profiles were mapped out geographically in **Figure 7.2**. As was determined in Chapter 4, only limited geographical clustering is found. The dominant genotype of the Italian isolates does not occur in Belgian isolates (blue), but the other two do (bright green and light blue).

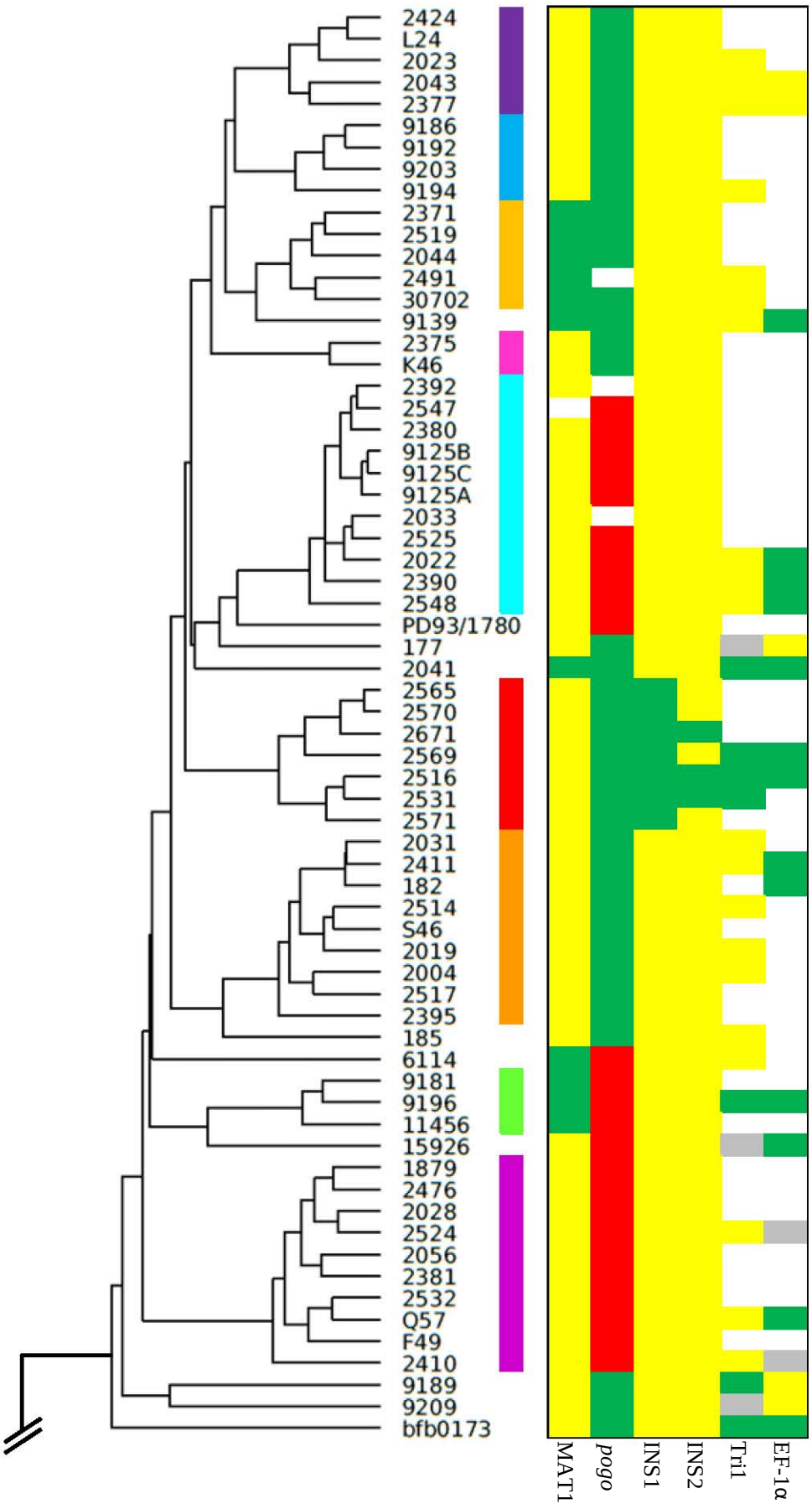
2424
L24
2023
2043
2377
9186
9192
9203
9194
2371
2519
2044
2491
30702
9139
2375
K46
2392
2547
2380
9125B
9125C
9125A
2033
2525
2022
2390
2548
PD93/1780
177
2041
2565
2570
2671
2569
2516
2531
2571
2031
2411
182
2514
S46
2019
2004
2517
2395
185
6114
9181
9196
11456
15926
1879
2476
2028
2524
2056
2381
2532
Q57
F49
2410
9189
9209
bfb0173
MAT1
pogo
INS1
INS2
Tri1
EF-1α

Figure 7.1 – Superposition of genetic markers on the AFLP tree of 64 *F. poae* isolates (and additionally two technical replicates). All *F. poae* isolates in **Table S4.1** were used for AFLP except 177, 2521, 7555, 6127 and 42824. White entries are markers for which no data was collected (for the *Tri1*and *EF-1α* markers) or could be collected (for the *MAT1* and *pogo* markers). *MAT1*: yellow is MAT1-1, green is MAT1-2 (see Chapter 4). *Tri1*: yellow and green are the major types defined in Chapter 5, grey are the three divergent isolates (15926, 9209 and 177; see **Figure 6.11**). *EF-1α*: yellow, green and grey represent the three different *EF-1α* types detected in Chapter 5 (see **Figure 5.3**). INS1 and INS2 are the major insertions of supernumerary sequence into chromosome 3 of a subset of isolates. Yellow indicates the absence of the insertion, green indicates the presence of the insertion. Eight isolates total were detected that have insertion 1 (closest to the telomere of chromosome 3), however isolate 2521 was not included in the AFLP analysis therefore only 7 are depicted here (isolates 2565, 2570, 2571, 2671, 2569, 2516 and 2531). Of the eight isolates with insertion 1 there are three that also contain insertion 2 (isolates 2671, 2516 and 2531). *Pogo*: green indicates presence of the *pogo* element between *Tri5* and *Tri6*, red indicates absence (see **Figure 6.8** and **Figure 6.9**). Clusters of isolates that share more than 90% genetic similarity according to the Dice similarity coefficient (see **Figure 5.2**) are grouped with the same colors.

The track and trace opportunities that are gained from TE insertions and RIP were demonstrated with the diagnostic PCR for the translocation of supernumerary sequence into chromosome 3 (**Figure 7.2**C). When in the future more insertions are used as genetic markers, as was already done for the *pogo* element between *Tri5* and *Tri6*, recombination between different groups of isolates should become more clear.

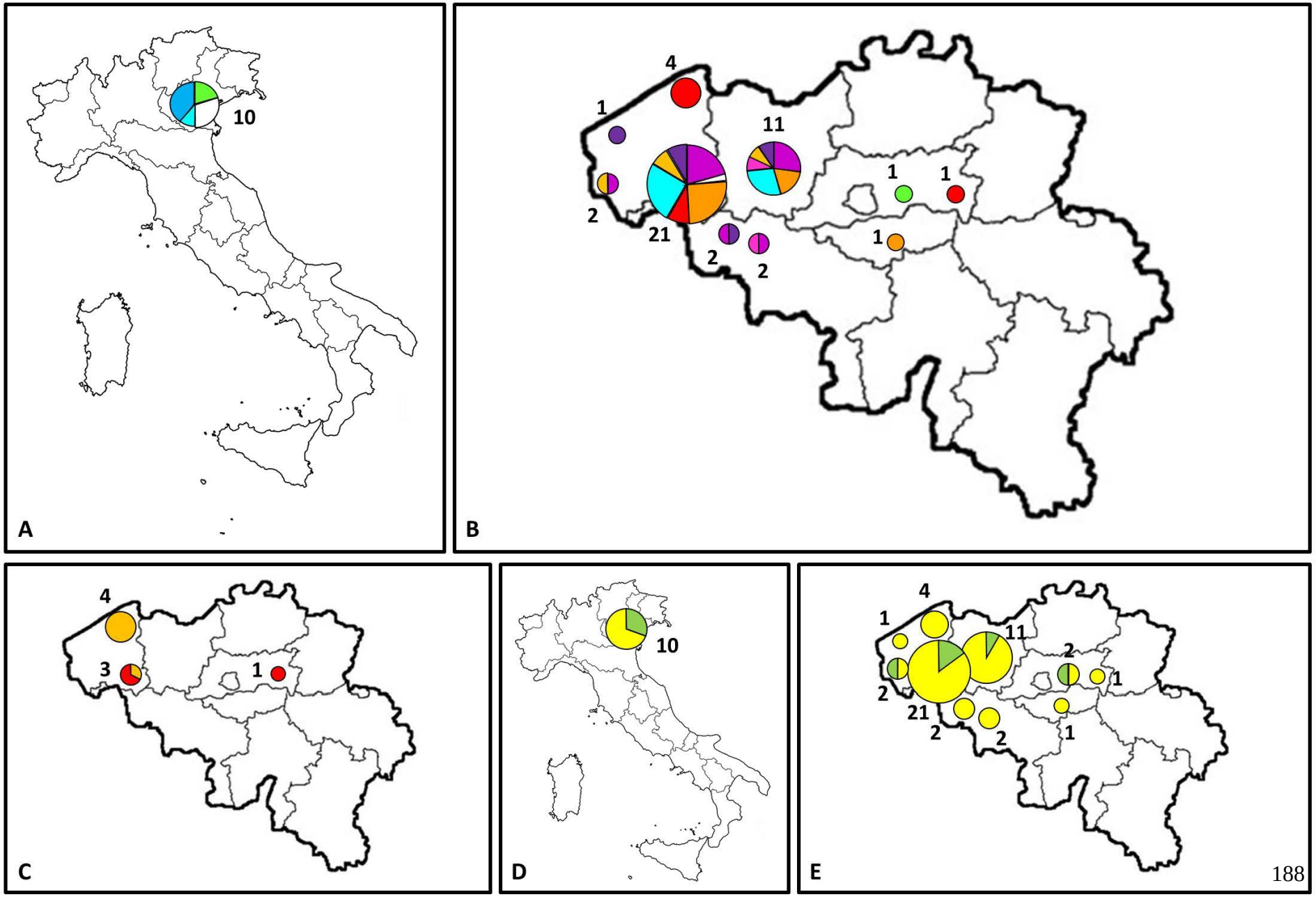
10
A
4
1
11
1
1
2
21
1
2
2
B
4
3
1
C
10
D
4
1
11
2
2
1
21
2
2
1
E

Figure 7.2 – Summary of *F. poae* isolates and the genetic markers that were investigated in this thesis. Note that isolates from locations other than Italy and Belgium are not shown. Pie charts and circles are scaled to the number of isolates collected at every location. **A** and **B**: genetic profiles as determined by AFLP analysis of Italian and Belgian isolates. Isolates that are part of a cluster with >90% genetic similarity based on the Dice coefficient are are given the same colours as in **Figure 7.1** and represent isolates that belong to the same genetic profile. From the 10 Italian isolates, 3 (isolates 9139, 9181 and 9196) did not belong to such as a cluster and are included as the white segment of the circle. For the Belgian isolates this was the case for one isolate (isolate 2041) from Zwevegem. Two Belgian isolate from Zwevegem (isolate 2521) and Heverlee (isolate 7555) were not included in the AFLP analysis and are not included on the map. **C**: Three locations where the genotype containing major supernumerary sequence translocations was detected. Orange: five isolates with only insertion 1 (closest to the telomere of chromosome 3). Red: three isolates with both insertion 1 and insertion 2. **D** and **E**: distribution of the mating type in Italian and Belgian isolates (see Chapter 4). Yellow = MAT1-1; green = MAT1-2. For the four locations where MAT1-1 and MAT1-2 are shown to co-occur, isolates from both mating types were collected in the same sampling year except for Heverlee, Belgium where the two isolates of opposing mating type were collected in 1965 and 1968. For one isolate from Zwevegem, Belgium (isolate 2547) no mating type could be determined and it is not included on the map.

A recent study indicated that a significant portion of the *F. poae* population may be homothallic, i.e. isolates contain genes from both the MAT1-1 and MAT1-2 idiomorphs within their genome (Dinolfo et al., 2014). In our set of sixty-nine isolates, we found no indications of homothallism. Within the genus *Fusarium*, the heterothallicmode of reproduction is the ancestral state and homothallic isolates belonging to the FGSC contain genes from the two idiomorphs closely linked together (O'Donnell et al., 2013); see **Box 2.1**. This is not always the case. In the *Cochliobolus* genus, there are also both heterothallic and homothallic species, and for three homothallic species the organization of the genes from the two idiomorphs is unique in every case (Yun et al., 1999). In the case of *C. luttrellii*, genes from the two idiomorphs have become fused through a recombination event between idiomorphs from heterothallic parents. On the other hand, in *Aspergillus*, heterothallism has been argued to be the derived state (Galagan et al., 2005). Isolates from the study by Dinolfo et al. (2014) should urgently be subjected to additional investigation in order to confirm the results of these authors, and to uncover how the genes of both idiomorphs are combined in any homothallic individuals.

It is not known how homothallism in the FGSC came to be. O'Donnell et al. (2004) proposed an unequal crossover event, bringing together the genes from the two opposing idiomorphs from the most recent heterothallic ancestors. **Box 2.1** shows that the homothallic configuration of *F. graminearum* has a complex relation to the heterothallic loci of *F. pseudograminearum*. The MAT1-1 locus in *F. poae* is identical as described in other fusaria. However, the MAT1-2 locus in *F. poae* contains an additional inversion, bordering the MAT1-2-3 gene when

compared to the loci of type B trichothecene producers (extracted from isolates 6114 and 30702, data not shown).

The heterothallic isolates collected within the scope of this thesis occur in a skewed distribution of MAT1-1/MAT1-2. Within the Italian isolates, 7 out of 10 isolates were of the MAT1-1 type. Mating type was determined for 48 Belgian isolates, 42 of which were of the MAT1-1 type (**Figure 7.2**D and E). This may indicate that sexual reproduction is infrequent within the population, though it is beyond doubt occurring considering the findings in this study. The skewed distribution of MAT1-1/MAT1-2 in Belgian *F. poae* populations was also found in a study at the UCL (Pierre Hellin, personal communication).

7.3 Lifestyle parallels between *Fusarium* species

We hypothesize that parallels can be drawn between *F. poae* and *F. langsethiae*. The *F. langsethiae* genome was recently sequenced, and by the state of its assembly it can be inferred that a great deal of repetitive sequence is present (dr. Erik Lysoe, personal communication). It stands to reason that RIP should be either completely inactive, or like in *F. poae* selective for certain regions of the genome. Long read sequencing and assembly will be able to answer this question in the future. However, supernumerary chromosomes are likely present within the genome of *F. langsethiae*, as evidenced by CHEF karyotyping (Lysoe et al., 2015). Moreover, karyotyping of *F. sporotrichioides*, a sister species of *F. langsethiae*, showed an identical karyotype as *F. poae* (Fekete et al., 1993). It will be interesting to see if *F. langsethiae* is able to combine sexual and asexual reproduction, or if it perhaps verges even further on the scale towards an asexual mode of reproduction. In any case, the different types of reproduction in *F. graminearum*, *F. poae* and potentially *F. langsethiae* is one of the exciting reasons for comparative studies between the three (**Table 7.1**).

Table 7.1 – Comparison between *F. graminearum*, *F. poae* and *F. langsethiae*; including interesting targets for future research. Some *F. langsethiae* findings are based on unpublished data (dr. Erik Lysoe, personal communication).

Parameter	*F. graminearum*	*F. poae*	*F. langsethiae*
Trichothecene chemotype	Type B	Type A+B	Type A
Pathogenesis	Necrotroph in late stages	Largely symptomless	Largely symptomless
Mode of reproduction	Predominantly sexual	Sexual + asexual?	Asexual?
Supernumerary chromosomes	No	Yes	Yes
High level of repetitive DNA	No	Yes	Yes
Triazole application	Efficient	Shift towards *F. poae*	Shift towards *F. langsethiae*

Sexual reproduction in *Fusarium* species has probably been best investigated in *F. graminearum*. Zeller et al. (2003) investigated the diversity of *F. graminearum* on wheat spikes in small quadrants. They detected a frequently recombining population, with limited spread after infection, as clonal isolates were almost exclusively detected from the same wheat ears. This is confirmed in a study by Manstretta et al. (2015) who investigated dispersal patterns of ascospores and conidia and found that 93% of the spores within a wheat canopy were ascospores. Liang et al. (2015) concluded from several large datasets and multiple studies that the *F. graminearum* population on wheat in the upper Midwestern United States is likely sexually more active that the population on barley.

7.4 Opportunities for pathogenomics

In Chapter 4, it was shown that the obtained genome assembly is a valuable tool for population monitoring of *F. poae* and understanding the balance between clonal and sexual reproduction. However, significant opportunities for pathogenomics are also available. Typically, novel sequenced genomes are mined for their secondary metabolite arsenal (Wiemann et al., 2013) and predicted effector genes and cell wall degrading enzymes (Gardiner et al., 2012). Investigations of this type offer invaluable insights into the epidemiology of the fungus. For example, *F. avenaceum* is a generalist pathogen occupying the extracellular space of a plethora of hosts, and this is reflected in the very high level of predicted secreted proteins (Lysoe et al., 2014). In the early stages of infection, *Z. tritici* is characterized by a latent biotrophic phase with little symptom development and during which it evades host defenses, termed "stealth pathogenesis". Accordingly, its genome contains a very low level of plant cell wall degrading enzymes (Goodwin et al., 2011).

Aside from an in depth look at the trichothecene biosynthesis loci, pathogenomics investigations like this have not been performed for *F. poae* yet and undoubtedly provide some of the most exciting opportunities for this species in the near future. The high quality genome annotation in Chapter 4 offers some interesting research questions. At least 31 genes have been duplicated to the supernumerary genome, several of which have predicted pathogenicity or secondary metabolite biosynthesis functions (**Table S4.2**).

The toxigenic potential of *Fusarium* species is not yet fully understood. As more genomes are sequenced, researchers find that a plethora of secondary metabolite clusters is present, for which no compound has been assigned or discovered yet. Moreover, *Fusarium* genomes up to now have in most cases contained unique clusters, not present in other species (Hansen et al., 2015).

These are part of the "cryptic genome" of the organism, regions on the chromosomes that are only expressed under specific circumstances such as under stress or during plant infection (Wiemann et al., 2013). Plant pathogenic *Fusarium* species contain record numbers of such secondary metabolite clusters, for example *F. avenaceum* contains up to 80 core genes involved in secondary metabolite biosynthesis (Lysoe et al., 2014). Prediction of secondary metabolite clusters, and their localization across the core and supernumerary genome of *F. poae*, should offer valuable insight into the toxigenic potential of this species. Often, phylogenetic studies on secondary metabolite biosynthesis clusters (SMCs) offer evidence of horizontal gene transfer between fungi, or even between different kingdoms (Gardiner et al., 2012; Sieber et al., 2014). The presence of TEs in or around SMCs such as the trichothecene cluster (see Chapter 6) may facilitate such horizontal gene transfer events.

A duplicated gene that is present in 10 copies (though not all full length; Table S4.2) is the *Dicer2* gene. This is a vital part of the RNA silencing machinery in fungal species (Segers et al., 2007), which has recently been confirmed for *F. graminearum* in particular (Chen et al., 2015). Notably, Dicer2 activity provides protection against mycoviruses, which are RNA viruses commonly infecting many fungal species. It has been stated that within the genus *Fusarium*, *F. poae* has particularly high levels of mycovirus infection (Fekete et al., 1995; Cho et al., 2013). This was confirmed by a *de novo* assembly of RNAseq reads collected in Chapter 4 (data not shown), as 2 mycoviruses (occurring within the nucleus) and 2 mitoviruses (occurring within the mitochondria) were detected. In light of the prevalence of RNA viruses in *F. poae*, the high copy number of the antiviral *Dicer2* gene is conspicuous and warrants further investigation.

The lessons learnt from the *F. poae* genome in Chapter 4 should hopefully help us to understand the genome dynamics of other *Fusarium* species, and pathogens from other genera. The genome dynamics that we detected between the core and supernumerary chromosomes were largely caused by the absence of RIP on the supernumerary genome. At least in *F. solani*, a similar exclusion could be ongoing as it was experimentally shown that a part of the genome was not affected by RIP. The supernumerary chromosomes of *F. solani* and of *F. oxysporum* f. sp. *lycopersici* have been shown to play a role in pathogenicity (Coleman et al., 2009; Ma et al., 2010), but it is not known if they have additional characteristics as those described in this thesis for *F. poae*. Several other *Fusarium* species have been shown to contain supernumerary chromosomes such as *F. sporotrichioides* (Fekete et al., 1993), *F. langsethiae* (Lysoe et al., 2015) and *F. asiaticum* (Galazka and Freitag, 2014), but for these either sequence information

or assembly quality is not yet sufficient to allow for an investigation as in depth as that carried out in Chapter 4. In a broader sense, different genome biology, rather than the currently widely adopted hypothesis of different origins could explain the differences between core and supernumerary genomes in many species.

During the genomics work that is described in Chapter 4, peculiar patterns of mutations were detected in the genomes of the four *F. poae* isolates. Blocks of high SNP levels between certain isolates alternated with blocks that contained little to no variation in a mosaic-like pattern. This is highly reminiscent of the situation in *Zymoseptoria pseudotritici*, a sister species of *Z. tritici* (Stukenbrock et al., 2012). It was found that this species originated through a single fusion event between two divergent individuals and all haplotypes that are present in current isolates of the species can be traced back to the divergence of the population founders. It will be highly interesting to investigate the origin of *F. poae* as a species, which is feasible with the highly contiguous assembly of its genome. Stukenbrock and McDonald (2008) reviewed the different origins of plant pathogens in agro-ecosystems and found several instances where hybridization led to the making of new pathogen. However, host and pathogen co-evolution is the more frequent scenario, often associated with the domestication of agricultural crops and the concordant loss in genetic diversity, both in the host and the pathogen. Finally, sudden host jumps and horizontal gene transfer may drastically alter the pathogenic potential of an organism and may lead to the formation of novel pathogens.

7.5 Longevity in the FHB complex

It is unknown whether *F. poae* fits the criteria of an "emerging" species or not. At least within the last decades it has been continuously prominent, as it has been detected frequently since the eighties of last century, and one study even assigns an important role to *F. poae* on wheat seeds of the 1930s-1940s (Gordon, 2006). It has also been detected from wheat samples collected in the early 1900s in the UK (dr. Cees Waalwijk, personal communication). Chapter 2 indicated that *F. poae* and *F. langsethiae* show an increased tolerance towards triazoles in field trials. We argue that this may contribute to upholding the share of these weaker pathogens in the population.

The genome sequence of *F. poae* was mined for the presence of the three *CYP51* known to *Fusarium* species (Becher et al., 2011). All three described genes are present in single copy in the genome; therefore copy number variation, for example by duplication to the supernumerary genome, is not responsible for higher triazoles tolerance. The genes code for functional proteins

(data not shown). We argue that like in *F. graminearum*, variation at the *CYP51* level may not be responsible for tolerance against triazoles. Transcriptional regulation (i.e. constitutively higher expression of the target genes, or higher expression upon triazoles exposure) has not been investigated yet.

Conclusively proving a link between elevated triazole mediation and a more toxic mycotoxin chemotype is troublesome. If efflux transporters of the ABC or MFS type are involved, there is significant substrate redundancy to cope with in experimental setups (Zwiers et al., 2003; Coleman and Mylonakis, 2009). Individual knockout of transporters are therefore not likely to offer convincing results. Micro-array or RNAseq experiments that monitor transporter upregulation under certain conditions may be more successful (Becher et al., 2011). It should be possible to uncover whether the same transporters are upregulated as a response to endogenous toxin production (e.g. as identified by Seong et al. (2009)) and exogenous triazole application. In *F. graminearum*, at least two such ABC transporters exist (FGSG_08830, FGSG_11028). For our hypothesis to be valid, self-protection of the fungus against its toxic trichothecenes should be more efficient or faster in *F. langsethiae* than in *F. graminearum*. Exposure experiments with DON and T-2 against both *F. graminearum* and *F. langsethiae* could help to elucidate this.

7.6 FHB and mycotoxin profiling

Chapter 3 of this thesis elaborated on the *Fusarium* survey work that was carried out for cereals and cereal-derived samples in a one year case study. Several of the measured trichothecenes are the subject of currently ongoing official investigation from legislative authorities. Traditionally, for mycotoxins that may pose a risk for human or animal health, the European Commission (EC; DG SANTE, Directorate General for Health and Food Safety) will ask the European Food Safety Authority (EFSA) to form a Scientific Opinion on that compound. For example, in the case of T-2/HT-2, this request was formulated in June 2010. The CONTAM (contaminants) panel of EFSA accepts the question and provides a deadline for the publication of a Scientific Opinion. Next, EFSA will ask the Member States of the European Union for scientific data and reports on the investigated subject, in an official "call for data". The data collected in the framework of Chapter 3 was submitted to EFSA as part of this procedure. EFSA will form a Scientific Opinion including a summary of available literature, values for lowest-observed-adverse-effect level (LOAEL) and no-observed-adverse-effect level (NOAEL), and occurrence data based on mycotoxin surveys. By combining this data, a risk assessment is performed for different target groups. In the case of the Scientific Opinion on T-2/HT-2, this was published

by EFSA in December 2011 (EFSA CONTAM Panel, 2011b). The EC uses the information provided in the Scientific Opinion to create legislation if necessary, such as was the case in 2013 when indicative values were set for T-2/HT-2 occurrence in cereals and cereal matrices (European Commission, 2013).

Scientific Opinions have been published in very recent years for *Fusarium* mycotoxins such as ZEN (EFSA CONTAM Panel, 2011a), T-2/HT-2 (EFSA CONTAM Panel, 2011b), NIV (EFSA CONTAM Panel, 2013) and BEAU/ENN (EFSA CONTAM Panel, 2014). Three Scientific Opinions for *Fusarium* mycotoxins are still ongoing, namely DON and its (masked) metabolites (deadline December 31st, 2015), MON (deadline December 31st, 2016) and DAS (deadline December 31st, 2016). This shows that the data collected in the framework of Chapter 3 is relevant for ongoing legislative efforts.

7.7 *Fusarium poae* epidemiology

Fusarium poae has been designated as one of the most prominent members of the FHB complex in Belgium during recent years. Together with *F. graminearum*, it was the most frequently isolated species by Audenaert et al. (2009). These researchers used a plating-based method, whereby colonies that emerge from wheat ears are characterized by diagnostic PCR and population distributions are calculated based on the total number of outgrowing colonies. In Chapter 3 of this thesis, we deployed a quantitative approach over a large number of samples, which shows less bias towards species that may have an *in vitro* advantage over slower growers. Importantly, even with this completely different approach, *F. graminearum* and *F. poae* were the two species with the highest incidence (the percentage of positive samples) and abundance (the amount of DNA normalized on plant DNA). This is a unifying trend over *F. poae* literature: despite the very different surveying strategies that are used by different research groups, *F. poae* stands as one of the most frequently encountered species within the FHB complex; Chapter 2 indicates that such reports existed already in the eighties of last century.

Much is still unclear about the epidemiology of *F. poae*. It has been described as a secondary species and its close correlation with other *Fusarium* species in field samples support this hypothesis. To improve our understanding of the epidemiology of *F. poae,* we need thorough field monitoring at different times in the growing season, which to the best of our knowledge has not been performed for *F. poae*. Moreover, to investigate the role of primary infection with *F. graminearum*, double inoculation experiments should be performed. It will be interesting to monitor whether *F. poae* profits from the metabolic changes that *F. graminearum* induces *in*

planta, such as increased concentration of metabolites from the polyamine pathway. Trichothecene biosynthesis in *F. poae* is likely regulated by yet unknown *in planta* signals, as L-arginine as the sole nitrogen source *in vitro* did not particularly stimulate type B trichothecene production, which is abundantly produced by *F. poae in planta* (Vogelgsang et al., 2008b). Nitrogen metabolism of both the plant and the fungus has a profound impact on the pathogenicity of the pathogen (Seifi et al., 2013; Subramaniam et al., 2015). One of the exciting questions for the future is to determine whether *F. poae*, and *F. langsethiae*, react differently to various nitrogen cues than *F. graminearum*.

The host preference of *F. poae* is unclear. In Chapter 3, we found that in Belgium it is more dominant on wheat than on barley. However, the literature review in Chapter 2 showed that in several countries, *F. poae* is dominant on barley as well, and the reason for this discrepancy is not known. The same samples that had low *F. poae* infestation in Chapter 3, had also higher DON levels (due to higher DON production by *F. graminearum*). Possibly the colonization of the ear with *F. graminearum* and DON was too high for *F. poae* to take hold.

7.8 Unique genome and chemotype at a crossroads

A type A + type B trichothecene chemotype was detected in *F. poae*, which is unstable *in vitro* with regard to the type B production when *F. poae* is cultured in trichothecene biosynthesis inducing medium. This can be explained by picturing the chemotype as a linear series of four compounds, DAS, NEO, FUS-X and NIV, and the biosynthesis of these compounds does not necessarily continue all the way through to NIV. The *Tri* cluster and its environment are invaded by TEs, which can be seen as a consequence of the unique *F. poae* genome biology, as no other *Fusarium* species have been described with a similar invasion. It is tempting to speculate that isolates with a *pogo* element in the important *Tri6 – Tri5* backbone region are affected in their trichothecene biosynthesis, but the instability of the chemotype could not easily be linked to the presence of this element.

New trichothecene chemotypes and metabolites are regularly detected (Fruhmann et al., 2014; Varga et al., 2015). As recombining populations bring together the different alleles that are present at the trichothecene loci, new chemotypes can be expected to arise in the future (Liang et al., 2014). We illustrate in Chapter 6 that a combination of *Tri13* and *Tri1* alleles, respectively coding for enzymes with a broad substrate range (*F. sporotrichioides*-like) and the possibility of hydroxylation at both C7 and C8 (*F. graminearum*-like), is responsible for the type A + B trichothecene chemotype in *F. poae*. This model may explain other such chemotypes, as in *F.*

equiseti where simultaneous type A + B production has also been reported from isolates. Indeed, the TRI13 in *F. equiseti* is more closely related to to FsTRI13 (79.2%) than to FgTRI13 (72.1%). Nevertheless, we should take care with identifying the link between genotype and chemotype, and *in vitro* chemotypes may be very different from *in vivo* production depending on what methods are used. Predicting the chemotype of *F. poae* isolates by a genetic diagnostic method may be particularly troublesome, as all *F. poae* isolates have a "NIV genotype", but production of NIV, at the last stage of the biosynthetic grid, may be dependent on unknown environmental or epigenetic factors.

7.9 General conclusion and perspective

The goal of this thesis was to increase our understanding of *F. poae*, a species that is consistently described as weakly pathogenic, but is a prominent member of the FHB complex nevertheless. In a first major part of the thesis, we set out to ascertain whether we are right to call *F. poae* a "successful" species. Results of field trials indicate that *F. poae*, for reasons that are yet unknown, is more tolerant towards triazoles than other species of the complex. Moreover, field surveys have indicated that the biomass of *F. poae* in the wheat ear is at the same high level as *F. graminearum*. A literature survey showed that the species has occasionally been reported as one of the most frequently detected FHB species for decades. Therefore, it seems like by all accounts, *F. poae* is indeed a successful species despite its limited ability to induce FHB symptoms in cereals.

In a second major part of the thesis, some of the reasons for the endurance of *F. poae* in the FHB complex were investigated. With state of the art genomics, we uncovered genome dynamics within this organism that have not been described for any fungus before, as the supernumerary chromosomes are not under the control of genome defense, which may confer significant opportunities for adaptation, and should accelerate chromosomal and organismal evolution in *F. poae*. With a polyphasic *in vitro* approach, a unique chemotype of both type A and type B trichothecenes was detected and investigated at the mechanistic level. Moreover, indications were found that *F. poae* combines sexual and asexual reproduction. Both the unique genome dynamics of *F. poae*, and the unique chemotype are connected in the finding that the *Tri* cluster is invaded by TEs, nevertheless no clear consequences on the trichothecene chemotype could be detected.

A key *F. poae* research topic for the future includes determining the actual effects that the unique genome biology of *F. poae* has had on its lifestyle, for example by investigation the

function of genes that have been duplicated to the supernumerary genome by knockout experiments. It will be interesting to uncover whether dosage effects and neofunctionalization play a role for genes of interest such as those involved in production of secondary metabolites and host colonization.

To map the spread and reproductive strategy of *F. poae*, simple diagnostic PCRs similar to those developed in this thesis will be useful. It will be possible to determine whether the genotype with major translocation(s) of sequence has spread to other locations or neighbouring countries, and with thorough monitoring schemes even the speed of such spreading events could be ascertained. The current assembly of *F. poae* is among the best within the fungi and should aid in further understanding genome evolution and biology in fungi. However, some drawbacks remain, such as the lack of knowledge on the occurrence of meiosis. Future investigations should further attempt to induce sexual reproduction in the lab, or lacking that, redirect field surveys to monitoring the occurrence of the sexual cycle. By evaluating when/if (new) TE insertions become RIPped over and during growing seasons, it will be possible to identify the frequence of meiosis (using RIP as a proxy for the sexual cycle).

While this thesis provides an explanation for the genetic basis of the type A+B chemotype in *F. poae*, there was no attempt to identify whether this chemotype offers any advantages over other FHB pathogens. This is another important research question for the future. With gene swaps of *Tri1* and *Tri13*, it should be possible to develop mutant strains that produce only type A (DAS and NEO; *FlTri1* gene swap) and type B (FUS-X and NIV; *FgTri13* gene swap) trichothecenes. Combining these in comparative experiments with the wildtype, a *Tri5* knockout mutant (producing no trichothecenes) and a knockout at *Tri1* (producing only DAS) will help uncover what role trichothecenes play in the epidemiology of *F. poae*, both for colonization of the host *in planta* and in its competition with other FHB species. *In planta* studies will also shed more light on the production of type A and type B trichothecenes by *F. poae* in the field, and for this purpose analytical methods should include not only the major trichothecene end products but also their related compounds. These experiments will also shed light on whether the instability detected *in vitro* is also present *in planta*, and which cues stimulate NIV production by *F. poae*.

Summary

The disease *Fusarium* Head Blight (FHB) on small grain cereals such as wheat and barley, is caused by a complex of *Fusarium* species that co-occur on the ear. This complex is dynamic, and evolves during the growing season, but may also show drastic differences between growing seasons or over multiple years. Within this complex, *F. graminearum* is the most important species. It causes significant economic damage, primarily due to its production of deoxynivalenol (DON). This is a mycotoxin, i.e. a secondary metabolite produced by the fungus which is not vital for its survival, but does play a role in certain niches or under certain conditions. *F. poae* has repeatedly been described as one of the most frequently detected *Fusarium* species, which is surprising because of its limited aggressiveness to the cereal host. In contrast to its consistent occurrence, the knowledge on *F. poae* is limited, particularly in comparison to *F. graminearum*. The goal of this thesis therefore was to improve our understanding of *F. poae*.

Broadly, the research in this thesis may be divided into two parts. In a first part, we set out to uncover whether *F. poae* can rightfully be called a successful species, and in a second part some of the more fundamental reasons for this success were addressed.

From the information in Chapters 1 and 2, it can be concluded that *F. poae* may be considered a successful species, despite its lack of aggressiveness. In field trials, it seems to profit from triazole application as its share in the *Fusarium* population increases while the share of other species such as *F. graminearum* decreases. The same finding holds true for *F. langsethiae*, which is morphologically similar to *F. poae*, and which is an emerging problem on oats in Scandinavian countries and the UK. A survey of literature indicates that it has been among the most prominently detected FHB species for decades, across a geographically broad distribution. Moreover, a detailed survey of Belgian small grain cereal field samples, indicated that *F. poae* biomass accumulates to levels similar to those of *F. graminearum* in wheat. Nevertheless, a lot is still unknown about its pathogenesis, and it remains to be seen how *F. poae* colonizes the wheat ear, but does not induce advanced necrosis – and particulary whether it may benefit the organism not to.

In Chapters 4, 5 and 6 we set out to identify determinants in the lifestyle of *F. poae* which may have contributed to its success. The basis for this approach was laid in Chapter 4, with the whole genome sequencing approach for four *F. poae* isolates. A high quality genome may galvanize

research of an organism, and therefore one isolate was sequenced with novel SMRT technology, which produces long reads and eventually leads to a more contiguous assembly. This provides otherwise impossible opportunities for genome biology and evolution studies. This allowed us to divide the genome of one *F. poae* isolate into a core and supernumerary component. The core genome is conserved and relatively stable between isolates, and it contains four chromosomes that show extensive synteny to those of *F. graminearum*. The supernumerary genome on the other hand is highly dynamic between isolates, and these chromosomes have been shown to differ in size and number between individuals. We found that the supernumerary chromosomes show high levels of TEs and paralogs, opposite to the situation on the core chromosomes. This was traced back to RIP, a fungus-specific defense mechanism against TEs, which is active on the core genome but not on the supernumerary genome.

The consequences of the core and supernumerary genome "living apart together" in *F. poae* were shown to be significant. The integration of TEs, and even whole blocks of supernumerary sequence, may accelerate evolution and adaptation in *F. poae*. By acting as a refuge from RIP for repetitive DNA, duplicated genes may persist in *F. poae* that would not have survived in *F. graminearum*. Elucidating the function of these duplicated genes will be one of the exciting *F. poae* related research questions for the future.

During the genome work on *F. poae*, clear indications surfaced that isolates of this species combine both sexual and asexual reproduction. RIP is only active during the pre-meiotic phase, and all the ingredients for the sexual cycle were found to be present within the genome. Both MAT1-1 and MAT1-2 mating types required for meiosis were found in the population, albeit in a heavily skewed but co-occurring fashion. A genotype where >200kb blocks of supernumerary sequence had translocated to the core chromosomes was found in three locations across Belgium, heavily indicative of clonal spread. For these purposes, a collection of 69 *F. poae* isolates was tested. In accordance with literature, we found that genome-wide intra-species diversity (determined with AFLP) heavily exceeded the diversity at the locus of a barcoding gene (EF-1α), which may be explained by the disruptive nature of TEs and supernumerary genome – mediated rearrangements on evolutionary short timescales. Indeed, the similar or even clonal nature of some (groups of) isolates may be obscured by TE proliferation.

Since DON has been shown to be an important part of the life cycle of *F. graminearum*, we set out to test which trichothecenes *F. poae* produces in a trichothecene biosynthesis inducing medium, and whether the described genome dynamics may have an effect on trichothecene production. We found that, uniquely, both type A and type B trichothecenes are produced in a

strictly sequential fashion, from DAS over NEO and FUS-X to NIV. If any of the compounds at the later stages is produced, all those coming before could also be detected. The triggers which are needed to move production all the way to NIV are still unknown. It was determined that this chemotype is not fixed, opposite to what has been described for the FGSC. All isolates are likely part of a universal NIV producing population, and opposed to the FGSC, defining a genetic "genotype" for this unstable chemotype may therefore be uninformative.

Different loci in the genomes of *Fusarium* species contain genes that are responsible for trichothecene production, grouped in clusters. Variation at the *Tri1* locus has been shown to be responsible for the switch between type A and type B production. In *F. poae*, we found different types of the *Tri1* gene with up to 3% divergence, however nearly all SNPs were synonymous. Clearly, TRI1 function is heavily constrained in this pathogen. In accordance with the unique genome dynamics of *F. poae*, the *Tri* cluster and its environment was found to be invaded by TEs. A RIPped *pogo* TE was found in the central region of the cluster in more than half of the isolates, however this could also not explain for any qualitative or quantitative differences in chemotype between the isolates. Like in several other *Fusarium* species, a recombination event was detected over the *Tri* cluster by using the TEs as genetic markers.

The production of both type A and type B trichothecenes was traced back to the combination of "opposing functions" by TRI1 and TRI13: TRI1 has *F. graminearum* – like function with the hydroxylation of its substrate at both C7 and C8, and TRI13 has *F. sporotrichioides* – like function by taking CAL as a substrate. In this manner, TRI13 mediates different paths along a complex biosynthesis grid.

In conclusion, we argue that the unique chemotype and genome dynamics of *F. poae* may be conducive to its continued persistence in the FHB complex, but as of yet a definitive link has not been shown. Future investigations will be able to elucidate whether characteristics such as a rapid generation of novel genotypes, a more toxic chemotype than its close relatives in the FHB complex, and the likely combination of sexual and asexual production have aided in the success of *F. poae* as a pathogen.

Samenvatting

De ziekte aarfusarium die vooral voorkomt op graangewassen zoals tarwe en gerst, wordt veroorzaakt door een gans complex van *Fusarium* species, die samen voorkomen op de aar van het gewas. De samenstelling van dit complex is zeer dynamisch, en kan gedurende het groeiseizoen veranderen, maar kan ook tussen verschillende groeiseizoenen grote verschillen vertonen. Binnen de verschillende species van het complex is *F. graminearum* allicht de belangrijkste. Ze leidt tot significante economische verliezen, vooral dan door de productie van de toxische stof deoxynivalenol (DON). Dit is een mycotoxine, d.w.z. een secundair metaboliet dat niet strikt noodzakelijk is voor het overleven van de schimmel, maar dat in bepaalde niches of onder bepaalde omstandigheden geproduceerd wordt. *F. poae* is in veel landen één van de meest gedetecteerde *Fusarium* species, een verrassende bevinding gezien het een vrij zwak pathogeen is. Het frequente voorkomen van *F. poae* staat in sterk contrast met de kennis die erover beschikbaar is, vooral in vergelijking met *F. graminearum*. Het doel van deze thesis was dan ook om een beter begrip te krijgen van *F. poae*.

In het algemeen kan deze thesis onderverdeeld worden in twee grote delen. In een eerste deel was het onze bedoeling om te bepalen als *F. poae* terecht een "succesvol" species mag genoemd worden. In een tweede deel werden een aantal verklaringen voor dit succes gezocht.

In Hoofdstukken 1 en 2 konden we vaststellen dat *F. poae* op veel vlakken een succesvol species is, ongeacht zijn beperkte aggressiviteit ten opzichte van de waardplant. In veldproeven die de efficiëntie van triazolen testten, konden we vaststellen dat *F. poae* mogelijk resistenter is dan andere species, en zo zijn aandeel in de populatie kan vergroten na fungiciden applicatie. Een gelijkaardig resultaat werd bekomen voor *F. langsethiae*, een opkomende species op haver in Scandinavische landen en het Verenigd Koninkrijk. Een literatuur studie toonde dat *F. poae* reeds tientallen jaren bij de meest gedetecteerde FHB species hoort, en dit over een geografisch wijde schaal. Ten laatste werd een gedetailleerde veld monitoring uitgevoerd, en deze toonde aan dat in België de graad van tarwe infestatie door *F. poae* gemiddeld even hoog is als deze door *F. graminearum*. Ongeacht deze duidelijke tekenen van "succes" als species, is slechts weinig geweten over de pathogenese van *F. poae*. Zo moet het nog onderzocht worden hoe de species de tarwe aar koloniseert, maar toch weinig symptomen induceert – en of dit misschien onderdeel is van de specifieke strategie van de schimmel.

In Hoofdstukken 4, 5 en 6 wilden we bepaalde karakteristieken van *F. poae* identificeren, die mogelijk hebben bijgedragen aan zijn succes. De solide basis voor deze aanpak werd gelegd in

Hoofdstuk 4, door de genoomsequentie van vier *F. poae* isolaten te bepalen. Een hoog kwalitatieve genoom sequentie kan onderzoek omtrent een organisme drastisch vooruit helpen, en daarom werd voor één isolaat SMRT technologie aangewend. Deze nieuwe techniek produceert lange DNA sequenties, en leidt daarom tot een meer continue genoom assemblage. Hierdoor worden nieuwe kansen aangesneden voor onderzoek naar de biologie en evolutie van een genoom. Het *F. poae* genoom kon onderverdeeld worden in een "basis" en "extra" deel. Het basisgenoom is sterk geconserveerd en vrij stabiel tussen de isolaten, en bestaat uit vier chromosomen die grote gelijkenis tonen met de chromosomen van, bijvoorbeeld, *F. graminearum*. Het "extra" genoom echter is zeer dynamisch, en de chromosomen hier verschillen in aantal en grootte tussen verschillende isolaten. Het basis en extra genoom verschillen onderling door hun niveau van repetitief DNA. We konden vastellen dat het ontbreken van "RIP" op het extra genoom, een verdedigingsmechanisme tegen "transposable elements", verantwoordelijk is voor de verschillen tussen het basis en extra genoom in *F. poae*.

De gevolgen van het samen voorkomen van het basis en extra genoom in *F. poae*, zijn significant. De dynamiek die ontstaat doordat TEs vanop het extra genoom naar het basisgenoom migreren, alsook door de volledige verplaatsing van grote stukken DNA, leidt tot een versnelde evolutie en groter adaptatie vermogen in *F. poae*. Doordat RIP niet actief is op het extra genoom, en repetitief DNA er niet uitgeschakeld wordt, ontstaan er gen duplicaties die in *F. graminearum* zouden uitgeschakeld zijn. Het uitzoeken van de functies van al deze gen duplicaties, is een interessante taak voor de toekomst.

Gedurende het onderzoek naar de genoomsequentie van *F. poae*, kwam overtuigend bewijs naar voor dat isolaten van deze species zich zowel seksueel als aseksueel voortplanten. RIP functioneert immers enkel tijdens de pre-meiotische fase, en op het basis genoom werd zeer duidelijk vastgesteld dat RIP recent actief was. Beide "mating types" die nodig zijn voor meiose (MAT1-1 en MAT1-2) werden teruggevonden in de populatie, doch niet in gelijke frequentie. Dit zijn aanduidingen dat isolaten zich seksueel voortplanten. Een specifiek genotype dat >200kb aan extra sequentie had in het basis genoom, ten gevolge van een unieke verplaatsing vanuit het extra genoom, werd aangetroffen op drie locaties over België. Dit type van verspreiding van een genotype is typisch voor aseksuele voortplanting, waarbij snel grote afstanden kunnen afgelegd worden. Een collectie van 69 *F. poae* isolaten werd getest op zijn genetische diversiteit, en zoals het ook in de literatuur beschreven wordt, werd een veel grotere variabiliteit vastgelegd op genoom-wijd niveau dan op het niveau van één typerings gen. We stellen voor dat de genoom dynamiek in *F. poae*, met z'n actieve TEs en "extra" genoom, kan

zorgen voor veel variabiliteit op evolutionair korte tijdsschaal. Zodoende zou de identieke aard van sommige isolaten gemaskeerd kunnen worden door TE mobilisatie.

Aangezien DON voor *F. graminearum* een belangrijk metaboliet is, wilden we achterhalen welke trichothecene mycotoxines *F. poae* aanmaakt op een inducerend medium. Zowel type A als type B trichothecenen werden geproduceerd in een strikt sequentieel patroon, van DAS, over NEO, over FUS-X, naar NIV. Wanneer een bepaalde stof verder in het schema was aangemaakt, konden ook al deze eerder in de rij gedetecteerd worden. Welke factoren nodig zijn om trichothecene productie tot en met NIV te bekomen is niet geweten. Dit "chemotype" was niet constant, in tegenstelling tot de situatie in het *F. graminearum* species complex. Alle isolaten van *F. poae* zijn waarschijnlijk onderdeel van een NIV producerende populatie, en een genetisch "genotype" vastleggen voor deze isolaten is dus allicht weinig betekenisvol.

Verschillende loci in het genoom van *Fusarium* species bevatten genen die samen verantwoordelijk zijn voor de productie van trichothecenen. In andere *Fusarium* species is het reeds aangetoond dat het onderscheid tusssen type A en type B trichothecenen wordt gemaakt door variatie van de *Tri1* locus. In *F. poae* vonden we verschillende types van het *Tri1* gen, met tot 3% sequentie divergentie. Bijna geen enkele SNP leidde echter tot aminozuur substituties, en de functie van TRI1 lijkt in *F. poae* zeer sterk beschermd. In navolging van de unieke genoom dynamiek binnen *F. poae*, werden verschillende TEs aangetroffen in en rond de trichothecene biosynthese cluster. Een *pogo* TE dat onderhevig was aan RIP ligt middenin de cluster in meer dan de helft van de *F. poae* isolaten, maar deze aanwezigheid was niet gecorreleerd met de chemotype variabiliteit. Finaal werd, net als in verschillende andere *Fusarium* species, eenr recombinatie event vastgesteld in de trichothecene biosynthese cluster.

De productie van zowel type A als type B trichothecene wordt veroorzaakt door de gecombineerde functie van twee enzymes met "tegengestelde" werking: TRI1 heeft een functie zoals in *F. graminearum*, het plaatst namelijk twee OH groepen op het substraat, terwijl TRI13 een functie zoals in *F. sporotrichioides* heeft, met een breed substraat spectrum. Op deze manier zou kunnen gesteld worden dat TRI13 verschillende routes langs het trichothecene biosynthese network aanstuurt. Finaal concluderen we dat de unique genoom dynamiek en het unique chemotype van *F. poae* ondersteunend kunnen zijn voor het voortdurende success van *F. poae* in het FHB complex, maar een definitieve link is nog niet aangetoond. Verder onderzoek zal moeten aantonen of eigenschappen zoals het snelle onstaan van nieuwe genotypes, een meer toxisch chemotype dan nauw verwante species, en de combinatie van seksuele en aseksuele reproductie bepalend geweest zijn in het succes van *F. poae* als een pathogeen.

Appendix

Note: dr. Marthe De Boevre carried out LC-MS/MS development and validation, and wrote the text for this Appendix.

Development and validation of LC-MS/MS method for detection of mycotoxins in grain, food and feed matrices

Reagents and chemicals, sample preparation and extraction

Methanol (LC-MS grade) was purchased from BioSolve BV (Valkenswaard, The Netherlands), while acetonitrile (Analar Normapur), n-hexane (Hipersolv Chromanorm) and ammonium acetate were obtained from VWR International (Zaventem, Belgium). Acetic acid (glacial, 100%) was supplied by Merck (Darmstadt, Germany). Water was obtained from a Milli-Q® SP Reagent water system from Millipore Corp. (Brussels, Belgium). Individual mycotoxin solid standards (1 mg) of DON, 3-ADON, 15-ADON, DOM, α-ZEL, β-ZEL, zearalanone (ZAN), HT-2, NEO, FUS-X and DAS were purchased from Sigma Aldrich NV/SA (Bornem, Belgium). T-2 solid standard (1 mg), and DON-3G (50.2 ng/µl in acetonitrile) were obtained from Biopure Referenzsubstanzen GmbH (Tulln, Austria). ZEN (5 mg) was supplied by Fermentek (Jerusalem, Israel). All mycotoxin solid standards were dissolved in methanol (1 mg/ml), and were storable for a minimum of 1 year at -18 °C (Spanjer et al., 2008). The DON-3G solution was kept at 4 °C.

Working solutions of DON, 3-ADON, 15-ADON, DOM, ZEN, α-ZEL, β-ZEL, ZAN, HT-2, T-2, DAS, NEO and FUS-X (10 ng/µl) were prepared in methanol, and stored at -18 °C, while DON-3G was dissolved in acetonitrile, and stored at 4 °C. The internal standard-mixture (including DOM and ZAN) was prepared in methanol, stored at -18 °C, and renewed monthly.

In short, after addition of the internal standards mix to every sample (DOM, 25 µg/kg; ZAN, 25 µg/kg), the ground material was extracted with 10 ml acetonitrile/water/acetic acid (79/20/1), combined with a hexane defatting (5 ml hexane). The sample extract was vigourously shaken on the Agitator decanter overheadshaker (Agitelec, J. Toulemonde & Cie, Paris, France) for 60 minutes. After centrifugation (3 000 g, 15 min), the supernatant (hexane layer) was removed; the aqueous layer was filtered and evaporated to dryness under a gentle stream of nitrogen (40 °C). The residue was dissolved in ‘mobile phase for injection’ (methanol/water (50/50) with 5 mM ammonium acetate and 0.3% glacial acetic acid) and centrifuged in an Ultrafree-MC centrifugal device (Millipore, Bedford, MA, USA) for 10 min at 10 000 g.

LC-MS/MS methodology

UPLC-MS/MS analysis was performed using a Waters Acquity UPLC system coupled to a Quattro Premier XE mass spectrometer (Waters, Milford, MA, USA) equipped with an electrospray interface (ESI) by injecting a volume of 10 µl. Chromatographic separation was performed applying a ZORBAX RRHD Eclipse Plus-C18-column (1.8 µm, 100 mm x 2.1 mm)

(Agilent Technologies, Diegem, Belgium). The column was kept at 30°C, while the autosampler was set at 10 °C. A mobile phase consisting of water/methanol (95/5, v/v (A)) and methanol/water (95/5, v/v (B)), both buffered with 5 mM ammonium acetate and 0.3% glacial acetic acid was used at a flow rate of 0.4 ml/min. The gradient elution program started at 50% mobile phase A for 3.5 minutes, followed with a linear increase to 99% mobile phase B by 7.5 minutes. An isocratic gradient of 99% mobile phase B initiated at 7.5 minutes for 1 minute. The duration of each UPLC run was 11 minutes, including reequilibration to 50% mobile phase A. The ESI interface was used in the positive electrospray ionisation mode (ESI+). The MS parameters include the following settings: ESI source block temperature 120 °C; desolvation temperature 300 °C; capillary voltage 4 kV; argon collision gas 9.10-6 bar; cone gas flow 50 L/h, desolvation gas flow 800 L/h, and multiplier 750 V. The acquisition of data was performed applying selected reaction monitoring (SRM), in order to increase the sensitivity and the selectivity of the mass spectrometric conditions. The cone voltage and the collision energy were optimized, and selected for the most suitable precursor ion of each analyte, implemented with 2 product ions. These MS-parameters are detailed in **Table A.1**. MassLynx™ version 4.1. and QuanLynx® version 4.1. software (Micromass, Manchester, UK) were used for the data acquisition and processing.

Table A.1 - Optimized ESI^+ MS/MS-parameters. The asterisk designates the quantifier ion.

Analyte	Precursor ion (m/z)	Molecular Ion	Cone Voltage (V)	Product Ions (m/z)	Collision Energy (eV)
DON	297.4	$[M+H]^+$	37	203.4*	14
				249.3	12
DON-3G	476.1	$[M+NH_4]^+$	15	248.6*	18
				296.9	12
3-ADON	356.1	$[M+NH_4]^+$	25	203.1*	16
				339.2	15
15-ADON	356.1	$[M+NH_4]^+$	18	137.4*	25
				339.2	8
HT-2	442.2	$[M+NH_4]^+$	27	215.3*	15
				263.3	15
T-2	484.1	$[M+NH_4]^+$	31	245.4*	14
				305.4	15
ZEN	319.2	$[M+H]^+$	37	283.3*	15
				301.4	10
α-ZEL	321.3	$[M+H]^+$	30	285.4*	12
				303.3	8
β-ZEL	321.0	$[M+H]^+$	25	285.1*	10
				303.3	8
FUS-X	355.0	$[M+H]^+$	18	174.9*	25
				137.0	20
NEO	400.00	$[M+NH_4]^+$	26	305.3*	19
				185.0	12
DAS	384.20	$[M+NH_4]^+$	21	307.1*	14
				247.0	12
DOM (IS)	281.1	$[M+H]^+$	30	108.8*	20
				233.3	12
ZAN (IS)	321.2	$[M+H]^+$	35	189.1*	22
				303.3	14

Internal quality control was guaranteed using a standard measuring program. First, a standard mixture was injected, followed by mobile phase for injection. After the insertion of a blank sample, the spikes were analysed for the construction of a calibration curve. Then, 20 samples were injected followed by a control spike, which is a repeated injection of a spike of the calibration curve. The results were interpreted and identified according to 4 quality parameters: the analytes should have at least 3 or more identification points; the signal to noise ratio of each ion should be more than 3; the relative intensity of the selected ions, expressed as the percentage of the intensity of the most abundant ion, must correspond with those of the ions of the spike with a comparable concentration, and the relative retention time (with regard to the internal standard) of the analyte in the sample must range within a margin of 2.5% of the relative

retention time of the spiked sample. For all components DOM was used as the internal standard, except for ZEN, α-ZEL and β-ZEL where ZAN was used as the internal standard.

Method validation

The method was validated based on the Commission Regulation (EC) No 401/2006 of February 23 2006 laying down the methods of sampling and analysis for the official control of the levels of mycotoxins in foodstuffs (European Commission, 2006c). The method was validated in terms of linearity, trueness, limit of detection (LOD), limit of quantification (LOQ), decision limit (CCα), detection capability (CCβ), precision, expanded measurement uncertainty and specificity.

Five blank samples of each matrix were spiked in triplicate during 3 consecutive days with the different mycotoxins at 5 concentration levels of 0.5; 0.75; 1.0; 1.5 and 2 times the cut-off level as indicated in **Table A.2**. DOM and ZAN were added as internal standards, and by using the relative standard peak area, DOM was applied as a structural analogue for DON, 3-ADON, 15-ADON, DON-3G, FUS-X, NEO, DAS, T-2 and HT-2, while ZAN was used for the myco-estrogens and their derivatives.

The linearity of the method was assessed for each toxin, by fitting the data with a linear regression model and description of the residual analysis. Establishing the linear regression model, no parallel curves were detected for both standard solution and matrix. Indeed, ion suppression was noted for the matrix curve, possibly due to interferences of matrix substances during ionisation. Hence, matrix-matched calibration curves were used for the determination of the analytes. In addition, the outcome of the residual analysis revealed a random distribution of the residues.

Because no certified reference materials were available, the trueness of the analysis was determined on the basis of the apparent recovery after spiking of the target toxins. The apparent recovery was determined using a matrix-matched calibration curve for all five concentration levels. The observed signal (expressed as the relative peak area) was plotted against the actual concentration. The measured concentration was determined using the calibration curves, and the apparent recovery was calculated by **Equation A.1**.

Equation A.1: Formula for the description of the trueness: apparent recovery

$$\frac{\text{measured concentration (µg/kg)}}{\text{actual spiked concentration (µg/kg)}} = \text{apparent recovery (\%)}$$

In general, the results obtained are presented in **Table A.3**, and proved to be acceptable from 90% to 107%, which fit the criteria mentioned in 401/2006.

The LOD and LOQ were calculated by establishing the concentration equal to 3 and 6 times, respectively, the residual standard error of the intercept, divided by the slope of the constructed calibration curve. The CCα, for compounds with a maximum permissible limit (DON, ZEN and T-2 and HT-2), was determined as the concentration equal to the y-curve plus 1.64 the residual standard error of the intercept. For compounds without a maximum permissible limt the concentration was equal to the concentration ressembling the maximum tolerable limit plus 1.64 the standard error of the intra-laboratory reproducibility. The detection capability (CCβ) is equal to CCα plus 1.64 the standard deviation of the intra-laboratory reproducibility of the mean measured amount at CCα level. All parameters were verified by the signal to noise ratio (s/n), which should be more than 3 and 10, respectively according to the IUPAC-guidelines. The developed method allowed the determination of all the target mycotoxins at a ppb-level lower than the maximum permissible levels (**Table A.2**).

The repeatibility of the method was determined by the analysis of three replicates at five different concentrations on the same day by calculating the variation coefficient (VC). The same approach was applied for the determination of the intra-laboratory reproducibility, differing in three days instead of one. The VC's were measured during the precision study at the five different concentration levels as pointed out in **Table A.3**. The repeatability and the intra-laboratory reproducibility data obtained were for most mycotoxins in accordance with the described criteria. These criteria have only been described for some mycotoxins, however by processing the results they were also implemented for 3-ADON, 15-ADON, DON-3G, NEO, DAS, FUS-X and the ZEN-derivatives. NEO has for both the repeatability and the intra-laboratory reproducibility high VC-values (29% and 23%, respectively) at the 0.5 * cut-off level.

The combined standard uncertainty (u_c) is an estimated standard deviation equal to the positive square root of the total variance obtained by combining the variance of repeatability (within day, $s^2_w = s^2_{r\ within\ day}$), the variance between days ($s^2_b = s^2_{L\ between\ day}$) and the bias of the uncertainty U (ó)² (**Equation A.2**). The expanded measurement uncertainty was calculated according to **Equation A.3**. The expanded measurement uncertainty (U) was obtained by multiplying u_c by a coverage factor 2, based on a desired approximate level of confidence of 95%.

Equation A.2: determination of the bias of uncertainty

$$U(ó)^2 = = ((s^2_R * (1-ɣ) * \left(\frac{ɣ}{\frac{n}{p}}\right))$$

with s^2_R reproducibility variance, $ɣ = s^2_r/s^2_R$, n = amount of series analysed, and p = amount of days analysed.

Equation A.3: determination of the expanded measurement uncertainty

$$u_c = 2 * \sqrt{(s^2_w + U(ó)^2 + s_b{}^2)}$$

with s^2_w variance of repeatability, the variance between days ($s^2_b = s^2_{L\ between\ day}$), and the bias of the uncertainty U $(ó)^2$.

The expanded measurement uncertainty (U), calculated at the several concentration levels is a criterion for the integral acceptability of the UPLC-MS/MS method and ranged for all mycotoxins from 6% to 41%, except for NEO where the U was high for the 2 * cut-off level. This high value was attributed to the high VC-levels as previously mentioned and are rather questionable for this specific mycotoxin.

The specificity was tested by the analysis of 20 blank samples of different matrices. The calculations were executed and processed using Microsoft Office Excel 2007 and IBM SPSS 19. The same batches were used for most validation parameters; however the sample preparation procedure was completely independent, leading to completely independent data. The analysis of the results confirmed that no interferences occurred in the several MRM-channels. The results of the performance characteristics of the UPLC-MS/MS method are presented in **Table A.2** and **Table A.3**, moreover these are in good agreement with the criteria mentioned in the Commission Regulation (EC) No 401/2006.

Table A.2: Performance characteristics for the UPLC-MS/MS method for the analysed mycotoxins: cut-off level (CO; µg/kg), limit of detection (LOD; µg/kg), limit of quantification (LOQ; µg/kg), decision limit (CCα; µg/kg) and detection capability (CCβ; µg/kg).

analyte	CO (µg/kg)	LOD (µg/kg)	LOQ (µg/kg)	CCα (µg/kg)	CCβ (µg/kg)
DON	100	31	62	17	27
3-ADON	100	40	81	23	33
15-ADON	100	25	49	15	22
DON-3G	100	72	143	39	72
ZEN	75	21	41	11	22
α-ZEL	75	27	54	15	23
β-ZEL	75	31	62	17	29
T-2	150	38	77	20	43
HT-2	150	52	104	27	53
FUS-X	300	170	341	94	272
DAS	150	60	119	31	64
NEO	150	44	87	84	453

Table A.3: Performance characteristics for the UPLC-MS/MS method for the analysed mycotoxins: repeatability (%), intra-laboratory reproducibility (%), apparent recovery (%) and expanded measurement uncertainty (%). CO = cut-off level.

	Repeatability (VC, %)					Intra-laboratory reproducibility (VC, %)					Apparent recovery (%)					Expanded measurement uncertainty (%)				
analyte	**½*CO**	**¾*CO**	**1*CO**	**3/2*CO**	**2*CO**	**½*CO**	**¾*CO**	**1*CO**	**3/2*CO**	**2*CO**	**½*CO**	**¾*CO**	**1*CO**	**3/2*CO**	**2*CO**	**½*CO**	**¾*CO**	**1*CO**	**3/2*CO**	**2*CO**
DON	12	10	7	4	2	2	6	8	2	1	96	98	104	100	99	14	17	22	15	8
3-ADON	12	6	9	10	3	14	5	9	8	3	100	105	96	99	101	17	12	25	36	19
15-ADON	8	3	6	3	2	9	7	5	3	1	107	98	98	99	101	12	12	15	14	8
DON-3G	7	7	9	3	4	6	1	2	3	1	107	101	109	105	105	10	9	19	14	15
ZEN	6	8	10	2	1	1	6	7	7	2	101	103	97	100	100	6	12	18	18	8
α-ZEL	6	12	12	6	3	9	2	8	3	2	102	104	95	99	101	8	15	24	14	10
β-ZEL	8	12	12	4	2	13	3	4	8	5	98	103	98	101	100	11	21	23	22	16
T-2	8	4	4	8	3	4	6	2	6	1	106	101	99	98	102	16	15	15	45	18
HT-2	12	9	7	5	1	19	10	10	3	2	100	100	102	100	100	34	34	37	31	21
FUS-X	16	7	7	4	4	17	20	15	3	1	90	113	97	96	101	67	66	70	49	41
DAS	9	11	11	10	4	7	12	6	2	1	107	102	95	96	102	18	40	13	43	25
NEO	29	25	16	16	11	23	8	7	10	7	99	114	91	110	96	54	66	45	37	80

References

A

Abou Ammar, G., Tryono, R., Doell, K., Karlovsky, P., Deising, H.B., and Wirsel, S.G.R. (2013). Identification of ABC Transporter Genes of *Fusarium graminearum* with Roles in Azole Tolerance and/or Virulence. PLoS One *8*, e79042.

Alexander, N.J., McCormick, S.P., Waalwijk, C., van der Lee, T., and Proctor, R.H. (2011). The genetic basis for 3-ADON and 15-ADON trichothecene chemotypes in *Fusarium*. Fungal Genetics and Biology *48*, 485-495.

Ameye, M., Audenaert, K., De Zutter, N., Steppe, K., Van Meulebroek, L., Vanhaecke, L., De Vleesschauwer, D., Haesaert, G., and Smagghe, G. (2015). Priming of Wheat with the Green Leaf Volatile Z-3-Hexenyl Acetate Enhances Defense against *Fusarium graminearum* But Boosts Deoxynivalenol Production. Plant Physiology *167*, 1671-1684.

Aoki, T., Ward, T., Kistler, H.C., and O'Donnell, K. (2012). Systematics, phylogeny and trichothecene mycotoxin potential of *Fusarium* head blight cereal pathogens. Mycotoxins *62*, 91-102.

Audenaert, K., Callewaert, E., Hofte, M., De Saeger, S., and Haesaert, G. (2010). Hydrogen peroxide induced by the fungicide prothioconazole triggers deoxynivalenol (DON) production by *Fusarium graminearum*. BMC Microbiology *10*, 112.

Audenaert, K., De Boevre, M., Vanheule, A., Callewaert, J., Bekaert, B., Höfte, M., De Saeger, S., and Haesaert, G. (2013). Mycotoxin glucosylation in commercial wheat varieties: Impact on resistance to *Fusarium graminearum* under laboratory and field conditions. Food Control *34*, 756-762.

Audenaert, K., Landschoot, S., Vanheule, A., Waegeman, W., De Baets, B., and Haesaert, G. (2011). Impact of Fungicide Timing on the Composition of the *Fusarium* Head Blight Disease Complex and the Presence of Deoxynivalenol (DON) in Wheat. In Fungicides: beneficial and harmful aspects, N. Thajuddin, ed. (Rijeka, Croatia: InTech), pp. 79-98.

Audenaert, K., Van Broeck, R., Bekaert, B., De Witte, F., Heremans, B., Messens, K., Hofte, M., and Haesaert, G. (2009). *Fusarium* head blight (FHB) in Flanders: population diversity, inter-species associations and DON contamination in commercial winter wheat varieties. European Journal of Plant Pathology *125*, 445-458.

Audenaert, K., Vanheule, A., Hofte, M., and Haesaert, G. (2014). Deoxynivalenol: A Major Player in the Multifaceted Response of *Fusarium* to Its Environment. Toxins *6*, 1-19.

B

Baayen, R.P., O'Donnell, K., Bonants, P.J., Cigelnik, E., Kroon, L.P., Roebroeck, E.J., and Waalwijk, C. (2000). Gene genealogies and AFLP analyses in the *Fusarium oxysporum* complex identify monophyletic and nonmonophyletic formae speciales causing wilt and rot disease. Phytopathology *90*, 891-900.

Barreto, D., Carmona, M., Ferrazini, M., Zanelli, M., and Perez, B.A. (2004). Occurrence and pathogenicity of *Fusarium poae* in barley in Argentina. Cereal Research Communications *32*, 53-60.

Barros, G., Zanon, M.S.A., Palazzini, J.M., Haidukowski, M., Pascale, M., and Chulze, S. (2012). Trichothecenes and zearalenone production by *Fusarium equiseti* and *Fusarium semitectum* species isolated from Argentinean soybean. Food Additives and Contaminants Part a-Chemistry Analysis Control Exposure & Risk Assessment *29*, 1436-1442.

Bebber, D.P., Ramotowski, M.A.T., and Gurr, S.J. (2013). Crop pests and pathogens move polewards in a warming world. Nature Climate Change *3*, 985-988.

Becher, R., Hettwer, U., Karlovsky, P., Deising, H.B., and Wirsel, S.G.R. (2010). Adaptation of *Fusarium graminearum* to Tebuconazole Yielded Descendants Diverging for Levels of Fitness, Fungicide Resistance, Virulence, and Mycotoxin Production. Phytopathology *100*, 444-453.

Becher, R., Weihmann, F., Deising, H.B., and Wirsel, S.G.R. (2011). Development of a novel multiplex DNA microarray for *Fusarium graminearum* and analysis of azole fungicide responses. BMC Genomics *12*, 52.

Berthiller, F., Crews, C., Dall'Asta, C., De Saeger, S., Haesaert, G., Karlovsky, P., Oswald, I.P., Seefelder, W., Speijers, G., and Stroka, J. (2013). Masked mycotoxins: A review. Molecular Nutrition & Food Research *57*, 165-186.

Berthiller, F., Dall'asta, C., Corradini, R., Marchelli, R., Sulyok, M., Krska, R., Adam, G., and Schuhmacher, R. (2009). Occurrence of deoxynivalenol and its 3--D-glucoside in wheat and maize. Food Additives and Contaminants Part a-Chemistry Analysis Control Exposure & Risk Assessment *26*, 507-511.

Berthiller, F., Krska, R., Domig, K.J., Kneifel, W., Juge, N., Schuhmacher, R., and Adam, G. (2011). Hydrolytic fate of deoxynivalenol-3-glucoside during digestion. Toxicology Letters *206*, 264-267.

Blitzblau, H.G., Bell, G.W., Rodriguez, J., Bell, S.P., and Hochwagen, A. (2007). Mapping of meiotic single-stranded DNA reveals double-strand-break hotspots near centromeres and telomeres. Current Biology *17*, 2003-2012.

Boddu, J., Cho, S., Kruger, W.M., and Muehlbauer, G.J. (2006). Transcriptome analysis of the barley-*Fusarium graminearum* interaction. Molecular Plant-Microbe Interactions *19*, 407-417.

Bolger, A.M., Lohse, M., and Usadel, B. (2014). Trimmomatic: a flexible trimmer for Illumina sequence data. Bioinformatics *30*, 2114-2120.

Bonin, A., Bellemain, E., Bronken Eidesen, P., Pompanon, F., Brochmann, C., and Taberlet, P. (2004). How to track and assess genotyping errors in population genetics studies. Molecular Ecology *13*, 3261-3273.

Booth, C. (1971). The genus *Fusarium*. The genus *Fusarium*. Commonwealth Mycological Institute, Kew, UK. 237p.

Bowden, R.L., and Leslie, J.F. (1999). Sexual recombination in *Gibberella zeae*. Phytopathology *89*, 182-188.

Brennan, J.M., Leonard, G., Fagan, B., Cooke, B.M., Ritieni, A., Ferracane, R., Nicholson, P., Simpson, D., Thomsett, M., and Doohan, F.M. (2007). Comparison of commercial European wheat cultivars to *Fusarium* infection of head and seedling tissue. Plant Pathology *56*, 55-64.

Brown, D.W., Dyer, R.B., McCormick, S.P., Kendra, D.F., and Plattner, R.D. (2004). Functional demarcation of the *Fusarium* core trichothecene gene cluster. Fungal Genetics and Biology *41*, 454-462.

Broz, K.L., and Kistler, H.C. (2014). Cellular localization of proteins involved in trichothecene biosynthesis in *Fusarium graminearum*. Phytopathology *104*, 20-20.

Bryden, W.L. (2012). Mycotoxin contamination of the feed supply chain: Implications for animal productivity and feed security. Animal Feed Science and Technology *173*, 134-158.

C

Cambareri, E.B., Jensen, B.C., Schabtach, E., and Selker, E.U. (1989). Repeat-induced G-C to A-T mutations in *Neurospora*. Science *244*, 1571-1575.

Camiolo, S., and Porceddu, A. (2013). gff2sequence, a new user friendly tool for the generation of genomic sequences. BioData Mining *6*, 15.

Catlett, N.L., Lee, B.-N., Yoder, O.C., and Turgeon, B.G. (2003). Split-Marker Recombination for Efficient Targeted Deletion of Fungal Genes. Fungal Genetics Newsletter *50*, 9-11.

Chen, Y., Gao, Q., Huang, M., Liu, Y., Liu, Z., Liu, X., and Ma, Z. (2015). Characterization of RNA silencing components in the plant pathogenic fungus *Fusarium graminearum*. Scientific Reports *5*, 12500.

Cho, W.K., Lee, K.-M., Yu, J., Son, M., and Kim, K.-H. (2013). Insight into Mycoviruses Infecting *Fusarium* Species. In Advances in Virus Research, Vol 86: Mycoviruses, S.A. Ghabrial, ed., pp. 273-288.

Chulze, S.N., Ramirez, M.L., Torres, A., and Leslie, J.F. (2000). Genetic variation in *Fusarium* section Liseola from no-till maize in Argentina. Applied and Environmental Microbiology *66*, 5312-5315.

Clear, R.M., and Patrick, S.K. (1993). Prevalence of some seed-borne fungi on soft white winter-wheat seed from Ontario, Canada. Canadian Plant Disease Survey *73*, 143-149.

Clutterbuck, A.J. (2011). Genomic evidence of repeat-induced point mutation (RIP) in filamentous ascomycetes. Fungal Genetics and Biology *48*, 306-326.

Coghlan, A., Eichler, E.E., Oliver, S.G., Paterson, A.H., and Stein, L. (2005). Chromosome evolution in eukaryotes: a multi-kingdom perspective. Trends in Genetics *21*, 673-682.

Coleman, J.J., and Mylonakis, E. (2009). Efflux in Fungi: La Piece de Resistance. PLoS Pathogens *5*, e1000486.

Coleman, J.J., Rounsley, S.D., Rodriguez-Carres, M., Kuo, A., Wasmann, C.C., Grimwood, J., Schmutz, J., Taga, M., White, G.J., Zhou, S., *et al.* (2009). The Genome of *Nectria haematococca*: Contribution of Supernumerary Chromosomes to Gene Expansion. PLoS Genetics *5*, e1000618.

Connolly, L.R., Smith, K.M., and Freitag, M. (2013). The *Fusarium graminearum* Histone H3 K27 Methyltransferase KMT6 Regulates Development and Expression of Secondary Metabolite Gene Clusters. PLoS Genetics *9*, e1003916.

Correll, J.C., Klittich, C.J.R., and Leslie, J.F. (1987). Nitrate non-utilizing mutants of *Fusarium oxysporum* and their use in vegetative compatibility tests. Phytopathology *77*, 1640-1646.

Covarelli, L., Beccari, G., Prodi, A., Generotti, S., Etruschi, F., Juan, C., Ferrer, E., and Manes, J. (2015). *Fusarium* species, chemotype characterisation and trichothecene contamination of durum and soft wheat in an area of central Italy. Journal of the Science of Food and Agriculture *95*, 540-551.

Croll, D., and McDonald, B.A. (2012). The Accessory Genome as a Cradle for Adaptive Evolution in Pathogens. PLoS Pathogens *8*, e1002608.

Croll, D., Zala, M., and McDonald, B.A. (2013). Breakage-fusion-bridge Cycles and Large Insertions Contribute to the Rapid Evolution of Accessory Chromosomes in a Fungal Pathogen. PLoS Genetics *9*, e1003567.

Cuomo, C.A., Gueldener, U., Xu, J.-R., Trail, F., Turgeon, B.G., Di Pietro, A., Walton, J.D., Ma, L.-J., Baker, S.E., Rep, M., *et al.* (2007). The *Fusarium graminearum* genome reveals a link between localized polymorphism and pathogen specialization. Science *317*, 1400-1402.

D

D'mello, J., Placinta, C., and Macdonald, A. (1999). *Fusarium* mycotoxins: a review of global implications for animal health, welfare and productivity. Animal Feed Science and Technology *80*, 183-205.

De Boevre, M., Di Mavungu, J.D., Landschoot, S., Audenaert, K., Eeckhout, M., Maene, P., Haesaert, G., and De Saeger, S. (2012a). Natural occurrence of mycotoxins and their masked forms in food and feed products. World Mycotoxin Journal *5*, 207-219.

De Boevre, M., Di Mavungu, J.D., Maene, P., Audenaert, K., Deforce, D., Haesaert, G., Eeckhout, M., Callebaut, A., Berthiller, F., Van Peteghem, C., *et al.* (2012b). Development and validation of an LC-MS/MS method for the simultaneous determination of deoxynivalenol, zearalenone, T-2-toxin and some masked metabolites in different cereals and cereal-derived food. Food Additives and Contaminants Part a-Chemistry Analysis Control Exposure & Risk Assessment *29*, 819-835.

De Boevre, M., Jacxsens, L., Lachat, C., Eeckhout, M., Di Mavungu, J.D., Audenaert, K., Maene, P., Haesaert, G., Kolsteren, P., De Meulenaer, B., *et al.* (2013). Human exposure to mycotoxins and their masked forms through cereal-based foods in Belgium. Toxicology Letters *218*, 281-292.

De Boevre, M., Vanheule, A., Audenaert, K., Bekaert, B., Di Mavungu, J.D., Werbrouck, S., Haesaert, G., and De Saeger, S. (2014). Detached leaf in vitro model for masked mycotoxin biosynthesis and subsequent analysis of unknown conjugates. World Mycotoxin Journal *7*, 305-312.

Dedeurwaerder, G., Ghysselinckx, J., Hellin, P., Janssen, F., Duvivier, M., and Legreve, A. (2014). Detection of *Fusarium langsethiae* on wheat in Belgium. European Journal of Plant Pathology *139*, 453-455.

Desjardins, A.E. (2008). Natural product chemistry meets genetics: When is a genotype a chemotype? Journal of Agricultural and Food Chemistry *56*, 7587-7592.

Desjardins, A.E., McCormick, S.P., and Appell, M. (2007). Structure-activity relationships of trichothecene toxins in an *Arabidopsis thaliana* leaf assay. Journal of Agricultural and Food Chemistry *55*, 6487-6492.

Dhillon, B., Gill, N., Hamelin, R.C., and Goodwin, S.B. (2014). The landscape of transposable elements in the finished genome of the fungal wheat pathogen *Mycosphaerella graminicola*. BMC Genomics *15*, 1132.

Dill-Macky, R., and Jones, R.K. (2000). The effect of previous crop residues and tillage on *Fusarium* head blight of wheat. Plant Disease *84*, 71-76.

Ding, L., Xu, H., Yi, H., Yang, L., Kong, Z., Zhang, L., Xue, S., Jia, H., and Ma, Z. (2011). Resistance to Hemi-Biotrophic *F. graminearum* Infection Is Associated with Coordinated and Ordered Expression of Diverse Defense Signaling Pathways. PLoS One *6*, e19008.

Dinolfo, M.I., Barros, G.G., and Stenglein, S.A. (2012). Development of a PCR assay to detect the potential production of nivalenol in *Fusarium poae*. FEMS Microbiology Letters *332*, 99-104.

Dinolfo, M.I., Castanares, E., and Stenglein, S.A. (2014). Characterization of a *Fusarium poae* world-wide collection by using molecular markers. European Journal of Plant Pathology *140*, 119-132.

Dinolfo, M.I., Stenglein, S.A., Moreno, M.V., Nicholson, P., Jennings, P., and Salerno, G.L. (2010). ISSR markers detect high genetic variation among *Fusarium poae* isolates from Argentina and England. European Journal of Plant Pathology *127*, 483-491.

Divon, H.H., Razzaghian, J., Udnes-Aamot, H., and Klemsdal, S.S. (2012). *Fusarium langsethiae* (Torp and Nirenberg), investigation of alternative infection routes in oats. European Journal of Plant Pathology *132*, 147-161.

Doohan, F.M., Brennan, J., and Cooke, B.M. (2003). Influence of climatic factors on *Fusarium* species pathogenic to cereals. European Journal of Plant Pathology *109*, 755-768.

Doohan, F.M., Parry, D.W., and Nicholson, P. (1999). *Fusarium* ear blight of wheat: the use of quantitative PCR and visual disease assessment in studies of disease control. Plant Pathology *48*, 209-217.

E

Edwards, S.G. (2009a). *Fusarium* mycotoxin content of UK organic and conventional barley. Food Additives and Contaminants Part a-Chemistry Analysis Control Exposure & Risk Assessment *26*, 1185-1190.

Edwards, S.G. (2009b). *Fusarium* mycotoxin content of UK organic and conventional oats. Food Additives and Contaminants Part a-Chemistry Analysis Control Exposure & Risk Assessment *26*, 1063-1069.

Edwards, S.G. (2009c). *Fusarium* mycotoxin content of UK organic and conventional wheat. Food Additives and Contaminants Part a-Chemistry Analysis Control Exposure & Risk Assessment *26*, 496-506.

Edwards, S.G. (2011). Zearalenone risk in European wheat. World Mycotoxin Journal *4*, 433-438.

Edwards, S.G., Imathiu, S.M., Ray, R.V., Back, M., and Hare, M.C. (2012). Molecular studies to identify the *Fusarium* species responsible for HT-2 and T-2 mycotoxins in UK oats. International Journal of Food Microbiology *156*, 168-175.

EFSA CONTAM Panel (EFSA Panel on Contaminants in the Food Chain), 2011a. Scientific Opinion on the risks for public health related to the presence of zearalenone in food. EFSA Journal 2011, *9*, 2197.

EFSA CONTAM Panel (EFSA Panel on Contaminants in the Food Chain), 2011b. Scientific Opinion on the risks for animal and public health related to the presence of T-2 and HT-2 toxin in food and feed. EFSA Journal 2011, *9*, 2481.

EFSA CONTAM Panel (EFSA Panel on Contaminants in the Food Chain), 2013. Scientific Opinion on risks for animal and public health related to the presence of nivalenol in food and feed. EFSA Journal 2013, *11*, 3262.

EFSA CONTAM Panel (EFSA Panel on Contaminants in the Food Chain), 2014. Scientific Opinion on the risks to human and animal health related to the presence of beauvericin and enniatins in food and feed. EFSA Journal 2014, *12*, 3802.

Eudes, F., Comeau, A., Rioux, S., and Collin, J. (2000). Phytotoxicity of eight mycotoxins associated with *Fusarium* in wheat head blight. Canadian Journal of Plant Pathology-Revue Canadienne De Phytopathologie *22*, 286-292.

European Commission (2006a). Commission Regulation (EC) No 1881/2006 of 19 December 2006 setting maximum levels for certain contaminants in foodstuffs. Official Journal of the Union, *L364*, 5-24.

European Commission (2006b). Commission Recommendation 2006/576/EC of 17/08/2006 on the presence of deoxynivalenol, zearalenone, ochratoxin A, T-2 and HT-2 and fumonisins in products intended for animal feeding. Official Journal of the European Union, *L229*, 7-9.

European Commission (2006c). Commission Regulation (EC) No 401/2006 of 23/02/2006 laying down the methods of sampling and analysis for the official control of the levels of mycotoxins in foodstuffs. Official Journal of the European Communities, *L70*, 12-34.

European Commission (2013). Commission Recommendation 2013/165/EC of 27/03/2013 on the presence of T-2 and HT-2 in cereals and cereal products. Official Journal of the European Union, *L91*, 12-15.

F

Fan, J.R., Urban, M., Parker, J.E., Brewer, H.C., Kelly, S.L., Hammond-Kosack, K.E., Fraaije, B.A., Liu, X.L., and Cools, H.J. (2013). Characterization of the sterol 14 alpha-demethylases of *Fusarium graminearum* identifies a novel genus-specific CYP51 function. New Phytologist *198*, 821-835.

Fekete, C., Giczey, G., Papp, I., Szabo, L., and Hornok, L. (1995). High frequencey occurrence of virus-like particles with double stranded RNA genome in *Fusarium poae*. FEMS Microbiology Letters *131*, 295-299.

Fekete, C., and Hornok, L. (1997). A repetitive DNA sequence associated with karyotype variability in *Fusarium poae*. Acta Phytopathologica et Entomologica Hungarica *32*, 29-38.

Fekete, C., Nagy, R., Debets, A.J., and Hornok, L. (1993). Electrophoretic karyotypes and gene mapping in eight species of the *Fusarium* sections *Arthrosporiella* and *Sporotrichiella*. Current Genetics *24*, 500-504.

Fernandez, M.R., Huber, D., Basnyat, P., and Zentner, R.P. (2008). Impact of agronomic practices on populations of *Fusarium* and other fungi in cereal and noncereal crop residues on the Canadian Prairies. Soil & Tillage Research *100*, 60-71.

Feschotte, C. (2008). Opinion - Transposable elements and the evolution of regulatory networks. Nature Reviews Genetics *9*, 397-405.

Fisher, M.C., Henk, D.A., Briggs, C.J., Brownstein, J.S., Madoff, L.C., McCraw, S.L., and Gurr, S.J. (2012). Emerging fungal threats to animal, plant and ecosystem health. Nature *484*, 186-194.

Fredlund, E., Gidlund, A., Sulyok, M., Borjesson, T., Krska, R., Olsen, M., and Lindblad, M. (2013). Deoxynivalenol and other selected *Fusarium* toxins in Swedish oats - Occurrence and correlation to specific *Fusarium* species. International Journal of Food Microbiology *167*, 276-283.

Freitag, M., Williams, R.L., Kothe, G.O., and Selker, E.U. (2002). A cytosine methyltransferase homologue is essential for repeat-induced point mutation in *Neurospora crassa*. Proceedings of the National Academy of Sciences *99*, 8802-8807.

Fruhmann, P., Mikula, H., Wiesenberger, G., Varga, E., Lumpi, D., Stoeger, B., Haeubl, G., Lemmens, M., Berthiller, F., Krska, R., *et al.* (2014). Isolation and Structure Elucidation of Pentahydroxyscirpene, a Trichothecene *Fusarium* Mycotoxin. Journal of Natural Products *77*, 188-192.

G

Galagan, J.E., Calvo, S.E., Borkovich, K.A., Selker, E.U., Read, N.D., Jaffe, D., FitzHugh, W., Ma, L.J., Smirnov, S., Purcell, S., *et al.* (2003). The genome sequence of the filamentous fungus *Neurospora crassa*. Nature *422*, 859-868.

Galagan, J.E., Calvo, S.E., Cuomo, C., Ma, L.J., Wortman, J.R., Batzoglou, S., Lee, S.I., Basturkmen, M., Spevak, C.C., Clutterbuck, J., *et al.* (2005). Sequencing of *Aspergillus nidulans* and comparative analysis with *A. fumigatus* and *A. oryzae*. Nature *438*, 1105-1115.

Galagan, J.E., and Selker, E.U. (2004). RIP: the evolutionary cost of genome defense. Trends in Genetics *20*, 417-423.

Galazka, J.M., and Freitag, M. (2014). Variability of chromosome structure in pathogenic fungi - of 'ends and odds'. Current Opinion in Microbiology *20*, 19-26.

Gardiner, D.M., Kazan, K., and Manners, J.M. (2009). Nutrient profiling reveals potent inducers of trichothecene biosynthesis in *Fusarium graminearum*. Fungal Genetics and Biology *46*, 604-613.

Gardiner, D.M., Kazan, K., Praud, S., Torney, F.J., Rusu, A., and Manners, J.M. (2010a). Early activation of wheat polyamine biosynthesis during *Fusarium* head blight implicates putrescine as an inducer of trichothecene mycotoxin production. BMC Plant Biology *10*, 289.

Gardiner, D.M., McDonald, M.C., Covarelli, L., Solomon, P.S., Rusu, A.G., Marshall, M., Kazan, K., Chakraborty, S., McDonald, B.A., and Manners, J.M. (2012). Comparative Pathogenomics Reveals Horizontally Acquired Novel Virulence Genes in Fungi Infecting Cereal Hosts. PLoS Pathogens *8*, e1002952.

Gardiner, S.A., Boddu, J., Berthiller, F., Hametner, C., Stupar, R.M., Adam, G., and Muehlbauer, G.J. (2010b). Transcriptome Analysis of the Barley-Deoxynivalenol Interaction: Evidence for a Role of Glutathione in Deoxynivalenol Detoxification. Molecular Plant-Microbe Interactions *23*, 962-976.

Geiser, D.M., Aoki, T., Bacon, C.W., Baker, S.E., Bhattacharyya, M.K., Brandt, M.E., Brown, D.W., Burgess, L.W., Chulze, S., Coleman, J.J., *et al.* (2013). One Fungus, One Name: Defining the Genus *Fusarium* in a Scientifically Robust Way That Preserves Longstanding Use. Phytopathology *103*, 400-408.

Geiser, D.M., Jimenez-Gasco, M.D., Kang, S.C., Makalowska, I., Veeraraghavan, N., Ward, T.J., Zhang, N., Kuldau, G.A., and O'Donnell, K. (2004). *FUSARIUM*-ID v. 1.0: A DNA sequence database for identifying *Fusarium*. European Journal of Plant Pathology *110*, 473-479.

Gerlach, W., and Nirenberg, H. (1982). The genus *Fusarium*--a pictorial atlas. Mitteilungen aus der Biologischen Bundesanstalt fur Land-und Forstwirtschaft, Berlin-Dahlem, Germany. 406p.

Giraud, F., Pasquali, M., El Jarroudi, M., Vrancken, C., Brochot, C., Cocco, E., Hoffmann, L., Delfosse, P., and Bohn, T. (2010). *Fusarium* head blight and associated mycotoxin occurrence on winter wheat in Luxembourg in 2007/2008. Food Additives and Contaminants Part a-Chemistry Analysis Control Exposure & Risk Assessment *27*, 825-835.

Glynn, E., Brennan, J.M., Walsh, E., Feechan, A., and McDonnell, K.P. (2015). The potential of *Miscanthus* to harbour known cereal pathogens. European Journal of Plant Pathology *141*, 35-44.

Godfrey, S.A.C., Lovell, H.C., Mansfield, J.W., Corry, D.S., Jackson, R.W., and Arnold, D.L. (2011). The Stealth Episome: Suppression of Gene Expression on the Excised Genomic Island PPHGI-1 from *Pseudomonas syringae* pv. *phaseolicola*. PLoS Pathogens *7*, e1002010.

Goodwin, S.B., Ben M'Barek, S., Dhillon, B., Wittenberg, A.H.J., Crane, C.F., Hane, J.K., Foster, A.J., Van der Lee, T.A.J., Grimwood, J., Aerts, A., *et al.* (2011). Finished Genome of the Fungal Wheat Pathogen *Mycosphaerella graminicola* Reveals Dispensome Structure, Chromosome Plasticity, and Stealth Pathogenesis. PLoS Genetics *7*, e1002070.

Gordon, W.L. (2006). The occurrence of *Fusarium* species in Canada - I. Species of *Fusarium* isolated from farm samples of cereal seed in Manitoba. Canadian Journal of Plant Pathology-Revue Canadienne De Phytopathologie *28*, S111-S115.

Goswami, R.S., and Kistler, H.C. (2004). Heading for disaster: *Fusarium graminearum* on cereal crops. Molecular Plant Pathology *5*, 515-525.

Grenier, B., and Oswald, I.P. (2011). Mycotoxin co-contamination of food and feed: meta-analysis of publications describing toxicological interactions. World Mycotoxin Journal *4*, 285-313.

Guindon, S., and Gascuel, O. (2003). A simple, fast, and accurate algorithm to estimate large phylogenies by maximum likelihood. Systematic Biology *52*, 696-704.

H

Haas, B.J., Kamoun, S., Zody, M.C., Jiang, R.H.Y., Handsaker, R.E., Cano, L.M., Grabherr, M., Kodira, C.D., Raffaele, S., Torto-Alalibo, T., *et al.* (2009). Genome sequence and analysis of the Irish potato famine pathogen *Phytophthora infestans*. Nature *461*, 393-398.

Haave, R. (1985). Forekomst og patogenitet av *Fusarium* arter pa korn i Norge (As: Agricultural University).

Hane, J.K., and Oliver, R.P. (2008). RIPCAL: a tool for alignment-based analysis of repeat-induced point mutations in fungal genomic sequences. BMC Bioinformatics *9*, 478.

Hansen, F.T., Gardiner, D.M., Lysoe, E., Fuertes, P.R., Tudzynski, B., Wiemann, P., Sondergaard, T.E., Giese, H., Brodersen, D.E., and Sorensen, J.L. (2015). An update to polyketide synthase and non-ribosomal synthetase genes and nomenclature in *Fusarium*. Fungal Genetics and Biology *75*, 20-29.

Hatta, R., Ito, K., Hosaki, Y., Tanaka, T., Tanaka, A., Yamamoto, M., Akimitsu, K., and Tsuge, T. (2002). A conditionally dispensable chromosome controls host-specific pathogenicity in the fungal plant pathogen *Alternaria alternata*. Genetics *161*, 59-70.

Hazkani-Covo, E., Zeller, R.M., and Martin, W. (2010). Molecular Poltergeists: Mitochondrial DNA Copies (numts) in Sequenced Nuclear Genomes. PLoS Genetics *6*, e1000834.

Hoff, K.J., Lange, S., Lomsadze, A., Borodovsky, M., and Stanke, M. (2015). BRAKER1: Unsupervised RNA-Seq-Based Genome Annotation with GeneMark-ET and AUGUSTUS. Bioinformatics, available online pre-print, doi: 10.1093/bioinformatics/btv661.

Hu, J., Chen, C., Peever, T., Dang, H., Lawrence, C., and Mitchell, T. (2012). Genomic characterization of the conditionally dispensable chromosome in *Alternaria arborescens* provides evidence for horizontal gene transfer. BMC Genomics *13*, 171.

Hu, X., Xiao, G., Zheng, P., Shang, Y., Su, Y., Zhang, X., Liu, X., Zhan, S., St Leger, R.J., and Wang, C. (2014). Trajectory and genomic determinants of fungal-pathogen speciation and host adaptation. Proceedings of the National Academy of Sciences of the United States of America *111*, 16796-16801.

Hudec, K., and Rohacik, T. (2003). *Fusarium* spp. and Microdochium nivale infestation of asymptomatic wheat kernels in Slovakia. Cereal Research Communications *31*, 415-420.

Hudec, K., and Rohacik, T. (2009). The Occurrence and Predominance of *Fusarium* Species on Barley Kernels in Slovakia. Cereal Research Communications *37*, 101-109.

I

Imathiu, S.M., Edwards, S.G., Ray, R.V., and Back, M.A. (2013). *Fusarium langsethiae* - a HT-2 and T-2 Toxins Producer that Needs More Attention. Journal of Phytopathology *161*, 1-10.

Imathiu, S.M., Ray, R.V., Back, M., Hare, M.C., and Edwards, S.G. (2009). *Fusarium langsethiae* pathogenicity and aggressiveness towards oats and wheat in wounded and unwounded in vitro detached leaf assays. European Journal of Plant Pathology *124*, 117-126.

Ioos, R., Belhadj, A., and Menez, M. (2004). Occurrence and distribution of *Microdochium nivale* and *Fusarium* species isolated from barley, durum and soft wheat grains in France from 2000 to 2002. Mycopathologia *158*, 351-362.

J

Jansen, C., von Wettstein, D., Schafer, W., Kogel, K.H., Felk, A., and Maier, F.J. (2005). Infection patterns in barley and wheat spikes inoculated with wild-type and trichodiene synthase gene disrupted

Fusarium graminearum. Proceedings of the National Academy of Sciences of the United States of America *102*, 16892-16897.

Jenkinson, P., and Parry, D.W. (1994). Isolation of *Fusarium* species from common broad-leaved weeds and their pathogenicity to winter-wheat. Mycological Research *98*, 776-780.

Jestoi, M. (2008). Emerging *Fusarium*-mycotoxins fusaproliferin, beauvericin, enniatins, and moniliformin—A review. Critical reviews in food science and nutrition *48*, 21-49.

Joffe, A. (1974). Toxicity of *Fusarium poae* and *F. sporotrichioides* and its relation to alimentary toxic aleukia. Mycotoxins, 229-262.

Jones, N., and Houben, A. (2003). B chromosomes in plants: escapees from the A chromosome genome? Trends in Plant Science *8*, 417-423.

Jones, R.N. (1995). Tansley review no 85 - B chromosomes in plants. New Phytologist *131*, 411-434.

Junier, T., and Zdobnov, E.M. (2010). The Newick utilities: high-throughput phylogenetic tree processing in the Unix shell. Bioinformatics *26*, 1669-1670.

K

Kasuga, T., White, T.J., and Taylor, J.W. (2002). Estimation of nucleotide substitution rates in eurotiomycete fungi. Molecular Biology and Evolution *19*, 2318-2324.

Kazan, K., Gardiner, D.M., and Manners, J.M. (2012). On the trail of a cereal killer: recent advances in *Fusarium graminearum* pathogenomics and host resistance. Molecular Plant Pathology *13*, 399-413.

Keller, N.P., Turner, G., and Bennett, J.W. (2005). Fungal secondary metabolism - From biochemistry to genomics. Nature Reviews Microbiology *3*, 937-947.

Kelley, L.A., Mezulis, S., Yates, C.M., Wass, M.N., and Sternberg, M.J.E. (2015). The Phyre2 web portal for protein modeling, prediction and analysis. Nature Protocols *10*, 845-858.

Kelly, A., Clear, R.M., O'Donnell, K., McCormick, S., Turkington, K., Tekauz, A., Gilbert, J., Kistler, H., Busman, M., and Ward, T. (2015). Diversity of *Fusarium* head blight populations and trichothecene toxin types reveals regional differences in pathogen composition and temporal dynamics. Fungal Genetics and Biology *82*, 22-31.

Kema, G.H., and Weise, S. (2013). Pathogens: Appeal for funds to fight banana blight. Nature *504*, 218-218.

Kerenyi, Z., Moretti, A., Waalwijk, C., Olah, B., and Hornok, L. (2004). Mating type sequences in asexually reproducing *Fusarium* species. Applied and Environmental Microbiology *70*, 4419-4423.

Kerenyi, Z., Taborhegyi, E., Pomazi, A., and Hornok, L. (1997). Variability amongst strains of *Fusarium poae* assessed by vegetative compatibility and RAPD polymorphism. Plant Pathology *46*, 882-889.

Kim, D., Pertea, G., Trapnell, C., Pimentel, H., Kelley, R., and Salzberg, S.L. (2013). TopHat2: accurate alignment of transcriptomes in the presence of insertions, deletions and gene fusions. Genome Biology *14*, R36.

Kimura, M., Kaneko, I., Komiyama, M., Takatsuki, A., Koshino, H., Yoneyama, K., and Yamaguchi, I. (1998). Trichothecene 3-O-acetyltransferase protects both the producing organism and transformed yeast from related mycotoxins - Cloning and characterization of *Tri101*. Journal of Biological Chemistry *273*, 1654-1661.

Kimura, M., Tokai, T., Takahashi-Ando, N., Ohsato, S., and Fujimura, M. (2007). Molecular and genetic studies of *Fusarium* trichothecene biosynthesis: Pathways, genes, and evolution. Bioscience Biotechnology and Biochemistry *71*, 2105-2123.

King, R., Urban, M., Hammond-Kosack, M.C., Hassani-Pak, K., and Hammond-Kosack, K.E. (2015). The completed genome sequence of the pathogenic ascomycete fungus *Fusarium graminearum*. BMC Genomics *16*, 544.

Knutsen, A.K., Torp, M., and Holst-Jensen, A. (2004). Phylogenetic analyses of the *Fusarium poae*, *Fusarium sporotrichioides* and *Fusarium langsethiae* species complex based on partial sequences of the translation elongation factor-1 alpha gene. International Journal of Food Microbiology *95*, 287-295.

Kokkonen, M., Magan, N., and Medina, A. (2014). Comparative effects of fungicides and environmental factors on growth and T-2+HT-2 toxin production by *Fusarium sporotrichioides* and *Fusarium langsethiae* strains on an oat-based matrix. World Mycotoxin Journal *7*, 177-186.

Koren, S., and Phillippy, A.M. (2015). One chromosome, one contig: complete microbial genomes from long-read sequencing and assembly. Current Opinion in Microbiology *23*, 110-120.

Kosiak, B., Torp, M., Skjerve, E., and Andersen, B. (2004). *Alternaria* and *Fusarium* in Norwegian grains of reduced quality - a matched pair sample study. International Journal of Food Microbiology *93*, 51-62.

Kosiak, B., Torp, M., Skjerve, E., and Thrane, U. (2003). The prevalence and distribution of *Fusarium* species in Norwegian cereals: a survey. Acta Agriculturae Scandinavica Section B-Soil and Plant Science *53*, 168-176.

Kristensen, R., Torp, M., Kosiak, B., and Holst-Jensen, A. (2005). Phylogeny and toxigenic potential is correlated in *Fusarium* species as revealed by partial translation elongation factor 1 alpha gene sequences. Mycological Research *109*, 173-186.

Krzywinski, M., Schein, J., Birol, I., Connors, J., Gascoyne, R., Horsman, D., Jones, S.J., and Marra, M.A. (2009). Circos: An information aesthetic for comparative genomics. Genome Research *19*, 1639-1645.

Kulik, T., and Jestoi, M. (2009). Quantification of *Fusarium poae* DNA and associated mycotoxins in asymptomatically contaminated wheat. International Journal of Food Microbiology *130*, 233-237.

Kulik, T., and Pszczolkowska, A. (2011). Multilocus sequence analysis of *Fusarium poae*. Journal of Plant Pathology *93*, 119-126.

Kurtz, S., Phillippy, A., Delcher, A.L., Smoot, M., Shumway, M., Antonescu, C., and Salzberg, S.L. (2004). Versatile and open software for comparing large genomes. Genome Biology *5*, R12.

Kvas, M., Marasas, W.F.O., Wingfield, B.D., Wingfield, M.J., and Steenkamp, E.T. (2009). Diversity and evolution of *Fusarium* species in the *Gibberella fujikuroi* complex. Fungal Diversity *34*, 1-21.

L

Landschoot, S. (2012). Prediction of *Fusarium* head blight and deoxynivalenol content in winter wheat with regression-based learning algorithms. PhD thesis, Ghent University.

Landschoot, S., Audenaert, K., Waegeman, W., Pycke, B., Bekaert, B., De Baets, B., and Haesaert, G. (2011). Connection between primary *Fusarium* inoculum on gramineous weeds, crop residues and soil samples and the final population on wheat ears in Flanders, Belgium. Crop Protection *30*, 1297-1305.

Landschoot, S., Waegeman, W., Audenaert, K., Vandepitte, J., Baetens, J.M., De Baets, B., and Haesaert, G. (2012). An empirical analysis of explanatory variables affecting *Fusarium* head blight infection and deoxynivalenol content in wheat. Journal of Plant Pathology *94*, 135-147.

Landschoot, S., Waegeman, W., Audenaert, K., Van Damme, P., Vandepitte, J., De Baets, B., and Haesaert, G. (2013). A field-specific web tool for the prediction of *Fusarium* head blight and deoxynivalenol content in Belgium. Computers and Electronics in Agriculture *93*, 140-148.

Larkin, M.A., Blackshields, G., Brown, N.P., Chenna, R., McGettigan, P.A., McWilliam, H., Valentin, F., Wallace, I.M., Wilm, A., Lopez, R., *et al.* (2007). Clustal W and clustal X version 2.0. Bioinformatics *23*, 2947-2948.

Lazzaro, I., Moretti, A., Giorni, P., Brera, C., and Battilani, P. (2015). Organic vs conventional farming: Differences in infection by mycotoxin-producing fungi on maize and wheat in Northern and Central Italy. Crop Protection *72*, 22-30.

Lee, T., Han, Y.K., Kim, K.H., Yun, S.H., and Lee, Y.W. (2002). *Tri13* and *Tri7* determine deoxynivalenol- and nivalenol-producing chemotypes of *Gibberella zeae*. Applied and Environmental Microbiology *68*, 2148-2154.

Lemmens, M., Haim, K., Lew, H., and Ruckenbauer, P. (2004). The effect of nitrogen fertilization on *Fusarium* head blight development and deoxynivalenol contamination in wheat. Journal of Phytopathology *152*, 1-8.

Leroux, P., Albertini, C., Gautier, A., Gredt, M., and Walker, A.S. (2007). Mutations in the CYP51 gene correlated with changes in sensitivity to sterol 14α-demethylation inhibitors in field isolates of *Mycosphaerella graminicola*. Pest Management Science *63*, 688-698.

Leslie, J.F. (1991). Mating populations in *Gibberella fujikuroi* (*Fusarium* section *Liseola*). Phytopathology *81*, 1058-1060.

Li, H., Handsaker, B., Wysoker, A., Fennell, T., Ruan, J., Homer, N., Marth, G., Abecasis, G., Durbin, R., and Genome Project Data, P. (2009). The Sequence Alignment/Map format and SAMtools. Bioinformatics *25*, 2078-2079.

Li, Y., van der Lee, T.A.J., Evenhuis, A., van den Bosch, G.B.M., van Bekkum, P.J., Forch, M.G., van Gent-Pelzer, M.P.E., van Raaij, H.M.G., Jacobsen, E., Huang, S.W., *et al.* (2012). Population Dynamics of *Phytophthora infestans* in the Netherlands Reveals Expansion and Spread of Dominant Clonal Lineages and Virulence in Sexual Offspring. G3-Genes Genomes Genetics *2*, 1529-1540.

Li, Y.S., Wang, Z.H., Beier, R.C., Shen, J.Z., De Smet, D., De Saeger, S., and Zhang, S.X. (2011). T-2 Toxin, a Trichothecene Mycotoxin: Review of Toxicity, Metabolism, and Analytical Methods. Journal of Agricultural and Food Chemistry *59*, 3441-3453.

Liang, J., Lofgren, L., Ma, Z., Ward, T.J., and Kistler, H. (2015). Population subdivision of *Fusarium graminearum* from barley and wheat in the upper Midwestern United States at the turn of the century. Phytopathology *105*, 1466-1474.

Liang, J.M., Xayamongkhon, H., Broz, K., Dong, Y., McCormick, S.P., Abramova, S., Ward, T.J., Ma, Z.H., and Kistler, H.C. (2014). Temporal dynamics and population genetic structure of *Fusarium graminearum* in the upper Midwestern United States. Fungal Genetics and Biology *73*, 83-92.

Lindblad, M., Gidlund, A., Sulyok, M., Borjesson, T., Krska, R., Olsen, M., and Fredlund, E. (2013). Deoxynivalenol and other selected *Fusarium* toxins in Swedish wheat - Occurrence and correlation to specific *Fusarium* species. International Journal of Food Microbiology *167*, 284-291.

Liu, W.Z., and Sundheim, L. (1996). Nitrate nonutilizing mutants and vegetative compatibility groups in *Fusarium poae*. Fungal Genetics and Biology *20*, 12-17.

Liu, W.Z., Sundheim, L., and Langseth, W. (1998). Trichothecene production and the relationship to vegetative compatibility groups in *Fusarium poae*. Mycopathologia *140*, 105-114.

Logrieco, A., Mule, G., Moretti, A., and Bottalico, A. (2002). Toxigenic *Fusarium* species and mycotoxins associated with maize ear rot in Europe. European Journal of Plant Pathology *108*, 597-609.

Lukashin, A.V., and Borodovsky, M. (1998). GeneMark.hmm: new solutions for gene finding. Nucleic Acids Research *26*, 1107-1115.

Lynch, M., Bürger, R., Butcher, D., and Gabriel, W. (1993). The mutational meltdown in asexual populations. Journal of Heredity *84*, 339-344.

Lysoe, E., Divon, H.H., Terzi, V., Orrù, L., Lamontanara, A., Kolseth, A.-K., Frandsen, R.J.N., Nielsen, K.F., and Thrane, U. (2015). The draft genome of *Fusarium langsethiae*, a T-2/HT-2 mycotoxin producer. Paper presented at: 13th European *Fusarium* Seminar (Martina Franca, Italy).

Lysoe, E., Harris, L.J., Walkowiak, S., Subramaniam, R., Divon, H.H., Riiser, E.S., Llorens, C., Gabaldon, T., Kistler, H.C., Jonkers, W., *et al.* (2014). The Genome of the Generalist Plant Pathogen *Fusarium avenaceum* Is Enriched with Genes Involved in Redox, Signaling and Secondary Metabolism. PLoS One *9*, e112703.

Lysoe, E., Seong, K.-Y., and Kistler, H.C. (2011). The Transcriptome of *Fusarium graminearum* During the Infection of Wheat. Molecular Plant-Microbe Interactions *24*, 995-1000.

M

Ma, L.-J., Geiser, D.M., Proctor, R.H., Rooney, A.P., O'Donnell, K., Trail, F., Gardiner, D.M., Manners, J.M., and Kazan, K. (2013). *Fusarium* Pathogenomics. Annual Review of Microbiology *67*, 399-416.

Ma, L.-J., van der Does, H.C., Borkovich, K.A., Coleman, J.J., Daboussi, M.-J., Di Pietro, A., Dufresne, M., Freitag, M., Grabherr, M., Henrissat, B., *et al.* (2010). Comparative genomics reveals mobile pathogenicity chromosomes in *Fusarium*. Nature *464*, 367-373.

Madgwick, J.W., West, J.S., White, R.P., Semenov, M.A., Townsend, J.A., Turner, J.A., and Fitt, B.D.L. (2011). Impacts of climate change on wheat anthesis and *Fusarium* ear blight in the UK. European Journal of Plant Pathology *130*, 117-131.

Maier, F.J., Miedaner, T., Hadeler, B., Felk, A., Salomon, S., Lemmens, M., Kassner, H., and Schafer, W. (2006). Involvement of trichothecenes in fusarioses of wheat, barley and maize evaluated by gene disruption of the trichodiene synthase (Tri5) gene in three field isolates of different chemotype and virulence. Molecular Plant Pathology *7*, 449-461.

Manning, V.A., Pandelova, I., Dhillon, B., Wilhelm, L.J., Goodwin, S.B., Berlin, A.M., Figueroa, M., Freitag, M., Hane, J.K., Henrissat, B., *et al.* (2013). Comparative Genomics of a Plant-Pathogenic Fungus, *Pyrenophora tritici-repentis*, Reveals Transduplication and the Impact of Repeat Elements on Pathogenicity and Population Divergence. G3-Genes Genomes Genetics *3*, 41-63.

Manstretta, V., Gourdain, E., and Rossi, V. (2015). Deposition patterns of *Fusarium graminearum* ascospores and conidia within a wheat canopy. European Journal of Plant Pathology *143*, 873-880.

Marin, P., Moretti, A., Ritieni, A., Jurado, M., Vazquez, C., and Teresa Gonzalez-Jaen, M. (2012). Phylogenetic analyses and toxigenic profiles of *Fusarium equiseti* and *Fusarium acuminatum* isolated from cereals from Southern Europe. Food Microbiology *31*, 229-237.

Mateo, E.M., Valle-Algarra, F.M., Jimenez, M., and Magan, N. (2013). Impact of three sterol-biosynthesis inhibitors on growth of *Fusarium langsethiae* and on T-2 and HT-2 toxin production in oat grain under different ecological conditions. Food Control *34*, 521-529.

McCormick, S.P., Alexander, N.J., and Proctor, R.H. (2006). Heterologous expression of two trichothecene P450 genes in *Fusarium verticillioides*. Canadian Journal of Microbiology *52*, 220-226.

McCormick, S.P., Harris, L.J., Alexander, N.J., Ouellet, T., Saparno, A., Allard, S., and Desjardins, A.E. (2004). Tri1 in *Fusarium graminearum* encodes a P450 oxygenase. Applied and Environmental Microbiology *70*, 2044-2051.

McCormick, S.P., Stanley, A.M., Stover, N.A., and Alexander, N.J. (2011). Trichothecenes: From Simple to Complex Mycotoxins. Toxins *3*, 802-814.

McDonald, B.A., and Linde, C. (2002). Pathogen population genetics, evolutionary potential, and durable resistance. Annual Review of Phytopathology *40*, 349-379.

McMullen, M., Bergstrom, G., De Wolf, E., Dill-Macky, R., Hershman, D., Shaner, G., and Van Sanford, D. (2012). A Unified Effort to Fight an Enemy of Wheat and Barley: *Fusarium* Head Blight. Plant Disease *96*, 1712-1728.

Meek, I.B., Peplow, A.W., Ake, C., Phillips, T.D., and Beremand, M.N. (2003). *Tri1* encodes the cytochrome P450 monooxygenase for C-8 hydroxylation during trichothecene biosynthesis in *Fusarium sporotrichioides* and resides upstream of another new *Tri* gene. Applied and Environmental Microbiology *69*, 1607-1613.

Mehrabi, R., Bahkali, A.H., Abd-Elsalam, K.A., Moslem, M., Ben M'Barek, S., Gohari, A.M., Jashni, M.K., Stergiopoulos, I., Kema, G.H.J., and de Wit, P.J.G.M. (2011). Horizontal gene and chromosome transfer in plant pathogenic fungi affecting host range. FEMS Microbiology Reviews *35*, 542-554.

Menke, J., Dong, Y., and Kistler, H.C. (2012). *Fusarium graminearum* Tri12p Influences Virulence to Wheat and Trichothecene Accumulation. Molecular Plant-Microbe Interactions *25*, 1408-1418.

Mesterhazy, A. (1995). Types and components of resistance to *Fusarium* head blight of wheat. Plant Breeding *114*, 377-386.

Mestres, J. (2005). Structure conservation in cytochromes P450. Proteins-Structure Function and Bioinformatics *58*, 596-609.

Michielse, C.B., and Rep, M. (2009). Pathogen profile update: *Fusarium oxysporum*. Molecular Plant Pathology *10*, 311-324.

Mitchell, L.A., and Boeke, J.D. (2014). Circular permutation of a synthetic eukaryotic chromosome with the telomerator. Proceedings of the National Academy of Sciences of the United States of America *111*, 17003-17010.

Monk, B.C., Tomasiak, T.M., Keniya, M.V., Huschmann, F.U., Tyndall, J.D.A., O'Connell, J.D., III, Cannon, R.D., McDonald, J.G., Rodriguez, A., Finer-Moore, J.S., *et al.* (2014). Architecture of a single membrane spanning cytochrome P450 suggests constraints that orient the catalytic domain relative to a bilayer. Proceedings of the National Academy of Sciences of the United States of America *111*, 3865-3870.

Morton, V., and Staub, T. (2008). A short history of fungicides. Online, APSnet Features. doi: 10.1094/APSnetFeature-2008-0308.

Mueller, U.G., and Wolfenbarger, L.L. (1999). AFLP genotyping and fingerprinting. Trends in Ecology & Evolution *14*, 389-394.

Mullenborn, C., Steiner, U., Ludwig, M., and Oerke, E.C. (2008). Effect of fungicides on the complex of *Fusarium* species and saprophytic fungi colonizing wheat kernels. European Journal of Plant Pathology *120*, 157-166.

Müller, M.E., and Korn, U. (2013). *Alternaria* mycotoxins in wheat–A 10 years survey in the Northeast of Germany. Food Control *34*, 191-197.

N

Nakagawa, H., Ohmichi, K., Sakamoto, S., Sago, Y., Kushiro, M., Nagashima, H., Yoshida, M., and Nakajima, T. (2011). Detection of a new *Fusarium* masked mycotoxin in wheat grain by high-resolution LC-Orbitrap (TM) MS. Food Additives and Contaminants Part a-Chemistry Analysis Control Exposure & Risk Assessment *28*, 1447-1456.

Nakagawa, H., Sakamoto, S., Sago, Y., Kushiro, M., and Nagashima, H. (2013). Detection of masked mycotoxins derived from type A trichothecenes in corn by high-resolution LC-Orbitrap mass spectrometer. Food Additives and Contaminants Part a-Chemistry Analysis Control Exposure & Risk Assessment *30*, 1407-1414.

Namiki, F., Matsunaga, M., Okuda, M., Inoue, I., Nishi, K., Fujita, Y., and Tsuge, T. (2001). Mutation of an arginine biosynthesis gene causes reduced pathogenicity in *Fusarium oxysporum* f. sp *melonis*. Molecular Plant-Microbe Interactions *14*, 580-584.

Nazari, L., Pattori, E., Terzi, V., Morcia, C., and Rossi, V. (2014). Influence of temperature on infection, growth, and mycotoxin production by *Fusarium langsethiae* and *F. sporotrichioides* in durum wheat. Food Microbiology *39*, 19-26.

Neiman, A.M. (2005). Ascospore formation in the yeast *Saccharomyces cerevisiae*. Microbiology and Molecular Biology Reviews *69*, 565-584.

Nganje, W.E., Bangsund, D.A., Leistritz, F.L., Wilson, W.W., and Tiapo, N.M. (2004). Regional economic impacts of *Fusarium* head blight in wheat and barley. Applied Economic Perspectives and Policy *26*, 332-347.

Nicolaisen, M., Supronien, S., Nielsen, L.K., Lazzaro, I., Spliid, N.H., and Justesen, A.F. (2009). Real-time PCR for quantification of eleven individual *Fusarium* species in cereals. Journal of Microbiological Methods *76*, 234-240.

Nielsen, L.K., Cook, D.J., Edwards, S.G., and Ray, R.V. (2014). The prevalence and impact of *Fusarium* head blight pathogens and mycotoxins on malting barley quality in UK. International Journal of Food Microbiology *179*, 38-49.

Nor, N.M.I.M. (2014). Genetics of Southeast Asian populations and interspecific hybrids of *Fusarium* spp. PhD thesis, Kansas State University.

Nucci, M., and Anaissie, E. (2007). *Fusarium* infections in immunocompromised patients. Clinical Microbiology Reviews *20*, 695-704.

Nur, U., Werren, J.H., Eickbush, D.G., Burke, W.D., and Eickbush, T.H. (1988). A selfish B-chromosome that enhances its transmission by eliminating the paternal genome. Science *240*, 512-514.

O

O'Donnell, K., Rooney, A.P., Proctor, R.H., Brown, D.W., McCormick, S.P., Ward, T.J., Frandsen, R.J.N., Lysoe, E., Rehner, S.A., Aoki, T., *et al.* (2013). Phylogenetic analyses of RPB1 and RPB2

support a middle Cretaceous origin for a clade comprising all agriculturally and medically important fusaria. Fungal Genetics and Biology *52*, 20-31.

O'Donnell, K., Ward, T.J., Aberra, D., Kistler, H.C., Aoki, T., Orwig, N., Kimura, M., Bjornstad, A., and Klemsdal, S.S. (2008). Multilocus genotyping and molecular phylogenetics resolve a novel head blight pathogen within the *Fusarium graminearum* species complex from Ethiopia. Fungal Genetics and Biology *45*, 1514-1522.

O'Donnell, K., Ward, T.J., Geiser, D.M., Kistler, H.C., and Aoki, T. (2004). Genealogical concordance between the mating type locus and seven other nuclear genes supports formal recognition of nine phylogenetically distinct species within the *Fusarium graminearum* clade. Fungal Genetics and Biology *41*, 600-623.

Oerke, E.-C. (2006). Crop losses to pests. The Journal of Agricultural Science *144*, 31-43.

Opoku, N., Back, M., and Edwards, S.G. (2013). Development of *Fusarium langsethiae* in commercial cereal production. European Journal of Plant Pathology *136*, 159-170.

P

Paoletti, M., Rydholm, C., Schwier, E.U., Anderson, M.J., Szakacs, G., Lutzoni, F., Debeaupuis, J.P., Latge, J.P., Denning, D.W., and Dyer, P.S. (2005). Evidence for sexuality in the opportunistic fungal pathogen *Aspergillus fumigatus*. Current Biology *15*, 1242-1248.

Parikka, P., Hakala, K., and Tiilikkala, K. (2012). Expected shifts in *Fusarium* species' composition on cereal grain in Northern Europe due to climatic change. Food Additives and Contaminants Part a-Chemistry Analysis Control Exposure & Risk Assessment *29*, 1543-1555.

Parry, D.W., Jenkinson, P., and McLeod, L. (1995). *Fusarium* ear blight (Scab) in small-grain cereals - a review. Plant Pathology *44*, 207-238.

Parry, D.W., and Nicholson, P. (1996). Development of a PCR assay to detect *Fusarium poae* in wheat. Plant Pathology *45*, 383-391.

Pasquali, M., and Migheli, Q. (2014). Genetic approaches to chemotype determination in type B-trichothecene producing Fusaria. International Journal of Food Microbiology *189*, 164-182.

Peplow, A.W., Meek, I.B., Wiles, M.C., Phillips, T.D., and Beremand, M.N. (2003). Tri16 is required for esterification of position C-8 during trichothecene mycotoxin production by *Fusarium sporotrichioides*. Applied and Environmental Microbiology *69*, 5935-5940.

Pereyra, S.A., and Dill-Macky, R. (2008). Colonization of the residues of diverse plant species by Gibberella zeae and their contribution to *Fusarium* head blight inoculum. Plant Disease *92*, 800-807.

Pitt, J. (2000). Toxigenic fungi: which are important? Medical Mycology *38*, 17-22.

Placinta, C., D'mello, J., and Macdonald, A. (1999). A review of worldwide contamination of cereal grains and animal feed with *Fusarium* mycotoxins. Animal Feed Science and Technology *78*, 21-37.

Plotree, D., and Plotgram, D. (1989). PHYLIP-phylogeny inference package (version 3.2). cladistics *5*, 163-166.

Polley, R.W., and Turner, J.A. (1995). Surveys of stem base diseases and *Fusarium* ear diseases in winter-wheat in England, Wales and Scotland, 1989-1990. Annals of Applied Biology *126*, 45-59.

Pomraning, K. (2012). Characterization of *Neurospora crassa* and *Fusarium graminearum* Mutants Defective in Repeat-induced Point Mutation. PhD thesis, Oregon State University.

Pritsch, C., Muehlbauer, G.J., Bushnell, W.R., Somers, D.A., and Vance, C.P. (2000). Fungal development and induction of defense response genes during early infection of wheat spikes by *Fusarium graminearum*. Molecular Plant-Microbe Interactions *13*, 159-169.

Proctor, R.H., McCormick, S.P., Alexander, N.J., and Desjardins, A.E. (2009). Evidence that a secondary metabolic biosynthetic gene cluster has grown by gene relocation during evolution of the filamentous fungus *Fusarium*. Molecular Microbiology *74*, 1128-1142.

Punt, P.J., Oliver, R.P., Dingemanse, M.A., Pouwels, P.H., and Vandenhondel, C. (1987). Transformation of *Aspergillus* based on the hygromycin-B resistance marker from *Escherichia coli*. Gene *56*, 117-124.

Q

Quarta, A., Mita, G., Haidukowski, M., Santino, A., Mule, G., and Visconti, A. (2005). Assessment of trichothecene chemotypes of *Fusarium culmorum* occurring in Europe. Food Additives and Contaminants *22*, 309-315.

Quinlan, A.R., and Hall, I.M. (2010). BEDTools: a flexible suite of utilities for comparing genomic features. Bioinformatics *26*, 841-842.

R

R Core Team (2012). R: A language and environment for statistical computing. R Foundation for Statistical Computing, Vienna, Austria. http://www.R-project.org/.

Reverberi, M., Ricelli, A., Zjalic, S., Fabbri, A.A., and Fanelli, C. (2010). Natural functions of mycotoxins and control of their biosynthesis in fungi. Applied Microbiology and Biotechnology *87*, 899-911.

Ropars, J., Dupont, J., Fontanillas, E., de la Vega, R.C.R., Malagnac, F., Coton, M., Giraud, T., and Lopez-Villavicencio, M. (2012). Sex in Cheese: Evidence for Sexuality in the Fungus *Penicillium roqueforti*. PLoS One *7*, e49665.

Rouxel, T., Grandaubert, J., Hane, J.K., Hoede, C., van de Wouw, A.P., Couloux, A., Dominguez, V., Anthouard, V., Bally, P., Bourras, S., *et al.* (2011). Effector diversification within compartments of the *Leptosphaeria maculans* genome affected by Repeat-Induced Point mutations. Nature Communications *2*, 202.

S

Saleh, D., Xu, P., Shen, Y., Li, C., Adreit, H., Milazzo, J., Ravigne, V., Bazin, E., Notteghem, J.-L., Fournier, E., *et al.* (2012). Sex at the origin: an Asian population of the rice blast fungus *Magnaporthe oryzae* reproduces sexually. Molecular Ecology *21*, 1330-1344.

Sarver, B.A.J., Ward, T.J., Gale, L.R., Broz, K., Kistler, H.C., Aoki, T., Nicholson, P., Carter, J., and O'Donnell, K. (2011). Novel *Fusarium* head blight pathogens from Nepal and Louisiana revealed by multilocus genealogical concordance. Fungal Genetics and Biology *48*, 1096-1107.

Scauflaire, J., Gourgue, M., and Munaut, F. (2011). *Fusarium temperatum* sp nov from maize, an emergent species closely related to *Fusarium subglutinans*. Mycologia *103*, 586-597.

Scherm, B., Balmas, V., Spanu, F., Pani, G., Delogu, G., Pasquali, M., and Migheli, Q. (2013). *Fusarium culmorum*: causal agent of foot and root rot and head blight on wheat. Molecular Plant Pathology *14*, 323-341.

Schmidt, H., Adler, A., Holst-Jensen, A., Klemsdal, S.S., Logrieco, A., Mach, R.L., Nirenberg, H.I., Thrane, U., Torp, M., Vogel, R.F., *et al.* (2004a). An integrated taxonomic study of *Fusarium langsethiae*, *Fusarium poae* and *Fusarium sporotrichioides* based on the use of composite datasets. International Journal of Food Microbiology *95*, 341-349.

Schmidt, H., Niessen, L., and Vogel, R.F. (2004b). AFLP analysis of *Fusarium* species in the section Sporotrichiella - evidence for *Fusarium langsethiae* as a new species. International Journal of Food Microbiology *95*, 297-304.

Schollenberger, M., Drochner, W., and Mueller, H.-M. (2007). *Fusarium* toxins of the scirpentriol subgroup: a review. Mycopathologia *164*, 101-118.

Schollenberger, M., Mueller, H.-M., Liebscher, M., Schlecker, C., Berger, M., and Hermann, W. (2011). Accumulation Kinetics of Three Scirpentriol-Based Toxins in Oats Inoculated in Vitro with Isolates of *Fusarium sporotrichioides* and *Fusarium poae*. Toxins *3*, 442-452.

Segers, G.C., Zhang, X., Deng, F., Sun, Q., and Nuss, D.L. (2007). Evidence that RNA silencing functions as an antiviral defense mechanism in fungi. Proceedings of the National Academy of Sciences of the United States of America *104*, 12902-12906.

Seifi, H.S., Van Bockhaven, J., Angenon, G., and Höfte, M. (2013). Glutamate metabolism in plant disease and defense: friend or foe? Molecular Plant-Microbe Interactions *26*, 475-485.

Seong, K.-Y., Pasquali, M., Zhou, X., Song, J., Hilburn, K., McCormick, S., Dong, Y., Xu, J.-R., and Kistler, H.C. (2009). Global gene regulation by *Fusarium* transcription factors *Tri6* and *Tri10* reveals adaptations for toxin biosynthesis. Molecular Microbiology *72*, 354-367.

Shewry, P.R. (2009). Wheat. Journal of Experimental Botany *60*, 1537-1553.

Sieber, C.M.K., Lee, W., Wong, P., Muensterkoetter, M., Mewes, H.-W., Schmeitzl, C., Varga, E., Berthiller, F., Adam, G., and Gueldener, U. (2014). The *Fusarium graminearum* Genome Reveals More Secondary Metabolite Gene Clusters and Hints of Horizontal Gene Transfer. PLoS One *9*, e110311.

Sievers, F., Wilm, A., Dineen, D., Gibson, T.J., Karplus, K., Li, W., Lopez, R., McWilliam, H., Remmert, M., Soeding, J., *et al.* (2011). Fast, scalable generation of high-quality protein multiple sequence alignments using Clustal Omega. Molecular Systems Biology *7*, 539.

Simão, F.A., Waterhouse, R.M., Ioannidis, P., Kriventseva, E.V., and Zdobnov, E.M. (2015). BUSCO: assessing genome assembly and annotation completeness with single-copy orthologs. Bioinformatics *31*, 3210-3212.

Singh, R.P., Hodson, D.P., Huerta-Espino, J., Jin, Y., Bhavani, S., Njau, P., Herrera-Foessel, S., Singh, P.K., Singh, S., and Govindan, V. (2011). The emergence of Ug99 races of the stem rust fungus is a threat to world wheat production. Annual Review of Phytopathology *49*, 465-481.

Sinzelle, L., Izsvak, Z., and Ivics, Z. (2009). Molecular domestication of transposable elements: From detrimental parasites to useful host genes. Cellular and Molecular Life Sciences *66*, 1073-1093.

Siou, D., Gelisse, S., Laval, V., Suffert, F., and Lannou, C. (2015). Mutual Exclusion between Fungal Species of the *Fusarium* Head Blight Complex in a Wheat Spike. Applied and Environmental Microbiology *81*, 4682-4689.

Smit, A., and Hubley, R. (2008-2015). RepeatModeler Open-1.0.

Somma, S., Alvarez, C., Ricci, V., Ferracane, L., Ritieni, A., Logrieco, A., and Moretti, A. (2010). Trichothecene and beauvericin mycotoxin production and genetic variability in *Fusarium poae* isolated from wheat kernels from northern Italy. Food Additives and Contaminants Part a-Chemistry Analysis Control Exposure & Risk Assessment *27*, 729-737.

Spanjer, M.C., Rensen, P.M., and Scholten, J.M. (2008). LC-MS/MS multi-method for mycotoxins after single extraction, with validation data for peanut, pistachio, wheat, maize, cornflakes, raisins and figs. Food Additives and Contaminants Part a-Chemistry Analysis Control Exposure & Risk Assessment *25*, 472-489.

Stanke, M., Schoffmann, O., Morgenstern, B., and Waack, S. (2006). Gene prediction in eukaryotes with a generalized hidden Markov model that uses hints from external sources. BMC Bioinformatics *7*, 62.

Starkey, D.E., Ward, T.J., Aoki, T., Gale, L.R., Kistler, H.C., Geiser, D.M., Suga, H., Toth, B., Varga, J., and O'Donnell, K. (2007). Global molecular surveillance reveals novel *Fusarium* head blight species and trichothecene toxin diversity. Fungal Genetics and Biology *44*, 1191-1204.

Stenglein, S., Barreto, D., Nicholson, P., Chandler, E., Brambilla, V., Piris, E.M., Saliva, V., Mitidieri, M., and Salerno, G. (2009). First report of *Fusarium poae* on tomato in Argentina. Plant Pathology *58*, 401-401.

Stenglein, S.A., Dinolfo, M.I., Barros, G., Bongiorno, F., Chulze, S.N., and Moreno, M.V. (2014). *Fusarium poae* Pathogenicity and Mycotoxin Accumulation on Selected Wheat and Barley Genotypes at a Single Location in Argentina. Plant Disease *98*, 1733-1738.

Stenglein, S.A., Rodriguero, M.S., Chandler, E., Jennings, P., Salerno, G.L., and Nicholson, P. (2010). Phylogenetic relationships of *Fusarium poae* based on EF-1 alpha and mtSSU sequences. Fungal Biology *114*, 96-106.

Stergiopoulos, I., Zwiers, L.H., and De Waard, M.A. (2002). Secretion of natural and synthetic toxic compounds from filamentous fungi by membrane transporters of the ATP-binding cassette and major facilitator superfamily. European Journal of Plant Pathology *108*, 719-734.

Streit, E., Schwab, C., Sulyok, M., Naehrer, K., Krska, R., and Schatzmayr, G. (2013). Multi-Mycotoxin Screening Reveals the Occurrence of 139 Different Secondary Metabolites in Feed and Feed Ingredients. Toxins *5*, 504-523.

Stukenbrock, E.H. (2013). Evolution, selection and isolation: a genomic view of speciation in fungal plant pathogens. New Phytologist *199*, 895-907.

Stukenbrock, E.H., Christiansen, F.B., Hansen, T.T., Dutheil, J.Y., and Schierup, M.H. (2012). Fusion of two divergent fungal individuals led to the recent emergence of a unique widespread pathogen species. Proceedings of the National Academy of Sciences of the United States of America *109*, 10954-10959.

Stukenbrock, E.H., and Croll, D. (2014). The evolving fungal genome. Fungal Biology Reviews *28*, 1-12.

Stukenbrock, E.H., and McDonald, B.A. (2008). The origins of plant pathogens in agro-ecosystems. Annual Review of Phytopathology *46*, 75-100.

Subramaniam, R., Narayanan, S., Walkowiak, S., Wang, L., Joshi, M., Rocheleau, H., Ouellet, T., and Harris, L.J. (2015). Leucine metabolism regulates TRI6 expression and affects deoxynivalenol production and virulence in *Fusarium graminearum*. Molecular Microbiology *98*, 760-769.

Sugiura, Y., Fukasaku, K., Tanaka, T., Matsui, Y., and Ueno, Y. (1993). *Fusarium poae* and *Fusarium crookwellense*, fungi responsible for the natural occurrence of nivalenol in Hokkaido. Applied and Environmental Microbiology *59*, 3334-3338.

Swofford, D. (2003). PAUP*: phylogenetic analysis using parsimony, version 4.0 b10.

Szewczyk, E., Nayak, T., Oakley, C.E., Edgerton, H., Xiong, Y., Taheri-Talesh, N., Osmani, S.A., and Oakley, B.R. (2006). Fusion PCR and gene targeting in *Aspergillus nidulans*. Nature Protocols *1*, 3111-3120.

T

Tag, A.G., Garifullina, G.F., Peplow, A.W., Ake, C., Phillips, T.D., Hohn, T.M., and Beremand, M.N. (2001). A novel regulatory gene, *Tri10*, controls trichothecene toxin production and gene expression. Applied and Environmental Microbiology *67*, 5294-5302.

Talas, F., and McDonald, B. (2015). Significant variation in sensitivity to a DMI fungicide in field populations of *Fusarium graminearum*. Plant Pathology *64*, 664-670.

Tavanti, A., Gow, N.A.R., Maiden, M.C.J., Odds, F.C., and Shaw, D.J. (2004). Genetic evidence for recombination in *Candida albicans* based on haplotype analysis. Fungal Genetics and Biology *41*, 553-562.

Thorp, G.L., and Jennings, P. (2015). Monitoring of the UK wheat *Fusarium* population 2000-2014. Paper presented at: 13th European *Fusarium* Seminar (Martina Franca, Italy).

Thrane, U., Adler, A., Clasen, P.E., Galvano, F., Langseth, W., Logrieco, A., Nielsen, K.F., and Ritieni, A. (2004). Diversity in metabolite production by *Fusarium langsethiae*, *Fusarium poae*, and *Fusarium sporotrichioides*. International Journal of Food Microbiology *95*, 257-266.

Torp, M., and Adler, A. (2004). The European *Sporotrichiella* project: a polyphasic approach to the biology of a new *Fusarium* species. International Journal of Food Microbiology *95*, 241-245.

Torp, M., and Langseth, W. (1999). Production of T-2 toxin by a *Fusarium* resembling *Fusarium poae*. Mycopathologia *147*, 89-96.

Torp, M., and Nirenberg, H.I. (2004). *Fusarium langsethiae* sp nov on cereals in Europe. International Journal of Food Microbiology *95*, 247-256.

Trott, O., and Olson, A.J. (2010). Software News and Update AutoDock Vina: Improving the Speed and Accuracy of Docking with a New Scoring Function, Efficient Optimization, and Multithreading. Journal of Computational Chemistry *31*, 455-461.

Turgeon, B.G. (1998). Application of mating type gene technology to problems in fungal biology. Annual Review of Phytopathology *36*, 115-137.

U

Ueno, Y. (1983). Trichothecenes. Chemical, biological and toxicological aspects. Elsevier. 328p.

V

van der Fels-Klerx, H.J., de Rijk, T.C., Booij, C.J.H., Goedhart, P.W., Boers, E.A.M., Zhao, C., Waalwijk, C., Mol, H.G.J., and van der Lee, T.A.J. (2012). Occurrence of *Fusarium* Head Blight species and *Fusarium* mycotoxins in winter wheat in the Netherlands in 2009. Food Additives and Contaminants Part a-Chemistry Analysis Control Exposure & Risk Assessment *29*, 1716-1726.

van der Lee, T., Zhang, H., van Diepeningen, A., and Waalwijk, C. (2015). Biogeography of *Fusarium graminearum* species complex and chemotypes: a review. Food Additives and Contaminants Part a-Chemistry Analysis Control Exposure & Risk Assessment *32*, 453-460.

Varga, E., Wiesenberger, G., Hametner, C., Ward, T.J., Dong, Y., Schöfbeck, D., McCormick, S., Broz, K., Stückler, R., Schuhmacher, R., *et al.* (2015). New tricks of an old enemy: isolates of *Fusarium graminearum* produce a type A trichothecene mycotoxin. Environmental Microbiology *17*, 2588–2600.

Vendl, O., Crews, C., MacDonald, S., Krska, R., and Berthiller, F. (2010). Occurrence of free and conjugated *Fusarium* mycotoxins in cereal-based food. Food Additives and Contaminants Part a-Chemistry Analysis Control Exposure & Risk Assessment *27*, 1148-1152.

Verstraete, F. (2013). Aflatoxin contamination in maize in 2012-2013. Paper presented at: Mycotoxin Forum (Brussels).

Vogelgsang, S., Sulyok, M., Baenziger, I., Krska, R., Schuhmacher, R., and Forrer, H.-R. (2008a). Effect of fungal strain and cereal substrate on in vitro mycotoxin production by *Fusarium poae* and *Fusarium avenaceum*. Food Additives and Contaminants Part a-Chemistry Analysis Control Exposure & Risk Assessment *25*, 745-757.

Vogelgsang, S., Sulyok, M., Hecker, A., Jenny, E., Krska, R., Schuhmacher, R., and Forrer, H.-R. (2008b). Toxigenicity and pathogenicity of *Fusarium poae* and *Fusarium avenaceum* on wheat. European Journal of Plant Pathology *122*, 265-276.

Vujosevic, M., and Blagojevic, J. (2004). B chromosomes in populations of mammals. Cytogenetic and Genome Research *106*, 247-256.

W

Waalwijk, C., Kastelein, P., de Vries, I., Kerenyi, Z., van der Lee, T., Hesselink, T., Kohl, J., and Kema, G. (2003). Major changes in *Fusarium* spp. in wheat in the Netherlands. European Journal of Plant Pathology *109*, 743-754.

Waalwijk, C., van der Heide, R., de Vries, I., van der Lee, T., Schoen, C., Costrel-de Corainville, G., Hauser-Hahn, I., Kastelein, P., Kohl, J., Lonnet, P., *et al.* (2004). Quantitative detection of *Fusarium* species in wheat using TaqMan. European Journal of Plant Pathology *110*, 481-494.

Wagacha, J.M., Steiner, U., Dehne, H.-W., Zuehlke, S., Spiteller, M., Muthomi, J., and Oerke, E.-C. (2010). Diversity in Mycotoxins and Fungal Species Infecting Wheat in Nakuru District, Kenya. Journal of Phytopathology *158*, 527-535.

Walter, S., Nicholson, P., and Doohan, F.M. (2010). Action and reaction of host and pathogen during *Fusarium* head blight disease. New Phytologist *185*, 54-66.

Ward, T.J., Bielawski, J.P., Kistler, H.C., Sullivan, E., and O'Donnell, K. (2002). Ancestral polymorphism and adaptive evolution in the trichothecene mycotoxin gene cluster of phytopathogenic *Fusarium*. Proceedings of the National Academy of Sciences of the United States of America *99*, 9278-9283.

Ward, T.J., Clear, R.M., Rooney, A.P., O'Donnell, K., Gaba, D., Patrick, S., Starkey, D.E., Gilbert, J., Geiser, D.M., and Nowicki, T.W. (2008). An adaptive evolutionary shift in *Fusarium* head blight pathogen populations is driving the rapid spread of more toxigenic *Fusarium graminearum* in North America. Fungal Genetics and Biology *45*, 473-484.

Warris, S., Yalcin, F., Jackson, K.J.L., and Nap, J.P. (2015). Flexible, Fast and Accurate Sequence Alignment Profiling on GPGPU with PaSWAS. PLoS One *10*, e0122524.

Watters, M.K., Randall, T.A., Margolin, B.S., Selker, E.U., and Stadler, D.R. (1999). Action of repeat-induced point mutation on both strands of a duplex and on tandem duplications of various sizes in *Neurospora*. Genetics *153*, 705-714.

Wicker, T., Oberhaensli, S., Parlange, F., Buchmann, J.P., Shatalina, M., Roffler, S., Ben-David, R., Dolezel, J., Simkova, H., Schulze-Lefert, P., *et al.* (2013). The wheat powdery mildew genome shows the unique evolution of an obligate biotroph. Nature Genetics *45*, 1092-1096.

Wicker, T., Sabot, F., Hua-Van, A., Bennetzen, J.L., Capy, P., Chalhoub, B., Flavell, A., Leroy, P., Morgante, M., Panaud, O., *et al.* (2007). A unified classification system for eukaryotic transposable elements. Nature Reviews Genetics *8*, 973-982.

Wiemann, P., Sieber, C.M.K., Von Bargen, K.W., Studt, L., Niehaus, E.-M., Espino, J.J., Huss, K., Michielse, C.B., Albermann, S., Wagner, D., *et al.* (2013). Deciphering the Cryptic Genome: Genome-wide Analyses of the Rice Pathogen *Fusarium fujikuroi* Reveal Complex Regulation of Secondary Metabolism and Novel Metabolites. PLoS Pathogens *9*, e1003475.

Windels, C.E. (2000). Economic and social impacts of *Fusarium* head blight: changing farms and rural communities in the northern great plains. Phytopathology *90*, 17-21.

Wittenberg, A.H.J., van der Lee, T.A.J., Ben M'Barek, S., Ware, S.B., Goodwin, S.B., Kilian, A., Visser, R.G.F., Kema, G.H.J., and Schouten, H.J. (2009). Meiosis Drives Extraordinary Genome Plasticity in the Haploid Fungal Plant Pathogen *Mycosphaerella graminicola*. PLoS One *4*, e5863.

Wyand, R., and Brown, J. (2005). Sequence variation in the CYP51 gene of *Blumeria graminis* associated with resistance to sterol demethylase inhibiting fungicides. Fungal Genetics and Biology *42*, 726-735.

X

Xu, X. (2003). Effects of environmental conditions on the development of *Fusarium* ear blight. European Journal of Plant Pathology *109*, 683-689.

Xu, X.M., Nicholson, P., Thomsett, M.A., Simpson, D., Cooke, B.M., Doohan, F.M., Brennan, J., Monaghan, S., Moretti, A., Mule, G., *et al.* (2008). Relationship between the fungal complex causing *Fusarium* head blight of wheat and environmental conditions. Phytopathology *98*, 69-78.

Xu, X.M., Parry, D.W., Nicholson, P., Thomsett, M.A., Simpson, D., Edwards, S.G., Cooke, B.M., Doohan, F.M., Brennan, J.M., Moretti, A., *et al.* (2005). Predominance and association of pathogenic fungi causing *Fusarium* ear blight in wheat in four European countries. European Journal of Plant Pathology *112*, 143-154.

Y

Yandell, M., and Ence, D. (2012). A beginner's guide to eukaryotic genome annotation. Nature Reviews Genetics *13*, 329-342.

Yang, L., van der Lee, T., Yang, X., Yu, D., and Waalwijk, C. (2008). *Fusarium* populations on chinese barley show a dramatic gradient in mycotoxin profiles. Phytopathology *98*, 719-727.

Yin, Y., Liu, X., Li, B., and Ma, Z. (2009). Characterization of sterol demethylation inhibitor-resistant isolates of *Fusarium asiaticum* and *F. graminearum* collected from wheat in China. Phytopathology *99*, 487-497.

Yli-Mattila, T. (2010). Ecology and evolution of toxigenic *Fusarium* species in cereals in Northern Europe and Asia Journal of Plant Pathology *92*, 7-18.

Yli-Mattila, T., Gagkaeva, T., Ward, T.J., Aoki, T., Kistler, H.C., and O'Donnell, K. (2009). A novel Asian clade within the *Fusarium graminearum* species complex includes a newly discovered cereal head blight pathogen from the Russian Far East. Mycologia *101*, 841-852.

Yu, J.H., Hamari, Z., Han, K.H., Seo, J.A., Reyes-Dominguez, Y., and Scazzocchio, C. (2004). Double-joint PCR: a PCR-based molecular tool for gene manipulations in filamentous fungi. Fungal Genetics and Biology *41*, 973-981.

Yun, S.H., Berbee, M.L., Yoder, O.C., and Turgeon, B.G. (1999). Evolution of the fungal self-fertile reproductive life style from self-sterile ancestors. Proceedings of the National Academy of Sciences of the United States of America *96*, 5592-5597.

Z

Zadoks, J.C., Chang, T.T., and Konzak, C.F. (1974). A decimal code for the growth stages of cereals. Weed research *14*, 415-421.

Zeller, K.A., Bowden, R.L., and Leslie, J.F. (2003). Diversity of epidemic populations of *Gibberella zeae* from small quadrats in Kansas and north Dakota. Phytopathology *93*, 874-880.

Zhao, C., Waalwijk, C., de Wit, P.J.G.M., Tang, D., and van der Lee, T. (2013). RNA-Seq analysis reveals new gene models and alternative splicing in the fungal pathogen *Fusarium graminearum*. BMC Genomics *14*, 21.

Zhao, C., Waalwijk, C., de Wit, P.J.G.M., Tang, D., and van der Lee, T. (2014). Relocation of genes generates non-conserved chromosomal segments in *Fusarium graminearum* that show distinct and co-regulated gene expression patterns. BMC Genomics *15*, 191.

Zhou, H.Y., and Zhou, Y.Q. (2002). Distance-scaled, finite ideal-gas reference state improves structure-derived potentials of mean force for structure selection and stability prediction. Protein Science *11*, 2714-2726.

Zwiers, L.H., Stergiopoulos, I., Gielkens, M.M.C., Goodall, S.D., and De Waard, M.A. (2003). ABC transporters of the wheat pathogen *Mycosphaerella graminicola* function as protectants against biotic and xenobiotic toxic compounds. Molecular Genetics and Genomics *269*, 499-507.

Curriculum vitae

PERSONALIA

NAME	Adriaan J. C. Vanheule
ADDRESS	Fernard Bernierstraat 62, 1060 Sint-Gillis
BIRTH	05/10/1988, Veurne
CONTACT	+32 498 22 92 58
	adriaan_vanheule@hotmail.com

PROFESSIONAL EXPERIENCE

EUROPEAN COMMISSION, BRUSSELS, BELGIUM 2015-2016
Blue Book Trainee at the Directorate-General for Health and Food Safety

GHENT UNIVERSITY, GHENT, BELGIUM 2011-2015
PhD researcher working in the areas of microbiology, plant disease and food safety

WAGENINGEN UR, WAGENINGEN, THE NETHERLANDS 2014-2015
Research internship of six months to study fungal genomics

MARTIN LUTHER UNIVERSITÄT OF HALLE-WITTENBERG, HALLE, GERMANY 2014
Research internship of one month to study molecular techniques in fungal transformation

EDUCATION

GHENT UNIVERSITY, GHENT, BELGIUM 2009-2011
Master of Science in Bioscience Engineering: Agricultural Sciences
Grade: distinction
Dissertation: Pathological and microscopic study of powdery mildew on its new host triticale

GHENT UNIVERSITY, GHENT, BELGIUM 2006-2009
Bachelor of Science in Bioscience Engineering
Grade: distinction

AWARDS

AGRISCIENCES YOUNG RESEARCHERS 2015 2015
JEALOTT'S HILL, UNITED KINGDOM
2nd place for best Oral Presentation

13th EUROPEAN FUSARIUM SEMINAR, MARTINA FRANCA, ITALY 2015
Marasas Prize for Best Oral Presentation

BIJZONDER ONDERZOEKSFONDS (BOF), GHENT, BELGIUM 2014
Funding award for completing doctoral research

FONDS WETENSCHAPPELIJK ONDERZOEK (FWO), GHENT, BELGIUM 2013
Travel award for internship at Wageningen UR

PUBLICATIONS

Vanheule, A, Audenaert, K, Warris, S, van de Geest, H, Schijlen, E, Höfte, M, De Saeger, S, Haesaert, G, Waalwijk, C, van der Lee, T. Living apart together: crosstalk between the core and supernumerary genomes in a fungal plant pathogen. *Submitted to BMC Genomics.*

Vanheule, A, Audenaert, K, De Boevre, M, Landschoot, S, Bekaert, B, Munaut, F, Eeckhout, M, Hofte, M, De Saeger, S, Haesaert, G. (2014) The compositional mosaic of *Fusarium* species and their mycotoxins in unprocessed cereals, food and feed products in Belgium. International Journal of Food Microbiology, 181, 28-36.

Troch, V, Audenaert, K, Vanheule, A, Bekaert, B, Hofte, M, Haesaert, G. (2014) The importance of non-penetrated papillae formation in the resistance response of triticale to powdery mildew (*Blumeria graminis*). Plant Pathology, 63, 129-139.

De Boevre, M, Vanheule, A, Audenaert, K, Bekaert, B, Di Mavungu, J Diana, Werbrouck, S, Haesaert, G, De Saeger, S. (2014) Detached leaf *in vitro* model for masked mycotoxin biosynthesis and subsequent analysis of unknown conjugates. World Mycotoxin Journal, 7, 305-312.

Audenaert, K, De Boevre, M, Vanheule, A, Callewaert, J, Bekaert, B, Hofte, M, De Saeger, S, Haesaert, G. (2013) Mycotoxin glucosylation in commercial wheat varieties: Impact on resistance to *Fusarium graminearum* under laboratory and field conditions. Food Control, 34, 756-762.

Audenaert, K, Vanheule, A, Hofte, M, Haesaert, G. (2013) Deoxynivalenol: a major player in the multifaceted response of *Fusarium* to its environment. Toxins, 6, 1-19.

Troch, V, Audenaert, K, Vanheule, A, Bekaert, B, Hofte, M, Haesaert, G. (2013) Evaluation of resistance to powdery mildew in triticale seedlings and adult plants. Plant Disease, 97, 410-417.

Audenaert, K, Vanheule, A, De Baets, B, Haesaert, G, Landschoot, S, Waegeman, W. (2011) Impact of fungicide timing on the composition of the *Fusarium* head blight disease complex and the presence of deoxynivalenol (DON) in wheat, in: Fungicides - Beneficial and Harmful Aspects, edited by Nooruddin Thajuddin, INTECH Open Access Publisher.

SCIENTIFIC CONFERENCES

ORAL CONTRIBUTIONS

64th International Symposium on Crop Protection, May 22nd 2012, Ghent, Belgium. Vanheule, A, Audenaert, K, De Saeger, S, Höfte, M, and Haesaert, G. *Fusarium poae*: chemotypes, plant-pathogen interactions and reaction to stress triggers.

27th Meeting of the Fusarium working group of the Koninklijke Nederlandse Planteziektenkundige Vereniging, October 31st 2012, Utrecht, The Netherlands. Vanheule, A, Audenaert, K, De Saeger, S, Höfte, M, and Haesaert, G. *Fusarium poae*: chemotypes, plant-pathogen interactions and reaction to stress triggers.

35th Mycotoxin Workshop, May 22nd – May 24th 2013, Ghent, Belgium. Vanheule, A, Audenaert, K, De Saeger, S, Höfte, M, Haesaert, G. *Fusarium poae*: chemotype, plant-pathogen interaction and response oxidative stress triggers.

Agricultural contaminants – Mycotoxin Forum, September 5th – September 6th 2013, European Commission, Brussels, Belgium. Vanheule, A, De Boevre, M. Results from the MytoxPlex project.

29th Meeting of the Fusarium working group of the Koninklijke Nederlandse Planteziektenkundige Vereniging, October 29st 2014, Utrecht, The Netherlands. Vanheule, A, Audenaert, K, De Boevre, M, Bekaert, B, Waalwijk, C, van der Lee, T, Höfte, M, De Saeger, S, Wirsel, S, Haesaert, G. *Fusarium poae*: proposed pathway for a novel trichothecene chemotype.

13th European Fusarium Seminar, May 10th – May 14th 2015, Martina Franca, Italy. Vanheule, A, Audenaert, K, Warris, S, van de Geest, H, Höfte, M, Waalwijk, C, Haesaert, G, van der Lee, T. Presenting the fully assembled genome of *Fusarium poae*: repeats shed light on a cryptic sexual cycle.

13th European Fusarium Seminar, May 10th – May 14th 2015, Martina Franca, Italy. Vanheule, A, Audenaert, K, De Boevre, M, Bekaert, B, Waalwijk, C, van der Lee, T, Höfte, M, De Saeger, S, Wirsel, S, Haesaert, G. *Fusarium poae*: proposed pathway for a novel trichothecene chemotype.

SCI Agrisciences Young Researchers 2015: Crop Production, Protection and Utilisation, July 8th 2015, Jealott's Hill, UK. Vanheule, A, Audenaert, K, Höfte, M, Warris, S, van de Geest, H, Waalwijk, C, Haesaert, G, van der Lee, T. Supernumerary chromosomes evade genome defence in a fungal plant pathogen.

POSTER CONTRIBUTIONS

12th European Fusarium Seminar, May 12th – May 16th 2013, Bordeaux, France. Vanheule, A, Audenaert, K, De Saeger, S, Höfte, M, and Haesaert, G. *Fusarium poae*: the implication of a unique blend of mycotoxins.

International Mycotoxin Conference, May 19th – May 23rd 2014, Beijing, China. Vanheule, A, Audenaert, K, Wirsel, S, De Saeger, S, Höfte, M, Haesaert, G. *Fusarium poae*: identifying the molecular switches of a unique chemotype.

TUTORSHIP MASTER THESES

MICHIEL DEGRAUWE 2011-2012
Fusarium poae in Vlaamse wintertarwe: isolatie, chemotypering en fytopathologische karakterisatie

JANNES DECADT 2012-2013
In vitro en *in vivo* screening van de interactie wintertarwe – *Fusarium poae*

Dankwoord

Fiieeeuuuwwww.

Het was een lange, soms zware, maar achteraf bekeken vooral heel leerzame en verrijkende weg die me tot hier heeft gebracht, en het is niet zonder trots dat ik nu een afgewerkt doctoraat voor stel. Doctoreren is een speciale bezigheid, en multidisciplinair onderzoek doe je niet alleen. Er zijn heel wat mensen geweest zonder wie het absoluut niet zou gelukt zijn, en ik wil hen toch even speciaal bedanken.

Eerst en vooral: Kris. Ik durf heel eerlijk stellen dat zonder jou dit doctoraat er niet zou liggen. Je was er elke dag voor de (in mijn geval: broodnodige) begeleiding, met onuitputtelijke wetenschappelijke nieuwsgierigheid en enthousiasme. Nog belangrijker echter: je was er op de momenten dat de experimenten minder vlot gingen en ik het wat minder zag zitten, en met een gezonde portie realisme en optimisme wist je mij opnieuw 100% te motiveren. Een schitterende gave waar in de toekomst een heel indrukwekkend team van gaat kunnen genieten, daar ben ik zeker van. Vanuit de grond van mijn hart: bedankt!

Ik had de eer om gesteund te worden door meer dan 1 promotor. Geert, bedankt voor het vertrouwen en de kansen die je me 4 jaar lang gegeven hebt. Je liet me vrij om ietwat mijn eigen richting te kiezen, en met de regelmatige updates op het vierde verdiep hield je tegelijkertijd een sterk geapprecieerd oogje in het zeil – bedankt daarvoor. Monica, doorheen mijn doctoraat hebben we denk ik een handvol vergaderingen gehad over de stand van zaken, en ik ben vrij zeker dat elk van hen bepalend geweest zijn voor het verdere verloop van het onderzoek. Ik vond het fantastisch om na zo'n vergadering buiten te komen met een hoofd vol nieuwe ideeën en inspiratie. Sarah – bedankt voor de fijne omgeving op de FFW waarin in me steeds welkom gevoeld heb, en bedankt voor de oprechte interesse in mijn onderzoek.

I would like to thank the members of the examination committee for the (significant!) amount of work that they put into reading and improving my PhD thesis.

Het is onmogelijk om alle collega's waar ik me mee geamuseerd heb op te noemen (want de BIOT/GTB/BW15/… groep is echt fantastisch), maar een aantal pik ik er toch uit. Maarten en Nathalie – thanks voor de fijne tijden op de bureau – het was super om samen met jullie zowel vreudge en leed in het onderzoek te delen. Sofie – ik kon altijd bij jou terecht voor de stomste statistiek vragen (en er waren er heel wat). Boris… jou kan ik eigenlijk niet genoeg bedanken. Onwaarschijnlijk hoeveel geduld je hebt opgebracht om telkens maar weer het volgende gekke

idee in verband met transformanten of weet-ik-veel-wat te ondernemen. Je rol in dit doctoraat kan niet onderschat worden – merci! Jolien, Michiel, Dènny, Jelle, Katrien, Leen, Joris, Helena, Aingebourg, Stephanie, en alle andere fantastische collega's die ik vergeet: bedankt om de werkomgeving bij ons zo fantastisch leuk te maken met allerhande (al dan niet spontane) drinks, het jaarlijks weekend, leuke (al dan niet nerdy) koffiepauzes, … Een aantal "anciens" wil zeker niet vergeten: Hans, Nick – mijn voorbeelden als beginnend doctoraatstudent. Veronique, met jou is eigenlijk alles begonnen en van jou heb ik de beginselen van onderzoek geleerd – bedankt!

Ongeveer 7 maanden van mijn doctoraat heb ik doorgebracht in Wageningen, en dat waren 7 zeer leerrijke en deugddoende maanden. Cees en Theo, ik wil jullie oprecht bedanken voor het vertrouwen dat jullie in mij geplaatst hebben, voor de uitstekende begeleiding, en voor de voortdurende interesse in het onderzoek. Ik heb me bij jullie ontzettend goed geamuseerd, en mijn periode in Wageningen zie ik zowat als het hoogtepunt binnen mijn PhD. Bedankt – voor alles! The "Radix people" of Wageningen made my stay all the more pleasant – thank you guys for the fun jenever drinking, house parties, … Bedankt Els en Marga voor de steun in het lab en het geduld dat daarbij nodig was ;-). Sven, Henri, bedankt voor de fijne samenwerking, ik heb veel van jullie geleerd!

De Mytox groep en in het bijzonder de mensen aan de FFW verdienen een speciale vermelding. Ik kwam graag langs op het labo Bromatologie en dat is ongetwijfeld te danken aan de super fijne mensen daar. Marthe – jij verdient eigenlijk een dankwoord op jezelf. Ik heb heel veel van je geleerd, en ben erg dankbaar voor je optimisme en (onwaarschijnlijk groot) geduld. Annie, Christ'l, Melanie, Ellen, Christof, Nathan, … bedankt voor de leuke ervaringen (ik denk maar aan BBQ, quiz, organisatie van de Mycotoxin Workshop, …).

Throughout my PhD I had the pleasure to work in a few excellent external research labs. Françoise, thank you for welcoming me in Louvain-la-Neuve. Céline, thank you for the help with the AFLP! Jonathan and Pierre – thank you to you as well for the pleasant interaction (and conference shenanigans ;-)). Dr. Stefan Wirsel – thank you for the guidance and interest you have shown, both during my time in Halle and afterwards.

Aan mijn vrienden – hopelijk toont dit boekje aan waar ik 4 jaar mee bezig ben geweest, en is het een beter antwoord op de vragen "hoe is 't in de schimmels?" en "is dat nu nog altijd niet opgelost?" dan deze die ik de voorbije jaren heb gegeven ;-). Merci aan mijn broers en zussen voor het supporteren. Mama en papa, jullie verdienen een medaille voor de kansen en de steun

die jullie geboden hebben. Hopelijk zijn jullie vandaag trots en kan je ervan uit gaan dat het goed komt.

Er rest me nog 1 iemand te bedanken. Mikkie, jij hebt de keerzijde van doctoreren gezien. De talloze avonden aan de computer, ganse weekends in het labo, teleurstelling en frustratie als iets weer eens mislukte, … Jij was er elke keer opnieuw, zelfs als ik het eigenlijk niet verdiende, en zonder jou zou het niet gelukt zijn. Merci voor je grenzeloos optimisme, voor je steun, voor alles.

Adriaan Vanheule

Februari 2016, Brussel

"Piled Higher and Deeper" by Jorge Cham
www.phdcomics.com